

**Electrochemical synthesis and
characterisation of
polypyrrole/chitosan films doped with
molecular anions**



NUI MAYNOOTH

Ollscoil na hÉireann Má Nuad

Emer Moloney, B.Sc. (Hons)

**Department of Chemistry
National University of Ireland Maynooth**

February 2014

**Thesis Submitted to the National University of Ireland in
Fulfillment of the requirements for the Degree of Doctor of
Philosophy**

Supervisors: Prof. Carmel B. Breslin

Head of Department: Dr. John Stephens

Table of Contents

Declaration	vi
Acknowledgments.....	vii
Dedication	viii
Abstract	ix
1. Introduction and Literature Review	2
1.1 Research Topic and Relevance.....	2
1.2 Objectives and Achievements	2
1.3 Conducting polymers (CP).....	4
1.3.1 The conductivity and doping levels of conducting polymers	7
1.3.2 Synthesis of polypyrrole	12
1.4 Polypyrrole for biomedical applications	20
1.4.1 Polypyrrole in tissue engineering applications and neuroprosthetics ..	22
1.4.2 Polypyrrole in drug delivery applications	22
1.5 Chitosan.....	27
1.5.1 Biomedical applications	30
1.6 Polypyrrole/chitosan composites.....	31
1.7 Challenges	32
1.7.1 Electrical properties	32
1.7.2 Biological and physical properties	33
1.8 Summary	33
References	34
2 Experimental	47
2.1 Introduction.....	47
2.2 The electrochemical set-up	48
2.2.1 The electrochemical workstation	48
2.2.2 The electrochemical cell	49
2.3 Chemicals and preparation of polymers.....	53

2.3.1 Chemicals	53
2.3.2 Preparation of chitosan solution.....	53
2.3.3 Preparation of polymers	54
2.3.4 Vapour phase polymerisation of pyrrole on to chitosan	54
2.4 Experimental techniques	55
2.4.1 Potentiostatic technique	55
2.4.2 Cyclic voltammetry	56
2.4.3 Open-circuit potential.....	60
2.4.4 Electrochemical impedance spectroscopy (EIS).....	60
2.4.5 Electrochemical quartz crystal microbalance (EQCM)	65
2.4.6 Scanning electron microscopy (SEM) with energy dispersive X-Ray (EDX) Analysis.....	67
2.4.7 Differential scanning calorimetry (DSC)	70
2.4.8 Fourier transform infrared spectroscopy (FT-IR)	71
2.4.9 Ultra violet visible spectroscopy (UV-Vis).....	72
2.4.10 Adhesion tests of the polymer coatings	73
2.4.11 Wettability test of polymer coatings	73
2.4.12 Data-handling and statistics	74
References	74
3. Electrochemical synthesis and characterisation of polypyrrole chloride (PpyCl)/chitosan composite films	79
3.1 Introduction	79
3.2 Experimental	82
3.3 Results and discussion.....	83
3.3.1 Redox stability of a chitosan coated electrode.....	83
3.3.2 Electrochemical synthesis of the chitosan-polypyrrole chloride (Chit/PpyCl) film.....	84
3.3.3 Characterisation of the composite	89
3.3.4 Cyclic Voltammetry (CV).....	100
3.3.5 Open-circuit potential experiments	107
3.3.6 Electrochemical impedance spectroscopy (EIS) studies.....	108

3.4	Effect of lysozyme.....	129
3.4.1	The effect of lysozyme solution on chitosan using EQCM	130
3.4.2	Open-circuit potential of Chit/PpyCl immersed in lysozyme solution	131
3.5	Adhesion test	133
3.6	Wettability of the composite	135
3.7	Summary of results.....	138
	References	139
4.	Electrochemical synthesis and characterisation of polypyrrole methyl orange (PpyMO)/chitosan composite films	151
4.1	Introduction	151
4.2	Experimental	153
4.3	Results and discussion.....	154
4.3.1	Redox properties of Methyl Orange.....	154
4.3.2	Electrochemical synthesis of the polypyrrole methyl orange film and composite	155
4.3.3	Cyclic Voltammetry (CV).....	165
4.3.4	Electrochemical impedance spectroscopy (EIS).....	179
4.3.5	Adhesion test.....	196
4.3.6	Methyl orange release studies	197
4.4	Summary	202
	References	203
5.	Electrochemical synthesis and characterisation of polypyrrole oxacillin (PpyOx)/chitosan composite films.....	212
5.1	Introduction	212
5.2	Experimental	214
5.3	Results and discussion.....	214
5.3.1	Redox properties of Oxacillin	214
5.3.2	Electrochemical synthesis of the polypyrrole oxacillin (PpyOx) films	215
5.3.3	SEM-EDX.....	221

5.3.4	Cyclic Voltammetry	223
5.3.5	Electrochemical Impedance spectroscopy	235
5.3.6	Adhesion test.....	250
5.3.7	Release of oxacillin	251
5.3.8	Detection of oxacillin.....	252
5.4	Summary	256
	References	257
	Conclusion	264
6.	Conclusions	265
6.1	Future work	268
	References	268

Declaration

I hereby certify that this thesis, which I now submit for assessment on the programme of study leading to the award of PhD has not been submitted, in whole or part, to this or any other University for any degree and is, except where otherwise stated the original work of the author.

Emer Moloney, B.Sc (Hons)

National University of Ireland, Maynooth

February 2014

Acknowledgments

I would like to express my sincere gratitude to my supervisor Prof. Carmel B. Breslin, for her exemplary guidance and being more than generous with her time, for sharing her expertise and giving me the independence to develop my research skills.

I am grateful to all the technical staff in the Chemistry Department at NUI Maynooth, especially to Dr. Ken Maddock, Ollie Fenelon, and Noel Williams and to Mr. Paul Tierney at the Institute of Technology, Tallaght.

I am fortunate to have met my good friends Wayne and Orla through this endeavour. I would like to thank Orla for her meticulous proof-reading and Wayne for helping me with formatting (I anticipate). A special mention to Karen Herdman and David Branagan, I wish you both the best of luck. I would like to extend my best wishes to the rest of the department.

On the home front; I am deeply grateful to my parents; Eamon and Kay. A special mention for my late grandmother, Kay Moloney, and my extended family. I must also thank my brother, Owen, and my best friend Róisín, for taking an interest in my work, and being a welcomed distraction when needed. Without all their continuing love and support I would not have been able to fulfill my ambitions.

A heartfelt thank you to my wonderful partner, Dan, for being so supportive, loving, patient and understanding.

Finally, I want to thank my sons; Liam and Conor, for keeping me on my toes and enriching my life. Although there were times they showered me with nerf bullets as I wrote, I drew a lot of strength from their love.

“We can lick gravity, but sometimes the paperwork is overwhelming”

Wernher von Braun

Dedication

To Dan, Liam, and Conor.

For the joy you bring to my life

Abstract

In this thesis, results are presented and discussed on the synthesis of polypyrrole-chitosan composite films. These films were investigated for the incorporation and release of methyl orange (a model anionic dopant), dexamethasone (an anti-inflammatory drug) and oxacillin (an antibiotic). All drug-doped films were grown at a constant potential of 0.80 V vs SCE until a charge density of 0.25 C cm^{-2} was achieved. Initially, a novel approach was developed to prepare the polypyrrole-chitosan composite films by electrochemically polymerising pyrrole in a chitosan hydrogel network directly on an electrode surface. The electrochemical properties of the chitosan and the polypyrrole films differ, however the properties of polypyrrole are not adversely affected by the presence of chitosan, and it appears that the chitosan provides some mechanical reinforcement to the composite.

A second approach was investigated and in this case, chitosan was cast on to the doped polypyrrole post electropolymerisation and then cured under an infrared lamp. This was found to be more suitable for incorporating larger anionic species. A comprehensive electrochemical characterisation of the polypyrrole-chitosan composite films was obtained using cyclic voltammetry and electrochemical impedance spectroscopy. The redox peaks were identified and explained in terms of anion transport for the polypyrrole-chloride films and cation transport for polypyrrole-methyl orange films. Electrochemical impedance data were fitted to equivalent circuits and the charge transfer resistance, the double-layer capacitance, charge-storage capacitance, and conductivity were determined. The morphology of the composites varied with the dopant. Using scanning electron microscopy (SEM), the typical cauliflower structure was observed for the chloride-doped films, tubular-like structures were seen for the methyl orange-doped polymer films and the oxacillin-doped polymer

films were smooth. The adhesion properties were tested using the “peel-test” and the adhesion properties improved with the addition of the chitosan layer.

A constant potential was used to release methyl orange and oxacillin from the corresponding composites, and the stimulated release was investigated at various potentials, while the release was also investigated at open-circuit potentials. UV-visible spectroscopy was used to determine the concentrations of methyl orange and oxacillin. The release of methyl orange increased with an increase in the release period and as the applied potential was varied from 0.30 V to -0.60 V vs SCE. The release of oxacillin, on the other hand, did not vary significantly as a function of the applied potential, but did vary over time. The presence of chitosan did not significantly influence the release of oxacillin at 0.30 V vs SCE or at open-circuit potentials but did have an effect on the release at -0.60 V vs SCE.

Chapter 1

Introduction and Literature Review

1. Introduction and Literature Review

1.1 Research Topic and Relevance

The initial aim of this study was to prepare a composite of a conducting polymer (polypyrrole) with a natural polysaccharide (chitosan) with the view that such a composite could be useful for biomedical engineering. The polypyrrole-chitosan composite was successfully prepared using electropolymerisation. Previous work from this laboratory supports the utilising of polypyrrole in biomedical applications. For example, polypyrrole was deposited on to medical grade titanium and was found to be biocompatible^{1,2}, it was used to detect dopamine³⁻⁵ and it was a suitable candidate for the inclusion and release of anionic drugs⁶⁻⁸. The specific properties of polypyrrole are greatly influenced by the dopant^{7,9} and polymerisation technique¹⁰. However in some cases, polypyrrole can give a brittle amorphous material¹⁰. By combining chitosan with polypyrrole this may be prevented. This research topic is relevant to biomedical applications where polypyrrole and chitosan have independently shown promising results for tissue regeneration applications and drug delivery applications.

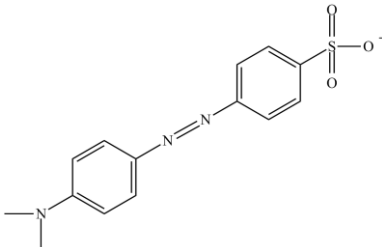
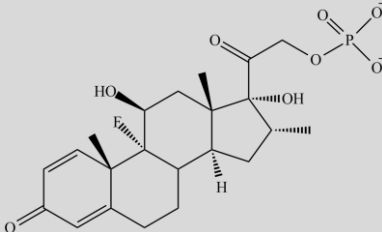
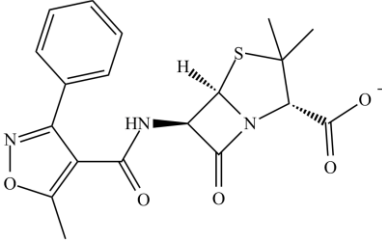
1.2 Objectives and Achievements

The main objective of the present work was to electropolymerise pyrrole within a chitosan polymer matrix on an electrode surface which would give some mechanical reinforcement to the polypyrrole without adversely affecting its electrochemical and electronic properties. In the early stages of this research work, polypyrrole doped with chloride anions, was successfully formed in the chitosan polymer matrix. However, this was not possible with larger anions and as an alternative; chitosan was cast on to the doped polypyrrole post electropolymerisation and cured under an infrared lamp.

Other objectives were to study the electrochemical and electronic properties using cyclic voltammetry (CV) and electrochemical impedance spectroscopy (EIS). The doped polypyrrole was assessed with and without the chitosan to determine the effects of chitosan on the electrochemical and electronic properties. The polypyrrole was doped

with anions of various sizes, chloride, methyl orange (as a model drug), dexamethasone (as an anti-inflammatory drug) and oxacillin (as an antibiotic). In Table 1.1 the dopants used in this study and their molecular structure, weights and pK_a values are summarised. The nature and size of the dopant anions and the release medium play crucial roles in the successful incorporation and release of the anion from polypyrrole¹¹, this will be discussed further in Section 1.4.2.1.

Table 1.1: The structure, molecular weight (M), and the pK_a values in aqueous solution for the anions of the model drugs used in this study.

dopant anion	structure	M of sodium salt (g mol ⁻¹)	pK_a
chloride (Cl ⁻)	Cl ⁻	58.44	-
methyl orange (MO ⁻)		327.33	3.8
dexamethasone (Dex ²⁻)		516.40	6.4
oxacillin (Ox ⁻)		423.42	2.7

All materials chosen in this study were relevant to biomedical applications. Electropolymerisation was performed at room temperature using a constant potential and using distilled water as the solvent. The electropolymerisation electrolyte was maintained near a neutral pH (pH at approximately 6.0 to 6.3) and the costs of the dopants were taken into consideration. It is worth mentioning that the films were not designed to deliver therapeutic amounts of the drug but to determine how the dopant affects the nature of the polypyrrole film and how it would respond also with the addition of chitosan. Dopants facilitate a way of altering the polypyrrole films properties. In this chapter, a description of conducting polymers is given with an emphasis on polypyrrole and its use and modifications for biomedical applications. Then, chitosan is considered and finally polypyrrole-chitosan composites are introduced and discussed.

1.3 Conducting polymers (CP)

Historically, polymers exhibiting conductivity were once considered undesirable¹², this section introduces seminal work that revolutionised conducting polymers. In 1862, Letherby reported the first the anodic oxidation of aniline to form polyaniline on a platinum electrode using electrolysis¹². In 1876, Goppelsroeder discovered that oligomers were formed by anodic oxidation of aniline¹³. In 1916, Angeli and Alessandri obtained polypyrrole (Ppy) from a solution of pyrrole and hydrogen peroxide¹⁴, at the time it was called “pyrrole black”. In 1958, Natta *et al.*¹⁵ were the first to synthesis polyacetylene using a Ziegler-Natta catalyst. They reported that the films of *cis* and *tran* PA had metallic-like appearance, but they did not have good conductivity^{16,17}. In 1963, McNeil *et al.*^{18, 19} prepared polypyrrole from the pyrolysis of tetraiodopyrrole, they were the first to recognise that polypyrrole had semiconducting properties which decreased when exposed to water vapour and oxygen. In 1968, Dall’olio *et al.* were the first to prepare polypyrrole from the electrochemical oxidation of pyrrole¹⁴. In 1975, Green and Street²⁰ reported the first conducting conjugated inorganic polymer, polysulfur nitride. They reported that the polymer had metallic conductivity and becomes superconducting at 0.26 ± 0.03 K. In 1977, Shirakawa, MacDiarmid, and Heeger were the first to achieve a conducting conjugated organic polymer, partially oxidised polyacetylene, shown in Figure 1.1. They discovered that by oxidising polyacetylene (PA) with chloride, bromine,

or iodine vapour, they made the PA 1×10^7 times more conducting²¹. This breakthrough in conducting conjugated organic polymers has led to extensive research in the field of conducting polymers. In 2000, the Nobel prize in Chemistry was awarded to MacDiarmid, Heeger, and Shirawaka, “for the discovery and development of electrically conducting polymers”²².

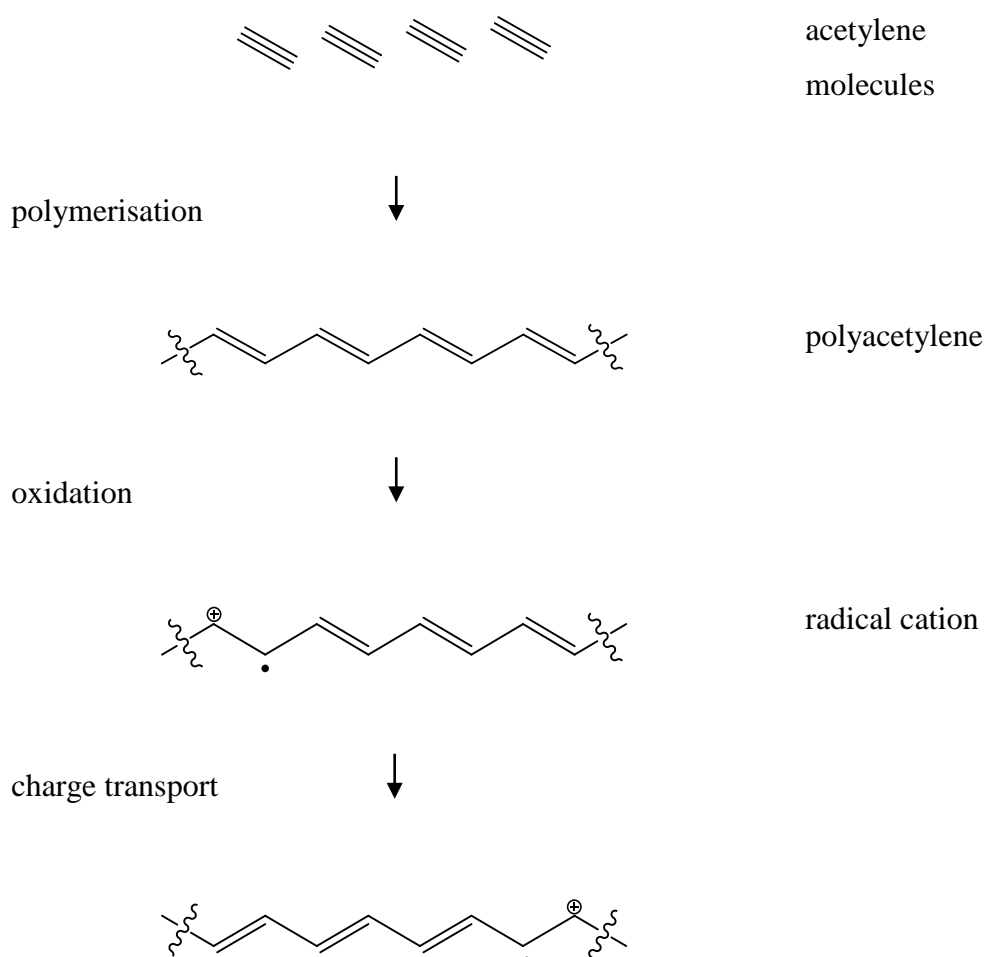
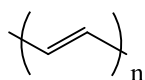


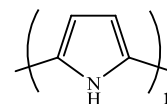
Figure 1.1: Polymerisation of acetylene, showing charge transport.

Although PA, which is a non-aromatic polyene, has metal-like conductivity, the use of PA is limited because it is air sensitive²³⁻²⁶. The development of aromatic conducting polyheterocycles and their derivatives particularly; polyaniline (PANI), polypyrrole (Ppy), polythiophene (PT) and poly(3,4-ethylenedioxythiophene) (PEDOT) have received because of their good stability, conductivity and ease of synthesis²⁶. Figure 1.2 shows the structure of the most commonly encountered conducting polymers in the

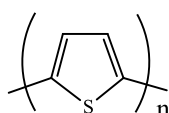
literature along with their electrical conductivities and type of doping. Electrical conductivity is the ability of a material to pass an electric current; it is a fundamental property of conducting polymers. Doping is the process of oxidising (p-doping) or reducing (n-doping) a neutral polymer which is balanced by a counter anion or cation (i.e., dopant), respectively. This is discussed further in section 1.3.1.



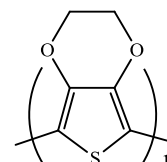
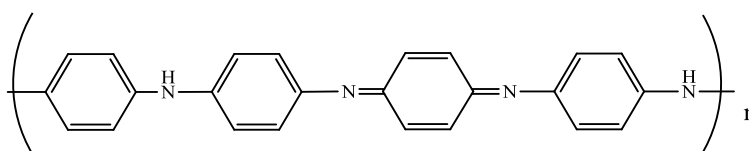
polyacetylene (PA)



polypyrrole (Ppy)



polythiophene (PT)

poly(3,4-ethylenedioxythiophene)
(PEDOT)

polyaniline (PANI)

Figure 1.2: Chemical structures of the most common conducting polymers.

Table 1.2: Conductivity of common organic conducting polymers adapted from Collier *et al.*²⁷

Conducting polymers	Conductivity ($\Omega^{-1} \text{ cm}^{-1}$)	Type of doping
Polyacetylene (PA)	200 - 1000	n, p
Polydiphenylamine (PDPA)	500	n, p
Polyaniline (PANI)	5	n, p
Polypyrrole (Ppy)	40 - 200	p
Polythiophene (PT)	10 - 100	p
Poly(3,4ethylenedioxythiophene) (PEDOT)	1 - 50	n, p

1.3.1 The conductivity and doping levels of conducting polymers

Conductivity (σ) is the ability of a material to pass an electric current, it relates the current density (I) to the electric field (E), as shown in Equation 1.1:

$$I = \sigma E \quad (1.1)$$

Where σ is the conductivity of the conductor in $\Omega^{-1} \text{ m}^{-1}$, I is the magnitude of current density in A m^{-2} , and E is the magnitude of the electric field in V m^{-1} . Materials are often classified in terms of their conductivity. In general, materials with conductivities less than $10^{-8} \Omega^{-1} \text{ m}^{-1}$ are classified as insulators, e.g., diamond, materials with conductivities between 10^{-8} and $10^2 \Omega^{-1} \text{ m}^{-1}$ are classified as semi-conductors, e.g., silicon, and materials with conductivities greater than $10^2 \Omega^{-1} \text{ m}^{-1}$ are classified as conductors, such as metals²⁸. This is illustrated in Figure 1.3 where the materials are classified in terms of the conductivity values. Conducting polymers have a broad range of conductivities, varying from that of insulators to metals. The variation in conductivities is attributed to the number of different polymers, dopants and available doping levels. Typical values for the conductivity in the range 10^2 to $10^5 \Omega^{-1} \text{ m}^{-1}$ are observed for doped PANI, Ppy, PT and their derivatives²⁹.

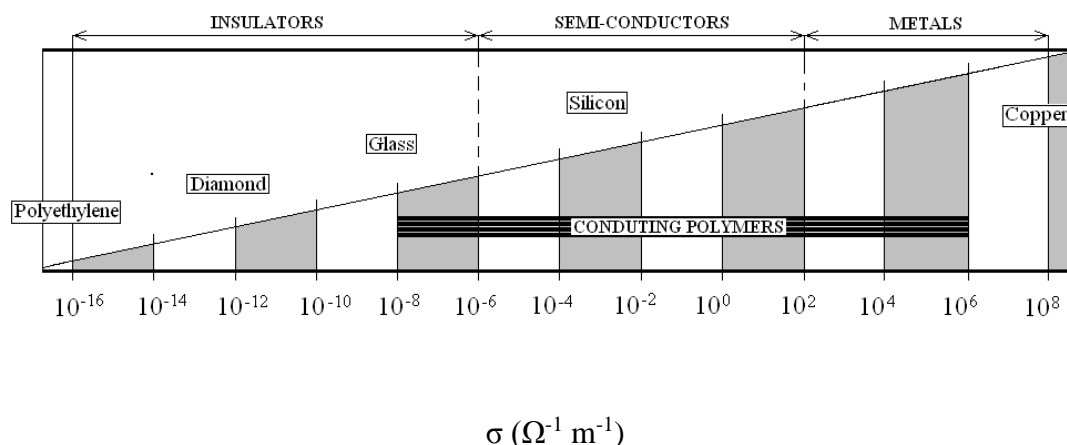


Figure 1.3: Classification of materials in order of electrical conductivity, σ .²⁸

Conductivity in conjugated polymers is attributed to the unique alternating double and single bonds that form the π conjugated system (delocalised $2p_z$ orbitals). Along the backbone of conducting polymers, σ -bonds hold each carbon atom together by concentrating electrons between them. The π -bonds, which constitute the second bond in each double bond, strengthen the connection between their atoms by attracting electrons above and below the plane of the molecule. This forms delocalised $2p_z$ orbitals which allows the generation and movement of charge carrier entities such as solitons, polarons and bipolarons³⁰.

A summary is given here of Brédas and Street's electronic band structure of solids to describe the conductivity of conducting polymers, in their publication, they give a comprehensive description of charge carrier entities; solitons, polarons, and bipolarons.

A soliton is formed at the transition point between two co-existing conjugated structures called "domains", on the same conducting polymer molecule. It results from two competing domains that satisfy the condition of degeneracy i.e., they have the same ground state. This allows the soliton to move freely as the overall charge on both sides of the domain is the same³¹. Heeger *et al.*³⁰ have identified solitons as being the primary

charge carriers in *trans*-PA, this may explain the wide conductivity range of PA in Table 1.2. Most conducting polymers, such as polypyrrole, do not satisfy the condition of degeneracy because they only have a near degeneracy, for this reason polaron and bipolarons are the main charge carriers in conducting polymers³⁰.

A polaron is formed through an oxidation or reduction reaction which leaves a positive or negative charge on the polymer. The portion of the polymer subjected to this process is distorted by the local excess of charge which is stabilised by the electrostatic interaction of a dopant anion or cation. This process forms localised electronic states within the band gap³¹.

A bipolaron is formed through further oxidation or reduction of the polymer. In this case the distortion due to the local excess of charge is greater than that of a polaron due to the effect of double charging. The formation of a bipolaron results when the stabilisation energy gained by the interaction with the distorted lattice -is larger than the coulomb repulsion between the two charges of the same sign. This process forms bipolaron electronic states inside the band gap³¹.

The delocalisation of electrons is limited by both disorder and coulombic forces between electrons and holes. However, these polymer systems are only conducting when doped and the electrical conduction depends on the extent of doping. Doping is the process of oxidising (p-doping) or reducing (n-doping) a neutral polymer and providing a counter anion or cation (i.e., dopant), respectively. Polypyrrole is a p-doped conducting polymer. The ordered motion of these charge carrier ions along the conjugated conducting polymer backbone produces electrical conductivity.

Polymers and materials in general, can be characterised based on their electrical conductivity as insulators, semiconductors or conductors. Brédas and Street³¹ used the electronic band structure of solids to describe the conductivity of conducting polymers. As shown in Figure 1.4, the highest occupied electronic levels gives the valance band (VB) and the lowest unoccupied level, gives the conduction band (CB). The band gap (E_g) between the VB and the CB determines the conducting properties of the polymer, as shown in the band gap diagram in Figure 1.4. If $E_g > 10$ eV, it is difficult to excite electrons into the CB and an insulator forms. In semiconductors, E_g is approximately 1

eV, which means the gap is small enough that electrons can be excited between the VB and CB. For conductors, the VB overlaps the CB resulting in the CB being partially filled with electrons and metallic conduction is observed. The smaller the band gap energy (i.e., the distance between the conduction and valence bands) the more conductive the material becomes.

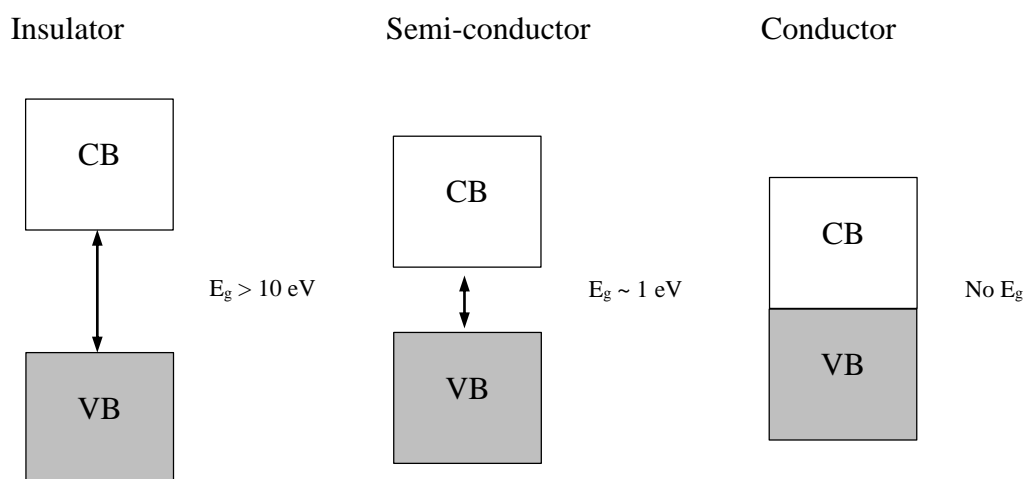
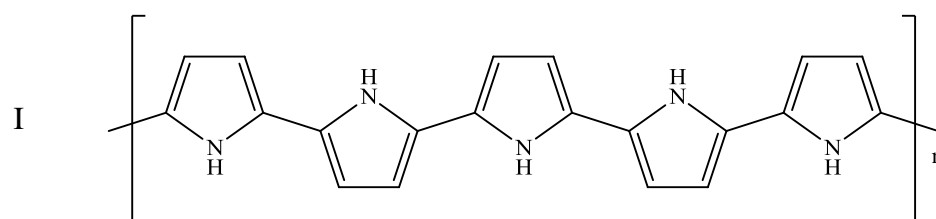
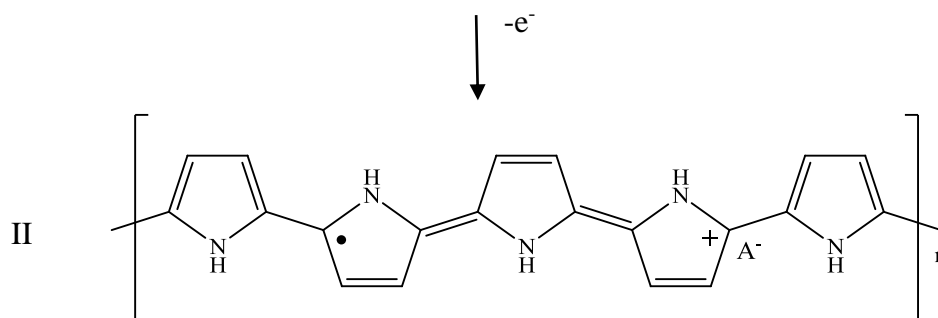


Figure 1.4: Band gap diagram, depicting the difference in energy band gaps E_g for an insulator, semi-conductor and conductor.

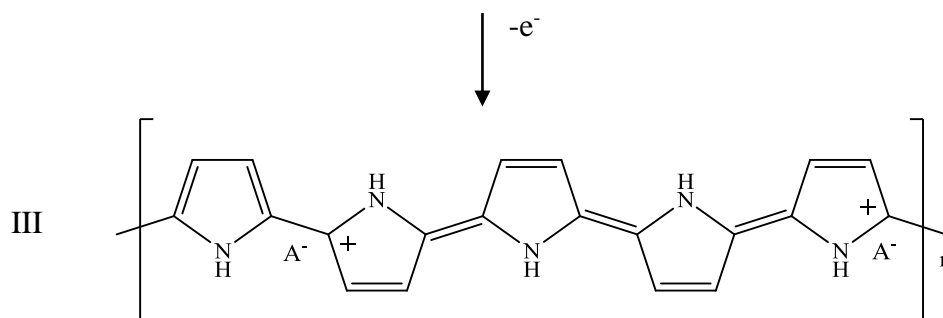
Conjugated polymers are essentially insulating until doped, doping can be performed chemically or electrochemically. Upon doping, the conjugated polymer becomes a conducting system and a net charge of zero is produced due to the close association of counter ions with the charged polymer backbone. This process introduces charge carriers, in the form of charged polarons, i.e., radical ions, or bipolarons, i.e., dications or dianions, into the polymer²⁶, as shown for polypyrrole in Figure 1.5. The ordered movement of these charge carriers along the conjugated Ppy backbone gives rise to electrical conductivity.



polypyrrole



Polaron (radical cation showing lattice distorted, quinoid-like, structure)



Bipolaron (dication showing strong lattice distortion)

Figure 1.5: Structural representation of (I) neutral Ppy, (II) partially oxidised Ppy with the formation of a polaron, (III) fully oxidised Ppy with the formation of a bipolaron.

In the undoped state, the Ppy band gap is 3.2 eV. The attraction of an electron in one repeat-unit to the nuclei in the neighbouring unit leads to the formation of a polaron. A quinoid-like geometry occurs with the formation of the polaron (Figure 1.5 II) and this extends to about four pyrrole rings. The polaron levels are about 0.5 eV away from the band edges, as shown in Figure 1.6 a. The polaron binding energy is 0.12 eV, constituting

the difference between the 0.49 eV decrease in ionisation energy and the 0.37 eV ($\pi + \sigma$) energy required to bring about a change in geometry. When a second electron is taken out of the chain a bipolaron is formed, as shown in Figure 1.5 III. The empty bipolaron electronic levels in the band gap are approximately 0.75 eV away from the band edges (Figure 1.6 b). The bipolaron binding energy is 0.69 eV meaning that a bipolaron is favoured over two polarons by 0.45 eV³¹. At high doping levels bipolaron bands are formed as shown in Figure 1.6 c.

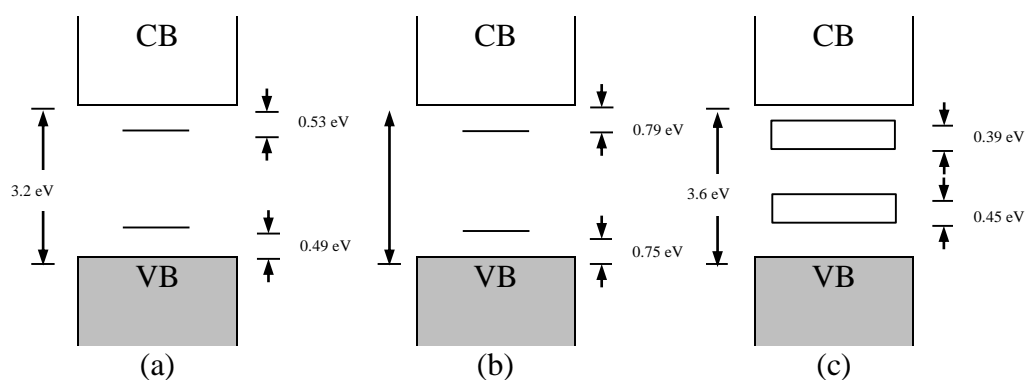


Figure 1.6: Evolution of polypyrrole band structure upon doping (a) low doping level, polaron formation, (b) moderate doping level, bipolaron formation, (c) high (33 mol %) doping level, formation of bipolaron bands.³¹

1.3.2 Synthesis of polypyrrole

The synthesis of conducting polymers is described in detail in several papers^{23, 32-40}. Conducting polymers can be synthesised in different ways³⁶ using chemical polymerisation, electrochemical polymerisation, photochemical polymerisation⁴¹, metathesis polymerisation⁴², concentrated emulsion polymerisation⁴³, inclusion polymerisation⁴⁴, solid-state polymerisation⁴⁵, plasma polymerisation⁴⁶, pyrolysis⁴⁷, and soluble precursor polymer preparation⁴⁸.

Polypyrrole is commonly synthesised by electrochemical methods or polymerised chemically with an oxidising agent. The chemical synthesis of polypyrrole involves the use of a chemical oxidant, such as ammonium peroxydisulfate ($(\text{NH}_4)_2\text{S}_2\text{O}_8$), hydrogen

peroxide (H_2O_2) and salts containing transition metal ions, for example, Fe^{3+} , Cu^{2+} , Cr^{6+} , Ce^{4+} , Ru^{3+} and Mn^{7+} salts⁴⁹. Wang *et al.*⁵⁰ evaluated the biocompatibility of chemically and electrochemically prepared polypyrrole, and they found that there were no adverse effects on cell cultures or on the animal models. Generally hydrogen peroxide⁵¹ and ferric chloride^{50, 52} (FeCl_3) are the preferred oxidants for biomedical considerations. The monomer can be oxidised in the appropriate solution leading to chemically active cation radicals of the monomer. These cation radicals attack the monomer molecules and results in the formation of an insoluble polymer. However, with this method it is difficult to deposit the CP onto a surface, as most of the CP precipitates within the solution phase. Chemical deposition of CPs can also be achieved using techniques such as vapour phase polymerisation (VPP). VPP is a technique in which the monomer is introduced to an oxidant-coated substrate in vapour form. Polymerisation then takes place at the oxidant vapour interface. VPP can be either chemical vapour phase polymerisation (CVPP) or electrochemical vapour phase polymerisation (EVPP). CVPP is a solvent free process used to give uniform, thin and highly conducting polymer layers on different substrates⁵³. This ensures that polymerisation only occurs at the desired surface with no bulk polymerisation taking place in the solution. The advantage of VPP is that the CP layers can be obtained on insulating surfaces unlike electrochemical polymerisation which is restricted to metal, carbon or other conducting materials⁵⁴. Spin coating, solvent casting or printing are other common techniques available for depositing thin and even polymer coatings⁵³. However, most conducting polymers are difficult to process using these techniques because they are insoluble in most solvents. Table 1.3 compares the advantages and disadvantages of chemical and electrochemical synthesis routes in the formation of conducting polymers.

Table 1.3: Comparison of chemical and electrochemical synthetic routes of the polymerisation of pyrrole, adapted from Guimard *et al.*²⁶

Synthesis method for preparing Ppy	Advantages	Disadvantages
Chemical polymerisation	Large yields	Cannot make thin films
	Can be functionalised in order to modify properties	Chemical synthesis is longer, more complicated and more expensive
Electrochemical polymerisation	Ease of synthesis, particularly thin films	Difficult to remove from substrate
	Doping is simultaneous	Not suitable for growth on many substrates

1.3.2.1 Electropolymerisation mechanism of pyrrole

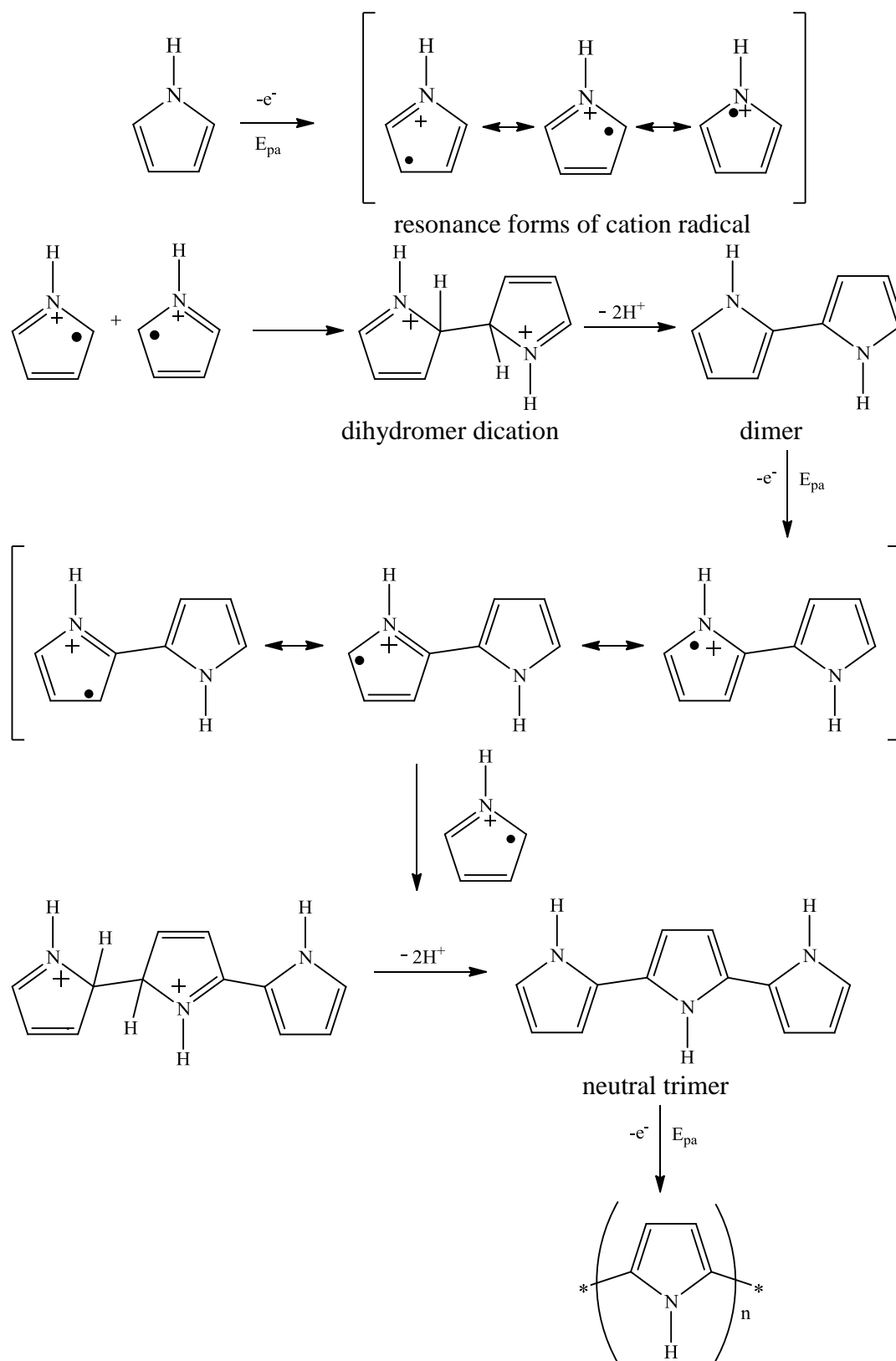
Various mechanisms for the electropolymerisation of pyrrole have been proposed and an excellent review is given by Sadki *et al.*⁵⁵. The mechanism described here is a summary of that proposed by Sadki *et al.*, which is based on the version originally proposed by Diaz *et al.*⁴⁰ in 1988. Waltman and Bargon⁵⁶ have confirmed this mechanism by theoretical studies based on the correlation between the reactivity and the unpaired electron density of the radical cations⁵⁵.

The mechanism proposed by Diaz is shown in Scheme 1.1. The initial step is the oxidation of pyrrole to form a radical cation. In chemical polymerisation the radical cation formed from the oxidation of the monomer attacks another monomer molecule generating a dimer radical cation. However, electrochemical polymerisation differs as the concentration of radical cations in the diffusion layer is much greater than the concentration of neutral monomers. The electron transfer is faster than the diffusion of pyrrole to the electrode surface and the concentration of the cation radicals increase. Polymerisation occurs

through a radical-radical coupling which results in a radical dication, as shown in Scheme 1.1.

These monomeric radical cations can undergo different reactions depending on their reactivity. The more stable cations diffuse into solution away from the electrode surface as a soluble product. The very reactive cations may react randomly with solvent or nucleophiles in the vicinity of the electrode and diffuse into solution as a soluble product⁵⁵. Between this reactivity the radical cations undergo a dimerisation reaction. The resonance structure at with the radical is at the 2-position is the most stable (having a greater unpaired electron density). Coupling between two radicals produces a dihydromer cation, and deprotonation occurs to give a neutral dimer product. The polymerisation follows with the oxidation of the dimer into a radical cation. Since the unpaired electron is now delocalised over the two rings the oxidation potential is lower than the monomer, thus the dimer is more inclined to oxidise, and another consequence of this stabilisation is that the dimer radical cation becomes less reactive than the monomer. The 5-5' α -position resonance form predominates, where the dimer radical cation at the 5-position reacts with the radical cation at the 2-position to form a trimer dication which deprotonates to give a neutral trimer. A neutral trimer is produced from the electro-oxidation of a trimer cation radical, which has several resonance forms (not shown here). The trimer 5-5' α -positions and the 3-3' β -positions can undergo coupling reactions with the other oligomers. The α -coupling will prevail until the oligomer chains increase along with the delocalisation of unpaired electrons resulting in a higher probability of β -bonds formed. The propagation continues with the same sequence of oxidation, coupling and deprotonation until the final polymer product is obtained, which is an oxidised form of polypyrrole with a positive charge for every three to four pyrrole units which are counterbalanced by anions¹⁴. This mechanism is believed to represent the electropolymerisation of pyrrole. Electron spin resonance (EPR) spectroscopy failed to identify the pyrrole radical when investigated using spin-trapping techniques; this supports the dimerisation pathway which follows the radical cation coupling pathway^{10, 14, 31}. The loss of hydrogen from the α -position indicated in the mechanism in Scheme 1.1 is in good agreement with the observed drop in pH of the solution during polymerisation⁵⁷. In addition, Genies *et al.*⁵⁸ used chronoabsorption to investigate the

rate-determining step (RDS) during film growth and concluded that the RDS is a coupling process and not monomer diffusion towards the electrode.



Scheme 1.1: Electrochemical polymerisation of pyrrole.

1.3.2.2 The influence of the electrochemical polymerisation parameters

Electrochemical polymerisation can be performed by using constant potential (galvanostatic), constant voltage (potentiostatic) or sweeping potentials (cyclic voltammetry). The synthesis results in a Ppy film doped with an anion at the surface of the working electrode. It is important that the working electrode does not oxidise concurrently with the pyrrole monomer. The electrode material also effects adhesion. Generally, substrates such as platinum, gold, indium tin oxide (ITO) and glassy carbon are chosen as the working electrode, however, a range of active metals which form oxides have also been used^{1, 59-62}. The potential window is also significant. Polypyrrole films prepared at lower current densities ($< 1.0 \text{ mA cm}^{-2}$), or at anodic potentials less than 0.80 V vs SCE, tend to be more dense and compact with homogeneous surfaces. Polymers deposited at higher current densities ($> 5.0 \text{ mA cm}^{-2}$) or greater than 0.90 V vs SCE, are inclined to form porous structures with irregular surfaces^{63, 64}. Furthermore, if the potential remains too high, over-oxidation occurs, reducing the electroactivity, and thus, the conductivity of the polymer. The polymer degrades resulting in a decrease in mechanical properties and loss of adhesion from the substrate. Oxidation of the monomer occurs at higher potentials than the redox properties of polypyrrole and during synthesis side reactions, crosslinking and overoxidation is possible⁶⁵. Overoxidation of polypyrrole occurs with the formation of C=O functional groups in the polymer backbone, as well as the formation of CO₂ at sufficiently positive potentials⁶⁶. The structure of overoxidised polypyrrole is shown in Figure 1.7. The coupling of the radical cations has a significant influence on the conductivity of the polypyrrole films. Waltman and Bargon⁵⁶ used theoretical calculations to predict the probability of α and β coupling occurring during electropolymerisation, β -coupling leads to disruption in conjugation, this increases the band gap and thus reduces the conductivity of the Ppy.

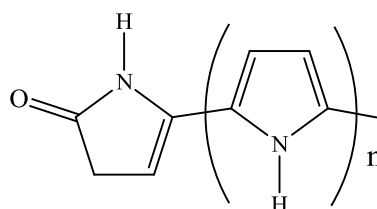


Figure 1.7: Representative structure of overoxidised polypyrrole, showing a ketone functional group.

Variation in the doping level⁶⁷ and the dopant used during synthesis has an effect on the film thickness, surface roughness, morphology^{68, 69}, surface energy and wettability⁷⁰. Dopants of various sizes have been studied including chlorides (Cl^-)^{71, 72}, perchlorates (ClO_4^-)^{73, 74}, nitrates (NO_3^-)⁷², *para*-toluene sulfonate ($p\text{TS}^-$)⁷⁵ poly(styrene sulfonate)^{76, 77} and dodecyl benzene sulfonate (DBS^-)^{78, 79}. When Ppy is doped with smaller anions, anion exchange is mainly displayed due to the high mobility of the small anions in the polymer matrix. Cation exchange generally takes place when Ppy is doped with large and bulky shaped anions, such as DBS^- . However, when counterions are medium in size, like $p\text{TS}^-$ for example, Ppy exhibits both anion and cation exchange behaviour. The concentration of pyrrole is another important factor. Yuan *et al.*⁸⁰ observed an increase in conductivity with increased pyrrole concentration. They explained this observation by applying the concept of electroneutrality coupling³¹. The more Ppy^+ sites produced for internal charge compensation in higher pyrrole concentrations, the more efficiently the anion will compensate the positive charge of the resulting Ppy^+ .

Solvent, pH and temperature during synthesis also affect the final properties of the polymer. Comparison across different solvents is difficult due to the solubility of the dopant and the pH variations. Acetonitrile is a common solvent used in organic systems^{81, 82}. Several studies have been carried out comparing the electrodeposition of Ppy in the presence of water, acetonitrile and mixtures of both water and acetonitrile⁸¹. Although the monomer oxidation potential is independent of the pH, the pH has an effect on the reactivity and stability of the Ppy formed at the electrode. In general, protons are produced after each oxidation at the electrode which consequently decreases the pH near the electrode. Zhou and Heinze⁵⁷ investigated the influence of pH on electropolymerisation of pyrrole from acetonitrile and found that neutral or weakly acidic pH favours polymerisation. This is consistent with Pletcher and co-workers⁸¹ who also found this to be the case when preparing a Ppy film at a Pt electrode from solutions of varying pH. In addition, pH affects the speed of polymerisation with Ppy forming more favourably with the addition of protons⁸³, slower in neutral pH, and not forming at all in basic solutions. However, a very low pH results in the formation of a film of low conductivity. This is due to the acid catalysed formation of non-conjugated trimers which further react to form a partly conjugated Ppy or become incorporated into the film⁸⁴. While at basic conditions,

cation radicals become deprotonated to neutral radicals which interferes with the radical-radical coupling reaction⁸⁵.

Finally, temperature plays an important role in the electropolymerisation. Sangian *et al.*⁸⁶ applied a low current density and a low temperature (-31°C) as a novel way of producing porous Ppy resulting in high conductivity. The rate of the electropolymerisation reaction is increased with increasing temperatures, however the Ppy that is deposited on the electrode is more likely to become over-oxidised and this has an insulating effect which hinders the further growth of the Ppy.

1.4 Polypyrrole for biomedical applications

There is ample evidence that polypyrrole is a promising candidate for biomedical applications and it is generally regarded that Ppy is biocompatible^{11, 13, 50, 87}. Some of the applications of polypyrrole and the associated advantages and disadvantages are summarised in Table 1.4. The potential applications range from artificial muscles, biosensors, neural probes, drug delivery to tissue engineering. The nature of the dopant and other excipients present, surface roughness, surface energy, conductivity and mechanical properties must also be considered¹¹. In 1994, Wong *et al.*⁸⁸ used polypyrrole to modulate cellular activity in mammalian cells. They demonstrated that extracellular matrix molecules, such as fibronectin, adsorb efficiently onto polypyrrole thin films and support cell attachment under serum-free conditions, suggesting that electrically conducting polymers may represent a type of culture substrate which could provide a non-invasive means to control the shape and function of adherent cells. This implied that if Ppy could modulate cellular reactions then it could be possible to limit the toxicity of implantable devices by incorporating biomolecules to influence biocompatibility opening up new vistas for polypyrrole in biomedical applications. In 2001 both the EU and the US FDA established new policies and guidelines (Directive 2004/27/EC) for drug/device combination products due to increased clinical and commercial interest⁸⁹. To date there are a number of FDA approved devices capable of electrical stimulation of the body, including pacemakers (bladder, cardiac, diaphragmatic and gastric), electrodes for deep-

brain stimulation (for the treatment of dystonia, essential tremor and Parkinson's disease), and spinal cord stimulators for pain management⁹⁰.

Table 1.4: Polypyrrole in biomedical applications, adapted from Guimard *et al.*²⁶

Application	Description of application	Advantages	Disadvantages	Ref.
Artificial muscles	Device with electrochemo-mechanical properties (volume change) capable of creating a mechanical force	Operational in physiological conditions. Requires low voltage (< 1.0 V) for actuation. Light weight	Short term redox stability. Delamination. Response limited by ion mobility	26, 91-96
Biosensors	Device containing biomolecules as sensing elements, integrated with electrical transducer	Electrochemical synthesis on metal electrode. Possible surface modifications. Efficient electric charge transfer from bio-reaction.	Cost of biocomponents Hydrophobicity can denature entrapped proteins	3, 26, 97-101
Neural Probes	Implantable electrode for recording or stimulating neuronal activity	Biocompatibility Good conductivity Increased surface area, decreased impedance	Poor electrical stability Stimulus induced depression of neuronal excitability ¹⁰²	52, 103-105
Drug Delivery	Implantable device capable of delivering drugs	Controlled release possible Ease of synthesis	Issues with long-term stability. Not suitable for all drugs	6, 63, 87, 106-109
Tissue engineering	Biocompatible, biodegradable scaffolds or cell culture substrates containing stimuli to enhance tissue regeneration	Biocompatible Good conductivity Modification to include chemical cues	Challenging Chemical, mechanical, and topological properties relevant to operation	27, 90, 110-112

1.4.1 Polypyrrole in tissue engineering applications and neuroprosthetics

There are several publications that review conducting polymers in biomedical applications^{11, 13, 26, 50}. Most cells respond to physical, chemical and electrical stimuli¹¹³, this is especially true for neurons. Polypyrrole has been reported to support cell adhesion and viability of many different cell types and has been shown to stimulate skeletal myoblasts¹¹¹ and cardiac myocytes¹¹⁴. Since 1994, Ppy has been reported to support cell adhesion and growth of a number of different cell types, including endothelial cells^{88, 115}, rat pheochromocytoma (PC12) cells²⁷, neurons and support cells^{105, 116, 117}. George *et al.*¹¹⁸ demonstrate that 3-D Ppy substrates can have a progressively positive biocompatibility profile with central nervous system (CNS) parenchyma *in vivo*. These results support future investigations aimed at using Ppy in the design and manufacture of neural prosthetics that are capable of integrating with CNS tissues based on specific chemical and physical properties of the Ppy polymer. Such prosthetics should enable reliable transmission of external and internal electrical signals for significant postoperative periods. Moreover, if judiciously formulated, they may stimulate damaged neural tissues to repair and reconnect. Conducting polymer coatings could potentially improve the electrode-tissue communication by providing a high surface area to cell and tissue integration and by significantly improving the charge transfer while requiring lower power to operate. Charge transfer is improved through reduced impedance and greater selectivity for both recording and stimulating applications. Since conducting polymers are typically softer materials, it is also hypothesised that inflammation is reduced due to the reduction in strain mismatch between tissue and electrode surface⁵². The outcome of this reduced inflammatory reaction is a decrease in thickness of the surrounding non-conductive fibrous tissue purported to cause signal degeneration⁵². Nodular polymeric structures can encourage cell attachment to produce a more intimate communication with neural tissue compared to conventional metallic electrodes, such as platinum and gold, which have minimal interactions with tissue^{119, 120}.

1.4.2 Polypyrrole in drug delivery applications

Controlled release polymer systems have been widely investigated since the introduction of the sustained release of proteins and macromolecules in 1976¹²¹. Not all drugs are

suitable for use in a conducting polymer based drug delivery system. Drugs evaluated for the suitability of drug delivery devices are generally commercially available drugs. The drug must not be electroactive at the potentials the system will experience during synthesis or during its working life. The biological activity of the drug could be compromised as a consequence of electroactivity¹¹. The pK_a of the drug must be considered as the charge on the drug will influence drug loading, film formation, and releasing capabilities⁶. Zinger and Miller¹²² showed that glutamate and dopamine can be released from a polypyrrole membrane using potential control. Pyo *et al.*¹²³ have demonstrated the release of adenosine 5'-triphosphate (ATP). Anionic drugs can be incorporated into the Ppy matrix during electrochemical polymerisation. Kontturi *et al.*⁶³ reported the controlled release of tosylate, salicylate, and naproxen. Cationic drugs have also been reported to have been incorporated into conducting polymers. Thompson *et al.*¹²⁴ discussed the mechanism for the incorporation of neurotrophin-3 (NT-3⁺) into polypyrrole which involved a combination of electrostatic and hydrophobic interactions between the drug, anionic dopant, *para*-toluene sulfonate (pTS^-) and the polymer, along with physical entrapment. Hepal and Mahdavi¹²⁵ used a polypyrrole composite as an ion gate membrane for the release of the cationic drug chlorpromazine. Anionic β -cyclodextrins (CD) were used as dopants to prepare Ppy and this allowed for subsequent incorporation of neutral drugs. The uncharged antipsychotic drug, *N*-methylphenothiazine (NMP), was loaded into CD doped Ppy by immersing the film in a 0.10 mol dm^{-3} NMP solution. The NMP was loaded into Ppy through encapsulation as the drug preferentially moves into the hydrophobic interior of the CD¹⁰⁶.

Implant associated infection is a common problem with implantable devices¹²⁶. Antibiotic-loaded coatings on an implant present a straight forward approach for preventing implant associated infection¹²⁶. The advantage of an antibiotic-loaded coating on an implant is that it can provide an immediate response to local infection but does not require an additional carrier for antibacterial agents other than the implant itself. This is most relevant to contemporary cementless orthopaedic implants which have increased in popularity due to overall better results in young patients compared to cemented prostheses¹²⁷.

1.4.2.1 Drug release strategies

The first reported controlled release system based on Ppy was reported by Zinger and Miller¹²² when glutamate anions were released on reduction of Ppy. More than 14 times the amount of glutamate was released when Ppy was exposed to a reduction potential of -1.00 V vs SCE than if no electrical stimulation was applied. In the late 1980s, Zhou and co-workers^{128, 129} demonstrated the release of dopamine from Ppy derivatives. By the 1990s several accounts in the literature were available on the release of anionic species such as anthraquinone-2,6-disulfonic acid (ASQA) from Ppy films and these were measured as a function of redox states¹³⁰. These publications demonstrate the release of anionic species through the application of a reduction potential. Cationic species such as chlorpromazine have been shown to be incorporated into a Ppy/melanin composite on reduction and released upon application of an oxidation potential¹²⁵. Actuation has also been used to achieve drug release. Sviriskis *et al.*¹³¹ demonstrated that the cationic drug, risperidone, could be released through the application of a reduction potential when the Ppy film was swollen to allow a greater diffusion of the drug.

Various forms of electrical stimulation can be applied to Ppy in an attempt to control the release of drugs, including constant potential, step potential (switching between step potentials) or CV (sweeping between potentials at a set rate)¹¹. As the Ppy redox state is altered a charged bioactive species will alternately experience attraction forces and the absence of attraction forces. Actuation can occur as the Ppy is switched between its redox states which may also influence drug movement. Several papers have compared step potentials with CV to release drugs. CV appears to be the more proficient method to release the ions^{64, 123, 130, 132, 133}. However, there are several drawbacks to this method. Thompson *et al.*¹²⁴ reported that CV released NT-3⁺ at faster rates than using either rapidly alternating potential steps or current pulses but the Ppy film was delaminated from the electrode upon handling. Contact with the underlying electrode was maintained when stimulation in the form of pulses, current or pulsed potential, was applied. Wadhwa *et al.*¹³² also found that CV was the more efficient method to stimulate drug release but after 30 cycles at 100 mV s⁻¹ cracks appeared in the Ppy film. This cracking is likely to be due to polymer actuation. Polymer delamination from the electrode and polymer cracking are both serious limitations for devices designed to release drugs over an extended period of

time. Furthermore, a drug release device that relies on CV is a far more complex electronic device than one relying on alternating pulses of potential or current. For these reasons, electrically stimulated release by CV may not necessarily be the best option. The most important electrochemical parameters to be considered, therefore, are the potential limits selected, the length of time spent at these limits and the corresponding redox states of the polymer¹¹.

Not all of the citations reviewed used stimulated release protocols. Aoki *et al.*¹³⁴ demonstrated that cells cultured on indium-tin oxide (ITO) showed a decrease of catecholamine release (neurotransmitter), compared to cells cultured on polypyrrole-coated iridium-tin oxide. They also demonstrated that cells cultured on a Ppy-coated ITO plate could be kept in culture, without any significant changes in morphology and in the secretory responsiveness to acetylcholine as compared with cells cultured on collagen. In contrast, the cells cultured on the ITO plate lost the responsiveness, while the amount of catecholamines synthesised was affected little by both Ppy and ITO surfaces. It is suggested that Ppy supports the secretory function of the chromaffin cells when they are cultured on the surface of the polymer¹³⁵. This research suggested early on that Ppy modified electrodes had advantages over traditional electrodes and that the modified electrodes support cell function. Alikacem *et al.*¹³⁶ studied the responses of various cell types on commercially available Ppy-woven polyester fabric known as Contex. Four different grades of conductivity were compared with uncoated polyester. Optimal cell responses were found for the Contex sample of intermediate conductivity. Collier *et al.*²⁷ showed that in vitro compatibility tests of a composite of Ppy and hyaluronic acid on PC-12 (rat phaeochromocytoma) cells confirmed the attachment and viability of the cells. These studies demonstrate that Ppy has enhanced neuroprosthetics interactions without applied external stimulus.

Some studies have shown that drugs can diffuse and exchange with the surrounding media without electrical stimulation^{108, 132, 137, 138}. Figure 1.8 illustrates how a drug may diffuse from a polymer matrix with respects to time.

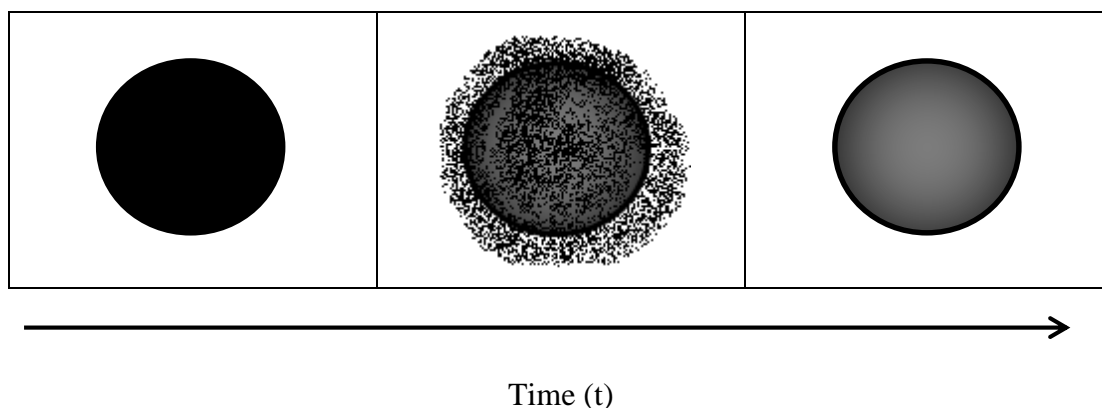


Figure: 1.8: Drug release from a polymer matrix.

Korsmeyer-Peppas's model can be used to analyse the release of therapeutic compounds from a polymeric matrix¹³⁹ when the release mechanism is unknown or there is a mix of release phenomena involved,

$$\frac{M_t}{M_\infty} = K_t^n \quad (1.2)$$

where M_t is the amount of drug release at time t , M_∞ is the amount of drug released at infinite time, K_t is the release rate constant and n is the an exponent of release. In this model, the value of n characterises the release mechanism of the drug^{140, 141}, release has a diffusion mechanism if $n = 0.5$ and is a zero-order release model if $n = 1$.

Novel methods of increasing the amount of drug that can be loaded into the polymers are continually being developed and these include increasing the surface area¹⁴² by forming nanostructures on the surface of the polymer^{137, 143}. Traditional methods include increasing polymer thickness which corresponds to increased drug loading. However, polymer film thickness can affect the release of the drug. The rate of charge passed during electrochemical polymerisation affects the speed of polymer deposition and subsequently the density, thickness and morphology of the film⁶⁴. Some research groups have reported the increase of polymer thickness with an increase in the total amount of drug that can be incorporated and thus released. Most of these studies compared films prepared under the same synthesis parameters. Assuming the doping level remains fairly constant, then a higher amount of polymer corresponds with more drug incorporated, and subsequently

more drug available for release. However, the level of drug release does not increase linearly with increasing film thickness; thinner films release a greater percentage of the incorporated drug than thicker films^{129, 133}. This may be due to thicker films being less electroactive¹²⁹ and changes in the diffusion coefficient with changing film thickness¹³³.

Wallace and co-workers¹³⁰ studied the factors influencing the release of ASQA from Ppy films. They demonstrated that the characteristics of the release medium, such as pH, ionic strength, polarity and hydrophobicity all affect the properties of Ppy and the release of the drugs. To correlate *in vitro* and *in vivo* release, the media used should mimic the targeted local environment where the system will be used.

1.5 Chitosan

Chitosan is derived from the deacetylation of chitin, the second most abundant polymer after cellulose. Chitin is often obtained from the waste of the seafood processing industry. It is subjected to *N*-deacetylation by treatment with a 40 to 45% NaOH solution, followed by purification procedures. The structure of chitosan is shown in Figure 1.8, it is a copolymer of *N*-acetyl-D-glucosamine and D-glucosamine¹⁴⁴ making it analogous to the structure of cellulose. It has a three dimensional α -helical configuration stabilised by intramolecular hydrogen bonding¹⁴⁵. Chitosan is insoluble in most solvents and water, but the presence of amino groups renders it soluble in acidic solutions¹⁴⁶, it has a pK_a of about 6.3¹⁴⁷. The solubilisation occurs by protonation of the $-NH_2$ function on the C-2 position of the D-glucosamine repeat unit, whereby the polysaccharide is converted to a polyelectrolyte in acidic media. Chitosan is the only pseudo-natural cationic polymer and thus, it finds many applications that follow from its unique character¹⁴⁸.

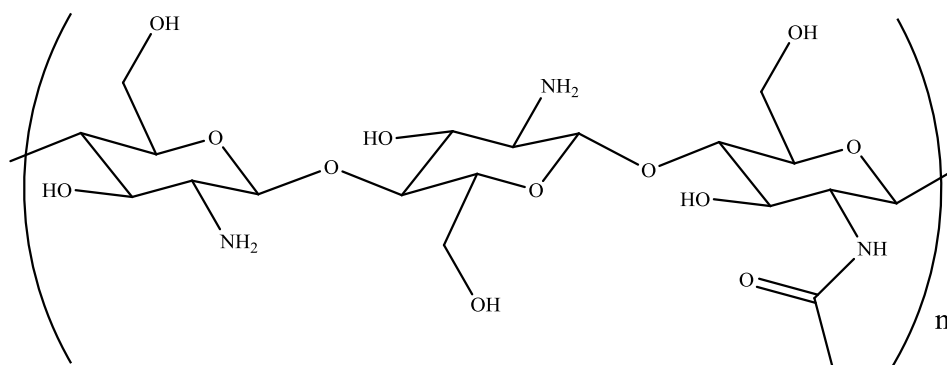


Figure 1.9: Structure of chitosan.

Chitosan hydrogels have been studied for biomedical and pharmaceutical applications. There are several definitions offered for a hydrogel¹⁴⁹, the IUPAC definition of a hydrogel is simply a gel in which the swelling agent is water¹⁵⁰, Peppas defined hydrogels as macromolecular networks swollen in water or biological fluids^{149, 151}. In this work, chitosan was observed to swell but the swelling index was not determined because of the restrictive volume size. Figure 1.10 shows the structures of chitosan crosslinked with itself reproduced from Gurny *et al.*'s¹⁴⁹ review of chitosan hydrogels. Crosslinking can occur between two chitosan units which may or may not belong to the same polymeric chain¹⁵². Alvarez-Lorenzo *et al.*¹⁵³ reported chitosan crosslinked with itself that exhibit pH-sensitive swelling. Argüelles-Monal¹⁵⁴ reported chitosan crosslinked with itself exhibit properties of an amorphous elastomer (gel). The reason they offer is that a network of chitosan crosslinked with itself may be stabilised by hydrophobic associations of *N*-acetyl groups, which restricted the mobility of a few covalent crosslinking points.

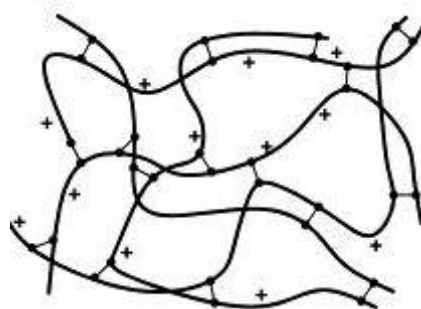


Figure 1.10: Structure of chitosan hydrogel crosslinked with itself¹⁴⁹.

It is important to realise that chitosan is not a single chemical product, it can be described as chitin which has been sufficiently deacetylated to form soluble amine salts¹⁵⁵, the degree of deacetylation necessary to obtain a soluble product being 40 to 98%. The grade of chitosan used in this thesis is classified as $\geq 75\%$. The molecular weights of chitosan polymers vary between 50 kDa to 2000 kDa. Physicochemical properties can be changed by varying the degree of deacetylation. Generally, increasing the molecular weight of chitosan increases the tensile strength, elongation and moisture absorption whereas an increase in deacetylation of chitosan can either decrease or increase depending on molecular weight¹⁵⁶. The higher the degree of deacetylation the more brittle and less hydrophilic it becomes¹⁵⁶.

The solubility of chitosan is highly influenced by the distribution of the amino groups, the molecular weight and the degree of deacetylation, indicating that the manufacturing process of chitosan can affect its solubility aspects^{157, 158}. In alkali medium, the elastic modulus increases as the pH increases due to the re-association of hydrogen bonds between networks¹⁵⁹. Chitosan with a degree of acetylation of 40 % has been found to be soluble up to a pH of 9.0, whereas chitosan with a degree of deacetylation of 85% is soluble up to a pH of 6.5, however solubility is also greatly influenced by the presence of salts in solution, and the ionic strength of the solution. The solubility of chitosan is lower at higher ionic strength. The microstructure of the polymer also contributes to dissolution¹⁶⁰. Structure can be controlled by drying temperature, and lyophilisation is generally used to produce porous structures resembling “sponge”^{161, 162}. An increase in the drying temperature results in decreased pore size. Infrared heating offers many advantages over conventional drying methods and it involves the exposure of a material to electromagnetic radiation, which facilitates drying from the inside out. Srinivasa *et al.*¹⁶³ observed that when films were dried using infrared (IR), they were superior in preserving desirable functional characteristics of the chitosan films. Although subtle variations in their crystallinity pattern were observed between differently dried chitosan films, no significant differences were observed in their properties. IR drying was found to be more efficient and produced more uniform films than the oven dried films. The tensile strength of the IR dried films (49.58 to 52.34 MPa) were less than that of the air dried films (56.78 to 59.38 MPa). There were no significant differences reported for burst

strength values, water vapour and oxygen transmission rate values in oven and IR dried films compared to the air dried films.

1.5.1 Biomedical applications

The interest in chitosan can be attributed to its unique chemical properties and various biological activities. The polycationic nature of chitosan contributes to its mucoadhesive properties¹⁶⁴. It has been investigated for potential use in gene delivery¹⁶⁵, vaccines¹⁶⁶, and as an antimicrobial agent¹⁶⁷. The structure of chitosan partially resembles glycosaminoglycans, which are important components of the connective tissue. As such, chitosan has been investigated for use in tissue engineering¹⁶⁸⁻¹⁷⁰. The regenerative properties of chitosan have been utilised to develop chitosan based wound dressings which have been approved by the FDA¹⁷¹.

Chitosan has been investigated as a pharmaceutical excipient¹⁷² for tablet binding and as a granulating agent for tablet formulations. Miyazaki *et al.*¹⁷³ showed that chitosan had a sustained release effect on diltiazem (calcium channel blocker). Bhise *et al.*¹⁷⁴ designed sustained release systems for the anionic drug naproxen using chitosan as a drug carrier matrix. Mura *et al.*¹⁷⁵ showed that chitosan can favourably affect the naproxen dissolution properties, yielding a dissolution efficiency improvement of up to about 8 times. Ilango *et al.*¹⁷⁶ demonstrated that chitosan has a sustained release effect on ibuprofen *in vivo*. It has also been shown that chitosan microspheres containing amoxicillin and metronidazole could improve the local absorption eradicating *Helicobacter pylori* infection¹⁷⁷. Making use of its *in situ* gelling properties, chitosan has been investigated for ophthalmic drug formulations¹⁷⁸.

Other uses of chitosan are in food, cosmetics and water treatment. The versatility of chitosan is very promising¹⁷⁹. However, the findings made by different researchers on the effects of molecular weight and degree of deacetylation on these properties are still controversial¹⁸⁰. The list of chitosan-based pharmaceutical and biomedical based technology is exhaustive. Bernkop-Schnürch¹⁸¹, Singla^{182, 183} and Kumar¹⁶⁰ have published excellent reviews on the application of chitosan in the biomedical industry.

1.6 Polypyrrole/chitosan composites

Figure 1.9 shows a bar chart illustrating a bibliometric analysis of the term polypyrrole/chitosan and shows the number of publications during the period 1992 to 2013. It is clear that the number of publications is increasing every year. The leading proponents, Sadrolhosseini *et al.*¹⁸⁴ have focused on the optical, electrical and thermal properties of the composite with the proposed application focused on electromagnetic interference (EMI) shielding. The analytical techniques and results shown by Sadrolhosseini *et al.*¹⁸⁴ are quite different to the body of work presented in this thesis. The first publication of polypyrrole-chitosan is a patent¹⁸⁵, the composite was prepared by chemical oxidation and the composite was dissolved in water making it a suitable material for biosensor that can immobilise enzymes. This patent is significant because it proposes a biomedical application. In 2004, the first paper on a polypyrrole chitosan composite was reported by Khor and Whey¹⁸⁶ where they employed chemical oxidation to prepare the composite and reported poor conductivity. Their endeavour was to prepare covalently bonded polypyrrole chitosan composites. Li *et al.*¹⁸⁷⁻¹⁹⁰ have reported novel nanocomposites of polypyrrole-chitosan. Yalçinkaya *et al.*¹⁹¹ prepared a polypyrrole-chitosan composite on a platinum electrode, in the presence of oxalic acid using cyclic voltammetry. Huang *et al.*¹⁹² reported the electrical regulation of schwann cells using polypyrrole chitosan composites prepared by chemical oxidation of pyrrole powder suspended in a solution of chitosan and then cast in a petri dish. Recently, Sajesh *et al.*¹¹² reported polypyrrole based conducting scaffolds by incorporating polypyrrole-alginate (Ppy-Alg) blended with chitosan using a lyophilisation technique. They employed this composite as a substrate for bone tissue engineering. A blend of Ppy-Alg was developed by oxidative chemical synthesis of polypyrrole using FeCl₃ as an oxidising agent. *In vitro* biomineralisation ability of the scaffold was assessed and thus the effectiveness of Ppy-Alg/chitosan scaffold in the field of tissue engineering was evaluated.

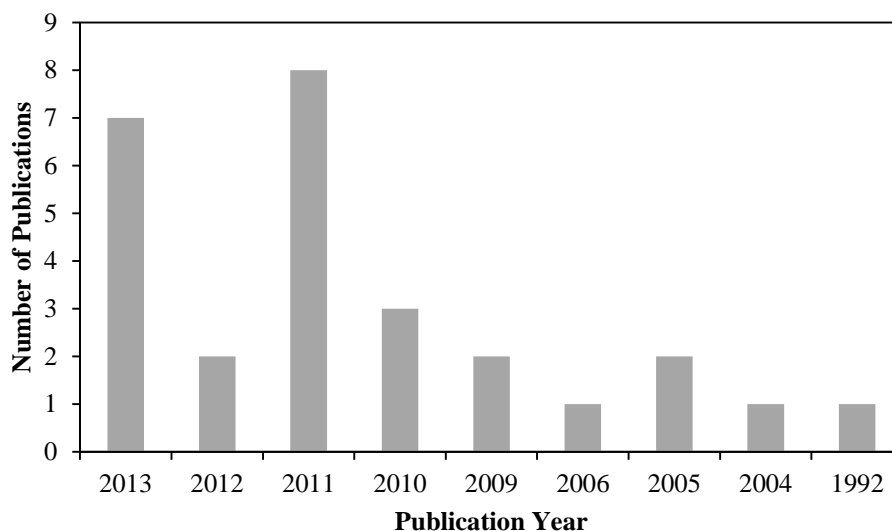


Figure 1.9: The numbers of publications using the term “polypyrrole chitosan” in their titles or abstracts, a total of 27 are accounted for including all publication types since 1992. Bibliometric analysis by SciFinder®.

1.7 Challenges

1.7.1 Electrical properties

As mentioned in Section 1.3.1 the high conductivity of polypyrrole is attributed to the dopant ions that serve as an electrical bridge between the polymer units. Long-term instability is a main drawback of conducting polymers¹⁹³ and for conductive implants, such as neural probes, dopant stability is important for electrical preservation¹⁹⁴. Few articles have reported the lifetime of their conducting polymer products. It was reported that Ppy doped with large anions can maintain conductivity for twenty years¹⁹⁵, and Ppy doped with amphiphilic anions can reduce the influence of water and oxygen⁸⁵. The potentials at which the overoxidation of Ppy occurs depends on the pH values of the aqueous solutions¹⁹⁶, and the species responsible for overoxidation have been identified as hydroxyl anions. On the contrary, the use of hydroxyl radical scavengers, such as methanol and dimethylthiourea, increases the stability of polypyrrole films under anodic potentials¹⁹⁷. Indeed, optimising a material involves some sort of trade off. Kim *et al.*¹⁹⁸ found that polypyrrole blended with a hydrogel had a negative effect on the electrical

conductivity of the conducting polymer as it caused both physical and chemical changes in the polymer.

1.7.2 Biological and physical properties

Some difficulties have been reported when bioactive molecules are incorporated during synthesis of Ppy. These include interference with polymer growth and decreased adherence of polymer to the underlying electrode^{122, 199}. Adherence is an extremely important factor for electrically stimulated drug release. Thompson *et al.*¹⁹⁹ addressed this issue by utilising a two layered synthesis approach, whereby a layer of Ppy doped with pTS^- was initially deposited onto the electrode before the second layer of Ppy containing the pTS^- and a bioactive molecule was deposited. This maintained the mechanical properties of Ppy and greatly improved adhesion of the polymer to the underlying electrode. Not all drugs can be released from Ppy, for example, Konturri *et al.*⁶³ found that nicoside did not release from Ppy upon reduction despite it being a smaller anion than naproxen. In an attempt to overcome this issue, Ppy was prepared with the 2-naphthalene sulfonate as it is twice the size of nicoside. This demonstrated that the size of the drug is not the only governing factor in drug release. For conducting polymers in biomedical applications most research is focused on the electrical characterisation, chemical composition and biological response with a gap in the performance metrics and mechanical properties. “Chitosan” applies to polymers of varying characteristics making cross referencing difficult to discern.

1.8 Summary

From the literature review, it is clear that there is interest in doping polypyrrole with therapeutic compounds; this has been supported by positive results from many studies. Particularly in the area of cell culture support and neural interfaces, in vitro studies have been encouraging (Section 1.4.1). Polypyrrole can be easily doped and undoped by

switching the potential, however many studies have shown that it is not necessary to control the potential for satisfactory results.

The greatest challenge is the long-term optimisation of Ppy to maintain its performance⁵². Chitosan can offer improved mechanical properties, it is insoluble in water but its hydrophilic properties make it an interesting hydrogel. Pure polypyrrole and pure chitosan films differ significantly in properties. Publications of polypyrrole with chitosan have been investigated, however the work presented in this thesis has taken a novel approach by electrochemically polymerising pyrrole in a chitosan hydrogel network directly on an electrode surface. The advantage of this procedure is that a comprehensive electrochemical characterisation can be obtained. These results are presented and discussed in Chapter 3. Polypyrrole chloride, which is a well-documented conducting polymer, was used in this study for comparison with the more novel anions such as methyl orange (Chapter 4) and oxacillin (Chapter 5).

References

1. S. T. Earley, D. P. Dowling, J. P. Lowry and C. B. Breslin, *Synthetic Metals*, 2005, **148**, 111-118.
2. M. Aziz-Kerrzo, K. G. Conroy, A. M. Fenelon, S. T. Farrell and C. B. Breslin, *Biomaterials*, 2001, **22**, 1531-1539.
3. C. C. Harley, A. D. Rooney and C. B. Breslin, *Sensors and Actuators B: Chemical*, 2010, **150**, 498-504.
4. C. Harley, National University of Ireland Maynooth., 2009.
5. R. Doyle, National University of Ireland Maynooth, 2011.
6. E. M. Ryan, C. B. Breslin, S. E. Moulton and G. G. Wallace, *Electrochimica Acta*, 2013, **92**, 276-284.
7. E. M. Ryan, NUI Maynooth, 2010.
8. G. M. Hendy, National University of Ireland Maynooth, 2009.
9. G. Zotti, G. Schiavon and N. Comisso, *Synthetic Metals*, 1991, **40**, 309-316.

10. A. I. Nazzal, G. B. Street and K. J. Wynne, *Molecular Crystals and Liquid Crystals*, 1985, **125**, 303-307.
11. D. Svirskis, J. Travas-Sejdic, A. Rodgers and S. Garg, *Journal of Controlled Release*, 2010, **146**, 6-15.
12. G. Inzelt, Conducting polymers a new era in electrochemistry, <http://dx.doi.org/10.1007/978-3-642-27621-7>.
13. D. D. Ateh, H. A. Navsaria and P. Vadgama, *Journal of The Royal Society Interface*, 2006, **3**, 741-752.
14. G. B. Street, T. C. Clarke, R. H. Geiss, V. Y. Lee, A. Nazzal, P. Pfluger and J. C. Scott, *Journal Physical Colloques*, 1983, **44**, 599-606.
15. G. Natta, G. Mazzanti and C. Corradini, *Atti della Accademia Nazionale dei Lincei. Classe di Scienze Fisiche, Matematiche e Naturali*, 1958, **25**, 1-2.
16. T. Ito, H. Shirakawa and S. Ikeda, *Journal of Polymer Science Part A-Polymer Chemistry*, 1974, **12**, 11-20.
17. T. Ito, H. Shirakawa and S. Ikeda, *Journal of Polymer Science Part A-Polymer Chemistry*, 1975, **13**, 1943-1950.
18. R. McNeill, R. Siudak, J. H. Wardlaw and D. E. Weiss, *Australian Journal of Chemistry*, 1963, **16**, 1056-1075.
19. B. A. Bolto, R. McNeill and D. A. Weiss, *Australian Journal of Chemistry*, 1963, **16**, 1090-1103.
20. R. L. Greene, G. B. Street and L. J. Suter, *Physical Review Letters*, 1975, **34**, 577-579.
21. C. K. Chiang, C. R. Fincher, Jr., Y. W. Park, A. J. Heeger, H. Shirakawa, E. J. Louis, S. C. Gau and A. G. MacDiarmid, *Phys. Rev. Lett.*, 1977, **39**, 1098-1101.
22. A. J. Heeger, *Reviews of Modern Physics*, 2001, **73**, 681-700.
23. W. J. Feast, J. Tsibouklis, K. L. Pouwer, L. Groenendaal and E. W. Meijer, *Polymer*, 1996, **37**, 5017-5047.
24. M. Aldissi, *Synthetic Metals*, 1984, **9**, 131-141.
25. M. C. De Jesus, Y. Fu and R. A. Weiss, *Polymer Engineering & Science*, 1997, **37**, 1936-1943.
26. N. K. Guimard, N. Gomez and C. E. Schmidt, *Progress in Polymer Science*, 2007, **32**, 876-921.

-
27. J. H. Collier, J. P. Camp, T. W. Hudson and C. E. Schmidt, *Journal of Biomedical Materials Research*, 2000, **50**, 574-584.
 28. E. Andreoli, *PhD Thesis*, NUI Maynooth, 2010.
 29. A. B. Kaiser, *Advanced Materials*, 2001, **13**, 927-941.
 30. A. J. Heeger, S. Kivelson, J. R. Schrieffer and W. P. Su, *Reviews of Modern Physics*, 1988, **60**, 781-850.
 31. J. L. Bredas and G. B. Street, *Accounts of Chemical Research*, 1985, **18**, 309-315.
 32. J. L. Garcia-Alvarez, *Current Organic Chemistry*, 2008, **12**, 1199-1219.
 33. C. Weder, *Chemical Communications*, 2005, 5378-5389.
 34. J. Jagur-Grodzinski, *Polymers for Advanced Technologies*, 2002, **13**, 615-625.
 35. J. L. Reddinger and J. R. Reynolds, in *Advances in Polymer Science, Volume 145*, Springer, 1999, pp. 57-122.
 36. D. Kumar and R. C. Sharma, *European Polymer Journal*, 1998, **34**, 1053-1060.
 37. J. D. Stenger-Smith, *Progress in Polymer Science*, 1998, **23**, 57-79.
 38. N. Toshima and S. Hara, *Progress in Polymer Science*, 1995, **20**, 155-183.
 39. C. R. Martin, *Accounts of Chemical Research*, 1995, **28**, 61-68.
 40. A. F. Diaz and J. C. Lacroix, *New Journal of Chemistry*, 1988, **12**, 171-180.
 41. M. Fujitsuka, T. Sato, H. Segawa and T. Shimidzu, *Synthetic Metals*, 1995, **69**, 309-310.
 42. M. Jeffries-El, G. Sauvé and R. D. McCullough, *Advanced Materials*, 2004, **16**, 1017-1019.
 43. J.-E. Österholm, Y. Cao, F. Klavetter and P. Smith, *Polymer*, 1994, **35**, 2902-2906.
 44. F. Cataldo, P. Ragni, O. Ursini and G. Angelini, *Radiation Physics and Chemistry*, 2008, **77**, 941-948.
 45. L. Chen, J. Jin, X. Shu and J. Xia, *Journal of Power Sources*, 2014, **248**, 1234-1240.
 46. N. D. Boscher, D. Duday, P. Heier, K. Heinze, F. Hilt and P. Choquet, *Surface and Coatings Technology*, 2013, **234**, 48-52.
 47. S. Yigit, J. Hacaloglu, U. Akbulut and L. Toppare, *Synthetic Metals*, 1997, **84**, 205-206.

-
48. H.-Q. Xie, C.-M. Liu and J.-S. Guo, *European Polymer Journal*, 1996, **32**, 1131-1137.
 49. L.-X. Wang, X.-G. Li and Y.-L. Yang, *Reactive and Functional Polymers*, 2001, **47**, 125-139.
 50. X. Wang, X. Gu, C. Yuan, S. Chen, P. Zhang, T. Zhang, J. Yao, F. Chen and G. Chen, *J. Biomed. Mater. Res., Part A*, 2004, **68A**, 411-422.
 51. A. Vaitkuvienė, V. Kasetas, J. Voronovic, G. Ramanauskaite, G. Biziuleviciene, A. Ramanaviciene and A. Ramanavicius, *Journal of Hazardous Materials*, 2013, **250-251**, 167-174.
 52. R. A. Green, N. H. Lovell, G. G. Wallace and L. A. Poole-Warren, *Biomaterials*, 2008, **29**, 3393-3399.
 53. A. T. Lawal and G. G. Wallace, *Talanta*, 2014, **119**, 133-143.
 54. A. Malinauskas, *Polymer*, 2001, **42**, 3957-3972.
 55. S. Sadki, P. Schottland, N. Brodie and G. Sabouraud, *Chemical Society Reviews*, 2000, **29**, 283-293.
 56. R. J. Waltman and J. Bargon, *Journal of Electroanalytical Chemistry and Interfacial Electrochemistry*, 1985, **194**, 49-62.
 57. M. Zhou and J. Heinze, *Electrochimica Acta*, 1999, **44**, 1733-1748.
 58. E. M. Genies, G. Bidan and A. F. Diaz, *Journal of Electroanalytical Chemistry and Interfacial Electrochemistry*, 1983, **149**, 101-113.
 59. A. Madhan Kumar and N. Rajendran, *Ceramics International*, 2013, **39**, 5639-5650.
 60. I. L. Lehr and S. B. Saidman, *Corrosion Science*, 2007, **49**, 2210-2225.
 61. V. Annibaldi, A. D. Rooney and C. B. Breslin, *Corrosion Science*, 2012, **59**, 179-185.
 62. A. M. Fenelon and C. B. Breslin, *Electrochimica Acta*, 2002, **47**, 4467-4476.
 63. K. Kontturi, P. Pentti and G. Sundholm, *Journal of Electroanalytical Chemistry*, 1998, **453**, 231-238.
 64. J.-M. Pernaut and J. R. Reynolds, *The Journal of Physical Chemistry B*, 2000, **104**, 4080-4090.
 65. H. Ge, G. Qi, E.-T. Kang and K. G. Neoh, *Polymer*, 1994, **35**, 504-508.
 66. I. Rodríguez, B. R. Scharifker and J. Mostany, *Journal of Electroanalytical Chemistry*, 2000, **491**, 117-125.

-
67. A. F. Diaz and B. Hall, *IBM Journal of Research and Development*, 1983, **27**, 342-347.
 68. T. Silk, Q. Hong, J. Tamm and R. G. Compton, *Synthetic Metals*, 1998, **93**, 59-64.
 69. T. Silk, Q. Hong, J. Tamm and R. G. Compton, *Synthetic Metals*, 1998, **93**, 65-71.
 70. K. S. Teh, Y. Takahashi, Z. Yao and Y.-W. Lu, *Sensors and Actuators A: Physical*, 2009, **155**, 113-119.
 71. G. A. Snook, G. Z. Chen, D. J. Fray, M. Hughes and M. Shaffer, *Journal of Electroanalytical Chemistry*, 2004, **568**, 135-142.
 72. M. J. Ariza and T. F. Otero, *Journal Membrane Science*, 2007, **290**, 241-249.
 73. R. A. Jeong, G. J. Lee, H. S. Kim, K. Ahn, K. Lee and K. H. Kim, *Synthetic Metals*, 1998, **98**, 9-15.
 74. X. Ren and P. G. Pickup, *Journal of Physical chemistry*, 1993, **97**, 5356-5362.
 75. H. Zhao, W. E. Price, C. O. Too, G. G. Wallace and D. Zhou, *Journal of Membrane Science*, 1996, **119**, 199-212.
 76. X. Ren and P. G. Pickup, *Electrochimica Acta*, 1996, **41**, 1877-1882.
 77. T. Komura, S. Goisihara, T. Yamaguti and K. Takahasi, *Journal of Electroanalytical Chemistry*, 1998, **456**, 121-129.
 78. M. D. Levi, C. Lopez, E. Vieil and M. A. Vorotyntsev, *Electrochimica Acta*, 1997, **42**, 757-769.
 79. K. P. Vidanapathirana, M. A. Careem, S. Skaarup and K. West, *Solid State Ionics*, 2002, **154–155**, 331-335.
 80. Y. J. Yuan, S. B. Adeloju and G. G. Wallace, *European Polymer Journal*, 1999, **35**, 1761-1772.
 81. A. J. Downard and D. Pletcher, *Journal of Electroanalytical Chemistry and Interfacial Electrochemistry*, 1986, **206**, 139-145.
 82. T. F. Otero and J. Rodriguez, *Synthetic Metals*, 1993, **55**, 1418-1423.
 83. T. F. Otero and J. Rodríguez, *Journal of Electroanalytical Chemistry*, 1994, **379**, 513-516.
 84. T. F. Otero and J. Rodríguez, *Electrochimica Acta*, 1994, **39**, 245-253.
 85. S. Shimoda and E. Smela, *Electrochimica Acta*, 1998, **44**, 219-238.
 86. D. Sangian, W. Zheng and G. M. Spinks, *Synthetic Metals*, 2014, **189**, 53-56.

-
87. S. Geetha, C. R. K. Rao, M. Vijayan and D. C. Trivedi, *Analytica Chimica Acta*, 2006, **568**, 119-125.
 88. J. Y. Wong, R. Langer and D. E. Ingber, *Proceedings of the National Academy of Sciences*, 1994, **91**, 3201-3204.
 89. P. Wu and D. W. Grainger, *Biomaterials*, 2006, **27**, 2450-2467.
 90. J. G. Hardy, J. Y. Lee and C. E. Schmidt, *Current Opinion in Biotechnology*, 2013, **24**, 847-854.
 91. T. F. Otero, I. Boyano, M. T. Cortés and G. Vázquez, *Electrochimica Acta*, 2004, **49**, 3719-3726.
 92. D. Zhou, G. M. Spinks, G. G. Wallace, C. Tiyaipiboonchaiya, D. R. MacFarlane, M. Forsyth and J. Sun, *Electrochimica Acta*, 2003, **48**, 2355-2359.
 93. G. Han and G. Shi, *Sensors and Actuators B: Chemical*, 2004, **99**, 525-531.
 94. G. Han and G. Shi, *Sensors and Actuators B: Chemical*, 2006, **113**, 259-264.
 95. G. M. Spinks, B. Xi, D. Zhou, V.-T. Truong and G. G. Wallace, *Synthetic Metals*, 2004, **140**, 273-280.
 96. E. Smela, *Advanced Materials*, 2003, **15**, 481-494.
 97. J. C. Soares, A. Brisolari, V. d. C. Rodrigues, E. A. Sanches and D. Gonçalves, *Reactive and Functional Polymers*, 2012, **72**, 148-152.
 98. S. Brahim, D. Narinesingh and A. Guiseppi-Elie, *Analytica Chimica Acta*, 2001, **448**, 27-36.
 99. S. Brahim, D. Narinesingh and A. Guiseppi-Elie, *Biosensors and Bioelectronics*, 2002, **17**, 53-59.
 100. M. Gerard, A. Chaubey and B. D. Malhotra, *Biosensors and Bioelectronics*, 2002, **17**, 345-359.
 101. G. G. Wallace, M. Smyth and H. Zhao, *TrAC Trends in Analytical Chemistry*, 1999, **18**, 245-251.
 102. D. B. McCreery, T. G. H. Yuen, W. F. Agnew and L. A. Bullara, *Biomedical Engineering, IEEE Transactions on*, 1997, **44**, 931-939.
 103. X. Cui, J. F. Hetke, J. A. Wiler, D. J. Anderson and D. C. Martin, *Sensors and Actuators A: Physical*, 2001, **93**, 8-18.
 104. X. Cui, J. Wiler, M. Dzaman, R. A. Altschuler and D. C. Martin, *Biomaterials*, 2003, **24**, 777-787.
 105. W. R. Stauffer and X. T. Cui, *Biomaterials*, 2006, **27**, 2405-2413.

-
106. G. Bidan, C. Lopez, F. Mendes-Viegas, E. Vieil and A. Gadelle, *Biosensors and Bioelectronics*, 1995, **10**, 219-229.
 107. D. Esrafilzadeh, J. M. Razal, S. E. Moulton, E. M. Stewart and G. G. Wallace, *Journal of Controlled Release*, 2013, **169**, 313-320.
 108. D. Ge, X. Tian, R. Qi, S. Huang, J. Mu, S. Hong, S. Ye, X. Zhang, D. Li and W. Shi, *Electrochimica Acta*, 2009, **55**, 271-275.
 109. L. Leprince, A. Dogimont and D. Magnin, *Journal of Materials Science: Materials in Medicine*, 2010, **21**, 925-930.
 110. L. Baosong and W. Yen, *Acta Polymerica Sinica*, 2010, **010**, 1399.
 111. K. J. Gilmore, M. Kita, Y. Han, A. Gelmi, M. J. Higgins, S. E. Moulton, G. M. Clark, R. Kapsa and G. G. Wallace, *Biomaterials*, 2009, **30**, 5292-5304.
 112. K. M. Sajesh, R. Jayakumar, S. V. Nair and K. P. Chennazhi, *International Journal of Biological Macromolecules*, 2013, **62**, 465-471.
 113. J. M. Fonner, L. Forciniti, N. Hieu, J. D. Byrne, Y.-F. Kou, J. Syeda-Nawaz and C. E. Schmidt, *Biomedical Materials*, 2008, **3**, 1-12.
 114. M. Nishizawa, H. Nozaki, H. Kaji, T. Kitazume, N. Kobayashi, T. Ishibashi and T. Abe, *Biomaterials*, 2007, **28**, 1480-1485.
 115. B. Garner, A. Georgevich, A. J. Hodgson, L. Liu and G. G. Wallace, *Journal of Biomedical Materials Research*, 1999, **44**, 121-129.
 116. N. Gomez and C. E. Schmidt, *Journal of Biomedical Materials Research Part A*, 2007, **81A**, 135-149.
 117. L. N. Novikova, J. Pettersson, M. Brohlin, M. Wiberg and L. N. Novikov, *Biomaterials*, 2008, **29**, 1198-1206.
 118. P. M. George, A. W. Lyckman, D. A. LaVan, A. Hegde, Y. Leung, R. Avasare, C. Testa, P. M. Alexander, R. Langer and M. Sur, *Biomaterials*, 2005, **26**, 3511-3519.
 119. X. Cui and D. C. Martin, *Sensors and Actuators A: Physical*, 2003, **103**, 384-394.
 120. R. A. Green, R. T. Hassarati, L. Bouchinet, C. S. Lee, G. L. M. Cheong, J. F. Yu, C. W. Dodds, G. J. Suaning, L. A. Poole-Warren and N. H. Lovell, *Biomaterials*, 2012, **33**, 5875-5886.
 121. R. Langer and J. Folkman, *Nature (London)*, 1976, **263**, 797-800.

-
122. B. Zinger and L. L. Miller, *Journal of the American Chemical Society*, 1984, **106**, 6861-6863.
 123. M. Pyo, G. Maeder, R. T. Kennedy and J. R. Reynolds, *Journal of Electroanalytical Chemistry*, 1994, **368**, 329-332.
 124. B. C. Thompson, S. E. Moulton, R. T. Richardson and G. G. Wallace, *Biomaterials*, 2011, **32**, 3822-3831.
 125. M. Hepel and F. Mahdavi, *Microchemical Journal*, 1997, **56**, 54-64.
 126. M. Zilberman and J. J. Elsner, *Journal of Controlled Release*, 2008, **130**, 202-215.
 127. R. W. Wysocki, C. J. Della Valle, S. Shott, A. G. Rosenberg, R. A. Berger and J. O. Galante, *The Journal of Arthroplasty*, 2009, **24**, 58-63.
 128. L. L. Miller and X. Q. Zhou, *Macromolecules*, 1987, **20**, 1594-1597.
 129. Q.-X. Zhou, L. L. Miller and J. R. Valentine, *Journal of Electroanalytical Chemistry and Interfacial Electrochemistry*, 1989, **261**, 147-164.
 130. Y. Lin and G. G. Wallace, *Journal of Controlled Release*, 1994, **30**, 137-142.
 131. D. Svirskis, B. E. Wright, J. Travas-Sejdic, A. Rodgers and S. Garg, *Electroanalysis*, 2010, **22**, 439-444.
 132. R. Wadhwa, C. F. Lagenaur and X. T. Cui, *Journal of Controlled Release*, 2006, **110**, 531-541.
 133. L. Li and C. Huang, *Journal of the American Society for Mass Spectrometry*, 2007, **18**, 919-926.
 134. T. Aoki, M. Tanino, K. Sanui, N. Ogata, K. Kumakura, T. Okano, Y. Sakurai and M. Watanabe, *Synthetic Metals*, 1995, **71**, 2229-2230.
 135. T. Aoki, M. Tanino, K. Sanui, N. Ogata and K. Kumakura, *Biomaterials*, 1996, **17**, 1971-1974.
 136. N. Alikacem, Y. Marois, Z. Zhang, B. Jakubiec, R. Roy, Martin W. King and R. Guidoin, *Artificial Organs*, 1999, **23**, 910-919.
 137. S. Jiang, Y. Sun, X. Cui, X. Huang, Y. He, S. Ji, W. Shi and D. Ge, *Synthetic Metals*, 2013, **163**, 19-23.
 138. C. Arbizzani, M. Mastragostino, L. Nevi and L. Rambelli, *Electrochimica Acta*, 2007, **52**, 3274-3279.
 139. R. W. Korsmeyer, R. Gurny, E. Doelker, P. Buri and N. A. Peppas, *International Journal of Pharmaceutics*, 1983, **15**, 25-35.

-
140. E. Shamaeli and N. Alizadeh, *International Journal of Pharmaceutics*, 2014, **472**, 327-338.
141. J. Siepmann and N. A. Peppas, *Advanced Drug Delivery Reviews*, 2001, **48**, 139-157.
142. X. W. Lou, L. A. Archer and Z. Yang, *Advanced Materials*, 2008, **20**, 3987-4019.
143. V. Bajpai, P. He and L. Dai, *Advanced Functional Materials*, 2004, **14**, 145-151.
144. M. G. Peter, *Journal of Macromolecular Science, Part A*, 1995, **32**, 629-640.
145. H. S. Kas, *J. Microencapsulation*, 1997, **14**, 689-711.
146. B. Krajewska, *Enzyme and Microbial Technology*, 2004, **35**, 126-139.
147. D. R. Bhumkar and V. B. Pokharkar, *AAPS PharmSciTech*, 2006, **7**, E50.
148. M. Rinaudo, *Progress in Polymer Science*, 2006, **31**, 603-632.
149. J. Berger, M. Reist, J. M. Mayer, O. Felt, N. A. Peppas and R. Gurny, *European Journal of Pharmaceutics and Biopharmaceutics*, 2004, **57**, 19-34.
150. J. V. Alemán, A. V. Chadwick, J. He, M. Hess, K. Horie, R. G. Jones, P. Kratochvíl, I. Meisel, I. Mita, G. Moad, S. Penczek and R. F. T. Stepto, in *Pure and Applied Chemistry*, 2007, vol. 79, p. 1801.
151. J. Berger, M. Reist, J. M. Mayer, O. Felt and R. Gurny, *European Journal of Pharmaceutics and Biopharmaceutics*, 2004, **57**, 35-52.
152. O. A. C. Monteiro Jr and C. Airoidi, *International Journal of Biological Macromolecules*, 1999, **26**, 119-128.
153. R. Barreiro-Iglesias, R. Coronilla, A. Concheiro and C. Alvarez-Lorenzo, *European Journal of Pharmaceutical Sciences*, 2005, **24**, 77-84.
154. W. Argüelles-Monal, F. M. Goycoolea, C. Peniche and I. Higuera-Ciapara, *Polymer Gels and Networks*, 1998, **6**, 429-440.
155. K. Pospiskova and I. Safarik, *Carbohydrate Polymers*, 2013, **96**, 545-548.
156. J. Nunthanid, S. Puttipatkhachorn, K. Yamamoto and G. E. Peck, *Drug Dev. Ind. Pharm.*, 2001, **27**, 143-157.
157. C. K. S. Pillai, W. Paul and C. P. Sharma, *Progress in Polymer Science*, 2009, **34**, 641-678.
158. C. M. P. Yoshida, V. B. V. Maciel, M. E. D. Mendonça and T. T. Franco, *LWT - Food Science and Technology*, 2014, **55**, 83-89.

-
159. K. D. Yao, W. G. Liu, Z. Lin and X. H. Qiu, *Polymer International*, 1999, **48**, 794-798.
160. M. N. V. R. Kumar, R. A. A. Muzzarelli, C. Muzzarelli, H. Sashiwa and A. J. Domb, *Chemical Reviews*, 2004, **104**, 6017-6084.
161. Y.-C. Lin, F.-j. Tan, K. G. Marra, S.-S. Jan and D.-C. Liu, *Acta Biomaterialia*, 2009, **5**, 2591-2600.
162. D. E. S. Santos, C. G. T. Neto, J. L. C. Fonseca and M. R. Pereira, *Journal of Membrane Science*, 2008, **325**, 362-370.
163. P. C. Srinivasa, M. N. Ramesh, K. R. Kumar and R. N. Tharanathan, *Journal of Food Engineering*, 2004, **63**, 79-85.
164. C.-M. Lehr, J. A. Bouwstra, E. H. Schacht and H. E. Junginger, *International Journal of Pharmaceutics*, 1992, **78**, 43-48.
165. O. M. Merkel, M. Zheng, H. Debus and T. Kissel, *Bioconjugate Chemistry*, 2011, **23**, 3-20.
166. L. Illum, I. Jabbal-Gill, M. Hinchcliffe, A. N. Fisher and S. S. Davis, *Advanced Drug Delivery Reviews*, 2001, **51**, 81-96.
167. M. Kong, X. G. Chen, K. Xing and H. J. Park, *International Journal of Food Microbiology*, 2010, **144**, 51-63.
168. I.-Y. Kim, S.-J. Seo, H.-S. Moon, M.-K. Yoo, I.-Y. Park, B.-C. Kim and C.-S. Cho, *Biotechnology Advances*, 2008, **26**, 1-21.
169. Y. Wan, H. Wu and D. Wen, *Macromolecular Bioscience*, 2004, **4**, 882-890.
170. Y. Wan, A. Yu, H. Wu, Z. Wang and D. Wen, *Journal of Materials Science: Materials in Medicine*, 2005, **16**, 1017-1028.
171. B. E. Benediktsdóttir, Ó. Baldursson and M. Másson, *Journal of Controlled Release*, 2014, **173**, 18-31.
172. L. Illum, *Pharmaceutical Research*, 1998, **15**, 1326-1331.
173. S. Miyazaki, A. Nakayama, M. Oda, M. Takada and D. Attwood, *International Journal of Pharmaceutics*, 1995, **118**, 257-263.
174. K. Bhise, R. Dhumal, A. Paradkar and S. Kadam, *AAPS PharmSciTech*, 2008, **9**, 1-12.
175. P. Mura, N. Zerrouk, N. Mennini, F. Maestrelli and C. Chemtob, *European Journal of Pharmaceutical Sciences*, 2003, **19**, 67-75.

-
176. R. Ilango, S. Kavimani, B. Jaykar and G. Umamaheshwari, *Indian Journal of Experimental Biology*, 1999, **37**, 505-508.
177. S. Shah, R. Qaqish, V. Patel and M. Amiji, *Journal of Pharmacy and Pharmacology*, 1999, **51**, 667-672.
178. A. M. De Campos, A. Sánchez and M. a. J. Alonso, *International Journal of Pharmaceutics*, 2001, **224**, 159-168.
179. E. Khor, *Current Opinion in Solid State and Materials Science*, 2002, **6**, 313-317.
180. H. K. S. Souza, J. M. Campiña, A. M. M. Sousa, F. Silva and M. P. Gonçalves, *Food Hydrocolloids*, 2013, **31**, 227-236.
181. A. Bernkop-Schnürch and S. Dünnhaupt, *European Journal of Pharmaceutics and Biopharmaceutics*, 2012, **81**, 463-469.
182. V. R. Sinha, A. K. Singla, S. Wadhawan, R. Kaushik, R. Kumria, K. Bansal and S. Dhawan, *International Journal of Pharmaceutics*, 2004, **274**, 1-33.
183. A. K. Singla and M. Chawla, *Journal of Pharmacy and Pharmacology*, 2001, **53**, 1047-1067.
184. A. R. Sadrolhosseini, M. M. Moxsin, W. M. M. Yunus, Z. A. Talib and M. M. Abdi, *Optical Review*, 2011, **18**, 331-337.
185. *Japan Pat.*, 1992.
186. E. Khor and J. L. H. Whey, *Carbohydrate Polymers*, 1995, **26**, 183-187.
187. CN102220622A, 2011.
188. CN102262114A, 2011.
189. Y. Chen, H. Feng, L. Li, S. Shang and M. Chun-Wah Yuen, *Journal Macromolecular Science, Part A: Pure and Applied Chemistry*, 2013, **50**, 1225-1229.
190. H. Huang, J. Wu, X. Lin, L. Li, S. Shang, M. C.-w. Yuen and G. Yan, *Carbohydrate Polymers*, 2013, **95**, 72-76.
191. S. Yalçinkaya, C. Demetgül, M. Timur and N. Çolak, *Carbohydrate Polymers*, 2010, **79**, 908-913.
192. J. Huang, X. Hu, L. Lu, Z. Ye, Q. Zhang and Z. Luo, *Journal of Biomedical Materials Research Part A*, 2010, **93A**, 164-174.
193. H. Bai and G. Shi, *Sensors*, 2007, **7**, 267-307.

194. M. F. a. L. F. a. H. N. a. J. D. B. a. Y.-F. K. a. J. S.-N. a. C. E. S. John, *Biomedical Materials*, 2008, **3**, 034124.
195. H. L. Ricks-Laskoski and L. J. Buckley, *Synthetic Metals*, 2006, **156**, 417-419.
196. Y. Li and R. Qian, *Electrochimica Acta*, 2000, **45**, 1727-1731.
197. C. Debiemme-Chouvy and T. T. M. Tran, *Electrochemistry Communications*, 2008, **10**, 947-950.
198. B. C. Kim, G. M. Spinks, C. O. Too, G. G. Wallace, Y. H. Bae and N. Ogata, *Reactive and Functional Polymers*, 2000, **44**, 245-258.
199. B. C. Thompson, S. E. Moulton, J. Ding, R. Richardson, A. Cameron, S. O'Leary, G. G. Wallace and G. M. Clark, *Journal of Controlled Release*, 2006, **116**, 285-294.

Chapter 2

Experimental

2 Experimental

2.1 Introduction

In this chapter, the techniques employed and the theory of the techniques used for the fabricating and characterisation of the composite material, polypyrrole with chitosan, are presented. One of the advantages of fabricating composite materials is that the new material can exhibit optimised performance, e.g., improved mechanical properties. The challenge with composite materials is that the heterogeneous nature of the material can make analysing the structure-property relationships difficult and well-established characterisation techniques are limited¹. However, in this research project with careful experimental design a detailed study of the electrochemical behaviour of the composite materials was possible.

Electrochemical synthesis experiments and a number of electroanalytical techniques were used throughout this study. The polypyrrole films (Ppy) were electrochemically synthesised with various anionic dopants to give PpyA, where A represents the anionic dopant. PpyA and chitosan composites were prepared by drop casting chitosan solution either on the metal substrate prior to electropolymerisation (Chapter 3) or as a layer at the PpyA interfaces, post-electropolymerisation. Traditional techniques used to characterise the materials in Chapter 3 were FT-IR (structural properties) and DSC (thermal properties). In Chapters 3, 4 and 5, SEM-EDX (morphology) was used. In Chapters 4 and 5 the composite yields were too small to obtain FT-IR or DSC results, and SEM-EDX served as an alternative characterisation technique. A simple microfabrication technique was developed for preparing drug doped polypyrrole composites and each chapter includes a comparison between the PpyA with and without the chitosan. The release of the dopant was monitored using UV-visible spectroscopy by applying an electrical stimulus or no electrical stimulus.

2.2 The electrochemical set-up

Electrochemistry is the study of chemical processes involving the transfer of electrons to or from an electrode surface, and the electrochemical measurements rely on these processes to provide readable data. According to Faraday's law of electrolysis, the amount of a substance deposited or evolved (m) during electrolysis is directly proportional to the current (I) and the time (t), i.e., the quantity of charge per unit area of a substance is related to the magnitude of the current.

$$m = \frac{Mit}{nF} = \frac{MQ}{nF} \quad (2.1)$$

In this equation, M is the molar mass of the substance, n is the number of moles of electrons, F is Faraday's constant and Q is the amount of charge consumed during electrolysis²⁻⁴. A wide range of electrochemical experiments can be performed with a commercial electrochemical workstation. The potential can be controlled and the resulting current is measured, giving the potentiostatic techniques or the current can be controlled and the potential is measured, giving the galvanostatic techniques.

2.2.1 The electrochemical workstation

The electrochemical measurements, including open-circuit potential, potentiostatic and cyclic voltammetry, were performed with a Solartron model SI1285 or SI1287 electrochemical interface operated by Scribner Associates' CorrWare for Windows™, Version 2.1. The CorrView programme for Windows™, Version 2.3, was used to display, analyse and graph the data. The potentiostat was connected to an electrochemical cell, as shown in Figure 2.1. The impedance measurements were performed using a Solartron Frequency response analyser, model SI1250 and SI1255B, coupled to a Solartron SI1287 electrochemical interface operated by Scribner Associates' ZPlot for Windows™, Version 2.1. The ZView programme for Windows™, Version 2.3, was used to display, analyse and graph the data. The electrochemical quartz crystal microbalance experiments were performed with a CH Instrument Potentiostat / Galvanostat, model CHI 440B, linked with a crystal oscillator. The experiments were operated by CHI Software package for Windows™, Version 1.0.0.1.

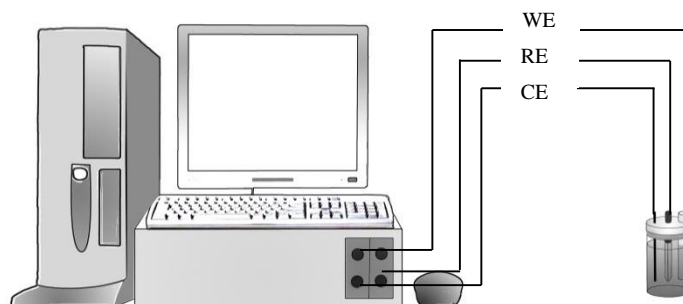


Figure 2.1: The electrochemical workstation: potentiostat and electrochemical cell.

2.2.2 The electrochemical cell

A conventional three electrode cell configuration was used to record the electrochemical data. The cell consisted of a glass sample vial with a capacity of 10 cm³ fitted with a customised polytetrafluoroethylene (PTFE) lid to accommodate a reference electrode (RE), a working electrode (WE) and a counter electrode (CE). The electrodes were connected to a potentiostat coupled to a compatible PC which collected and analysed the data, as depicted in Figure 2.1. A different cell design was used for the EQCM measurements and this is described in Section 2.4.5.

A saturated calomel electrode (SCE) was the reference electrode (RE) used most frequently except for when carrying out EQCM experiments. In this case, a custom made silver/silver chloride (Ag|AgCl) reference electrode was used. All potentials in this work are quoted against the reference electrode. The standard electrode potentials of the SCE and Ag|AgCl reference electrodes in aqueous solution are 0.241 V and 0.197 V, respectively, versus a standard hydrogen electrode (SHE) at 25 °C. The SCE was serviced regularly by refilling the internal solution with a saturated solution of super-purum KCl

(99.999+ %, Merck) and by checking the potential against a “virgin” SCE using a multimeter.

All electrode materials were supplied by Goodfellow Cambridge Ltd. and were sliced into discs with lengths of 1 cm. A platinum disc (99.99 % purity) with a diameter of 4 mm, and a gold disc (99.99 % purity) with a diameter of 3 mm, were employed as the electrodes. An electrical contact was made with copper wire glued with conducting silver epoxy to the base of the electrode. It was then encased in PTFE and secured in place by a non-conducting epoxy resin, a schematic of which is illustrated in Figure 2.2. The electrodes were polished with successively finer grades (30 μm , 15 μm , 6 μm and 1 μm) of diamond polishes (Buehler MetaDi Monocrystalline Diamond suspension) and 0.5 μm Al_2O_3 slurry on a Buehler micro-cloth, sonicated and rinsed with ethanol and distilled water to ensure a clean surface. Occasionally it was necessary to remove the polymer film from the electrode surface, and this was achieved using a Buehler METASERV grinder polisher with a Buehler SiC grinding paper (Grit P 2500). The electrode was then polished using the diamond polishes and Al_2O_3 slurry.

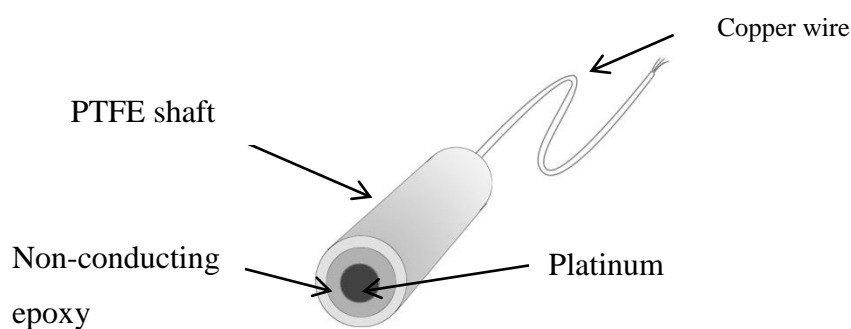


Figure 2.2: Illustration of disc electrode.

The counter electrode (CE) was a platinum wire with a high surface area of high purity (99.99+ %) supplied by Goodfellow Cambridge Ltd. Before every set of experiments, the

counter electrode was brushed with Buehler SiC grinding paper (Grit P 2500), cleaned with a cloth, sonicated in distilled water and finally rinsed with distilled water.

All experiments were carried out at atmospheric conditions, unless otherwise stated (room temperature 23 ± 2 °C). The supporting electrolytes were aqueous solutions of inorganic and organic salts.

The electrochemical cell was controlled by the potentiostat, as depicted in Figure 2.1. The block diagram in Figure 2.3 summarises the working relationship between the potentiostat and electrochemical cell. The potentiostat measures the voltage, V_{WE} , or the current of the working electrode, I_{WE} . It controls the voltage between the working electrode and counter electrode pair ($V_{WC} = V_{WE} - V_{CE}$), and adjusts this voltage to maintain the potential difference between the working electrode and reference electrode ($V_{WR} = V_{WE} - V_{RE}$) which it detects through a high-impedance feedback loop, where V_{RE} is a given arbitrary value. The current flow is measured between the counter electrode and working electrode ($I_{CE} = I_{WE} + I_{RE}$), and the potentiostat imposes a negative bias⁵ so that the value of I_{RE} is zero and $I_{CE} = I_{WE}$. If the solution has a high conductivity, then the current-voltage is not disturbed by the solution resistance, which creates an iR drop in the cell. The voltage is equal to the product of current and resistance, in accordance with Ohm's law, $V = iR$. When the current flow is appreciable the measured potential is distorted and shifts by an amount equal to iR , where R is the solution resistance⁶.

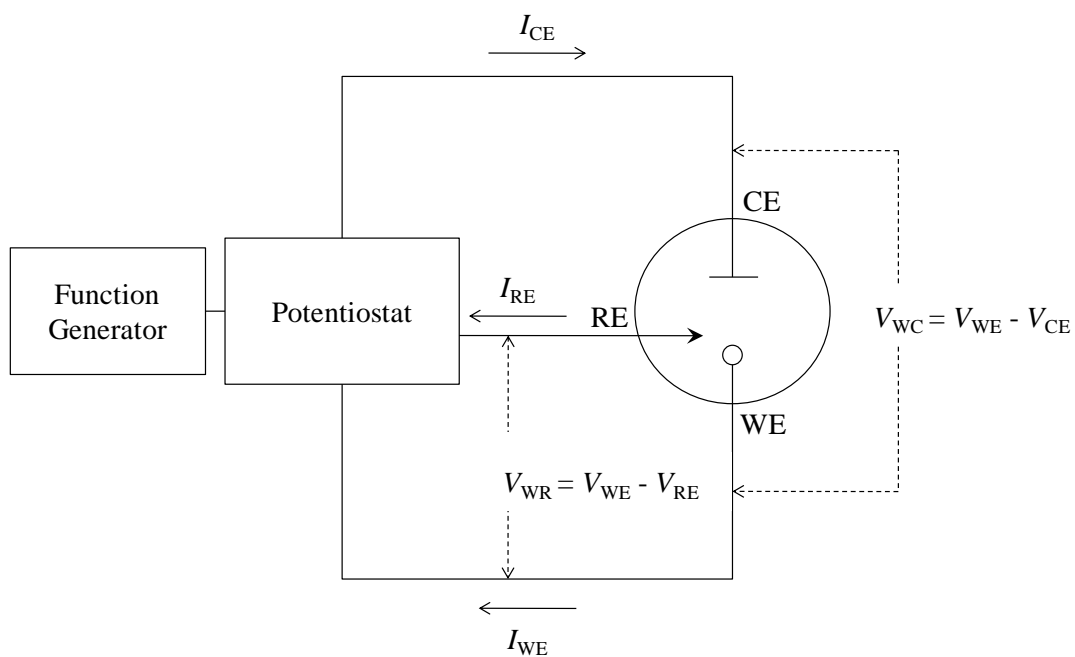


Figure 2.3: Block diagram representing the working relationship between a potentiostat and an electrochemical cell. Adapted from Bard and Faulkner⁷.

2.3 Chemicals and preparation of polymers

This section briefly summarises the techniques used to prepare the composite films, while the parameters are discussed in more detail in the relevant results sections.

2.3.1 Chemicals

The chemicals used in this research project were pyrrole (98 %), chitosan from shrimp shells (≥ 75 % deacetylated), lysozyme from chicken egg white (~ 70000 U mg^{-1}), methyl orange ACS reagent (85 % dye content), oxacillin sodium salt (~ 95 % TLC) and dexamethasone 21-phosphate disodium salt (≥ 98 %). The sodium chloride, sodium phosphate monobasic monohydrate, sodium hydroxide, calcium chloride, potassium chloride and lithium perchlorate were all ACS reagents (≥ 98 %). The hydrochloric acid, acetone, ethanoic acid and ethanol were AnalaR grade reagents supplied by VWR. High purity nitrogen and argon (99.95 %) were supplied by BOC. Distilled water was used to make up the solutions and Milli-Q purified water (14 M Ω cm, pH = 5.0) was used to make up the phosphate saline buffer. All the chemicals were used without further purification except for pyrrole (98 %). The pyrrole monomer was distilled under vacuum and stored in the dark at -18 °C under nitrogen, prior to use. Solution properties, such as pH and ionic conductivity, were determined using an Orion model 720A pH meter and a Jenway 4510 conductivity meter, respectively. The equipment was calibrated each time prior to experimental analysis using buffered solutions, pH 7.0 and 4.0, obtained from Fluka for calibration of the pH meter, and 0.01 mol dm^{-3} KCl from Sigma for calibration of the conductivity meter.

2.3.2 Preparation of chitosan solution

The chitosan solution was prepared by dissolving 0.125 g of chitosan in 25 cm^3 of 2.0 mol dm^{-3} ethanoic acid to give a 0.5 % (w/v) chitosan solution. The solution was stirred for 180 min using a magnetic stirrer and then it was filtered using Whatman™ filter paper. Chitosan films were deposited using a drop cast technique. The 0.5 % (w/v) chitosan solution was drop cast on to the electrode surface (10 μL / 0.13 cm^2), the film was dried for 10 min under an infrared lamp (55 - 60 °C) then let cool for 10 min. Occasionally, when

stand-alone experiments (e.g. gravimetric analysis) were performed on the chitosan film, microfilms were prepared by pipetting several quantities of the chitosan solution, 10 $\mu\text{L}/0.13\text{ cm}^2$, on to clear PVC sheets. They were cured as above and peeled away from the PVC substrate.

2.3.3 Preparation of polymers

The polypyrrole films doped with different anions were deposited from a solution containing the pyrrole monomer and an aqueous solution containing the anion as the supporting electrolyte. The formulation of the monomer electrolyte solutions for the films is summarised in Table 2.1, where the concentration of the pyrrole monomer was maintained at 0.1 or 0.2 mol dm^{-3} . The polymerisation solutions were prepared on a daily basis as it was of prime importance that the experimental parameters used were reproducible. The PpyA (where A is the dopant species) films were formed electrochemically at a constant potential of 0.80 V vs. SCE for a fixed duration or until the desired charge density was reached. The electrochemical preparation of PpyCl/chitosan is discussed in Chapter 3, PpyMO/chitosan is discussed in Chapter 4, and finally PpyOx/chitosan is discussed in Chapter 5.

Table 2.1: Summary of the formulation of the aqueous solutions used to fabricate the Ppy films.

Film	Pyrrole (mol dm^{-3})	Dopant (mol dm^{-3})
Polypyrrole chloride (PpyCl)	0.1	0.10
Polypyrrole methyl orange (PpyMO)	0.1	0.01
Polypyrrole dexamethasone (PpyDex)	0.1	0.01
Polypyrrole oxacillin (PpyOx)	0.2	0.02

2.3.4 Vapour phase polymerisation of pyrrole on to chitosan

The vapour phase polymerisation (VPP) of pyrrole to form a polypyrrole film with chitosan was investigated as a trial preparation method for obtaining greater yields. Winther-Jensen *et al.*⁸ reported the successful VPP of pyrrole and a similar protocol was

followed in this work. The chitosan film was prepared by pipetting 10 cm³ of 0.5% (w/v) chitosan solution onto a transparent PVC sheet. The film was dried under an IR lamp (55-60 °C) for 15 min. A solution of 0.5 mol dm⁻³ ferric chloride hexahydrate (FeCl₃·6H₂O, Sigma-Aldrich) in methanol was prepared as the oxidising agent. The chitosan film was peeled from the PVC and pre-treated by dipping the film into the oxidising solution and let air dry. The film was suspended over 1 cm³ of pyrrole monomer in a closed sample vial for 5 min at room temperature, 23 ± 2 °C. The polymerisation was observed instantaneously. The film was washed in methanol to remove unreacted oxidant, pyrrole monomer and by-products (FeCl₂).

2.4 Experimental techniques

A number of different techniques were employed in the formation and characterisation of the polypyrrole films and the polypyrrole with chitosan films. These techniques are described in this section.

2.4.1 Potentiostatic technique

In this experiment, a constant potential is applied to the electrode and the resulting current is measured as a function of time, $I = f(t)$. The experiment can be performed for a fixed duration or until a particular current or charge is reached. The data acquisition rate was set at five points per second. This technique was used as the preferred method to deposit the polymer films by applying a constant potential of 0.80 V vs. SCE to the electrode in the monomer-containing solution. Typical plots are shown in Figure 2.4, which depict the current-time response, the corresponding charge-time plot and the potential variation with time during the oxidation of the pyrrole. Sometimes it is more informative to plot the charge passed as a function of the time, as shown in Figure 2.4. The charge can be calculated at any time from the integral of the current.

It is well known that Ppy is reduced with the application of a cathodic potential and the dopant (depending on size) is forced out of the polymer so the polypyrrole can maintain its neutrality ($\text{Ppy}^+\text{A}^- + \text{e}^- \rightarrow \text{Ppy}^0 + \text{A}^-$)⁹. In this work constant potentials were applied,

varying from 0.3 V (a potential greater than the open-circuit potential) to 0.00 V, -0.30 V, -0.60 V and -0.90 V vs SCE, to reduce the polymer films and release the dopant species.

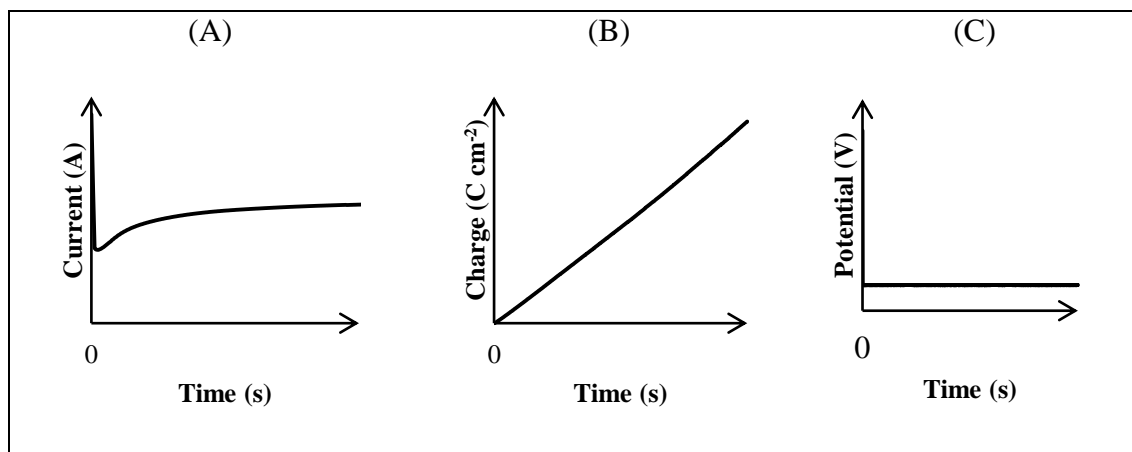


Figure 2.4: Potentiostat transients for the oxidation of pyrrole at 0.80 V vs. SCE (A) the current-time plot (B) the charge-time plot used to determine the total charge consumed on oxidation and (C) step waveform applied.

2.4.2 Cyclic voltammetry

Cyclic voltammetry (CV) is one of the most useful and widely applied techniques in electrochemistry¹⁰. It involves sweeping the applied potential between two potential limits at a constant scan rate and the resulting current is monitored. In this study, it was used to evaluate the suitability and the stability of the dopant species, i.e., its redox stability within the limits of proton reduction and water oxidation and to determine the redox behaviour of the polymer films.

In cyclic voltammetry, there are three main responses that depend on the reversibility of the redox process and each response is characterised by a different shape of the voltammogram, as shown in Figure 2.5. Adsorption processes can also be identified and these give rise to a different shape of the voltammogram, as shown in Figure 2.5(d). Three

key parameters, the peak current (I_p), the peak potential (E_p), and the potential width at half peak ($E_p - E_{p/2}$) are used to describe the reversibility of the redox process. The dependence of each parameter on the scan rate, ν , allows further characterisation of the electrochemical system. The E_p does not change with ν for reversible (Nernstian) systems, however for irreversible and quasi-reversible redox processes E_p increases with increasing ν . The I_p changes linearly with $\nu^{1/2}$ for reversible and quasi-reversible systems and with ν for reversible adsorbed species. The correlation between I_p and $\nu^{1/2}$ for quasi-reversible systems depend on scan rate and the electron transfer rate constant. Generally there is no correlation between I_p and $\nu^{1/2}$ at high scan rates and for reactions which display slow electron transfer kinetics¹¹. The cyclic voltammogram shown in Figure 2.5 (a) is an example of a reversible reaction. A reversible cyclic voltammogram can be obtained if both the oxidation and reduction species are in equilibrium with one another and if the kinetics of the electron transfer process is fast. A theoretical expression for the peak current for a reversible cyclic voltammogram can be derived as a function of the scan rate to give the Randles-Ševčík expression¹² (Equation 2.2). According to this relationship, the dependence of the peak current, I_p , on the scan rate, ν , follows a characteristic square-root law, which provides evidence of the presence of a diffusional-controlled process¹².

$$I_p = 0.4463nFAc_B^* \sqrt{\frac{nF\nu D}{RT}} \quad (2.2)$$

In this equation, n is the number of electrons, F is Faraday's constant, A is the electrode area (cm^2), c_B^* is the bulk concentration of the electrolyte (mol cm^{-3}), ν is the scan rate (V s^{-1}) and D is the apparent diffusion coefficient ($\text{cm}^2 \text{s}^{-1}$). It can be seen that the peak current is proportional to the concentration of the electroactive species and the square-root of the scan rate and diffusion coefficient. Therefore, a linear relationship between the current and the square-root of the scan rate indicates that the redox reaction of the electroactive species conforms to the Randles-Ševčík equation and is governed to some extent by a diffusion-controlled process.

Figure 2.5 (A) represents a reversible reactions, the ratio of the peak currents, $|I_{pa}/I_{pc}| = 1.0$ and the difference in the peak potentials, $\Delta E_p = 2.218RT/nF = 57/n$ mV at 298 K, and is independent of scan rate¹⁰. Figure 5.2 B shows an irreversible reaction the potential width at half peak, $|E_p - E_{p/2}| = 48/\alpha n$ mV at 298 K and increases as the scan rate increases¹³. If the charge transfer processes at the interface are slower, then the equilibrium condition does not prevail, and the reaction becomes quasi-reversible, as shown in Figure 2.5 (C). In this case, $|E_p - E_{p/2}| = 26\Delta(\Lambda, \alpha)$ mV at 298 K and increases as the scan rate increases⁷. The factor $\Delta(\Lambda, \alpha)$ is a function of α and Λ , where α is the transfer coefficient and $\Lambda = k^0/(vDF/RT)^{1/2}$, D is the diffusion coefficient of the electroactive species and k^0 is the standard heterogeneous rate constant, for quasi-reversible systems k^0 is between 1×10^{-1} and 1×10^{-5} cm s⁻¹. As Λ increases the properties become reversible¹⁴. Reversible voltammograms are not always governed by diffusional processes; Figure 5.2 (D) shows the voltammogram of an adsorption response, here $\Delta E_{p/2} = 90/n$ mV. The diagnostics for these systems are covered in many text books^{7, 10, 15, 16}.

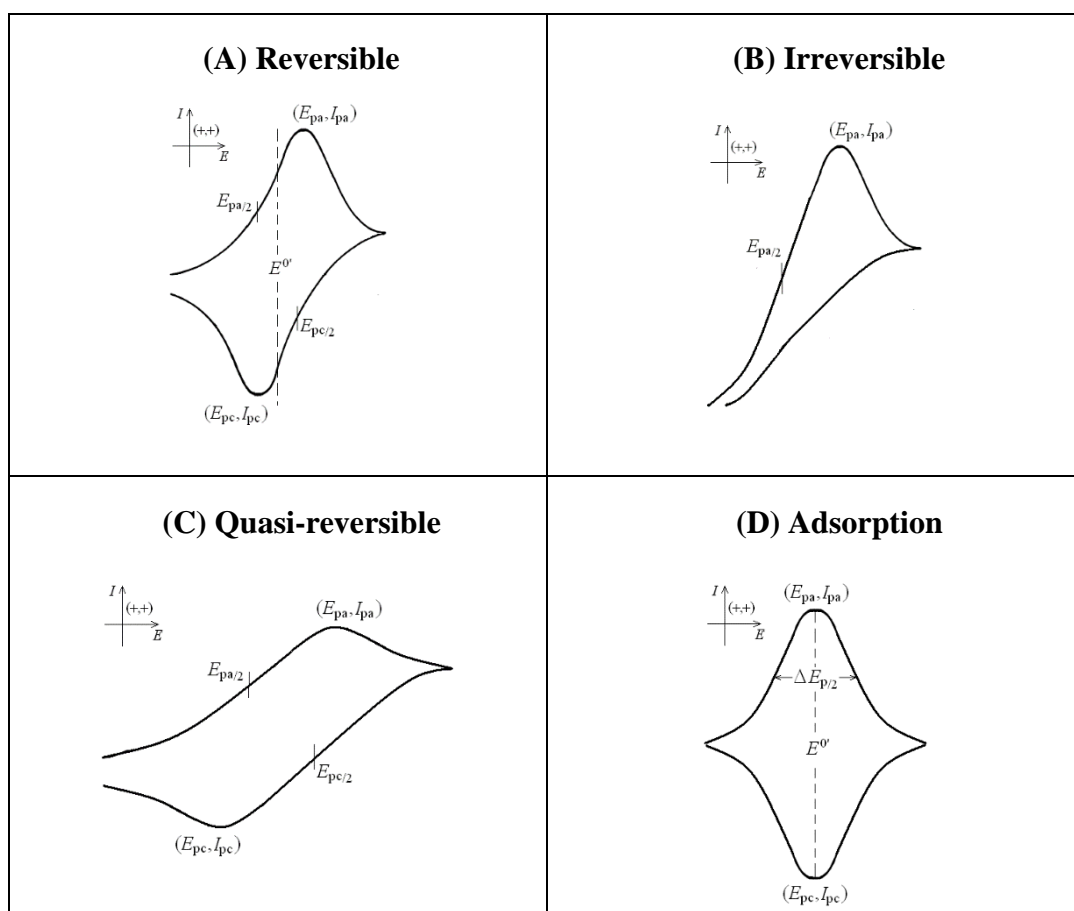


Figure 2.5: Cyclic voltammograms (CV) for (A) Reversible, (B) Irreversible, (C) Quasi-reversible and (D) Adsorption processes showing the peak current (I_p), peak potential (E_p), and potential width at half peak ($E_p - E_{p/2}$).¹¹

2.4.3 Open-circuit potential

In open-circuit potential experiments the “free” potential of the cell is monitored as a function of time. The experiment can be performed for a fixed duration or until a particular potential is reached, the result is a potential-time plot. The data acquisition rate was set at one point per second. This technique was used to determine the potential of the polymers and monitor changes in the oxidation state over a period of time in various solutions. It was also used to investigate the anion leaching from the polymer films (drug release without electrical stimuli). In this case a magnetic stirrer was used to aid diffusion of the released dopant at the electrode surface.

2.4.4 Electrochemical impedance spectroscopy (EIS)

Electrochemical impedance spectroscopy, EIS, was used to investigate the charge transfer resistance, double layer capacitance, redox capacitance or charge storage capacitance, and conductivity of the Ppy doped with various anionic species, and in the presence of chitosan. Experiments were recorded over a frequency range from 65,000 to 0.008 Hz at various applied potentials, this frequency range was sufficient to capture. As impedance is only applicable to electrochemical systems that behave linearly and are in a steady state condition, the polymer films were conditioned for 120 min to ensure the system was under steady-state conditions before the measurements were performed. Furthermore, the perturbing sinusoidal voltage was maintained at 10 mV, which is sufficiently small to keep the overall state of the system unchanged. The frequency of the AC wave was varied allowing the impedance of the system to be obtained as a function of frequency.

The underlining principle of EIS is that it is a transfer function between potential and current as shown in Equation 2.3.

$$E(t) = \Delta E \sin(\omega t) \xrightarrow{Z(\omega)} I(t) = \Delta I \sin(\omega t + \theta) \quad (2.3)$$

In this analysis, ω ($\omega = 2\pi f$, f is the frequency) is the angular frequency of the sinusoidal potential perturbation, and θ is the phase difference (phase angle, phase shift) between the potential and current. The impedance (Z) is defined using Equation 2.4, where Z' and Z'' are the real and imaginary components of Z , respectively, and $i = (-1)^{1/2}$.

$$Z = \frac{E(t)}{I(t)} = Z' + iZ'' \quad (2.4)$$

Impedance data can be plotted with the imaginary impedance (Z'') versus the real impedance (Z') at each sampled frequency giving a complex plot or the Nyquist plot, or the data may be plotted as the logarithm of the total impedance, $|Z|$, and the phase angle, θ , versus the logarithm of the frequency, giving a Bode plot. Typical Nyquist and Bode plots are shown in Figure 2.6. Once collected, the impedance data are usually fitted to equivalent circuits. The aim in fitting the experimental data to an equivalent circuit is to mimic the impedance response, where each circuit element is selected to correspond to a real physical component in the electrochemical cell.

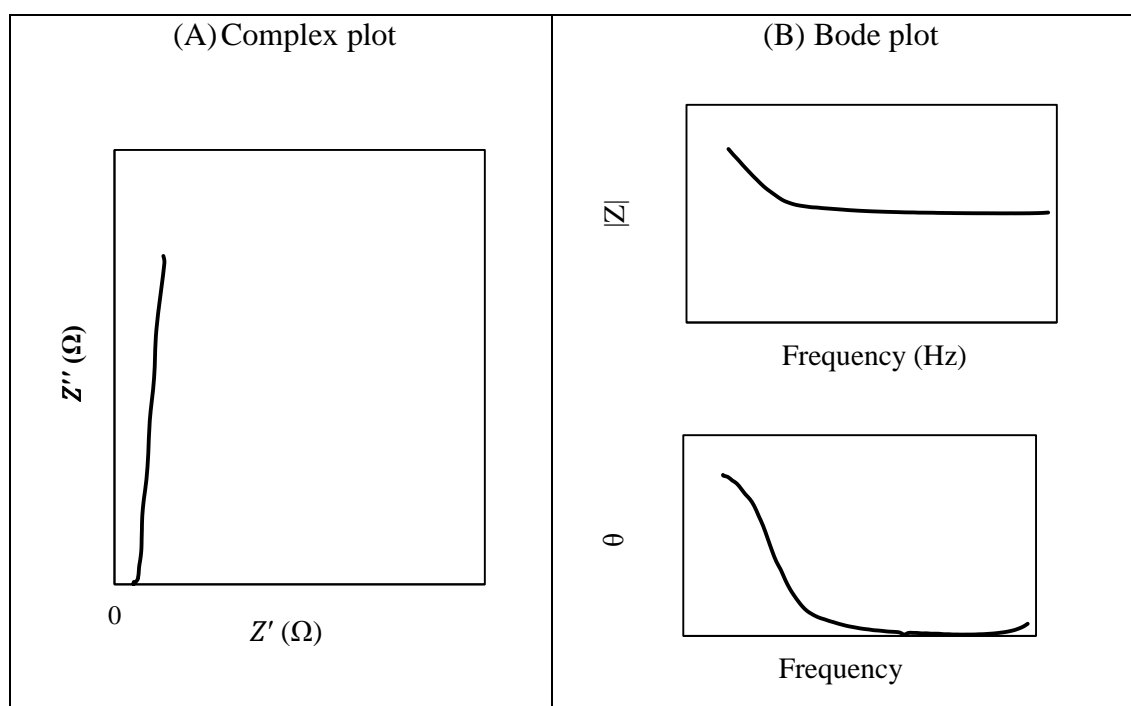


Figure 2.6: The impedance response of a typical polypyrrole film (A) complex plot or “Nyquist” plot and (B) the Bode plot.

The Zview software was used to fit the experimental data to equivalent electrical models. Initial estimates of the required parameters were obtained and then refined using a non-linear least square iterative process to improve the fit for the experimental data, the number of iterations was 100. Representative equivalent circuit model used in this study are presented in Figure 2.7. The two main circuit elements used were resistors and constant phase elements. The Zview software computes values for each component and estimates the error and % error by testing several solutions close to the best fit value by determining how much the value must change before the goodness of fit begins to decrease.

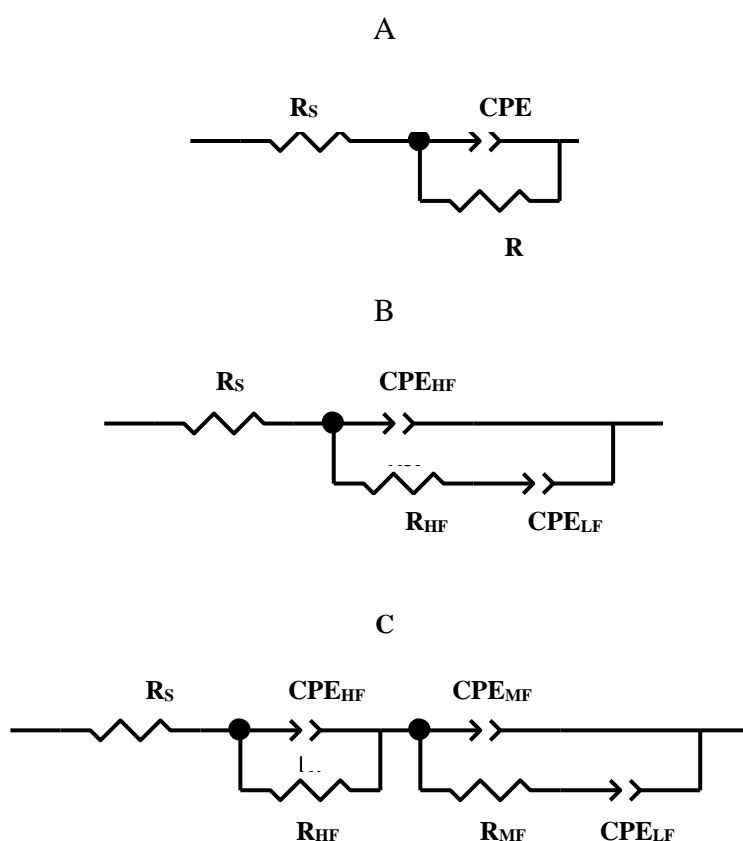


Figure 2.7: Electrical equivalent circuit model, where R_s is the solution resistance, CPE_{HF} is the constant phase element used at high frequency, R_{ct} is the charge-transfer resistance and the CPE_{LF} is the constant phase element at low frequency.

The sum of squares (SS), sum of the squared deviations, and chi-squared (χ^2) values were used to test whether the data were well described by the hypothesised function, i.e., it determines the goodness of fit. These important statistics are presented in the data tables of parameters for the circuit elements evaluated by fitting the impedance data to suitable equivalent circuits. As the system becomes more complex further circuit elements are added, and as a result the % error increases. For more complicated models a 10 % error was acceptable if the sum of squares < 1.0 , however for simpler circuits, the error were less than 5 %.

A resistor has no imaginary component therefore its magnitude is equal to the impedance of the system. Constant phase elements (CPE) define the inhomogeneity of the surface in EIS experiments and are often used to determine the capacitance of the interface¹⁷. A CPE has two parameters: T, an actual value, and α which is an exponent, as shown in Equation 2.5, where ω is the angular frequency.

$$\frac{1}{Z} = Y = T(i\omega)^\alpha \quad (2.5)$$

The magnitude of the exponent gives information on the nature of the physical processes¹⁸. For $\alpha = 1.0$, the CPE behaves as a capacitor, when $\alpha = 0$ the CPE behaves as a resistor, when $\alpha = 0.5$ diffusion processes are evident and for $\alpha = -1.0$, the CPE behaves as an inductor. When $\alpha = 1.0$, T has units of capacitance, $F \text{ cm}^{-2}$. When $\alpha \neq 1.0$, T has units of $\Omega^{-1} \text{ cm}^{-2} \text{ s}^\alpha$. When determining interfacial or double layer capacitance at high frequency (C_{HF}) it is incorrect to equate the CPE1-T as capacitance. Hsu and Mansfield¹⁹ proposed the use of Equation 2.6 for the correction of capacity to its real value when the CPE and R are parallel.

$$C_{\text{HF}} = T_{\text{HF}}(\omega''_{\text{max}})^{\alpha-1} \quad (2.6)$$

Jovic *et al.*²⁰ concluded that only in the case of a CPE and R parallel connection is Equation 2.6 valid. Huang *et al.*^{21, 22} developed Equation 2.7 which is an adaption from

the relationship used by Brug *et al.*²³ between the CPE1-T parameter and interfacial capacitance for a CPE and R in series.

$$\text{corrected } C_{\text{HF}} = T_{\text{HF}}^{(1/\alpha)} \left(\frac{R_s R_T}{R_s + R_T} \right)^{1/\alpha} \quad (2.7)$$

According to Orazem and Tribollet²⁴ Equation 2.7 is the most accurate for a disc electrode exhibiting faradaic behaviour and so it was used in this work to calculate the double layer capacitance at high frequency, C_{HF} .

The low frequency capacitance which is related to the charge storage in the film²⁵⁻²⁷, was estimated from the Bode plot. The data were normalised to the surface area and the solution resistance was found from the fitting. The solution resistance was then subtracted from the transmission line and an estimate of the capacitance was obtained from the Bode plot, where $|Z|$ is plotted against the logarithm of frequency in radians. The estimated capacitance at low frequency was calculated using the expression in Equation 2.8 where ω is the frequency and $|Z|$ is the y-intercept at $\omega = 1$ ($\log(\omega) = 0$).

$$|Z| = \frac{1}{\omega C} \quad (2.8)$$

At low frequency the magnitude of the impedance $|Z|$ changes linearly with the reciprocal of the angular frequency and thus the capacitance, C_{LF} , can be estimated directly from the Bode plot ($C_{\text{LF}} = 1/\text{slope}$). The calculation for determining C_{LF} is independent of film thickness^{28,29}. The circuit element R_{HF} represents resistance, or charge-transfer resistance, at high frequency which contains contributions from the electronic and ionic resistance³⁰, shown in equation 2.9. The total resistance, R_T , was computed using the expression in Equation 2.10 for resistors in series³¹.

$$R_{\text{HF}} = R_e + R_i \quad (2.9)$$

$$R_T = R_{HF} + R_{MF} \quad (2.10)$$

This resistance was then used to calculate the conductivity³¹, σ_T , as shown in Equation 2.11, where d is the nominal thickness of the dry film.

$$\sigma_T = \frac{1}{R_T} \times \frac{d}{A} \quad (2.11)$$

2.4.5 Electrochemical quartz crystal microbalance (EQCM)

EQCM is an acoustic wave microsensor that is capable of ultrasensitive mass measurements³². Under favourable conditions, a typical QCM can measure a mass change of 0.1 to 1.0 ng. This technique was utilised to obtain additional information on the polypyrrole films with chitosan and secondly to obtain the doping levels of oxacillin within the polypyrrole film. All EQCM experiments were carried out on a Chi440 EQCM and the equipment consisted of a quartz crystal oscillator, a potentiostat with a frequency counter and a computer. A schematic diagram, indicating the various components of the EQCM set-up, is shown in Figure 2.8. The polymers were deposited onto polished Au quartz crystal electrodes (Cambria Scientific) with an exposed surface area of 0.20 cm². The electrochemical cell consisted of a specially made PTFE holder in which the crystal was placed between two O-rings. The PTFE cell was assembled by carefully screwing the PTFE holder and PTFE cell body together.

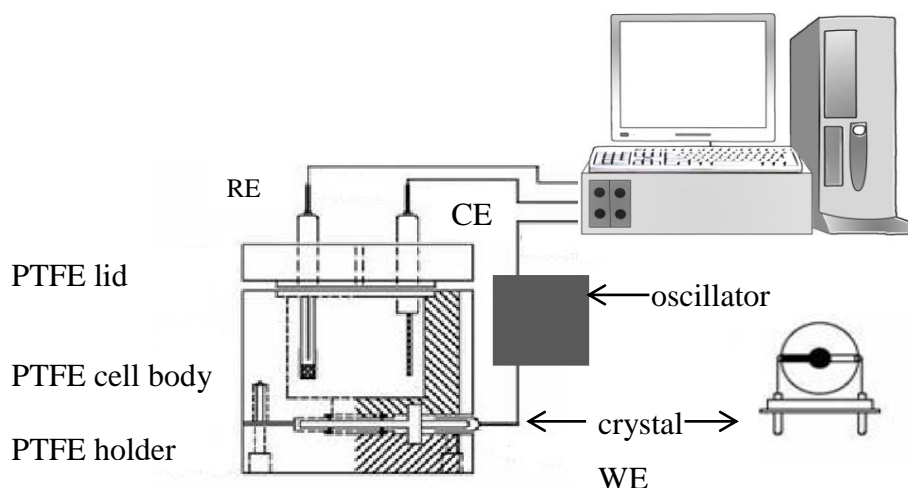


Figure 2.8: Schematic representation of a typical EQCM instrument. The top view of the EQCM-crystal is also shown³³.

During each experiment only one side of the metal electrode surfaces is in contact with the electrolyte. The quartz crystal is supported by two wires, one to carry current to the gold layer and the other to allow for crystal vibration and to record the frequency. The set-up is completed using a platinum wire counter electrode and a custom made Ag|AgCl reference electrode. In EQCM measurements, the frequency of the oscillating quartz crystal is monitored. Changes in the frequency are observed as the mass of the crystal changes³⁴. The changes in frequency are related to the changes in mass through the Sauerbrey equation³⁵, which is given as Equation 2.12.

$$\Delta f = f_c - f_o = - \frac{2f_o^2 \Delta m}{A(\rho_q \mu_q)^{1/2}} = -C_f \Delta m \quad (2.12)$$

Here, f_o is the resonant frequency, Δm is the mass change, A is the acoustically active area of the electrode, 0.203 cm^2 , ρ_q is the density of the quartz, 2.648 g cm^{-3} , and μ_q is the shear modulus of the quartz, $2.947 \times 10^{11} \text{ g cm}^{-1} \text{ s}^{-2}$. In this equation the change of resonant frequency (Δf) is related to the change in mass (Δm) per unit area (A) times a constant. The frequency, therefore, decreases as the mass increases. The frequency is also sensitive to changes in the viscosity of the film and the Sauerbrey equation is only valid for rigid thin layers³⁶. As a general rule, the equation is valid provided that the mass

change, Δm , is less than 1 % of the mass of the quartz crystal. It does not take into account solvent participation and it also assumes the current efficiency for the electropolymerisation of the monomer is 100 %¹⁰. The EQCM allows the simultaneous recording of the current-potential and mass changes at the AT-cut quartz crystal electrode. The technique can be used to measure the mass-to-charge ratio of electrodeposited materials and compare it to theoretical values in order to identify their nature. The potentiostatic deposition of a generic compound can be outlined as follows:



The average mass-to-charge ratio R for the electrodeposition of C is given by Equation 2.13 a derivation of Faraday's law, to estimate the doping levels of anions in polypyrrole³⁷.

$$R = \frac{\Delta m_C}{|Q_C|} = \pm \frac{M(C)}{nF} \qquad (2.13)$$

Here, Δm_C and Q_C are the experimental mass and charge of deposition calculated from the frequency change and the time integral of the current, respectively. The ratio R is simply the deposited mass per unit of charge (g C^{-1}), and it corresponds to the ratio of the molar mass of the deposit, $M(C)$, and the charge consumed per mole of it, nF . The absolute value of Q_C is used in order to obtain $R > 0$ for increasing mass ($\Delta m_C > 0$) and $R < 0$ for decreasing mass ($\Delta m_C < 0$) for both oxidation ($Q_C > 0$) and reduction ($Q_C < 0$) processes¹¹.

2.4.6 Scanning electron microscopy (SEM) with energy dispersive X-Ray (EDX) Analysis

The morphology of the materials was analysed using scanning electron microscopy. Scanning electron microscopy (SEM) produces high resolution micrographs of a surface. SEM micrographs appear as 3-D images and are therefore useful for analysing the surface structure of the sample. The primary electrons coming from the source strike the surface of the sample to generate different types of signals categorised by elastic or inelastic

interactions³⁸, as shown in Figure 2.9. The elastic scattering results from the deflection of incident electrons by atomic nuclei or shell electrons with similar energy. This, in turns, results in backscattered electrons (BSE) with negligible energy loss and scattering angles larger than 90° . The inelastic scattering results from interactions of the incident electrons with the nuclei and core electrons of the material, and generates signals with substantial energy loss. Auger electrons and X-Ray emissions belong to this group. The incident beam has a characteristic penetration volume in the sample and each signal originates from a different part of the sample. The BSE electrons have sufficient energy ($E > 50$ eV) to emerge from underneath the sample surface. Images generated from BSE electrons are characterised by Z contrast, with the brightness of the elements proportional to the atomic number (Z) as the backscattering yield increases with increasing Z. The resolution of these images is of the order of $1\ \mu\text{m}$ because of the high energy of the BSE electrons. The secondary electrons, SE, have lower energy ($E < 50$ eV) and consequently give topographical information of the sample surface. The low energy of SE electrons allows a resolution of about $100\ \text{nm}$ ³⁹.

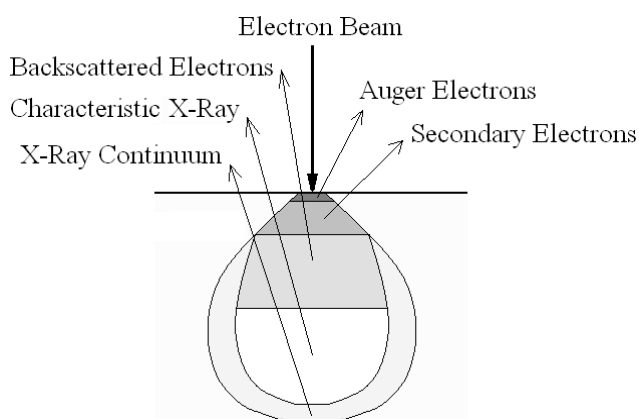


Figure 2.9: Schematic representation of the electron-material interaction in scanning electron microscopy (SEM)⁴¹.

Auger electrons are emitted from atoms ionised by the incident electron beam and their energy is characteristic of the elements. The characteristic X-Ray signal is used to perform the chemical microanalysis of the sample surface. This technique is called energy dispersive X-Ray (EDX) analysis. Energy dispersive X-Ray analysis (EDX) is routinely carried out in combination with SEM. EDX allows the micro-elemental analysis of the top few micrometers of the sample. X-Ray signals are generated when the high-energy

electron beam hits the sample surface. A characteristic X-Ray signal is produced from the interaction of a beam electron with an inner shell electron of the sample. The inner electron is ejected and replaced by an outer shell electron. This process gives rise to the emission of X-Rays with energies corresponding to the energy separation of the levels involved in the electronic transition. Since each element has its characteristic orbital energies, the X-Rays emitted by the sample are related to its chemical composition. An X-Ray continuum is also generated by the deceleration of the beam electrons which gives the broad background signal present in all EDX spectra. This background has much lower intensity than the elemental peaks and does not represent an issue in the qualitative analysis of the samples. The transitions involved in the characteristic X-ray emission are labelled after the K, L, M, N electronic shells. The EDX lines are also named α , β or γ depending on which outer shell electrons make the transition to fill the electron vacancy. Transitions of electrons immediately after the emptied level are α , the following level are β and γ in order of increasing energy. An EDX spectrum consists of a series of peaks at a specific energy depending on the chemical element and with intensity proportional to the number of counts. The number of counts is proportional to both the amount of chemical element in the sample and to the energy carried by the associated X-Ray signal. The resolution of the EDX probe is given by the size of the volume of interaction of the electron beam with the sample. The size is usually a few microns. The interaction of the BSE electrons with the surrounding zones of the probed point (the beam spot) can cause the emission of X-Rays that add up to the signal belonging to the point of analysis, as shown in Figure 2.10. The extent of such interference is a major limitation that affects the quantitative analysis³⁹. A quantitative EDX analysis is practicable only with high-quality flat-polished sample surfaces, and it must be performed against a known standard prepared and analysed in the same way. Quantitative analysis is possible by comparison of relative peak heights of the sample and a standard of known composition measured under the same conditions, however various correction factors due to matrix effects must be taken into account in order to obtain reliable data.

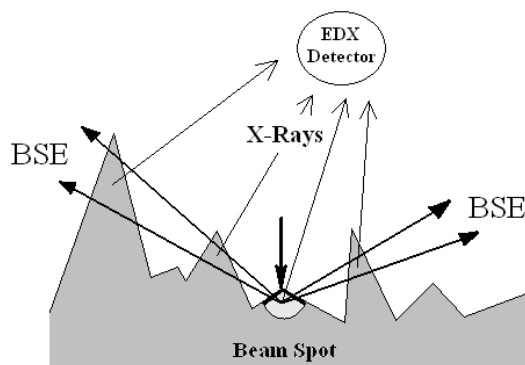


Figure 2.10: Schematic illustration of the effect of the surface roughness on the detection of the X-Ray signal¹¹.

A Hitachi S-3200-N microscope equipped with an Oxford Instrument INCAx-act EDX system was used to analyse the composite materials. Most of the films were too thin to remove from the electrode surface without compromising the integrity of the material, so it was necessary to customise disc electrodes. The customised electrodes had a short shaft modified with threads and an adaptable aluminium sample holder was made with compatible threads so that the electrode easily screwed into it. In order to achieve high resolution micrographs the samples were sputter coated with a thin film of gold (1.5 nm) with an AGAR Automatic Sputter Coater coupled to an AGAR Terminating Film Thickness Monitor unit.

2.4.7 Differential scanning calorimetry (DSC)

A PerkinElmer Pyris 6.0 DSC controlled by Pyris Data software was used to measure and to record the thermal properties and heat capacity (C_p) of the polymer films. The temperature range studied in this work was between 20 and 450 °C. A heating rate of 2 °C min⁻¹ was used and all samples were maintained under nitrogen during the analysis.

DSC is a thermoanalytical technique that compares the difference in the amount of heat (Δq) required to increase the temperature of a sample and a reference (ΔT), with a well-defined heat capacity, measured as a function of temperature, Equation 2.14.

$$(Cp) = \frac{\Delta q}{\Delta T} \quad (2.14)$$

A typical set-up is shown in Figure 2.11. A 1 mg of the sample was weighed and hermetically sealed in aluminium pans and both the sample and reference were maintained at the same temperature throughout the experiment. When the sample undergoes a physical transformation, such as a phase transition or thermal decomposition, heat must flow to or from the sample and this depends on whether the process is exothermic or endothermic. The difference in heat flow between the sample and reference also delivers the quantitative amount of energy absorbed or released during the transitions. This information can be obtained by integrating the endothermic and exothermic peaks.

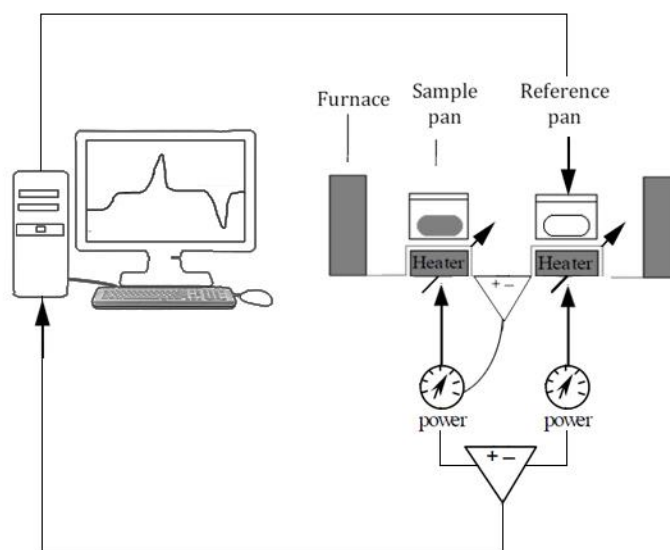


Figure 2.11: Schematic diagram of a DSC.

2.4.8 Fourier transform infrared spectroscopy (FT-IR)

Infrared spectroscopy is used for structural analysis as the functional group bands appear in the same range regardless of the molecular structure of the compound. The bands recorded in the low frequency region or the “fingerprint region”, from 700 to 1500 cm^{-1} ,

result from combined bending and stretching motions of the atoms and are unique for each compound. A PerkinElmer 2000 FT-IR model driven by Spectrum™ software was used to record the FT-IR data. All samples were prepared as potassium bromide pellets and were scanned between 4000 and 450 cm^{-1} , using an average of 8 scans and 4 cm^{-1} resolution. The spectra were compared to a background which was recorded of the air and under the same measurement conditions.

2.4.9 Ultra violet visible spectroscopy (UV-Vis)

UV-visible spectroscopy measures the amount of ultraviolet and visible light transmitted or absorbed by a sample placed in a spectrometer. The wavelength at which a chemical absorbs light is a function of its electronic structure and the intensity of the light absorption is related to the amount of the chemical species between the light source and the detector. In addition, UV-visible spectra can be used to identify some chemical species. A Varian Cary® 50 UV-Visible spectrometer controlled by Cary WinUV was used to record the UV-visible data. This spectrometer has a Xenon lamp and a maximum scan rate of 24 000 nm min^{-1} . The scan mode was used to identify the maximum absorption (λ_{max}) and measure the amount of the dopant species released from the polymer films. The spectrum was scanned between 600 and 300 nm for methyl orange and between 400 and 200 nm for oxacillin, as the λ_{max} values vary with the nature of the drugs, Table 2.2. The spectra were collected and analysed to calculate the amount of drug released upon application of a reduction potential or at the open-circuit potential. A quartz cuvette with a diameter of 1 cm was used for oxacillin and dexamethasone, while plastic disposable cuvettes were used for methyl orange detection. The amount of dopant released was determined by measuring the absorbance at the wavelength of maximum absorption (λ_{max}) for the drug in question and applying the Beer-Lambert law⁴⁰, Equation 2.15.

$$A = \log_{10} \left(\frac{P_{\lambda}^0}{P_{\lambda}} \right) = \epsilon cl \quad (2.15)$$

Here, A is the absorbance, P_{λ}^0 is the power of incident radiation, P_{λ} is the power of transmitted radiation, ϵ is the molar absorption coefficient, l is the path length and c is the concentration of the compound in solution. Calibration curves were generated for each drug. The slope was calculated from the linear relationship between the concentration and the absorbance.

Table 2.2: Summary of the λ_{\max} values for the drug.

Compound	λ_{\max} (nm)
Methyl Orange	465
Oxacillin	205

2.4.10 Adhesion tests of the polymer coatings

The adhesion of polypyrrole to a metal substrate is vital to its application as a biomaterial particularly where good electrical contact is necessary for stimulated drug delivery. A simple qualitative peel test was used to determine the adhesive properties of the polymers on the metal substrate. This peel-test, described by Idla *et al.*⁴¹, involves the application of a clear pressure sensitive tape (sellotape™) to the polymer and rapidly peeling it away. If the coating remains intact it is considered adhesive while it is considered non-adhesive if the coating delaminates partially or wholly.

2.4.11 Wettability test of polymer coatings

The wettability (hydrophilicity) of a surface can be determined with the use of contact angle measurements with deionised water, the lower the contact angle, the more wettable (hydrophilic) the surface⁴². Contact angle measurements were made using the sessile drop technique analysed with the goniometer method using the FTA 1000 software package. A drop of deionised water is applied on the samples. The software uses the contrast between the light and dark regions to calculate the contact angle of the droplet.

2.4.12 Data-handling and statistics

The data acquired from the experimental techniques are automatically stored as either binary files (.bin) or ASCII text files (.txt) so it was necessary to manually translate the data files into excel files (.xls) for mathematical and statistical analysis. The standard error bars are expressed in absolute units of measurement, represented by the standard error of the mean ($SE_{\bar{x}}$), i.e., standard deviation (s) divided by the square root of the sample size (n), as shown in Equation 2.16.

$$SE_{\bar{x}} = \frac{s}{\sqrt{n}} \quad (2.16)$$

Percent standard errors are expressed as a relative measured values $SE_{\bar{x}}(\%)$, where \bar{x} is the mean (Equation 2.17).

$$SE_{\bar{x}}(\%) = \frac{SE_{\bar{x}}}{\bar{x}} \times 100 \% \quad (2.17)$$

All experiments were carried out in triplicate unless otherwise stated.

References

1. G. Kickelbick, *Hybrid materials: synthesis, characterization and applications*, Wiley-VCH, 2007.
2. G. Inzelt, in *Electroanalytical Methods*, ed. F. Scholz, Springer Berlin Heidelberg, 2010, ch. 7, pp. 147-158.
3. M. Faraday, *Philosophical Transactions of the Royal Society of London*, 1834, **124**, 77-122.

-
4. F. C. Strong, *Journal of Chemical Education*, 1961, **38**, 98-98.
 5. A. Hickling, *Transactions of the Faraday Society*, 1942, **38**, 27-33.
 6. G. D. Christian, *Analytical chemistry*, Wiley, 2004.
 7. A. J. Bard and L. R. Faulkner, *Electrochemical methods. Fundamentals and applications*, Wiley, 2001.
 8. B. Winther-Jensen, J. Chen, K. West and G. Wallace, *Macromolecules*, 2004, **37**, 5930-5935.
 9. K. Kontturi, P. Pentti and G. Sundholm, *Journal of Electroanalytical Chemistry*, 1998, **453**, 231-238.
 10. F. Scholz and A. M. Bond, *Electroanalytical methods guide to experiments and applications*, Springer, 2010.
 11. E. Andreoli, *PhD Thesis*, NUI Maynooth, 2010.
 12. C. M. A. Brett and A. M. C. F. Oliveira Brett, *Journal of Electroanalytical Chemistry and Interfacial Electrochemistry*, 1989, **262**, 83-95.
 13. G. Inzelt, *Conducting Polymers A New Era in Electrochemistry*, Springer-Verlag, Berlin, Heidelberg, 2008.
 14. J. Wang, *Analytical Electrochemistry*, Wiley-VCH, 2006.
 15. C. M. A. Brett and A. M. O. Brett, *Electrochemistry: Principles, methods and applications*, Oxford University Press, 1993.
 16. G. Inzelt, Conducting polymers a new era in electrochemistry, <http://dx.doi.org/10.1007/978-3-642-27621-7>.
 17. M. E. Orazem, P. Shukla and M. A. Membrino, *Electrochimica Acta*, 2002, **47**, 2027-2034.
 18. D. D. Macdonald, *Electrochimica Acta*, 2006, **51**, 1376-1388.
 19. C. H. Hsu and F. Mansfeld, *Corrosion*, 2001, **57**, 747-748.
 20. V. D. Jović and B. M. Jović, *Journal of Electroanalytical Chemistry*, 2003, **541**, 13-21.
 21. I. Frateur, V. M.-W. Huang, M. E. Orazem, N. Pébère, B. Tribollet and V. Vivier, *Electrochimica Acta*, 2008, **53**, 7386-7395.
 22. V. M. Huang, S.-L. Wu, M. E. Orazem, N. Pébère, B. Tribollet and V. Vivier, *Electrochimica Acta*, 2011, **56**, 8048-8057.

-
23. G. J. Brug, A. L. G. van den Eeden, M. Sluyters-Rehbach and J. H. Sluyters, *Journal of Electroanalytical Chemistry and Interfacial Electrochemistry*, 1984, **176**, 275-295.
 24. M. E. Orazem and B. Tribollet, *Electrochemical Impedance Spectroscopy*, John Wiley & Sons, Inc., Hoboken, New Jersey, 2008.
 25. G. Garcia-Belmonte and J. Bisquert, *Electrochimica Acta*, 2002, **47**, 4263-4272.
 26. X. Ren and P. G. Pickup, *Journal of Electroanalytical Chemistry*, 1994, **372**, 289-291.
 27. T. Komura, S. Goisihara, T. Yamaguti and K. Takahasi, *Journal of Electroanalytical Chemistry*, 1998, **456**, 121-129.
 28. G. Garcia-Belmonte, Z. Pomerantz, J. Bisquert, J.-P. Lellouche and A. Zaban, *Electrochimica Acta*, 2004, **49**, 3413-3417.
 29. G. Garcia-Belmonte, *Electrochemistry Communications*, 2003, **5**, 236-240.
 30. W. J. Albery and A. R. Mount, *Journal of Electroanalytical Chemistry and Interfacial Electrochemistry*, 1991, **305**, 3-18.
 31. A. Kępas and M. Grzeszczuk, *Journal of Electroanalytical Chemistry*, 2005, **582**, 209-220.
 32. A. R. Hillman, *Journal of Solid State Electrochemistry*, 2011, **15**, 1647-1660.
 33. CH Instruments Inc, <http://chinstruments.com/chi400.shtml>.
 34. D. A. Buttry and M. D. Ward, *Chemical Reviews*, 1992, **92**, 1355-1379.
 35. G. Sauerbrey, *Zeitschrift für Physik*, 1959, **155**, 206-222.
 36. E. J. Calvo and R. A. Etchenique, in *Comprehensive Chemical Kinetics*, eds. R. G. Compton and G. Hancock, Elsevier, 1999, vol. 37, ch. 12, pp. 461-487.
 37. C. K. Baker and J. R. Reynolds, *Journal of Electroanalytical Chemistry and Interfacial Electrochemistry*, 1988, **251**, 307-322.
 38. Y. Ma, *Physical Review B*, 1994, **49**, 5799-5805.
 39. J. Goldstein, D. E. Newbury, D. C. Joy, C. E. Lyman, P. Echlin, E. Lifshin, L. Sawyer and J. R. Michael, *Scanning Electron Microscopy and X-ray Microanalysis*, Springer, 2003.
 40. D. F. Swinehart, *Journal of Chemical Education*, 1962, **39**, 333-335.
 41. J. Reut, A. Öpik and K. Idla, *Synthetic Metals*, 1999, **102**, 1392-1393.

42. K. S. Teh, Y. Takahashi, Z. Yao and Y.-W. Lu, *Sensors and Actuators A: Physical*, 2009, **155**, 113-119.

Chapter 3

Electrochemical synthesis and characterisation of polypyrrole chloride (PpyCl)/chitosan composite films

3. Electrochemical synthesis and characterisation of polypyrrole chloride (PpyCl)/chitosan composite films

3.1 Introduction

Incorporating a natural bioactive material with a synthetic, semi-conducting material is a well-documented strategy for optimising the biological activity in biomedical materials¹. In this chapter, films consisting of a blend of chitosan and polypyrrole were prepared and characterised for their electrical and physical properties. This chapter serves as a baseline study of a polypyrrole-chitosan composite film. Polypyrrole-chitosan composite films were prepared in two ways. The initial goal was to prepare polypyrrole (Ppy) in the presence of chitosan and this was successfully achieved. However, when the inclusion of larger anionic species (A) was investigated (results are presented and discussed in the proceeding chapters) it was found that the PpyA would not grow. A decision was made to grow the PpyA in the absence of chitosan and apply a layer of chitosan at the PpyA interface, post-electropolymerisation. This method has some advantages but the main drawback is the adhesion properties of the composite formed. Most of this chapter is devoted to polypyrrole grown in the presence of chitosan and herein will be denoted as Chit/PpyCl, while the rest of the thesis is devoted to PpyA (where A is the dopant) with chitosan added post electropolymerisation and will be denoted by PpyA/Chit.

Polypyrrole is one of the most extensively studied conducting polymers². The intense focus on polypyrrole is due to its easy synthesis, either through the chemical or electrochemical oxidation of its monomer (pyrrole), compatibility in aqueous systems, its commercial availability and intrinsic properties such as good redox properties, high electrical conductivity and good environmental stability³. Polypyrrole has several potential applications including batteries⁴, electrochemical sensors⁵, conductive textiles and fabrics⁶, electromagnetic interference (EMI) shielding⁷, anti-corrosion coatings⁸⁻¹⁰, mechanical actuators¹¹ and drug delivery¹². However, like other conducting polymers, polypyrrole itself cannot be easily fabricated as a thin film with good mechanical

properties. Polypyrrole blended with other polymers can overcome these practical limitations^{13, 14}. Recently, blends of conducting polymers and hydrogels have received much attention, where these two materials have been integrated and investigated for biomedical applications, such as biosensors^{15, 16} and drug delivery^{17, 18}.

Chitosan is a polysaccharide made up of β -(1 \rightarrow 4)-linked *N*-acetyl-D-glucosamine and D-glucosamine units (Section 1.5, Figure 1.8), it is commercially produced from the deacetylation of chitin, the main component of the exoskeleton of crustacean shells, such as shrimp¹⁹. Chitosan is normally insoluble in aqueous solution above pH 7.0, however, in dilute acids (pH < 6.0) it becomes soluble²⁰. It can be cast into films which possess hydrogel properties and for this reason it has a wide range of applications, such as wastewater treatment²¹, separation membranes²², food packaging²³, wound healing and drug delivery²⁴. The use of chitosan in drug delivery has received much attention as it is a commercially available pharmaceutical excipient due to its biocompatibility²⁵. Chitosan itself is not sufficient to induce healing properties and is usually blended as a component with polyethylene glycol²⁶ or polyglutamic acid²⁷.

Although polypyrrole has emerged as a promising material with substantial potential for biomedical applications²⁸ and as a drug delivery system¹², few of these studies have investigated the ion (biological molecules and drugs) transport within the polypyrrole blended with hydrogel. Even in an unstimulated (absence of an electrical stimulus) environment, polypyrrole can naturally auto undoped²⁹, i.e., the release of anions to maintain charge neutrality.

The first documented polypyrrole-chitosan composite was published by Hitoshi *et al.*³⁰ in 1992. They prepared the composite by oxidative chemical polymerisation in the presence of ferric *p*-toluene sulfonated trihydrate (I) and chitosan. They proposed that the composite could be widely used, particularly as a support material for enzyme immobilisation in biosensors. To date there have been some publications on these composites, usually in the presence of an additional component such as silver nanoparticles³¹, poly(DL-lactide)³² and silica³³. As mentioned previously in Section 1.6, most of these reported composites are produced chemically. In this study, the composite was formed electrochemically as films, using a facile fabrication technique with

reproducible results and a comprehensive study of its electrochemical behaviour. In a more recent publication by Yalçinkaya *et al.*³⁴, the composite was formed electrochemically from an electrosynthesis solution containing chitosan, oxalic acid and pyrrole and applying a sweeping potential technique. Although a preliminary electrochemical evaluation of the composite was presented using cyclic voltammetry, it was difficult to discern redox peaks in the electrochemical data. However, the composite was well characterised using FT-IR and DSC, which is relevant to the work presented in this chapter.

In-situ electropolymerisation of pyrrole has advantages over chemical polymerisation particularly for the immobilisation of biological species, such as neurotrophins³⁵, hyaluronic acid³⁶, enzymes³⁷ (urease and glutamate dehydrogenases) and laminin peptide sequences³⁸. For example, Haung *et al.*³⁹ combined a degradable variation of a polypyrrole-chitosan composite seeded with schwann cells to promote nerve cell adhesion and proliferation with and without an electrical stimuli.

This chapter presents the electrochemical synthesis and characterisation of a polypyrrole chitosan composite using chloride as a dopant. Chloride is a suitable anion because it is the most abundant physiological anion and is not cytotoxic to cells. Fonner *et al.*⁴⁰ studied cell growth viability on Ppy films and found that thick films of polypyrrole doped with chloride performed better than films doped with ToS and PSS. The sequential steps involved in the synthesis of the chitosan-polypyrrole composite are summarised in Figure 3.1. The steps vary from casting the chitosan film, curing the film under an IR lamp to the electropolymerisation of pyrrole. The sequence of steps varies with the formation of Chit/PpyCl or PpyCl/Chit. The results of an impedance study (EIS) are also presented and analysed using appropriate circuit models. On extensive literature review no references were found to contain discussions on the electrochemical properties of polypyrrole and chitosan composites using EIS, however, there are numerous reports on the electrochemical properties of polypyrrole with other polymeric materials^{16, 17, 41-45}. As an example, Aylward *et al.*⁴⁶ have analysed the anion and cation transport in composite films of polypyrrole with a sulfonated silica (ormosil) hydrogel.

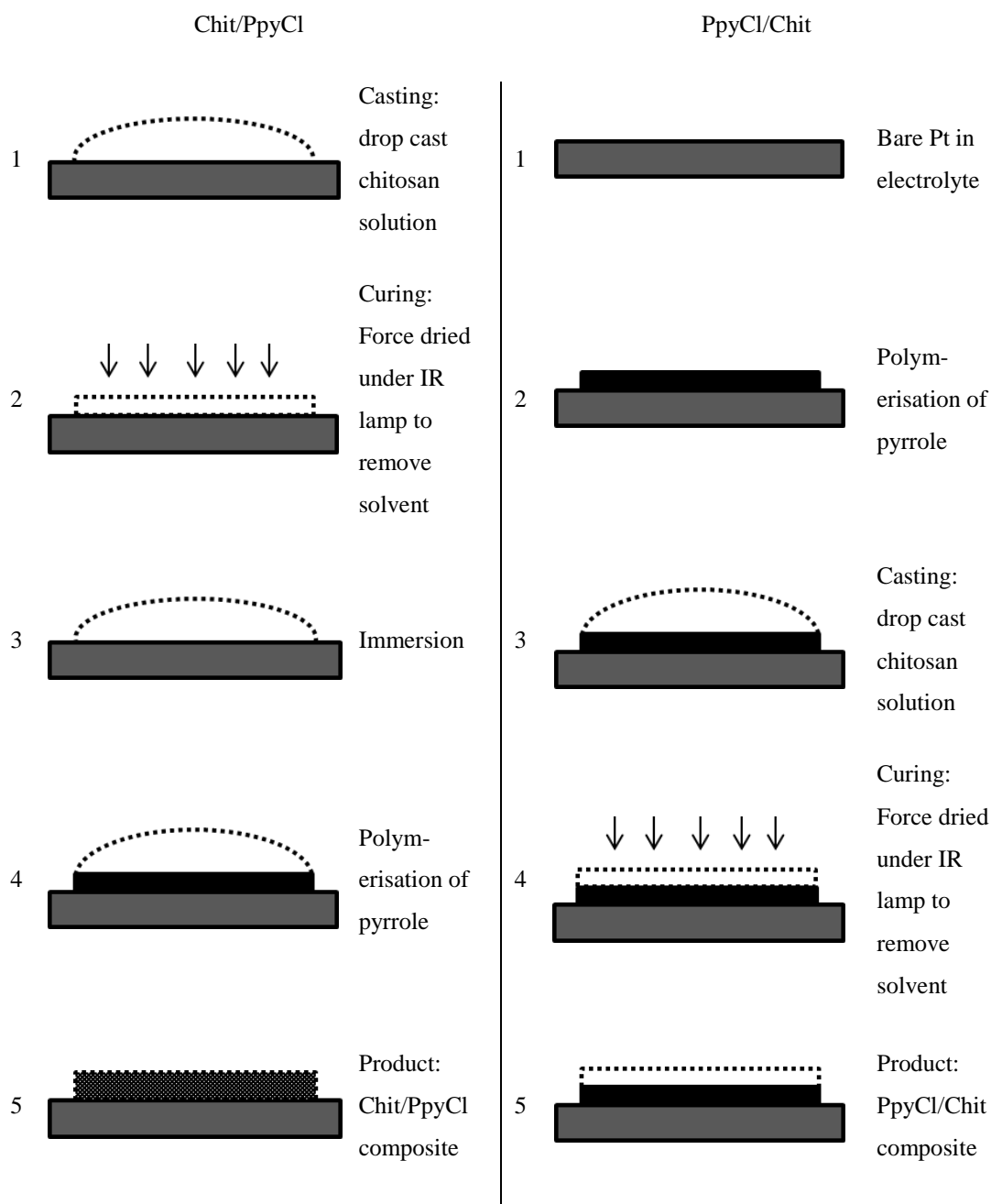


Figure 3.1: Sequential steps in the synthesis of Chit/PpyCl and PpyCl/Chit. Both synthetic routes yield a conducting composite.

3.2 Experimental

All electrochemical experiments were carried out with a conventional three-electrode cell at room temperature ($23 \pm 2^\circ\text{C}$) at atmospheric conditions. All potentials were measured

and are quoted with respect to a saturated calomel reference electrode (SCE). The working electrode was a platinum disc electrode (0.13 cm^2) and the counter electrode was platinum wire ($\gg 0.13 \text{ cm}^2$). Potentiostatic experiments and cyclic voltammetry measurements were carried out on a Solartron 1287. The experiments were controlled by CorrWare and the data were analysed with CorrView. Electrochemical impedance measurements were carried out with a frequency response analyser (FRA), Solartron 1250 or Solartron 1255B, coupled to a Solartron 1287 electrochemical interface. The experiments were controlled by Zplot and the data were analysed with ZView. All instrumentation, software and materials employed were described in Section 2.2.1 and 2.2.2, and the chemicals used were discussed in Section 2.3.1. The wettability tests were performed at the Institute of Technology Tallaght (ITT).

3.3 Results and discussion

3.3.1 Redox stability of a chitosan coated electrode

Cyclic voltammetry was used to gain information on the stability of a chitosan coated Pt electrode (Chit/Pt). The experiments were carried out on a bare Pt electrode and a chitosan coated Pt electrode by cycling the potential between -1.20 V and 1.00 V vs SCE at a scan rate of 50 mV s^{-1} in $0.1 \text{ mol dm}^{-3} \text{ NaCl}$. Typical cyclic voltammograms are shown in Figure 3.2 for bare Pt and Chit/Pt. It is clear that both display similar redox properties which are dominated by H^+ adsorption and $\text{H}_{2(\text{g})}$ evolution between approximately -0.90 V and -1.20 V vs SCE. This indicates that the electrochemistry of the bare Pt is dominant⁴⁷. Interestingly, the small peak centred at -0.45 V vs SCE for the Pt electrode is not evident for the Chit/Pt, which suggests that the chitosan film is stable following 20 cycles in the NaCl solution.

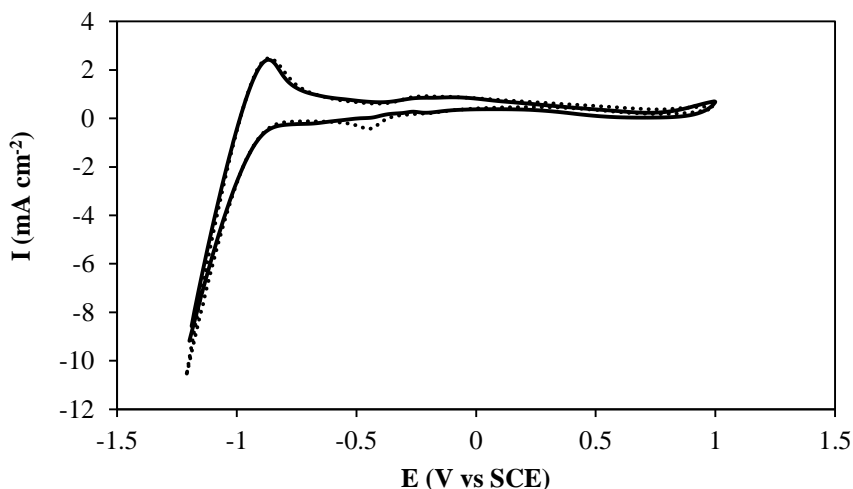


Figure 3.2: Cyclic voltammograms of a chitosan coated Pt electrode (20th cycle), the dashed trace corresponds to the bare Pt electrode in 0.1 mol dm⁻³ NaCl at 50 mV s⁻¹.

3.3.2 Electrochemical synthesis of the chitosan-polypyrrole chloride (Chit/ PpyCl) film

During electrosynthesis of Chit/PpyCl, chloride was incorporated into the polymer film as an anionic dopant. Initial synthesis of Chit/PpyCl was carried out by cyclic voltammetry (data not shown). Pyrrole was found to oxidise at 0.65 V vs SCE with subsequent cycles resulting in an increase in the current indicating that the electroactive polymer was deposited. However, the films produced were uneven and lacked reproducibility and this method was not employed. Galvanostatic growth has been used to prepare conducting polymer films doped with hydrogels⁴⁸. However, in this study all polymer films were synthesised by potentiostatic growth at a constant potential of 0.80 V vs SCE, as described in Section 2.4.1. This approach gave rise to highly reproducibility growth conditions.

The 0.5 % (w/v) of chitosan dissolved in 2.0 mol dm⁻³ acetic acid solution was cast on to the Pt electrode and was cured under an IR lamp for 10 min and let cool for a further 10

min, as illustrated in Figure 3.1. The chitosan coated Pt electrode was immersed in the electrolyte for 60 min prior to electropolymerisation. As shown in Figure 3.3, where data are presented for the formation of PpyCl and Chit/PpyCl, the electropolymerisation of pyrrole (Py) is fast. The current-time profiles for PpyCl and Chit/PpyCl grow to a charge density of 2.2 C cm^{-2} are shown in Figure 3.3 A, these growth profiles are typical of pyrrole electropolymerisation, both current-time plots show an initial increase in the current due to the nucleation of the polymer and a current plateau indicating further film growth⁴⁹. Although not evident in the current-time plots presented in Figure 3.3 A, on application of the potential there is an initial rapid decrease in the current, which arises from the charging of the double layer⁵⁰. This charging current decays rapidly and is followed by the nucleation of the polymer and a rising current transient, resulting from the increasing area available for the electrochemical reaction, as conducting polypyrrole is deposited on the electrode surface⁵⁰. The charge-time plots, presented in Figure 3.3 B, show a linear relationship between the charge and the electropolymerisation rate, indicating that the formation of both the conducting polymers films is successful and the polymers are deposited on the electrode surface^{47, 51}. A high degree of reproducibility was achieved using this approach, both the current and charges recorded were essentially identical.

Although the profiles presented in Figure 3.3 are similar for the PpyCl and Chit/PpyCl, a slightly lower rate of electropolymerisation is evident during the first 5 to 10 s for the Chit/PpyCl film, which corresponds to the nucleation of the film on the electrode substrate⁵². During the first 10 s the PpyCl grows rapidly, indicating efficient electropolymerisation. Although the rate of electropolymerisation is somewhat slower for the Chit/PpyCl film, both systems achieve similar current densities after about 50 s, indicating a faster rate of polypyrrole chain propagation within the hydrogel, after the initial nucleation period. Brahim *et al.*¹⁶ reported a similar phenomena within a poly(2-hydroxyethyl methacrylate) hydrogel network and proposed that this is due to the manifestation of localised availability of pyrrole monomers within the swollen hydrogel network, which influence the initial oxidation and coupling of polaronic species near the

electrode surface. Qualitatively, on visual inspection of the films, the PpyCl films appear as a shiny black film in contrast to the Chit/PpyCl which appears as a dull black film.

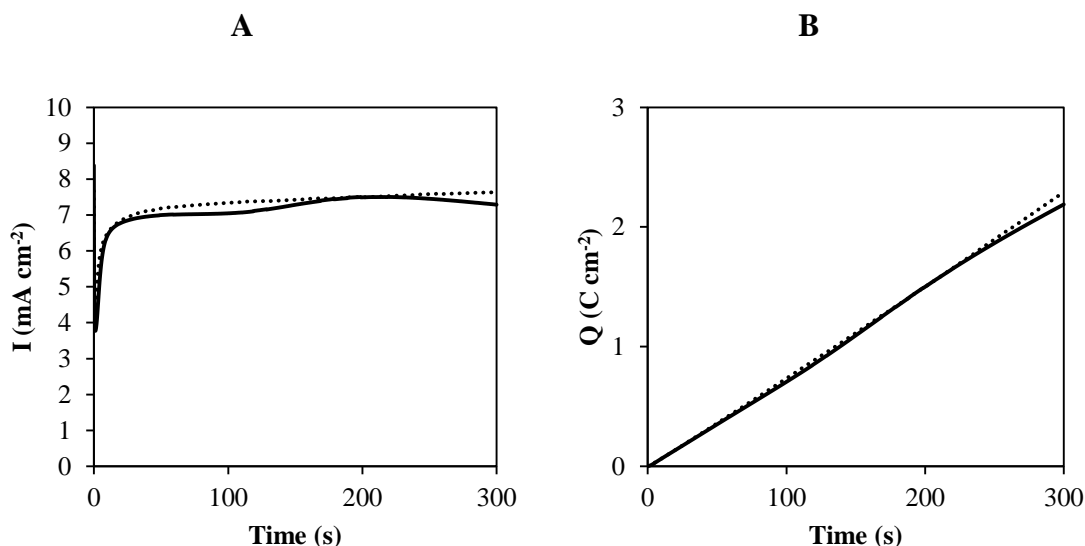


Figure 3.3: Current-time plots (A) and charge-time plots (B) for the growth of polypyrrole chloride (···· PpyCl) and chitosan/polypyrrole chloride (— Chit/PpyCl). The films were prepared by potentiostatic electropolymerisation at 0.80 V vs SCE for 300 s yielding a charge density of 2.20 C cm⁻² from a solution of 0.1 mol dm⁻³ Py and 0.1 mol dm⁻³ NaCl.

3.3.2.1 Influence of chitosan volume

The optimum volume of chitosan solution cast on the Pt electrode depends on the electroactive surface area of the electrode (0.13 cm²). A higher wet volume yields a higher dry volume or, more specifically, a higher hydrated volume during the immersion step. The pyrrole monomer and anions have to diffuse through the hydrated chitosan film to the surface electrode where the electropolymerisation takes place; the higher the volume of chitosan the longer it will take to hydrate and the further the distance the monomer and anions have to diffuse through. Optimum volume, in this case, is considered to be the volume at which the PpyCl forms in the presence of chitosan to the same charge density and duration that PpyCl requires in the absence of chitosan (2.2 C cm⁻²). The chitosan solution was cast on to the Pt electrode and was cured under an IR lamp for 10 min and let cool for a further 10 min. The chitosan coated Pt electrode was immersed in the electrolyte for 60 min prior to electropolymerisation. The influence of the volume of

chitosan is evident on comparing the current-time plots presented in Figure 3.4. There was no current increase for a volume of 30 μL indicating that no polymer was deposited (volumes $> 30 \mu\text{L}$ overflowed onto the epoxy casing). Indeed, there was no evidence of any polymer on the surface after the experiment. At a volume of 20 μL there was evidence of electropolymerisation and the optimum charge density was obtained but the duration of potentiostatic growth was in excess of 15 min. Exposing the PpyCl component of the composite to a high potential of 0.80 V vs SCE for long periods of time subjects the material to a risk of irreversible over-oxidation⁵³, resulting in an undesirable insulating material. A volume of 10 μL was sufficient to obtain reproducible PpyCl films with an optimum charge density of 2.2 C cm^{-2} in 300 s.

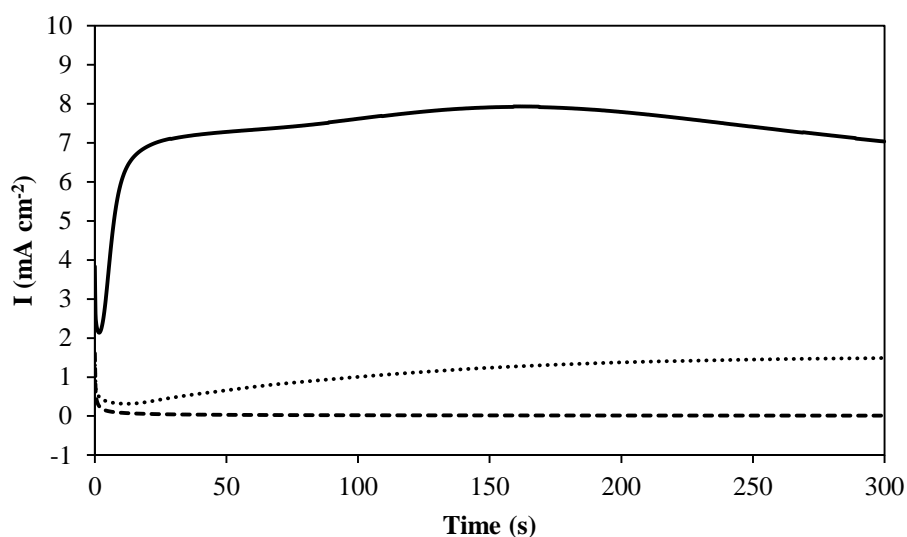


Figure 3.4: Current-time of PpyCl grown on a 0.13 cm^2 Pt electrode coated with various volumes of 5 % (w/v) chitosan (--- 30 μL), (····· 20 μL) and (— 10 μL). The films were prepared by potentiostatic electropolymerisation at 0.80 V vs SCE in 0.1 mol dm^{-3} Py 0.1 mol dm^{-3} NaCl.

3.3.2.2 Influence of immersion time

The optimum duration for which the chitosan coated Pt electrode needed to be immersed in the monomer and electrolyte solution was investigated at 10 min intervals. These microfabrication processes are a very fast and facile way of blending polymers, ideally additional steps such as solution casting and curing should not add too much time to the

full process and they should be very reproducible. The immersion step is necessary to allow the dry chitosan film to hydrate. Optimum duration is considered to be the immersion time required to give the same charge density (2.2 C cm^{-2}) and duration for the formation of PpyCl in the absence and presence of chitosan. Representative data are presented in Figure 3.5, where it is clear that after 20 min of immersion, the growth profile is very similar to the data recorded for the PpyCl film in the absence of chitosan, Figure 3.3. At 0 min immersion, the current increases indicating some deposition, but there was no polymer on the electrode when visually inspected. At 10 min there was some polymer visible, and some attempts yielded the optimum charge density and the optimum growth time but these results did not have satisfactory reproducibility. An immersion time of 20 min was found to be the optimum immersion time for the chitosan on the Pt electrode to swell in the electrolyte allowing the monomer and dopant to penetrate the chitosan layer.

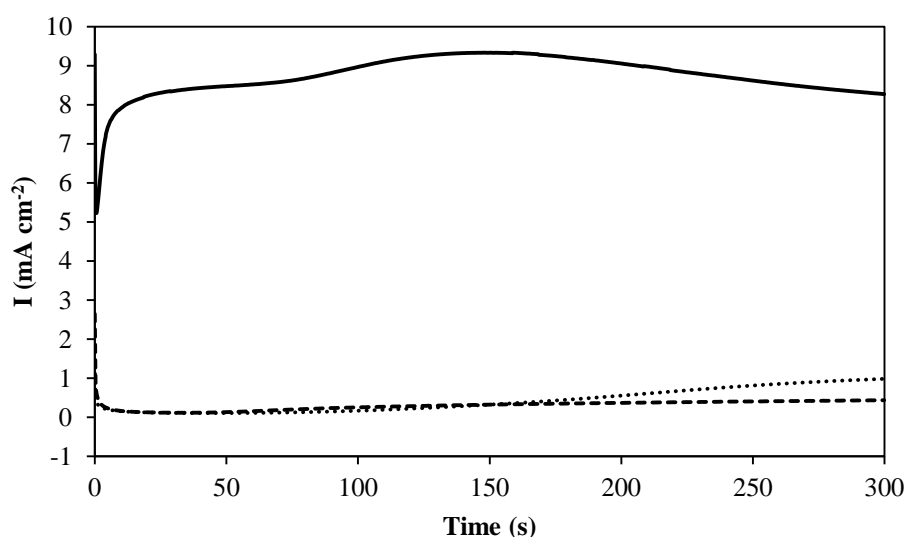


Figure 3.5: Current-time plots of PpyCl grown on a 0.13 cm^2 Pt electrode coated with $10 \mu\text{L}$ of 5 % (w/v) chitosan immersed in the monomer electrolyte prior to electropolymerisation (--- 0 min), (···· 10 min) and (— 20 min). The films were prepared by potentiostatic electropolymerisation at 0.80 V vs SCE in 0.1 mol dm^{-3} Py 0.1 mol dm^{-3} NaCl.

3.3.3 Characterisation of the composite

For the FT-IR and DSC characterisation techniques a stock of a representative sample was collected by carrying out numerous electrosynthesis experiments and carefully scraping the products away from the electrode surface with a scalpel. During the collection of the sample some of the polymer films stick to the blade and glass collection vial due to high surface energies presumably caused by the excess energy at the surface following electropolymerisation. For all these characterisation techniques, the PpyCl and Chit/PpyCl films were grown to a charge of 2.2 C cm^{-2} as attempts to remove thinner films were unsuccessful. The chitosan film was prepared by pipetting 1 cm^3 of 0.5 % (w/v) chitosan solution on to a clear PVC sheet. It was cured under an IR lamp and peeled away from the PVC substrate and was ground using a pestle and mortar. For the FT-IR samples, the materials were ground with dehydrated KBr using a pestle and mortar and pressed between two dies to make discs (Section 2.4.8). Using the same stock of Ppy and ChitPpy, DSC was also used to gain thermoanalytical information (Section 2.4.7). Heat Capacity is routinely used in pharmaceutical and polymer industries because it can determine the energy requirements and temperature thresholds of processing, in this work it is used to analyse heating events.

3.3.3.1 Composition of films (FT-IR)

FT-IR spectra of polypyrrole, chitosan, and the composite film are shown in Figure 3.6. As mentioned in Section 3.3.2, the black colour observed for PpyCl and Chit/PpyCl testifies to its presence, however, the transparent chitosan film makes it difficult to visually confirm its presence. There is no data given here to confirm the presence of a dopant anion in the Ppy or Chit/Ppy FT-IR spectra which is generally the case for many reports^{34, 54-57}. The band due to a C–Cl species may be superimposed by the polymer peaks present or it may appear outside the working range of the spectra recorded⁵⁵.

The FT-IR spectrum presented for the composite, Figure 3.6 (c), shows the main peaks of both constituents, PpyCl and chitosan, with the peak for the β –(1→4) glycosidic bond at 1157 cm^{-1} , clearly evident in the composite. The strong absorption peak from 3750 –

3000 cm^{-1} may be assigned to the presence of water⁵⁸. The peaks at 1638 cm^{-1} and 1636 cm^{-1} in for Chitosan, Ppy and Chit/Ppy may also be assigned to the presence of water⁵⁸, however, most reports assign this characteristic peak in Ppy to C=C stretching^{34, 54, 59-62}, in order to confirm that this peak is due to the C=C stretching a rigorous drying would be required, which was not done in this case. the black colour of polypyrrole yield relatively low intensity transmittance spectra. To minimise ambiguity, the FT-IR is employed in this work to identify the chitosan in Chit/Ppy and does not purport to give a comprehensive analysis of FT-IR peaks.

The peaks clearly seen at The FT-IR spectrum for chitosan shows a strong peak at 3390 cm^{-1} which was assigned to the asymmetrical stretching vibration of the O–H superimposed to the N–H stretching band and inter hydrogen bonds of the polysaccharide, C–H stretching at 2870 cm^{-1} . Polypyrrole also exhibits N–H stretching vibration at 3425 cm^{-1} . Figure 3.7 shows the magnified “fingerprint” region of the FT-IR spectrum (1800 – 800 cm^{-1}). Using the band assignments by Yalçinkaya *et al.*³⁴ the peak at 1654 cm^{-1} was assigned to the C=O stretching. Other clear peaks include the N–H bending at 1568 cm^{-1} , the C–N stretching coupled with N–H deformation at 1423 cm^{-1} , the symmetrical angular deformation of CH₃ at 1374 cm^{-1} , stretching of the C–N amino group at 1318 cm^{-1} , the β –(1→4) glycosidic bond at 1137 cm^{-1} , and the C–O–C stretching vibration at 1030 cm^{-1} .

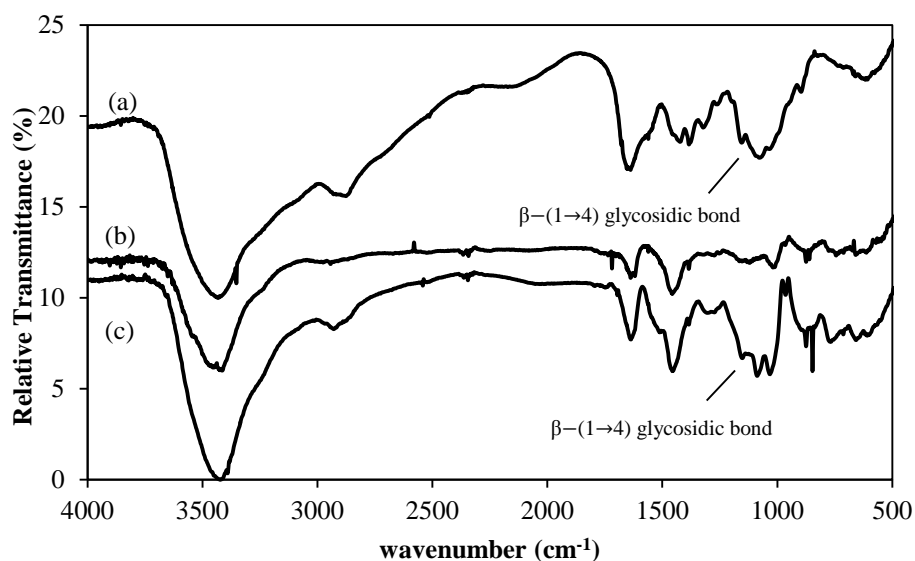


Figure 3.6: FT-IR spectra of (a) chitosan, (b) PpyCl and (c) Chit/PpyCl, showing the presence of the β -(1 \rightarrow 4) glycosidic bond at 1157 cm^{-1} in chitosan and 1152 cm^{-1} in Chit/PpyCl. The stock films were prepared by repeating the potentiostatic electropolymerisation at 0.80 V vs SCE to a charge density of 2.20 C cm^{-2} (0.1 mol dm^{-3} Py 0.1 mol dm^{-3} NaCl) and removing the material with a scalpel.

The spectrum of polypyrrole is shown in Figure 3.7 (b). Bands in the region of 1690 cm^{-1} are characteristic of α , β -unsaturated ketones, which are reported to lie between 1707 and 1687 cm^{-1} a nonconjugated carbonyl. The peak is assigned to the presence of a carbonyl group at the β -carbon of the pyrrole ring on overoxidation of the polymer and the concomitant CO_2 peak at 2347 cm^{-1} is also observed^{54, 59}. The peak at 1456 cm^{-1} is assigned to the C–N stretching vibration is characteristic of the Ppy ring, the peak at 1385 cm^{-1} C=C/C–C stretching vibration⁶⁴. 1318 cm^{-1} is ascribed to the =C–H in-plane deformation, the peak at 1121 cm^{-1} is ascribed to the C–N stretching vibration⁶⁰⁻⁶². The peak at 1019 cm^{-1} is due to C–H in plane stretching, the peak at 966 cm^{-1} may be due to C–C out of plane vibration, while the peaks at 875 cm^{-1} and 744 cm^{-1} may be assigned to the =C–H out of plane vibration^{60-62, 65}. According to Rodríguez *et al.*⁵⁴ a peak at 1152 cm^{-1} may indicate the presence of a conductive bipolaronic species of oxidised polypyrrole, its absence here suggests that the film is not in its conducting state but probably in a relaxed state.

The spectrum of the composite in Figure 3.7 (c), clearly indicates the presence of the β -(1 \rightarrow 4) glycosidic bond at 1152 cm^{-1} . The peak at 1636 cm^{-1} is assigned to the C=C stretch of the pyrrole ring.

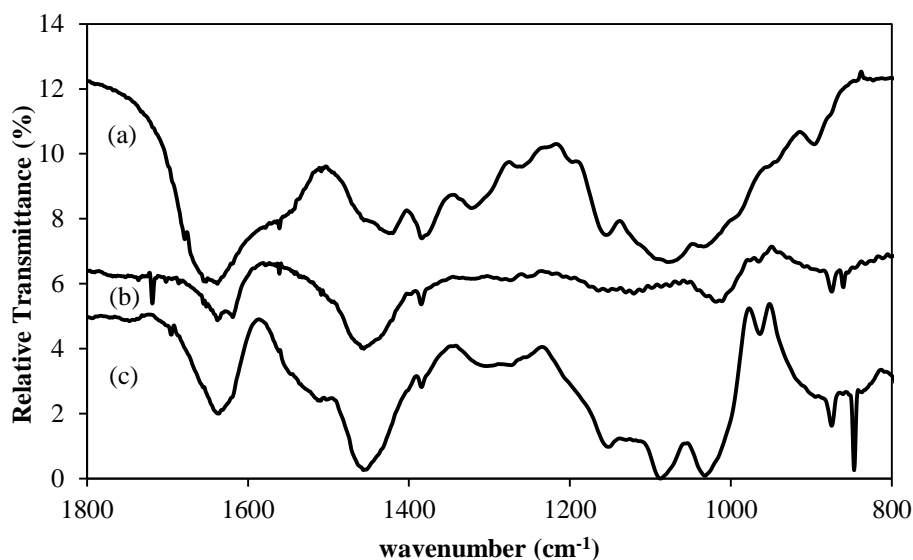


Figure 3.7: FT-IR spectra of (a) Chitosan (b) PpyCl and (c) Chit/PpyCl, is the fingerprint region. There is a small shift in the wavenumbers for the composite, indicating a weak interaction between the Ppy and Chit. The stock films were prepared by repeating the potentiostatic electropolymerisation at 0.80 V vs SCE to a charge density of 2.20 C cm^{-2} (0.1 mol dm^{-3} Py 0.1 mol dm^{-3} NaCl) and removing the material with a scalpel.

On comparing this spectrum with that recorded for PpyCl and chitosan, it is clear that no new peaks are formed and no peaks disappear. However, there is a small shift in the wavenumber which may be due to variances in the experiments, but does not discount the possibility of weak chemical interactions between the polypyrrole and chitosan such as, van der Waals, hydrogen bonding or electrostatic interactions. The stretching vibration of the O–H and N–H stretching band make it difficult to discern if hydrogen bonds exist between the chitosan and polypyrrole. Yalçinkaya *et al.*³⁴ prepared a polypyrrole chitosan composite and as a result of FT-IR data they proposed a structural representation with hydrogen bonding which is adapted and shown in Figure 3.8.

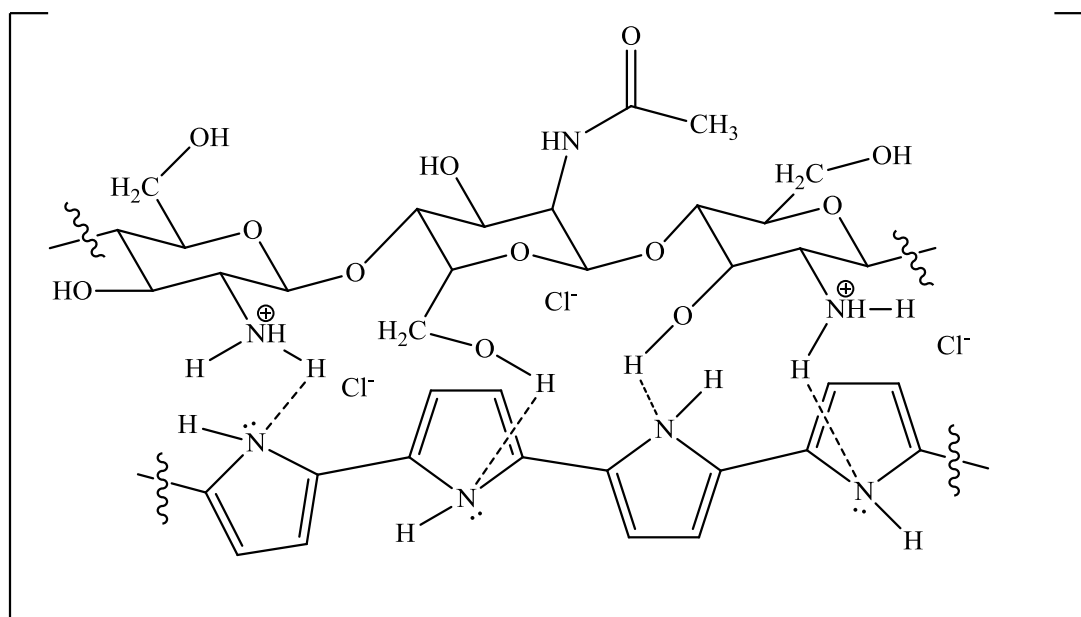


Figure 3.8: Structural representation of the Chit/PpyCl composite³⁴.

3.3.3.2 Thermal properties (DSC) of films

The thermal stability of 1 mg of dry polymers was studied by differential scanning calorimetry (DSC) under nitrogen to prevent atmospheric oxidation. The samples were heated from 20 °C to 450 °C at a heating rate of 2 °C min⁻¹. The resulting DSC curves are shown in Figure 3.9, for the PpyCl, chitosan and composite, Chit/PpyCl. The curve for chitosan shows two distinct peaks, a broad endothermic peak is observed between 30 °C and 105 °C with a maximum at 62 °C due to water elimination⁶⁶ and an exothermic peak is observed at 270 °C which is close to the recorded melting point of chitosan⁶⁷. The degree of deacetylation of chitosan does not significantly affect the glass transition temperature of chitosan films⁶⁸. For PpyCl and Chit/PpyCl there is a dip in the curve at 320 °C which may be due to the decomposition of the polymer⁶⁹.

When considering the data for the composite, it is likely that the chitosan content of the composite was too low for the characteristic peaks of chitosan to be obtained, however, it can be stated that the composite, Chit/PpyCl, exhibits a better thermal stability than chitosan and that the presence of chitosan does not compromise the high thermal stability of pure polypyrrole (> 400 °C).

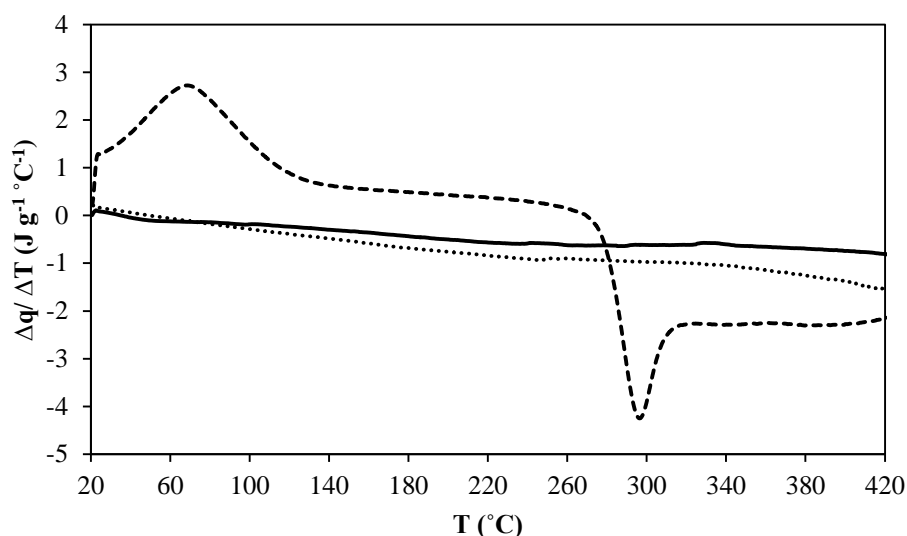


Figure 3.9: DSC curve for 1.0 mg of (···· PpyCl), (--- Chitosan) and (— Chit/PpyCl), working temperature range studied was between 20 and 450 °C at a heating rate of 2 °C min⁻¹ under nitrogen. The stock films were prepared by repeating the potentiostatic electropolymerisation at 0.80 V vs SCE to a charge density of 2.20 C cm⁻² (0.1 mol dm⁻³ Py 0.1 mol dm⁻³ NaCl) and removing the material with a scalpel.

3.3.3.3 Morphology (SEM) of films

Surface roughness is an inherent property of amorphous materials, the texture and roughness is an important consideration for cell adhesion in tissue regenerative technology. The surface topography of the polymers was studied by SEM. The scanning electron micrographs are presented in Figures 3.10, 3.11 and 3.12. The polymers were grown on a customised Pt electrode (Section 2.4.6) with a surface area of 0.13 cm². The polymers were washed thoroughly with distilled water to ensure the removal of excess electrolyte (NaCl) on the surface. They were air dried for several hours before imaging. These samples were not sputter coated prior to imaging.

Figure 3.10 shows a typical SEM micrograph of PpyCl which appears as globule structures or “cauliflower” structures, this is a well-documented morphology, typical of

the bulk polypyrrole⁴⁹. The globules are made up of micro-spherical grains, it has been reported that such a particular structure is related to the dopant intercalation difficulty in the disordered polymeric chain^{70,71}.

The exterior surface of the chitosan was very smooth and had no visible contrast which made imaging difficult. Other groups have reported similar results stating that the films are reproducibly homogeneous, smooth and without any visible pores on the surface^{72,73}. Figure 3.11 presents a typical SEM micrograph of a dry chitosan film with a defect deliberately made to allow imaging. The SEM micrograph of the polypyrrole chitosan composite is presented in Figure 3.12 and shows the same “cauliflower” morphology as the polypyrrole film, PpyCl⁷⁴. For comparison the morphology of the PpyCl film is shown as an inset in the top right corner. The cauliflower structures have similar sizes for both the PpyCl and composite, however, the visible “folds” seen with the composite, Figure 3.12, interconnecting the globules can be attributed to the presence of the chitosan.

It is worth noting that the films homogeneously cover the electrode without the appearance of any surface defects. EDX analysis was performed on these samples but similar spectra were recorded for the samples due to the abundance of C present at 0.3 keV in both the chitosan and polypyrrole. Chloride was detected at 2.62 keV in polypyrrole and the composite as the polymer films are doped with the chloride anions.

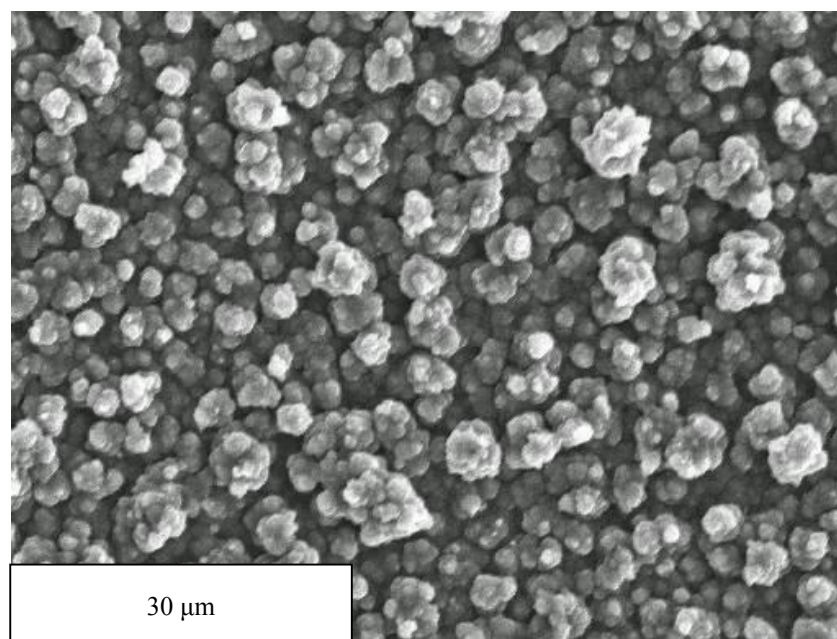


Figure 3.10: SEM micrograph of PpyCl grown on a 0.13 cm² customised Pt electrode showing “cauliflower” morphology. The films were prepared by potentiostatic electropolymerisation at 0.80 V vs SCE in 0.1 mol dm⁻³ Py 0.1 mol dm⁻³ NaCl grown to a charge density of 2.20 C cm⁻².

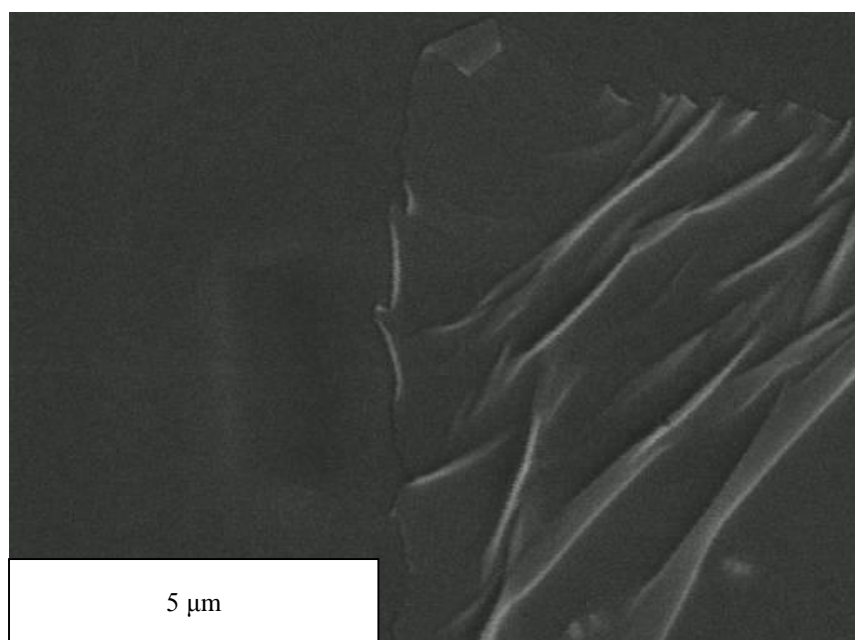


Figure 3.11: SEM micrograph of chitosan on a 0.13 cm² customised Pt electrode with a purposely made defect to allow imaging as an alternative to a featureless chitosan film.

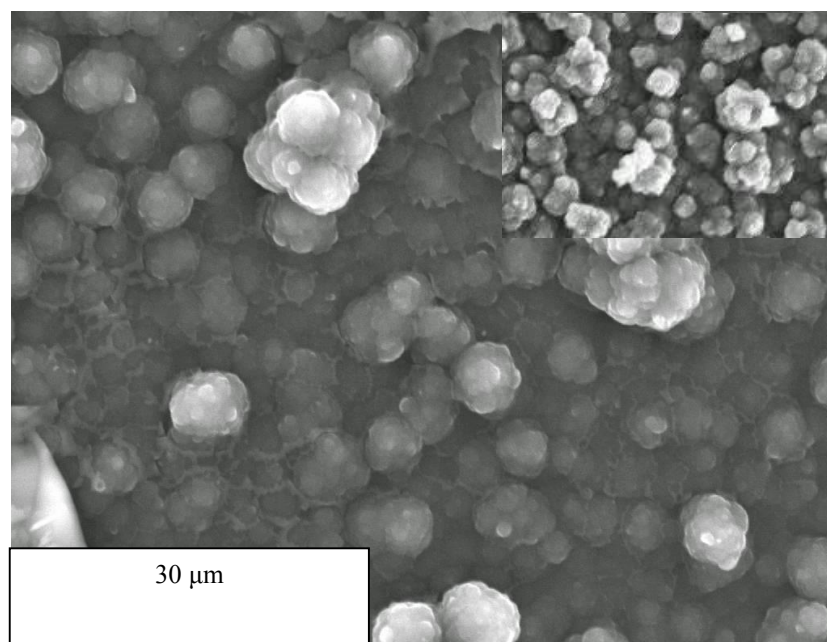


Figure 3.12: SEM micrograph of chitosan polypyrrole chloride, Chit/PpyCl, grown on a 0.13 cm² customised Pt electrode showing “cauliflower” morphology. The film was prepared by potentiostatic electropolymerisation at 0.80 V vs SCE to a charge density of 2.20 C cm⁻² from a solution of 0.1 mol dm⁻³ Py 0.1 mol dm⁻³ NaCl. The inset in the top right corner is polypyrrole chloride grown in the same conditions in the absence of chitosan.

3.3.3.4 Estimation of mass and doping levels

Quartz crystal microbalance measurements (EQCM) were performed and analysed to obtain information on the mass of the deposited PpyCl film and the doping level. In these studies, the PpyCl was grown to a charge of 11 mC (55 mC cm⁻²) by applying a constant potential of 0.85 V vs Ag|AgCl reference electrode. The frequency-charge plot and mass-charge plots for PpyCl are shown in Figure 3.13 A and B, respectively. A decrease in frequency is related to an increase in mass⁷⁵ described by the Sauerbrey relationship⁷⁶ (Equation 2.12 in Section 2.4.5).

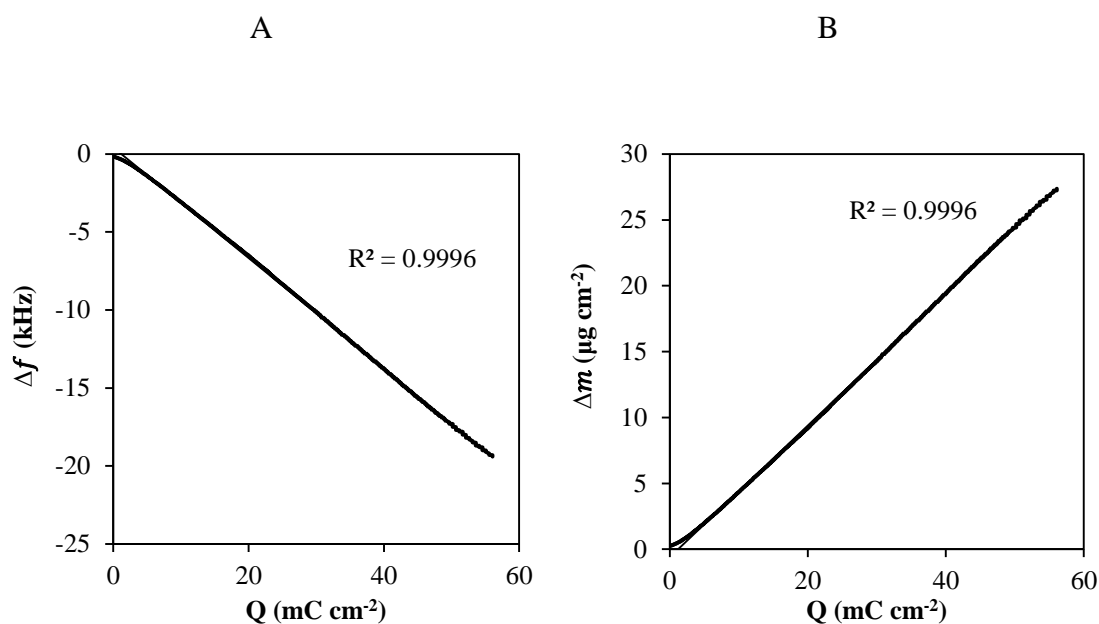


Figure 3.13: Frequency-charge plot (A) and mass charge plot (B) for the electropolymerisation of pyrrole to generate PpyCl to a charge density of 75 mC cm⁻² on an Au-EQCM crystal (0.20 cm²) recorded by EQCM measurements. The PpyCl was prepared by electropolymerisation at 0.80 V vs SCE.

The Sauerbrey equation can be re-arranged to solve for the mass change, as shown in Equation 3.1. As discussed in Section 2.4.5, this equation is only valid when the rigid film approximation is satisfied. This can be achieved by limiting the film thickness, for example; a 10 MHz quartz crystal is between 130 μm⁷⁷ and 170 μm⁷⁸ so a film thickness of 2 μm or less satisfies the rigid film approximation for a 10 MHz quartz crystal (< 2%)⁷⁷. Using a volume-to-charge ratio⁷⁹ (K) of 2.37×10^{-4} cm³ C⁻¹ for chloride⁸⁰ and a geometric area of 0.20 cm² a PpyCl film grown to a charge density of 55 mC cm⁻² is estimated to be 0.6 μm thick which agrees well with the approximation if we take into consideration that an 8 MHz quartz crystal is slightly thicker than a 10 MHz quartz crystal⁸¹ therefore a film thickness of 0.6 μm readily satisfies the rigid film approximation for an 8 MHz quartz crystal. (Terms are defined in Section 2.4.5).

$$\Delta m = - \frac{A \sqrt{(\rho_q \mu_q)}}{2f_o^2} = \frac{1}{C_f} \Delta f \quad (3.1)$$

The sensitivity factor (C_f) was found to be $7.087 \times 10^8 \text{ Hz cm}^2 \text{ g}^{-1}$. There is a linear increase in mass with charge when the charge exceeds 5 mC cm^{-2} . The doping level, p , of the polymer can be estimated with Equation 3.2 from the average slope of these mass-charge curves, which was computed as $R = 0.4209 \text{ mg C}^{-1}$.

$$R = \frac{m}{Q} = \frac{M_m + p M_A}{(n + p)F} \quad (3.2)$$

Here M_m and M_A are the formula weights of the monomer and anion. In the case of the chloride-doped polypyrrole, the molecular weight of pyrrole is 65.07 g mol^{-1} and chloride is 35.45 g mol^{-1} . The number of electrons, $n = 2$ and the value of p for Ppy has been reported to range from 0.2 to 0.5 dopant molecules per pyrrole unit⁸². For simple dopant anions such as Cl^- , the value of p is approximately 0.33, i.e., a 1:3 doping level. The value of p was calculated as 0.37 which is in reasonable agreement with the values reported in the literature. This value is slightly higher than the theoretical value where $p \leq 0.33$ but is still within experimental error. According to Snook *et al.*⁸³ a possible cause for inaccuracies may be adsorbed ions.

The average rate of growth of PpyCl was computed to be 2.03 mC s^{-1} . This is considerably slower than the rate of growth on a conventional Au disc electrode and Pt disc electrode which was computed to be 7.81 mC s^{-1} and 8.03 mC s^{-1} , respectively. The difference between the growth rates on a conventional Au disc and Pt disc can be explained in terms of the higher conductivity of Au facilitating a faster rate of electropolymerisation⁸⁴.

The thickness of the PpyCl films (δ_{film}) is directly proportional to the charge Q consumed during electropolymerisation⁸⁰, as shown in Equation 3.3.

$$\delta_{film} = K \frac{Q}{A} \quad (3.3)$$

Here, A is the geometric area of the film. For the PpyCl film grown to 2.2 C cm^{-2} and 0.25 C cm^{-2} the thickness was calculated as $4.0 \text{ }\mu\text{m}$ and $0.5 \text{ }\mu\text{m}$, respectively, using a volume-to-charge ratio⁷⁹ (K) of $2.37 \times 10^{-4} \text{ cm}^3 \text{ C}^{-1}$ for chloride⁸⁰ and a geometric area of 0.13 cm^2 .

The equation used to calculate the theoretical mass assumes the current efficiency for the electropolymerisation of the pyrrole monomer is 100 %⁸⁵.

The calculated mass, doping levels and thickness of the PpyCl films are summarised in Table 3.1.

Table 3.1: Summary of EQCM results, calculated mass, doping levels and thickness of PpyCl.

Results	PpyCl (Q = 55 mC cm⁻²)
Mass (μg cm⁻²)	27
Doping level, <i>p</i>	0.37
Doping Ratio,	1:3
Thickness (μm)	0.6

3.3.4 Cyclic Voltammetry (CV)

The electrochemical properties of PpyCl and Chit/PpyCl were characterised using cyclic voltammetry. The polymers were cycled in 0.1 mol dm⁻³ NaCl and the potential was swept from -0.95 V to 0.35 V vs SCE to avoid over-oxidising the polymer. Different scan rates, ranging from 5, 10, 25, 50, 100 and 150 mV s⁻¹, were used. Representative data are shown in Figure 3.14, where the voltammograms presented in Figures 3.14 A and C show the current-potential response at different scan rates for PpyCl and Chit/PpyCl films. In Figure 3.14 B and D the voltammograms recorded at 10 mV s⁻¹ are shown and compared to the electrochemical response of the bare Pt electrode using the same parameters. Reproducible voltammetric behaviour was attained after the first few cycles, usually 3 to 4 cycles and the data shown in Figure 3.14 were recorded following 9 cycles.

The voltammograms recorded for PpyCl and Chit/PpyCl are similar, showing a broad anodic peak and evidence of two reduction waves, which are more clearly evident in Figure 3.14 B and D. The anodic peak for PpyCl is centred at 0.10 V vs SCE at the higher

scan rates, but at low scan rates of 5 and 10 mV s^{-1} , this anodic peak appears at about -0.10 V vs SCE . There is a shift in the peak potential in the anodic direction with increasing scan rate and this is clearly shown in Figure 3.14 A. A cathodic peak is centred at -0.15 V vs SCE , and a drift in the peak is observed as the scan rate increases. A second cathodic peak is observed at -0.50 V vs SCE and drifts in the cathodic direction more significantly and becomes more pronounced at higher scan rates ($> 10 \text{ mV s}^{-1}$). This peak is associated with transient cation insertion⁸⁶. Similar voltammograms for PpyCl have been published and discussed^{40, 87-90}. The electroactivity of PpyCl is strongly influenced by ion transport properties, more specifically the anion transport, which has been extensively studied⁹¹⁻⁹⁶. However, there is little voltammetric data published or discussed with regard to the Chit/PpyCl composite. As shown in Figure 3.14 C and D, the chitosan component does not significantly alter the overall redox properties of the film and similar data are recorded for the PpyCl and Chit/PpyCl composite films. The anodic peak for Chit/PpyCl is centred at 0.16 V vs SCE at higher scan rates but appears to shift in the anodic direction at slow scan rates. The corresponding cathodic peak is observed at approximately -0.20 V vs SCE , while a second cathodic peak is observed at -0.65 V vs SCE and is less pronounced at lower scan rates ($< 50 \text{ mV s}^{-1}$). The electrochemical response of the Chit/PpyCl composite is clearly shown in Figure 3.14 D where the voltammograms recorded with Pt are compared with the composite at 10 mV s^{-1} . Two cathodic peaks are observed, centred at -0.20 V and -0.55 V vs SCE , which is similar to the data recorded for the PpyCl films (Figure 3.14 B). The latter peak is characteristic of cation insertion into polypyrrole^{46, 95}.

The electrochemical data are summarised in Table 3.2 for the main redox process, which appears to be predominantly the loss and uptake of anions. These polymer films doped with Cl^- anions demonstrate redox asymmetry typical of conducting polymers⁹⁷. The current ratios (I_{pc}/I_{pa}) of the main cathodic and anodic peaks deviate from 1.0. The values were computed as 0.7 and 0.6, for PpyCl and Chit/PpyCl, respectively, at a scan rate of 50 mV s^{-1} . This suggests that the system is not redox reversible⁴⁷. The midpoint potential, E_{mid} , was observed to shift to more positive potentials on increasing the scan rate from 5 to 150 mV s^{-1} . The midpoint potentials increased by 95 mV for PpyCl (-108 mV to 13 mV vs SCE) and 125 mV for Chit/PpyCl (-98 mV to 27 mV vs SCE). This indicates that the presence of the chitosan hydrogel has some effect on the anion

transport⁵¹. It is clear from the data presented in Table 3.2, that the electrochemical response of the PpyCl and Chit/PpyCl films are similar, with the peak currents increasing with scan rate and the peak separation increasing with scan rates, reaching values of 651 and 747 mV at 150 mV s⁻¹, respectively.

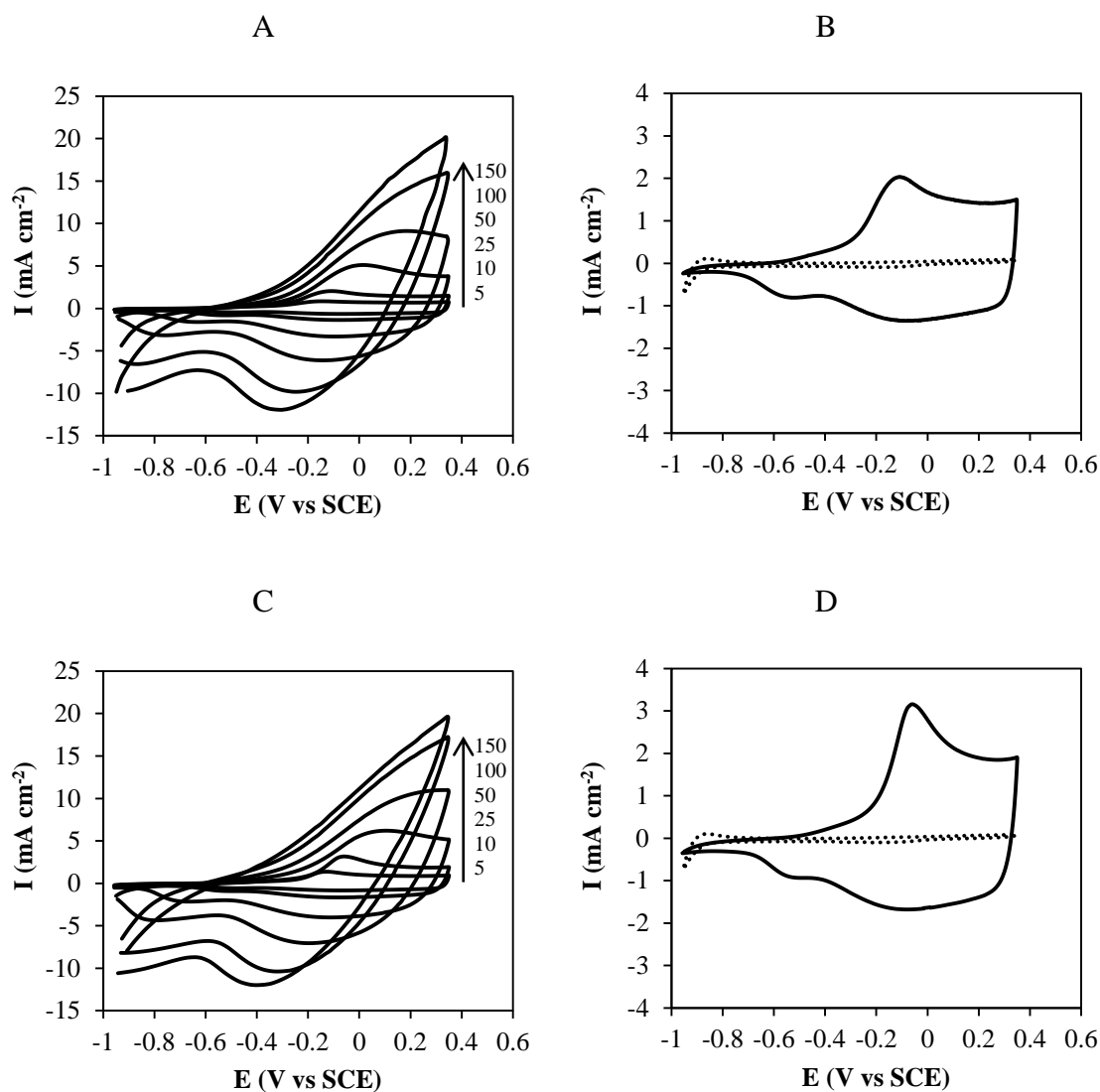


Figure 3.14: Cyclic voltammograms (10th cycle) of PpyCl (A and B) and Chit/ PpyCl (C and D) coated Pt electrode in 0.1 mol dm⁻³ NaCl. The dashed traces in (B) and (D) correspond to the voltammograms of bare Pt electrode. The scan rates in mV s⁻¹ are indicated on the plot. The films were prepared by potentiostatic electropolymerisation at 0.80 V vs SCE to a charge density of 2.20 C cm⁻². The PpyCl was prepared from a solution of 0.1 mol dm⁻³ Py and 0.1 mol dm⁻³ NaCl.

Table 3.2: Cyclic voltammetric data for the main redox process of PpyCl and Chit/PpyCl in 0.1 mol dm⁻³ NaCl.

PpyCl				
Scan rate (mV s ⁻¹)	E_{mid} (mV Vs SCE) ^a	ΔE_p (mV) ^b	I_{pa} (mA cm ⁻²)	I_{pc} (mA cm ⁻²)
5	-108	-66	1.0	1.0
10	-93	-26	2.0	1.0
25	-40	108	5.0	3.0
50	24	325	9.0	6.0
100	46	599	16.0	10.0
150	13	651	20.0	12.0

Chit/PpyCl				
Scan rate (mV s ⁻¹)	E_{mid} (mV vs SCE) ^a	ΔE_p (mV) ^b	I_{pa} (mA cm ⁻²)	I_{pc} (mA cm ⁻²)
5	-98	-60	1.0	1.0
10	-74	10	3.0	2.0
25	-4	220	6.0	4.0
50	69	533	11.0	7.0
100	12	670	17.0	10.0
150	27	747	26.0	16.0

^a Calculated from $1/2 (E_{p,c} + E_{p,a})$.

^b $\Delta E_p = E_{pa} - E_{pc}$.

Using a generalised capacitance curve (current divided by the potential scan rate) as described by Levi *et al.*⁹⁸, a more detailed analysis of the mass transfer processes can be obtained. A typical plot is presented in Figure 3.15 for the PpyCl and Chit/PpyCl films cycled at a scan rate of 5 mV s^{-1} . The oxidation and reduction peaks can be seen more clearly at the slow scan rates in both the PpyCl and Chit/PpyCl films using this approach. Four peaks are visible and these are labelled as I, II, III and IV. The secondary redox cation exchange process, peak I and IV, is centred at -0.50 V vs SCE . During oxidation there are two competing processes: the expulsion of the cation and the inclusion of the anion. Conversely, during reduction the expulsion of the anion and inclusion of the cation are the two competing processes. From Figure 3.15 it is clear that the anion transport is the dominant process during oxidation and reduction. The expulsion of the cation cannot be clearly seen even though the inclusion of the cation is clear and becomes more pronounced at faster scan rates.

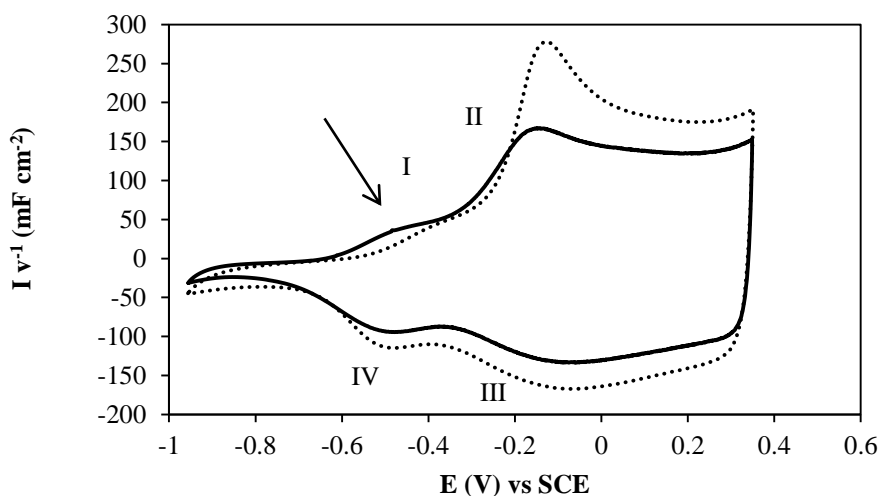
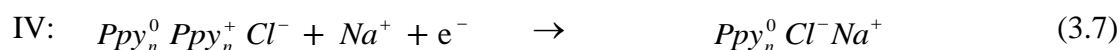
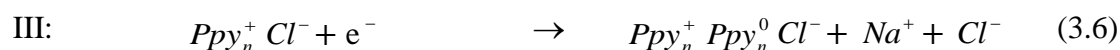
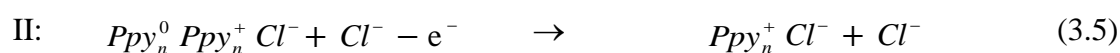
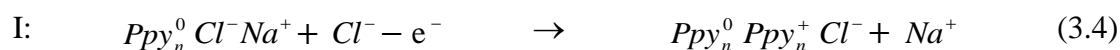


Figure 3.15: Generalised capacitance curve (where the current is divided by the scan rate v) for (— PpyCl) and (···· Chit/PpyCl) cycled in $0.1 \text{ mol dm}^{-3} \text{ NaCl}$ at 5 mV s^{-1} . The films were prepared by potentiostatic electropolymerisation at 0.80 V vs SCE to a charge density of 2.20 C cm^{-2} . The PpyCl was prepared from a solution of $0.1 \text{ mol dm}^{-3} \text{ Py}$ and $0.1 \text{ mol dm}^{-3} \text{ NaCl}$.

The possible processes occurring at the peaks labelled I, II, III, and IV are described in Equations 3.4, 3.5, 3.6 and 3.7. On re-oxidation of the PpyCl the polymer backbone

becomes positively charged. The charge neutrality is achieved by the expulsion of the sodium ion (Equation 3.4) and the incorporation of the chloride ion (Equation 3.5) from the electrolyte. When the PpyCl is reduced during subsequent cycles, the chloride anion is expelled into the electrolyte (Equation 3.6) and in order to maintain overall charge neutrality a sodium ion from the electrolyte is incorporated into the polymer (Equation 3.7).



In Figure 3.16, plots are shown of the peak potential (E_p) and peak current (I_p) as a function of the scan rate for PpyCl and Chit/PpyCl. The data recorded for the PpyCl film is shown in Figure 3.16 A, while similar data are presented for the composite in Figure 3.16 C. In both systems, the peak separation increases with scan rate and similar anodic peak potentials and cathodic peak potentials are observed with the PpyCl and Chit/PpyCl composite. The peak separations (ΔE_p) were 325 and 523 mV for PpyCl and Chit/PpyCl, respectively, at 50 mV s⁻¹. The peak currents for PpyCl and Chit/PpyCl increase linearly with increasing scan rate, indicating the absence of a kinetic or charge-transport limitation⁹⁵.

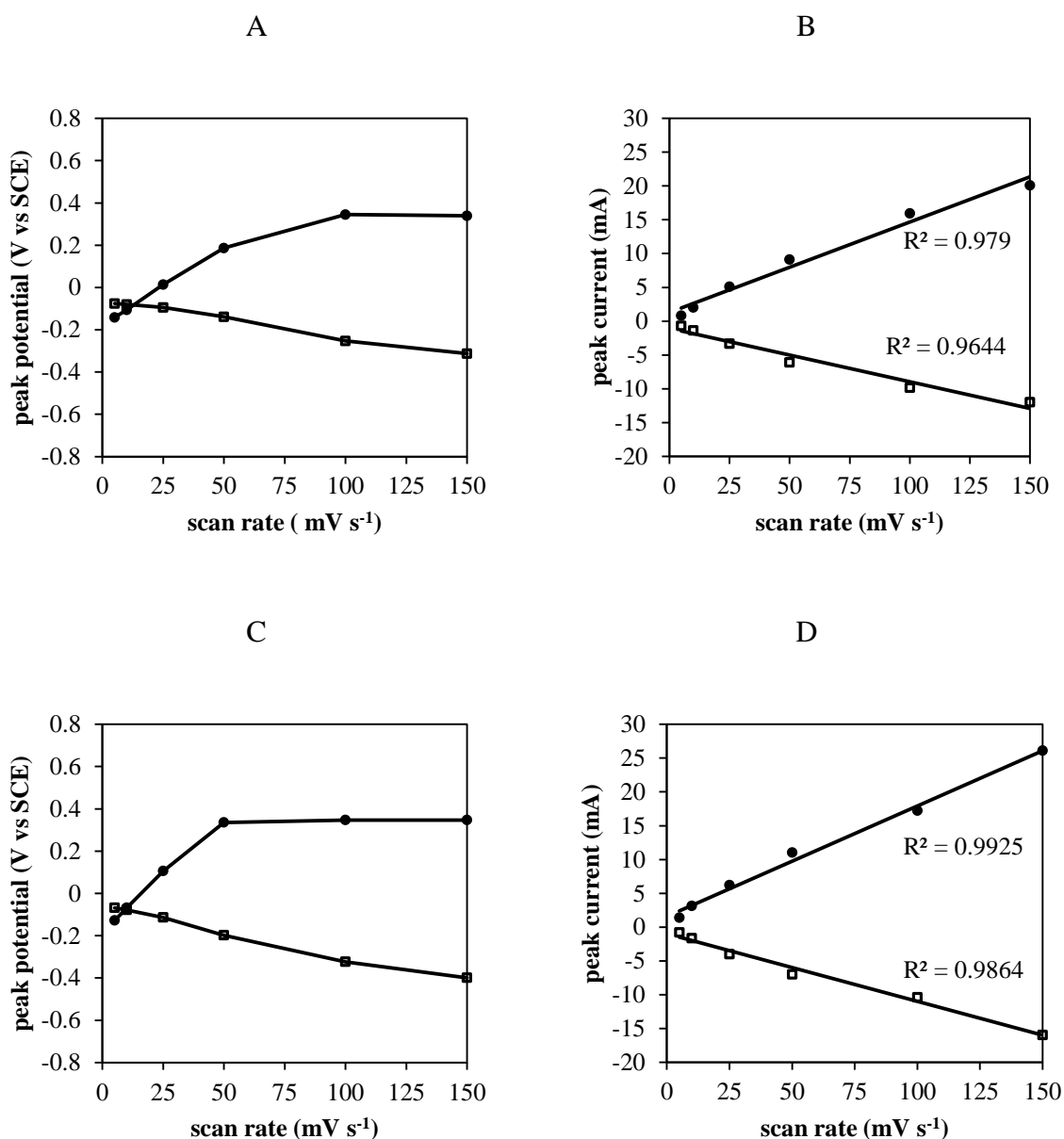


Figure 3.16: Peak potential plotted as a function of scan rate for PpyCl (A) and Chit/PpyCl (C) and peak current plotted as a function of scan rate PpyCl (C) and Chit/PpyCl (D) taken from the cyclic voltammograms (10th cycle) shown in Figure 3.14 A and C. Using the main anodic peak (●) and the main cathodic peak (□). The R^2 values for the linear trendline are indicated. The films were prepared by potentiostatic electropolymerisation at 0.80 V vs SCE to a charge density of 2.20 C cm^{-2} . The PpyCl was prepared from a solution of 0.1 mol dm^{-3} Py and 0.1 mol dm^{-3} NaCl.

3.3.5 Open-circuit potential experiments

The free potential, E_{oc} , of the PpyCl and Chit/PpyCl films was determined using open-circuit potential measurements. Figure 3.17 shows typical open-circuit potential plots for PpyCl and Chit/PpyCl recorded over a 12 h period. The open-circuit potential of the PpyCl film decays gradually from an initial potential of 0.12 V vs SCE and then reaches a plateau after approximately 180 min. Similar potentials are observed with the Chit/PpyCl composite. However, for these composite films the potential reached a constant value between 30 min and 180 min, presumably due to the cationic chitosan hydrogel slowing down the diffusion of chloride ions. After about 180 min, the potential decays further before reaching a final plateau. The average potentials, recorded after the 12 h period, were calculated as 0.04 V vs SCE for both films.

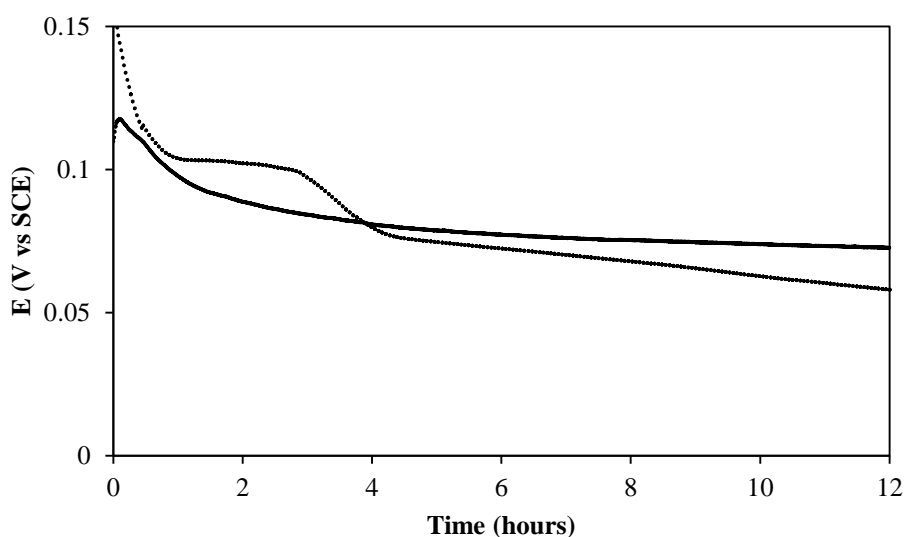


Figure 3.17: Open circuit potential-time plot for (— PpyCl) and (···· Chit/PpyCl) films recorded in $0.1 \text{ mol dm}^{-3} \text{ NaCl}$. PpyCl was prepared by potentiostatic electropolymerisation at 0.80 V vs SCE to a charge density of 2.20 C cm^{-2} . The PpyCl was prepared from a solution of $0.1 \text{ mol dm}^{-3} \text{ Py}$ and $0.1 \text{ mol dm}^{-3} \text{ NaCl}$.

3.3.6 Electrochemical impedance spectroscopy (EIS) studies

This section contains a detailed study of the complex-impedance of chitosan (Section 3.3.6.1), PpyCl (Section 3.3.6.2) and Chit/PpyCl (Section 3.3.6.3). The impedance response for chitosan, PpyCl and Chit/PpyCl is shown in the complex plane-impedance plots (Nyquist plots) and Bode plots in Figure 3.18. The imaginary and real components of the impedance are plotted to give the complex plane or Nyquist plots, while the modulus of the impedance and the phase angle are presented as a function of frequency to give the Bode plot. Reproducible results were obtained by polarising the electrodes at the required potential for 60 min. This period was sufficiently long to achieve steady-state conditions. The frequency range was varied from 65 kHz to 0.008 Hz. The impedance data, presented in Figure 3.18, were recorded for a Pt electrode coated with PpyCl, Chit/PpyCl films, 4 μm thick, and a chitosan film, 10 μL , at a constant potential of 0.10 V vs SCE.

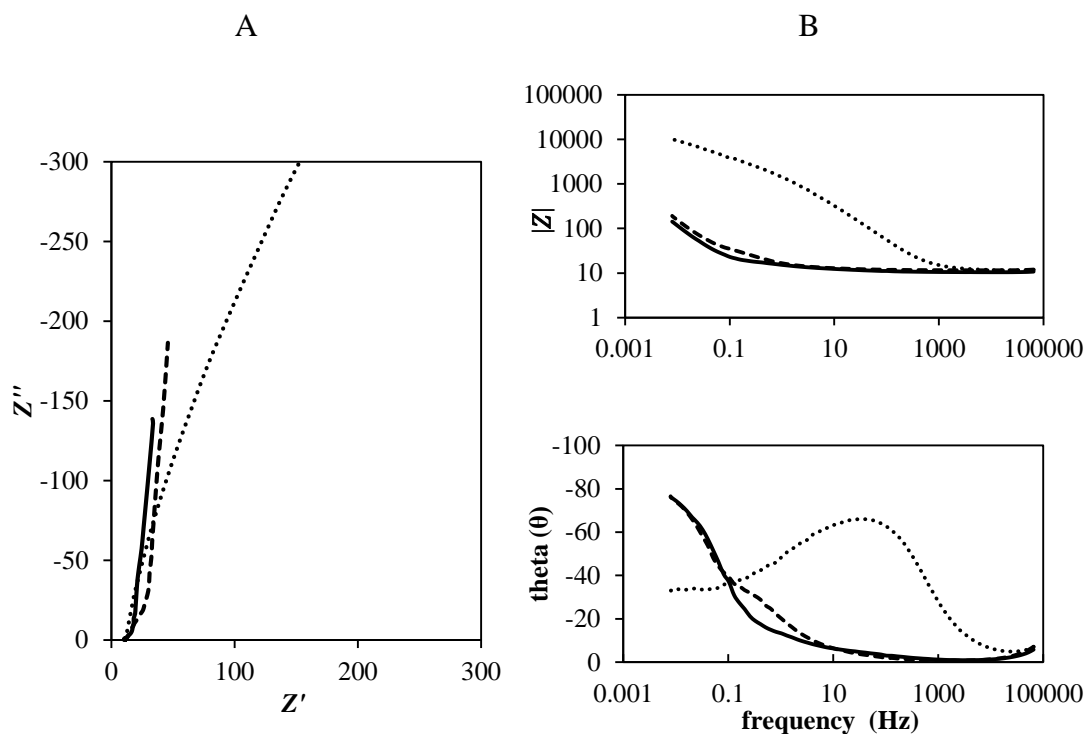


Figure 3.18: Complex-plane (A) and Bode impedance plots (B) for (— PpyCl), (···· Chit) and (--- Chit/PpyCl) coated 0.13 cm^2 Pt electrodes at 0.10 V vs SCE in 0.1 mol dm^{-3} NaCl. Frequency range shown from 65 kHz to 0.008 Hz . The films were prepared by potentiostatic electropolymerisation at 0.80 V vs SCE to a charge density of 2.20 C cm^{-2} . The PpyCl was prepared from a solution of 0.1 mol dm^{-3} Py and 0.1 mol dm^{-3} NaCl.

Two facts are immediately apparent from these data. The first observation is that the chitosan film exhibits a significantly higher resistance compared to the more conducting PpyCl and Chit/PpyCl films. Secondly, the presence of chitosan in the composite does not significantly alter the impedance response when compared to the data recorded for PpyCl.

In order to gain more information on the effect of chitosan in the Chit/PpyCl composite, the impedance measurements were recorded at fixed potentials between -0.80 V and 0.80 V vs SCE in 0.1 mol dm^{-3} NaCl. Data were collected in intervals of 0.10 V but only the data recorded at 0.20 V intervals are shown here. These data were fitted to the

equivalent circuits illustrated in Figure 3.19. using a non-linear least squares fitting minimisation method in the ZView fitting programme described in Section 2.4.4.

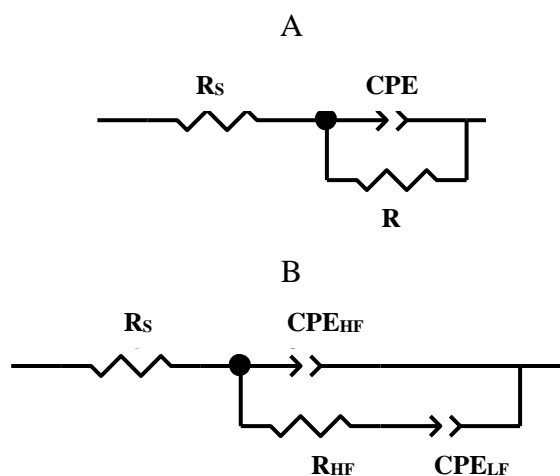


Figure 3.19: Equivalent circuits used for modelling the impedance data.

The circuit element R_{HF} represents resistance at high frequency, or charge-transfer resistance (R_{ct}), which contains contributions from the electronic and ionic resistance⁹⁹, as shown in Equation 3.8.

$$R_{HF} = R_e + R_i \quad (3.8)$$

Here, R_e is the electronic resistance and R_i is the ionic resistance. CPE_{HF} and CPE_{LF} elements are constant phase elements associated with high frequency impedance and low frequency impedance, respectively. Constant phase elements were used to determine the capacitance and were used rather than capacitors to take into account the inhomogeneity of the surface of the electrode^{100, 101}.

3.3.6.1 EIS of Chitosan films

The complex-plane impedance plots and Bode plots for the chitosan films are shown in Figure 3.20 A and B, respectively. There are few reports on the impedance of chitosan, however in some studies the impedance of chitosan solutions was reported¹⁰². The spectra

in the Nyquist plot show semi-circular arcs which are characteristic of the sinusoidal impedance curve which means only a resistance occurs, satisfying restrictive diffusion conditions¹⁰³.

The high to medium frequency region of the Nyquist plot and the Bode plot show superimposed transmission lines regardless of the applied potential until the lower frequency is reached ($\leq 20 - 25$ Hz). A simple Randles circuit (Figure 3.19 A) was used to model the impedance response at each applied potential. These changes can be explained by considering the processes that take place in the chitosan film.

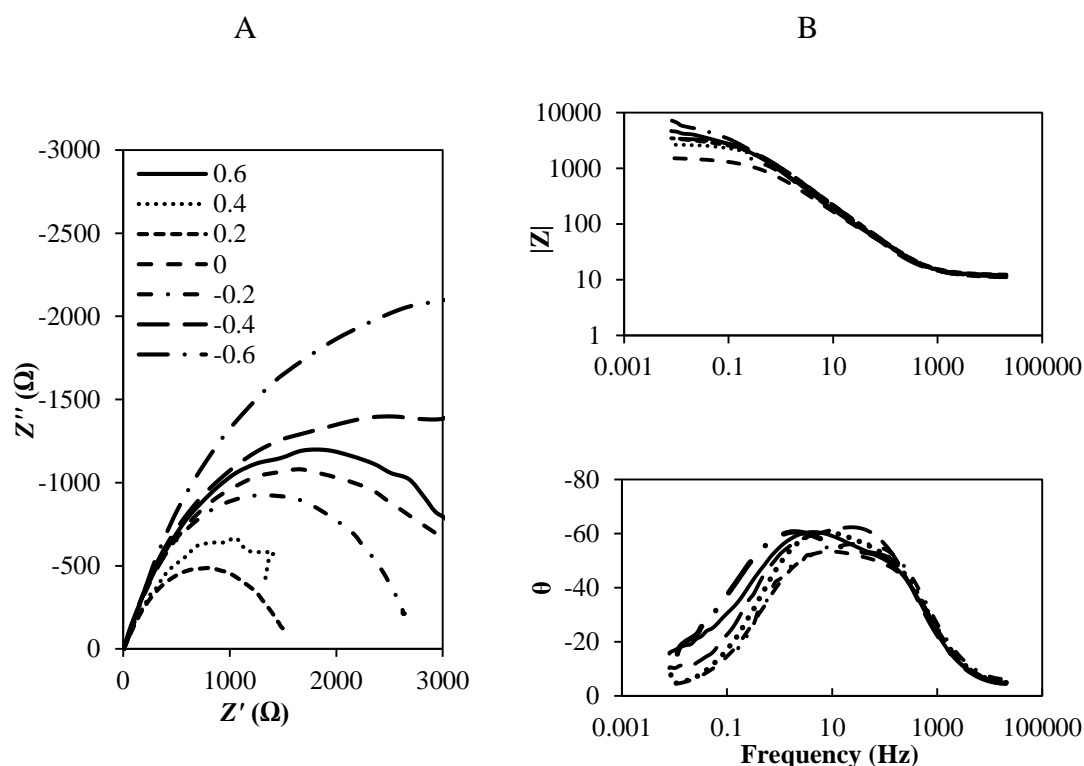


Figure 3.20: Complex-plane impedance plots (A) and the Bode plots (B) for chitosan coated 0.13 cm² Pt electrodes at various potentials in 0.1 mol dm⁻³ NaCl. Potentials are indicated in V vs SCE. Frequency range shown from 65 kHz to 0.008 Hz.

When water is incorporated into the chitosan film the free amino groups in the chitosan backbone become partially protonated¹⁰², as illustrated in Equation 3.9.



The NH_3^+ is bonded to the backbone of the chitosan but the OH^- is free to move (Equation 3.9). The mobility of these OH^- ions is connected with Equations 3.10 and 3.11, where the adsorption of cations clearly limits the mobility of the ions. At 0.80 V vs SCE, the ions are immobilised as $NH_3^+ OH^- Cl^-$, but as the potential is lowered, Equation 3.10 occurs giving higher concentrations of the mobile OH^- ions. This is consistent with the low resistance observed at 0.20 V vs SCE. As the potential is decreased further from 0.20 V to -0.60 V vs SCE, cation adsorption occurs limiting the mobility of counter-ions, as shown in Equation 3.11.



Table 3.3: Parameters for the circuit elements evaluated by fitting the impedance data of Chitosan to the equivalent circuit shown in Figure 3.19, $n=3$.

E (V vs SCE)	0.6	0.4	0.2	0.0	-0.2	-0.4	-0.6
R_s (Ω cm^2)	10.91 \pm 0.09	10.24 \pm 0.11	10.32 \pm 0.07	11.53 \pm 0.08	11.53 \pm 0.06	11.16 \pm 0.13	11.08 \pm 0.14
CPE-T (μF cm^{-2})	20.83 \pm 0.24	23.12 \pm 0.37	32.26 \pm 0.30	21.82 \pm 0.20	20.77 \pm 0.16	28.80 \pm 0.38	29.32 \pm 0.36
CPE-P	0.76 \pm 0.00	0.72 \pm 0.00	0.69 \pm 0.00	0.73 \pm 0.00	0.75 \pm 0.00	0.71 \pm 0.00	0.70 \pm 0.00
R ($k\Omega$ cm^2)	3.54 \pm 0.03	1.94 \pm 0.04	1.57 \pm 0.01	3.42 \pm 0.03	2.75 \pm 0.01	4.87 \pm 0.07	7.37 \pm 0.15
χ^2	0.00319	0.00258	0.00154	0.00202	0.00129	0.00498	0.00447
SS	0.4087	0.2525	0.1968	0.2580	0.1654	0.6377	0.5365

The charge transfer resistance, R , and the corrected capacitance, C , are plotted as a function of the applied potential in Figure 3.21 and Figure 3.22, respectively. As discussed above, it is clearly evident from Table 3.3 and Figure 3.21 that the charge-transfer resistance of the chitosan films vary with the potential, showing a minimum at 0.20 V vs SCE and a maximum at -0.60 V vs SCE.

Figure 3.22 shows the corrected capacitance, C , plotted as a function of the applied potential. The capacitance shows a maximum of $39 \mu\text{F cm}^2$ at 0.80 V vs SCE, the capacitance declines sharply to $22 \mu\text{F cm}^2$ with a minimum at 0.40 V vs SCE. Below 0.40 V vs SCE the capacitance appears to be independent of potential and remains at approximately $25 \mu\text{F cm}^2$.

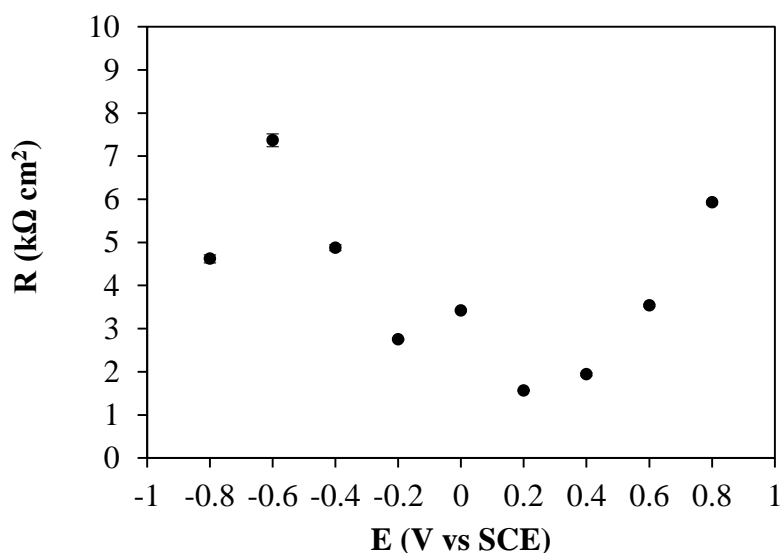


Figure 3.21: Charge transfer resistance, R , of chitosan coated 0.13 cm^2 Pt electrode plotted as a function of the applied potential in 0.1 mol dm^{-3} NaCl. $n=3$

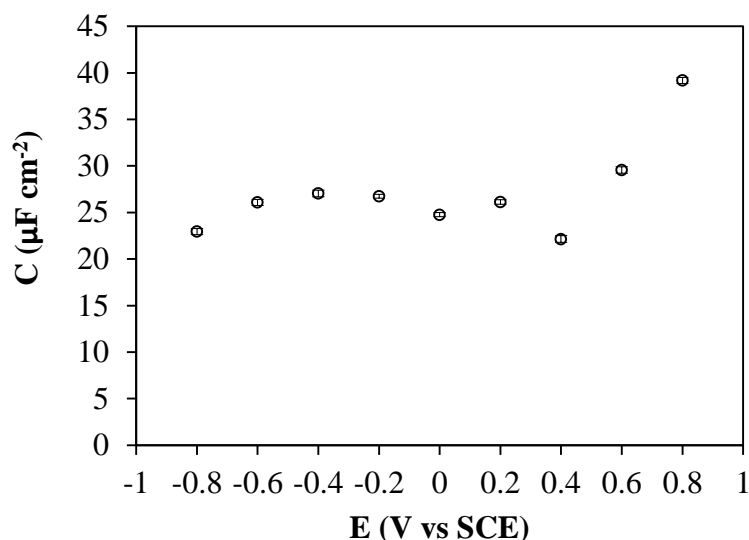


Figure 3.22: Corrected capacitance of chitosan coated 0.126 cm² Pt electrode plotted as a function of the applied potential in 0.1 mol dm⁻³ NaCl. n=3

3.3.6.2 EIS of PpyCl films

The complex-plane impedance plots and the Bode plots recorded for PpyCl show a range of electroactive behaviour, and the data are presented in Figures 3.23 and 3.24. In Figure 3.23 A and B, the impedance data recorded at 0.80, 0.60, 0.40, 0.20 and 0.00 V vs SCE are presented. It is evident from these data that the resistance of the PpyCl film is low at these potentials, but increases as the potential is increased from 0.00 to 0.60 V vs SCE before increasing sharply at 0.80 V vs SCE. It is evident from these data that the PpyCl polymer coated electrode behaves like a simple capacitor and the complex plane impedance plot becomes almost vertical. The impedance spectrum consists of a $\sim 45^\circ$ Warburg-type transmission line which can be seen more clearly in the inset of Figure 3.23 A. These data were fit to the equivalent circuit presented in Figure 3.19 B, which consists of an uncompensated solution resistance ($R_s = 11 \Omega \text{ cm}^2$) at the high frequency intercept. The CPE_{HF} represents the high frequency capacitance, or double layer capacitance, in parallel with R_{HF} . At oxidation potentials the value for R_{HF} is dominated by R_i . Based on

the well-known high electronic conductivity of PpyCl when it is even slightly oxidised, it can be assumed that the electronic resistance is negligible⁹⁵, i.e., ($R_i \gg R_e$). CPE_{LF} represents the low frequency capacitance, in this CPE_{LF} was replaced with a capacitor for an improved fit and lower errors.

Bowmaker *et al.*⁵⁵ found that Ppy over-oxidises irreversibly at potentials higher than 0.50 V vs SCE in the presence of chloride ions. This leads to a decrease in its redox activity and electronic conductivity as the β -C of pyrrole is oxidised to $C=O$ ^{104, 105}. At 0.80 V vs SCE, the PpyCl becomes over-oxidised and was modelled with a simple Randles cell circuit, shown in Figure 3.19 A.

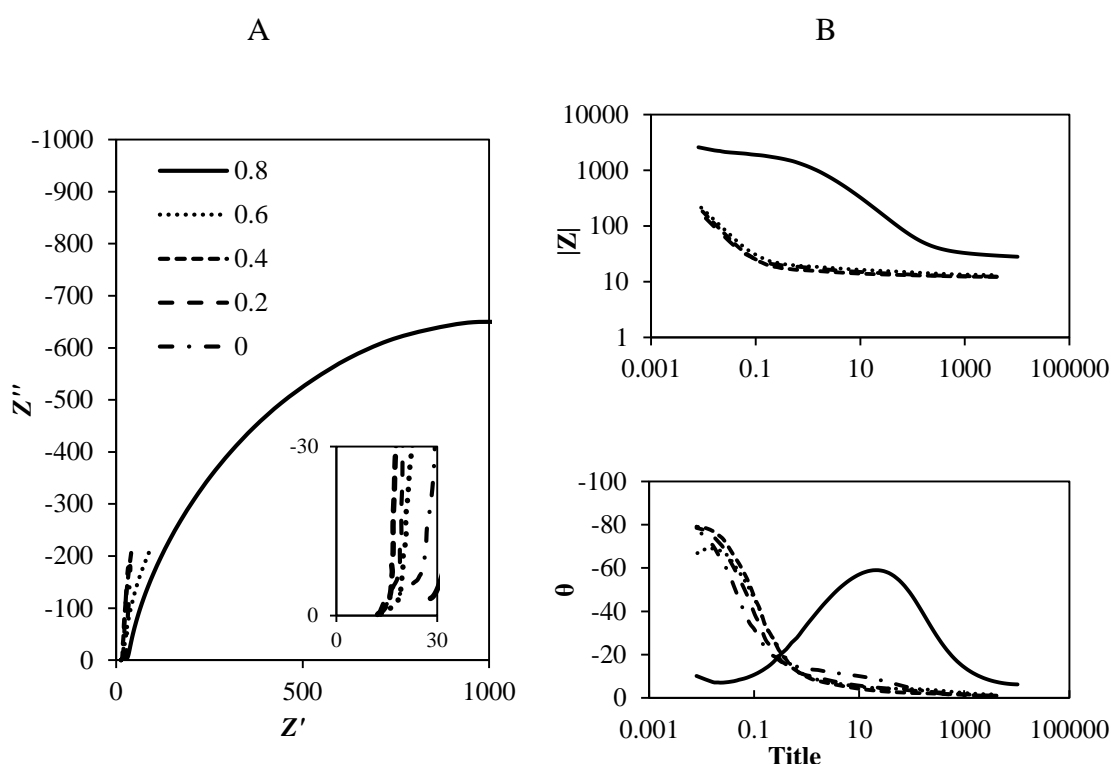


Figure 3.23: Complex-plane impedance plots (A) and Bode plots (B) for PpyCl coated 0.13 cm^2 Pt electrodes at various positive potentials in 0.1 mol dm^{-3} NaCl. Potentials are indicated in V vs SCE. Frequency range shown from 65 kHz to 0.008 Hz. The films were prepared by potentiostatic electropolymerisation at 0.80 V vs SCE to a charge density of 2.20 C cm^{-2} . The PpyCl was prepared from a solution of 0.1 mol dm^{-3} Py and 0.1 mol dm^{-3} NaCl.

In Figure 3.24 A and B, the complex-plane impedance plots and Bode plots are shown for PpyCl at a range of potentials varying from 0.00 to -0.80 V vs SCE. These data show a range of behaviours, with the resistance of the PpyCl film increasing tenfold from 0.00 V to -0.20 V vs SCE and a further tenfold increase in resistance from -0.20 V to -0.40 V vs SCE. The impedance response at 0.00 V vs SCE is almost vertical with a small $\sim 45^\circ$ incline, while the impedance at -0.20 V vs SCE displays a semi-circular configuration at the intermediate to low frequency region. Again these data were fit with the equivalent circuit in Figure 3.19 B.

At these potentials, the value for R_{HF} may not be dominated by the ionic resistance, and the contribution of electronic resistance becomes more significant, ($R_i < R_e$), as the potential is varied from -0.40 V to -0.80 V vs SCE. The PpyCl film becomes fully reduced at -0.80 V vs SCE and was modelled with the simple Randles cell circuit, shown in Figure 3.19 A. A summary of the values derived from the fitting is presented in Table 3.4, and the high frequency resistance, R_{HF} , and capacitance terms, C_{LF} and C_{HF} , are shown as a function of the applied potential in Figure 3.25.

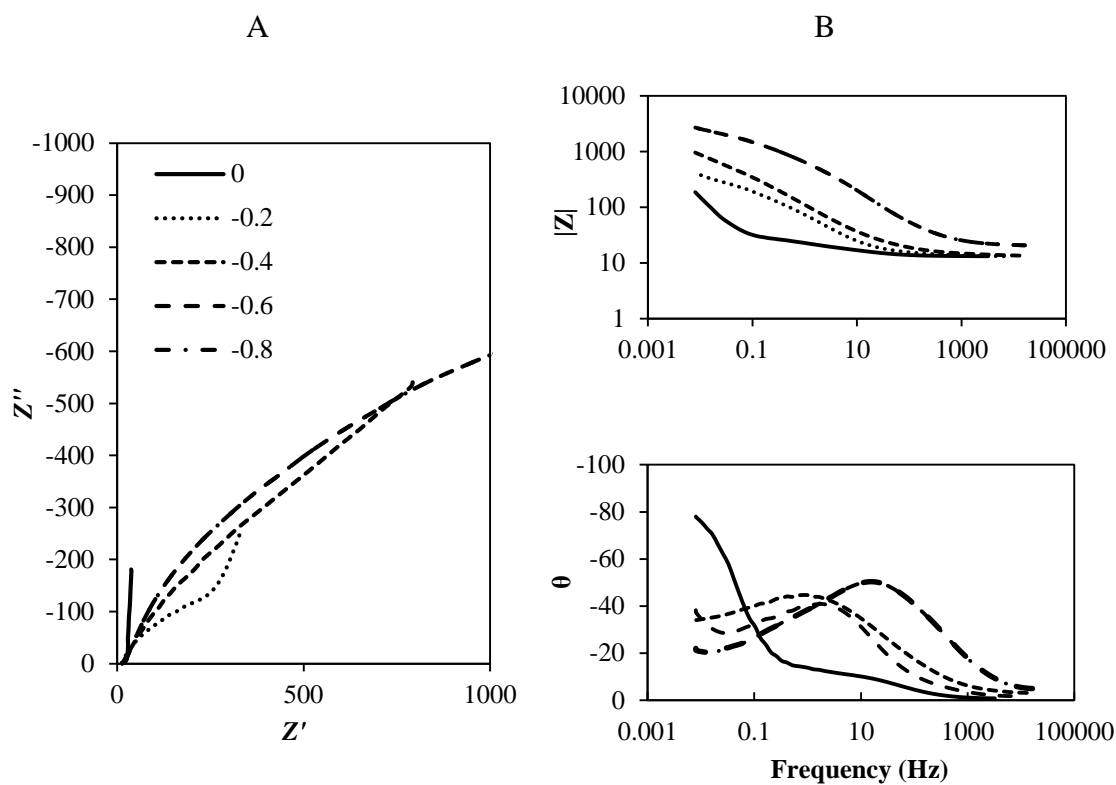


Figure 3.24: Complex-plane impedance plots (A) and Bode plots (B) for PpyCl coated Pt electrodes at various negative potentials in $0.1 \text{ mol dm}^{-3} \text{ NaCl}$. Potentials are indicated in V vs SCE. Frequency range shown from 65 kHz to 0.008 Hz. The films were prepared by potentiostatic electropolymerisation at 0.80 V vs SCE to a charge density of 2.20 C cm^{-2} . The PpyCl was prepared from a solution of $0.1 \text{ mol dm}^{-3} \text{ Py}$ and $0.1 \text{ mol dm}^{-3} \text{ NaCl}$.

Table 3.4: Parameters for the circuit elements evaluated by fitting the impedance data of PpyCl to the equivalent circuit shown in Figure 3.19, n=3.

E (V vs SCE)	0.6	0.4	0.2	0.0	-0.2	-0.4	-0.6
R_s (Ω cm²)	13.18 ± 0.11	12.62 ± 0.05	12.66 ± 0.07	13.32 ± 0.07	13.14 ± 0.05	13.20 ± 0.08	18.50 ± 0.31
CPE-T_{HF} (mF cm⁻²)	11.76 ± 0.42	14.51 ± 0.66	13.59 ± 0.58	12.05 ± 0.37	4.14 ± 0.05	3.50 ± 0.02	0.43 ± 0.01
CPE-P_{HF}	0.57 ± 0.01	0.77 ± 0.01	0.72 ± 0.01	0.67 ± 0.01	0.66 ± 0.00	0.56 ± 0.00	0.62 ± 0.00
R_{HF} (Ω cm²)	7.14 ± 0.19	4.47 ± 0.13	7.32 ± 0.18	16.79 ± 0.29	292 ± 8	2030 ± 59	2432 ± 60
CPE-T_{LF} (mF cm⁻²)	53.50 ± 0.79	67.74 ± 1.01	80.83 ± 1.24	81.94 ± 1.21	25.02 ± 1.39	- ± -	- ± -
CPE-P_{LF}	1 ± 0	1 ± 0	1 ± 0	1 ± 0	0.68 ± 0.02	- ± -	- ± -
χ²	0.00406	0.00490	0.00578	0.00367	0.00079	0.00215	0.00740
SS	0.4501	0.5535	0.6526	0.4079	0.0918	0.2671	0.8581

The CPE was replaced with a capacitor (C) in the lower branch of the circuit for parameters with a P value of 1 ± 0

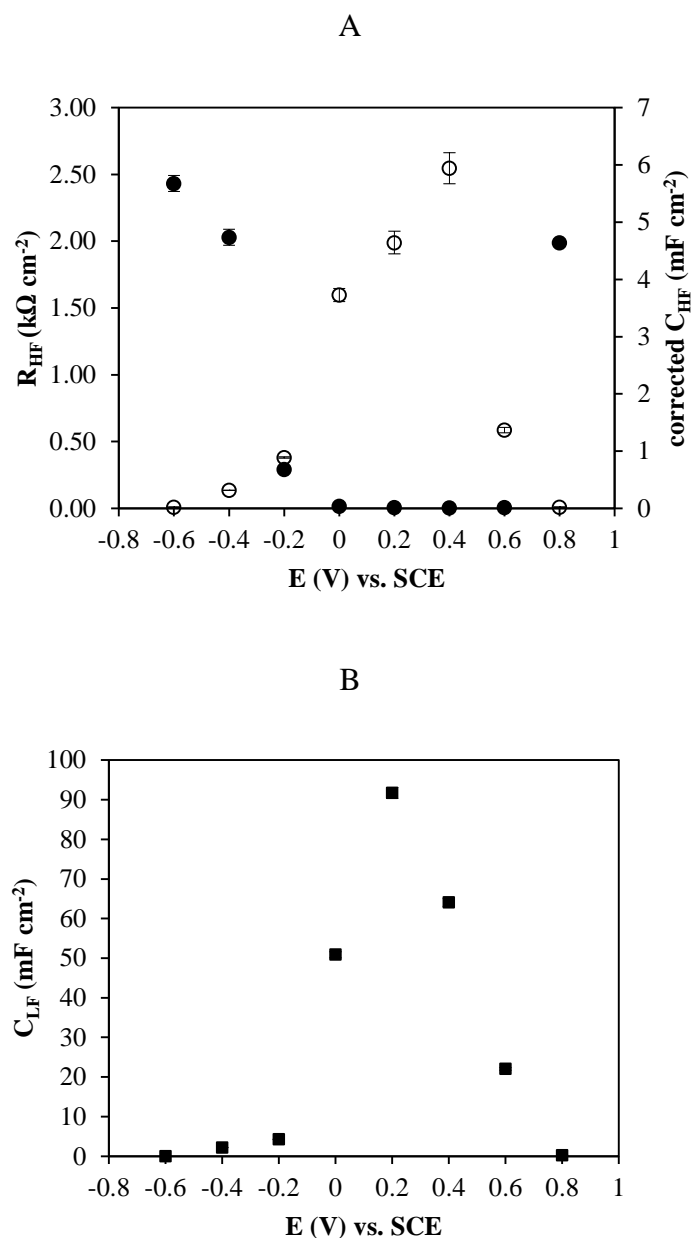


Figure 3.25: High frequency resistance, R_{HF} (●), corrected high frequency capacitance, C_{HF} (○) and low frequency capacitance, C_{LF} , (■) plotted as a function of applied potential for PpyCl in 0.1 mol dm^{-3} NaCl. The films were prepared by potentiostatic electropolymerisation at 0.80 V vs SCE to a charge density of 2.20 C cm^{-2} . The PpyCl was prepared from a solution of 0.1 mol dm^{-3} Py and 0.1 mol dm^{-3} NaCl. $n=3$

It is clearly evident from Table 3.4 and Figure 3.25 that the resistance, R_{HF} is high at 0.80 V vs SCE, and over-oxidation was identified as the probable cause^{104, 105}. The R_{HF} decreases considerably from 0.80 V to 0.60 V vs SCE, before reaching a minimum at 0.40 V vs SCE. The values increase again as the PpyCl film is fully reduced. The corrected high frequency capacitance, due to the double layer, increases as the applied potential is reduced from 0.80 V to 0.40 V vs SCE, which corresponds to the anion exchange. Figure 3.25 B shows a sharp peak in the low frequency capacitance possibly due to electron injection at the Pt|PpyCl interface and occurs close to the anion exchange at the PpyCl|electrolyte. The low frequency capacitance increases with the double layer capacitance and shows a maximum at 0.20 V vs SCE, possibly due to the increase in effective surface area¹⁰⁶.

3.3.6.3 EIS of Chit/PpyCl films

The impedance data were recorded using the same parameters and under the same conditions as stated for PpyCl, Section 3.3.6.2. The impedance data of Chit/PpyCl are presented in Figures 3.26 A and B and 3.27 A and B. Again, the applied potential has a considerable influence on the impedance response. In Figure 3.26 A and B, impedance data recorded at 0.00, 0.20, 0.40, 0.60 and 0.80 V vs SCE are presented as Nyquist impedance plots and Bode plots, respectively. Figure 3.27 show the complex-impedance at applied potentials from 0.00 V to -0.80 V vs SCE

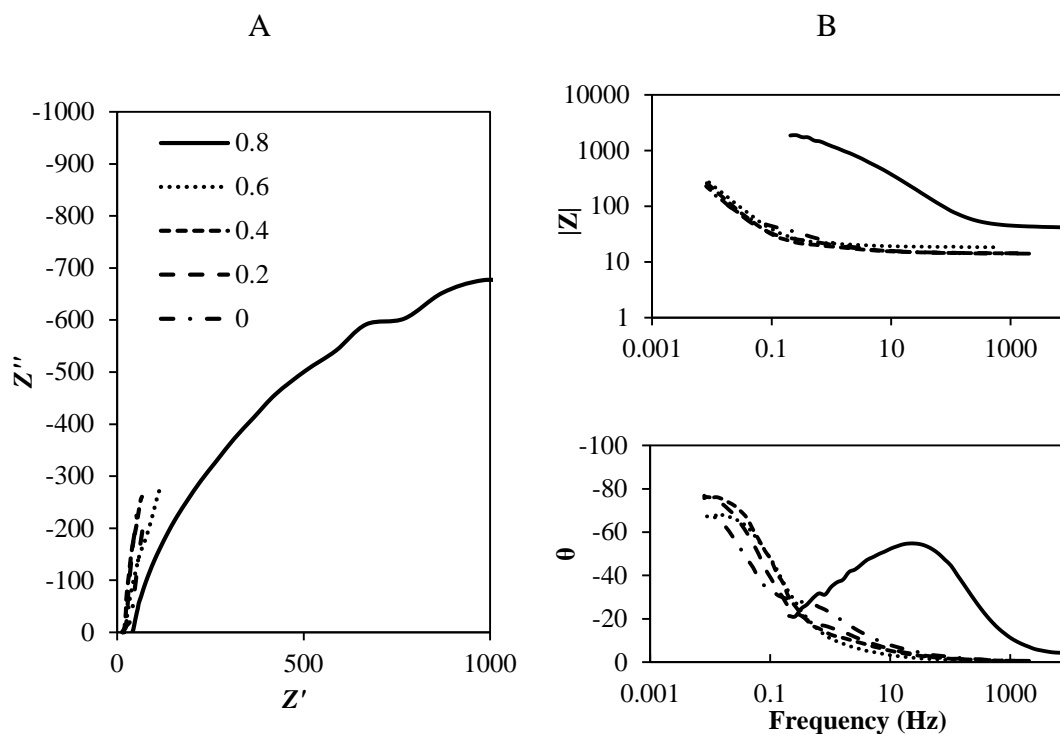


Figure 3.26: Complex-plane impedance plots (A) and Bode plots (B) for Chit/PpyCl coated 0.13 cm² Pt electrodes at various positive potentials in 0.1 mol dm⁻³ NaCl. Potentials are indicated in V vs SCE. Frequency range shown from 65 kHz to 0.008 Hz. The films were prepared by potentiostatic electropolymerisation at 0.80 V vs SCE to a charge density of 2.20 C cm⁻². The PpyCl was prepared from a solution of 0.1 mol dm⁻³ Py and 0.1 mol dm⁻³ NaCl.

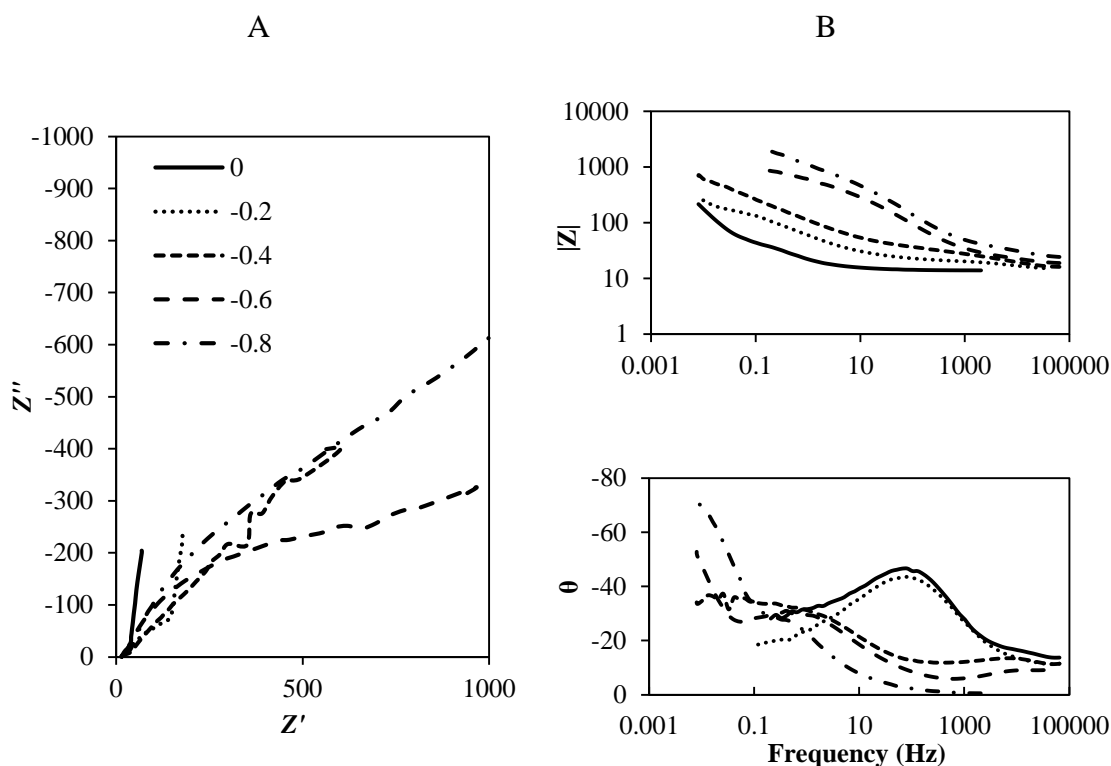


Figure 3.27: Complex-plane impedance plots (A) and Bode plots (B) for Chit/PpyCl coated Pt electrodes at various applied negative potentials in 0.1 mol dm^{-3} NaCl. Potentials are indicated in V vs SCE. Frequency range shown from 65 kHz to 0.008 Hz. The films were prepared by potentiostatic electropolymerisation at 0.80 V vs SCE to a charge density of 2.20 C cm^{-2} . The PpyCl was prepared from a solution of 0.1 mol dm^{-3} Py and 0.1 mol dm^{-3} NaCl.

The impedance data recorded from 0.60 V to -0.20 V vs SCE were analysed using the circuit in Figure 3.19 B. The simple Randles cell circuit, shown in Figure 3.19 A, was used to model the data at the lower applied potentials from -0.40 V to -0.60 V vs SCE. The fitted parameters are summarised in Table 3.5, while the charge-transfer resistance, R_{HF} , and the corrected double layer capacitance terms, C_{HF} and C_{LF} , are plotted as a function of the applied potential in Figure 3.28.

Table 3.5: Parameters for the circuit elements evaluated by fitting the impedance data of Chit/PyPyCl to the equivalent circuit shown in Figure 3.19, $n=3$.

E (V vs SCE)	0.6	0.4	0.2	0.0	-0.2	-0.4	-0.6
R_s (Ω cm^2)	18.44 \pm 0.06	14.42 \pm 0.05	14.51 \pm 0.04	14.20 \pm 0.04	16.46 \pm 0.07	6.71 \pm 0.36	17.98 \pm 0.26
CPE- T_{HF} (mF cm^{-2})	26.66 \pm 0.89	19.52 \pm 0.49	20.48 \pm 0.32	21.09 \pm 0.24	7.19 \pm 0.09	2.64 \pm 0.08	0.26 \pm 0.01
CPE- P_{HF}	0.78 \pm 0.01	0.80 \pm 0.00	0.79 \pm 0.00	0.72 \pm 0.00	0.55 \pm 0.00	0.27 \pm 0.00	0.59 \pm 0.01
R_{HF} (Ω cm^2)	7.88 \pm 0.54	9.24 \pm 0.24	17.01 \pm 0.28	51.11 \pm 0.86	250 \pm 5.27	50.09 \pm 1.31	911 \pm 25
CPE- T_{LF} (mF cm^{-2})	23.01 \pm 0.96	44.01 \pm 0.69	52.82 \pm 0.65	50.88 \pm 0.86	52.25 \pm 1.16	- \pm -	- \pm -
CPE- P_{LF}	1 \pm 0	1 \pm 0	1 \pm 0	1 \pm 0	1 \pm 0	- \pm -	- \pm -
χ^2	0.00146	0.00238	0.00160	0.00163	0.00102	0.00046	0.00454
SS	0.1183	0.2454	0.1650	0.1748	0.1012	0.0531	0.4538

The CPE was replaced with a capacitor (C) in the lower branch of the circuit for parameters with a P value of 1 ± 0

It is evident from a comparison of the impedance data recorded for the PpyCl and Chit/PpyCl films that the impedance response is similar but not identical. In this potential range, PpyCl and Chit/PpyCl have low resistance values indicating good electronic conductivity and the chitosan has no adverse effect on the PpyCl. At lower potentials (-0.40 V to -0.80 V vs SCE) a reduction process occurs and the resistance increases due to the loss of anions. The “Warburg-like” feature diminishes in the Chit/PpyCl and a circular arc indicative of the high charge-transfer resistance is observed in the impedance plots. The capacitance also decreases, this decrease in capacitance is observed as the dopant anion is released from the polymer film during reduction.

The presence of chitosan appears to modify the reduction of the PpyCl component. The resistance at 0.60 V vs SCE is $7.88 \Omega \text{ cm}^2$ and $7.14 \Omega \text{ cm}^2$ for Chit/PpyCl and PpyCl, respectively. The R_{HF} values remain comparable as the potential is reduced to -0.20 V vs SCE. As the potential is further reduced the resistance of the Chit/PpyCl steadily increases to $911 \Omega \text{ cm}^2$ at -0.60 V vs SCE, whereas the resistance of PpyCl increases to $2432 \Omega \text{ cm}^2$ at -0.60 V vs SCE. Frequency limits were difficult to attain for PpyCl at -0.80 V vs SCE, Chit/PpyCl on the other hand has an R_{HF} value of $2180 \Omega \text{ cm}^2$ at -0.80 V vs SCE, albeit with an increase in the sum of squares. This may be due to the mobility of counter-ions in the hydrogel. These results show that using chitosan in conjunction with PpyCl provides a good matrix for regulating ion-transport⁴⁶.

Again, the R_{HF} and C_{HF} values correspond showing a minimum in R_{HF} of $7.88 \Omega \text{ cm}^2$ at 0.60 V vs SCE and a corresponding maximum of 15.5 mF cm^{-2} for the capacitance, C_{HF} . This C_{HF} value is slightly higher than 5.94 mF cm^{-2} at 0.40 V vs SCE, which was obtained with the PpyCl film. The R_{HF} maximum has shifted from 0.40 V vs SCE in PpyCl to 0.60 V vs SCE in Chit/PpyCl. Similarly, the low frequency capacitance in Figure 3.28 has shifted from 0.20 V vs SCE for PpyCl to 0.40 V vs SCE for Chit/PpyCl. Maximum values obtained for the low frequency capacitance are similar at 91.7 mF cm^{-2} and 93.5 mF cm^{-2} for PpyCl and Chit/PpyCl, respectively. The C_{LF} values decrease as the potential decreases as the Chit/PpyCl becomes reduced due to the diminishing concentration of Cl^- anions in the film. The values are significantly different from that of chitosan in Figure 3.21 and Figure 3.22.

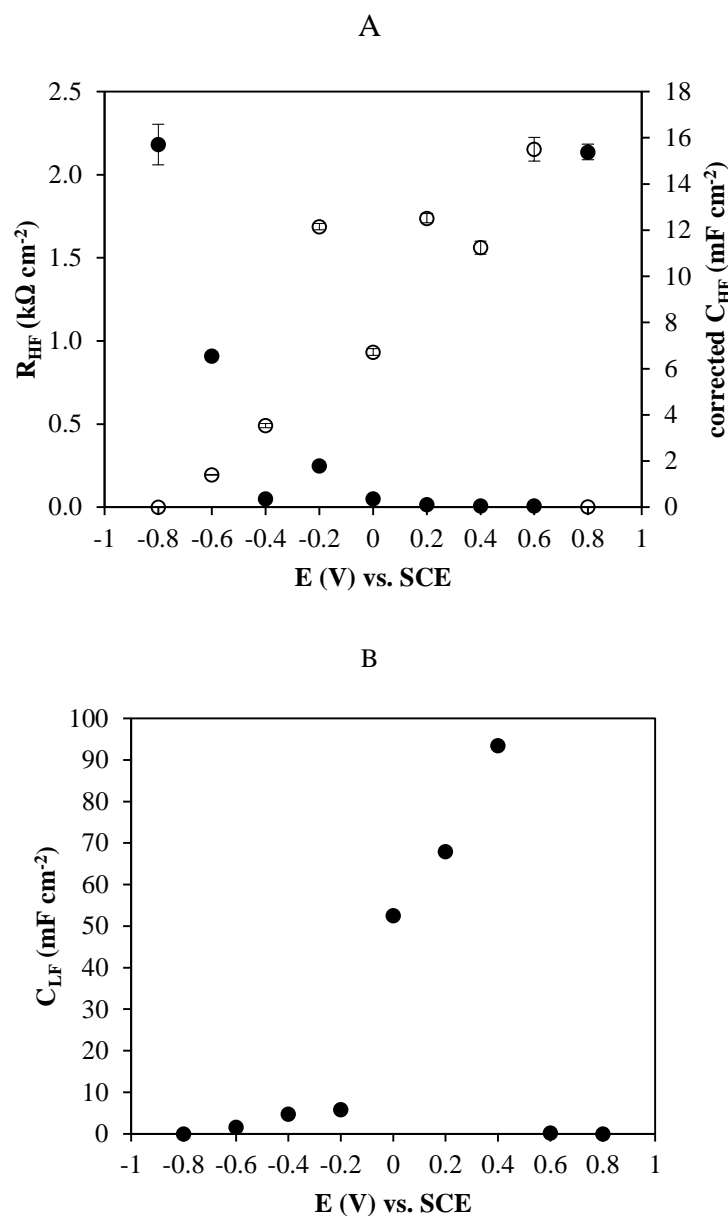


Figure 3.28: High frequency resistance, R_{HF} (●), corrected high frequency capacitance, C_{HF} (○) and low frequency capacitance, C_{LF} (■) plotted as a function of applied potential for Chit/PpyCl in 0.1 mol dm^{-3} NaCl. The films were prepared by potentiostatic electropolymerisation at 0.80 V vs SCE to a charge density of 2.20 C cm^{-2} . The PpyCl was prepared from a solution of 0.1 mol dm^{-3} Py and 0.1 mol dm^{-3} NaCl. $n=3$

3.3.6.4 Comparison between the composite films

Most of this chapter is devoted to the Chit/PpyCl composite system. In subsequent chapters, results are presented for the PpyA/Chit system where A is an anion (Cl^- , MO^-

, Dex^{2-} and Ox^-). In this section a comparison is made between the two chloride systems, Chit/PpyCl and PpyCl/Chit. As shown in Figure 3.1, the difference between these two composites is the order of addition of chitosan, either pre-electropolymerisation or post-electropolymerisation. In both cases 10 μL of chitosan was employed. However, the PpyCl component was deposited to a charge density of 2.2 and 0.25 C cm^{-2} for the Chit/PpyCl and PpyCl/Chit systems, respectively.

The impedance responses of Chit/PpyCl and PpyCl/Chit are shown in Figure 3.29, where the impedance data were recorded at 0.10 V vs SCE in 0.1 mol dm^{-3} NaCl.

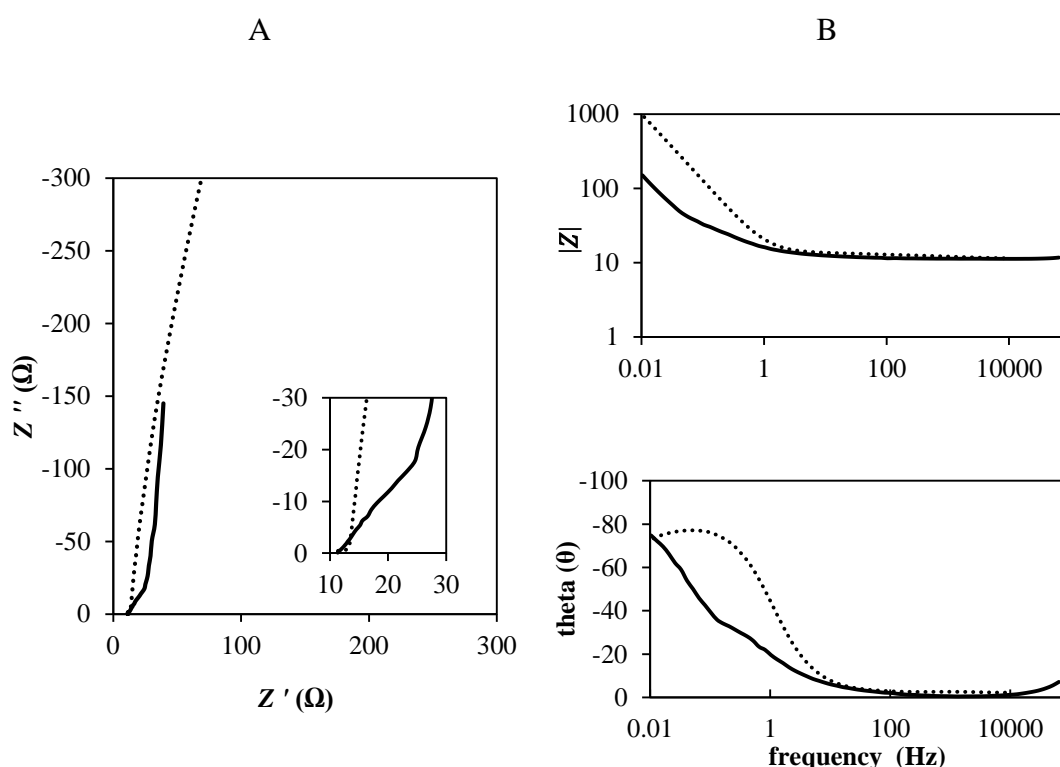


Figure 3.29: Complex-plane impedance plot (A) and Bode plot (B) for (\cdots Chit/PpyCl), (— PpyCl/Chit), coated Pt electrodes at 0.10 V vs SCE in 0.1 mol dm^{-3} NaCl. Frequency range shown from 65 kHz to 0.008 Hz. The films were prepared by potentiostatic electropolymerisation at 0.80 V vs SCE to a charge density of 2.20 C cm^{-2} for (\cdots Chit/PpyCl) and 0.25 C cm^{-2} for (— PpyCl/Chit). The Chit/PpyCl was prepared from a solution of 0.1 mol dm^{-3} Py and 0.1 mol dm^{-3} NaCl on a chitosan coated Pt electrode. Chitosan was added post-electropolymerisation for (— PpyCl/Chit).

The complex impedance plot shows a notable difference at the high frequency region, which is more evident in the inset. There is also a notable difference in the impedance response at the lower frequencies. This is clearly evident from a comparison of the Bode plots.

A summary of the data is presented in Table 3.6 along with PpyCl in the absence of chitosan and in the presence of chitosan, and pure chitosan is also included. The resistance values of PpyCl grown to different charge densities are similar but their double layer capacitance (corrected C_{HF}) and low frequency capacitance are quite different. This may be explained by the difference in film thickness influencing the effective surface area¹⁰⁷. Overall, the values recorded for the Chit/PpyCl and PpyCl (2.20 C cm⁻²) are similar, while the values obtained for the PpyCl/Chit and PpyCl (0.25 C cm⁻²) show a difference in resistance, this is possibly due to the influence that chitosan has on the ion mobility of chloride anions. Loss in conductivity is associated with reduced concentration of dopant species¹⁰⁸, and chitosan may aid in the preservation of electroactivity if dedoping is reduced. The values obtained for PpyCl are in good agreement with data reported by Li and Qian¹⁰⁹, taking into account the difference in electrode surface area. Chitosan has the highest resistance by three orders of magnitude due to the lack of conductivity.

Table 3.6: A comparison of the composite films and their components. Corrected capacitance C_{HF} , high frequency resistance R_{HF} , and low frequency capacitance, C_{LF} , in 0.1 mol dm⁻³ NaCl at 0.1 V vs SCE.

Sample (0.10 V)	corrected C_{HF} (mF cm⁻²)	R_{HF} (Ω cm²)	C_{LF} (mF cm⁻²)
Chit/PpyCl (2.20 C cm⁻²)	56.83 ± 0.75	37.2 ± 1.57	49.72 ± 0.59
PpyCl (2.20 C cm⁻²)	52.30 ± 0.84	9.5 ± 0.22	87.04 ± 1.41
PpyCl/Chit (0.25 C cm⁻²)	0.28 ± 0.06	2.5 ± 0.08	7.44 ± 0.2
PpyCl (0.25 C cm⁻²)	0.64 ± 0.03	14.9 ± 0.80	9.77 ± 1.37
Chitosan	22.13 ± 0.44	2629 ± 93.45	-

3.4 Effect of lysozyme

Biomedical materials for devices and drug delivery are an expanding area supporting the development of new drugs and therapeutics¹¹⁰. Natural polymers such as chitosan are of particular interest because of their non-toxic, biocompatible and antimicrobial properties¹¹¹. This present study was carried out to evaluate the suitability of Chit/PpyCl in the development of biomedical materials by investigating the enzymatic resistance of the Chit/PpyCl coated electrode. If the material is to be used in biomedical applications the enzymes present in-vivo must be taken into consideration. For chitosan, the corresponding cleaving enzyme is chitosanase¹¹² but it is expensive and unavailable in bulk¹¹³. In this study lysozyme was used as a ubiquitous enzyme because it is more abundant than chitosanase. Lysozyme is often used as an alternative to chitosanase for degradation studies of chitosan^{114, 115}, which appears to target acetylated residues. Its mode of action is similar to that of lysozyme which causes the hydrolysis of the (1→4)-β-glycosidic bond between *N*-acetyl-D-glucosamine residues¹¹⁶. Usually an enzymatic degradation study is carried out using a gravimetric technique^{115, 117} or by the determination of the reducing sugar content¹¹⁸. Unfortunately some difficulties were encountered when designing this degradation test. Therefore, in this study an in-vitro interaction of the chitosan with lysozyme was investigated using cyclic voltammetry (CV) in conjunction with the simultaneous measurements of the frequency response of an electrochemical quartz crystal microbalance (EQCM) electrode. The CV method was used to study peak current densities and peak potentials in relation to the lysozyme concentration in solution. Optimum measurement parameters were established using a gold disc electrode prior to using the Au-EQCM electrodes. The f_0 value was obtained from each experiment and was used to calculate the sensitivity factor (C_f) in Equation 3.1, which was found to be $7.09 \times 10^8 \text{ Hz cm}^2 \text{ g}^{-1}$. The lysozyme solutions were refreshed daily to ensure continuous enzyme activity

3.4.1 The effect of lysozyme solution on chitosan using EQCM

The volume of chitosan used to coat the Au-EQCM electrode was scaled-up from 10 μL for 0.13 cm^2 to 16.2 μL for 0.20 cm^2 . The 0.5 % (w/v) chitosan solution was pipetted onto the Au-EQCM electrode and the film was forced dried under an IR lamp (50 to 55 $^\circ\text{C}$) for 15 min. Prior to studying the effect of lysozyme on the chitosan coated Au-EQCM electrode, the bare Au-EQCM was cycled between 0.35 V and 0.50 V vs Ag|AgCl in 0.1 mol dm^{-3} NaCl solution until a reproducible voltammetric profile was obtained. The quality of the data for chitosan coated Au-EQCM electrodes was validated by recording cyclic voltammograms on a conventional Au electrode. The quality of the Au-EQCM voltammograms were verified by comparing them with previously recorded data on conventional Au electrodes. Open-circuit potential and cyclic voltammetry measurements were used to study the effect of the lysozyme solution on the electrochemical system. Two characteristic regions were observed for the gold electrodes, the non-faradaic current region (-0.35 V to 0.20 V vs SCE), and the steady state anodic peak between 0.20 V and 0.40 V vs SCE.

Studies on the adsorption of lysozyme at different concentrations and its coadsorption with Cl^- ions on Au in 0.1 mol dm^{-3} NaCl were performed for each concentration of lysozyme. The potential was cycled from -0.35 V to 0.50 V vs SCE. Representative data are shown in Figure 3.30 A and B where the voltammograms and the relative frequency were recorded in the presence of lysozyme with concentrations ranging from 1.5 $\mu\text{g mL}^{-1}$ to 1.0 mg mL^{-1} . Freier and Shoichet¹¹⁹ reported a maximum concentration of lysozyme in human serum to be 1.5 $\mu\text{g mL}^{-1}$. A 0.1 mol dm^{-3} NaCl solution served as the blank solution. There is little variation between the cyclic voltammograms and similar data are recorded in the lysozyme solutions. The relative frequency plots are similar for the blank solution and the solution containing 1.5 $\mu\text{g mL}^{-1}$ of lysozyme, while the plots are considerably different with the higher concentrations of lysozyme.

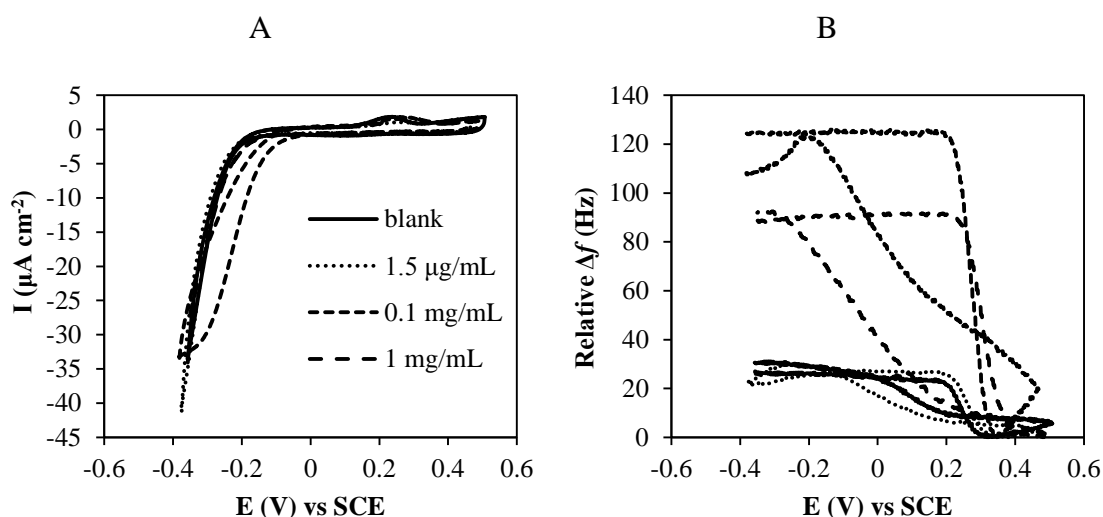


Figure 3.30: Representative EQCM data (A) cyclic voltammograms (10th cycle) and the corresponding (B) relative change in frequency (Δf) in different electrolyte solutions indicated in (A). Chit/PpyCl was prepared from a solution of 0.1 mol dm^{-3} Py and 0.1 mol dm^{-3} NaCl. The films were electropolymerisation at 0.80 V vs SCE to a charge density of 55 mC cm^{-2} on a chitosan coated Au-EQCM crystal (0.20 cm^2).

Although there are some reports in the literature of EQCM data on hydrogels^{120, 121}, it is not viable to determine a change in mass because hydrogels oppose certain preconditions of the Sauerbrey equation (Equation 3.1)¹²². The hydrogels are known to swell which, in this case, could be excessive¹⁰². Possible contributions to changes in the relative frequency include changes in surface morphology due to swelling and solution viscosity.

3.4.2 Open-circuit potential of Chit/PpyCl immersed in lysozyme solution

Open-circuit potential experiments were carried out in an attempt to determine the stability of Chit/PpyCl in the presence of lysozyme. The Chit/PpyCl coated electrodes were immersed in centrifuge tubes containing 0.1 mol dm^{-3} NaCl (control/blank) and a solution of lysozyme, $1.5 \text{ } \mu\text{g mL}^{-1}$ made up in 0.1 mol dm^{-3} NaCl (which served as an electrolyte). The solutions were refreshed daily over the 28 day period. The open-circuit potential is plotted as a function time, in days, for Chit/PpyCl immersed in 0.1 mol dm^{-3} NaCl and in the lysozyme-containing solution, in Figure 3.31. It is clear from these data that the open-circuit potentials recorded for the blank and lysozyme-containing solutions are similar over the 28-day period. The open-circuit potentials are reasonably constant and only vary from 0.12 V to 0.15 V vs SCE over the 28 day period. There is no evidence

to indicate that the lysozyme solution has modified the properties of the Chit/PpyCl composite.

After recording the open-circuit potential for 10 minutes, cyclic voltammetry was carried out over a short period of time (to avoid over-oxidation of the composite) in a small window between -0.35 and 0.50 V vs SCE, for 10 cycles at 50 mV s^{-1} . Figure 3.32 shows the total charge consumed during the 10th cycle of the cyclic voltammograms recorded in the presence and absence of the lysozyme. In both cases, the Chit/PpyCl composites immersed in the blank and 1.5 $\mu\text{g mL}^{-1}$ of lysozyme show a decrease in charge consumed during oxidative cycling (Figure 3.32 A) and a concomitant increase in charge consumed during reduction (Figure 3.32 B). Again, it can be concluded from these data that the lysozyme solutions have no significant effect on the stability of the Chit/PpyCl composites during electrochemical analysis. This is in good agreement to Ren and Ma's report on the very slow degradation process of chitosan (degree acetylation between 71.7 % and 93.5 %) in lysozyme over an 80 day period¹¹⁸.

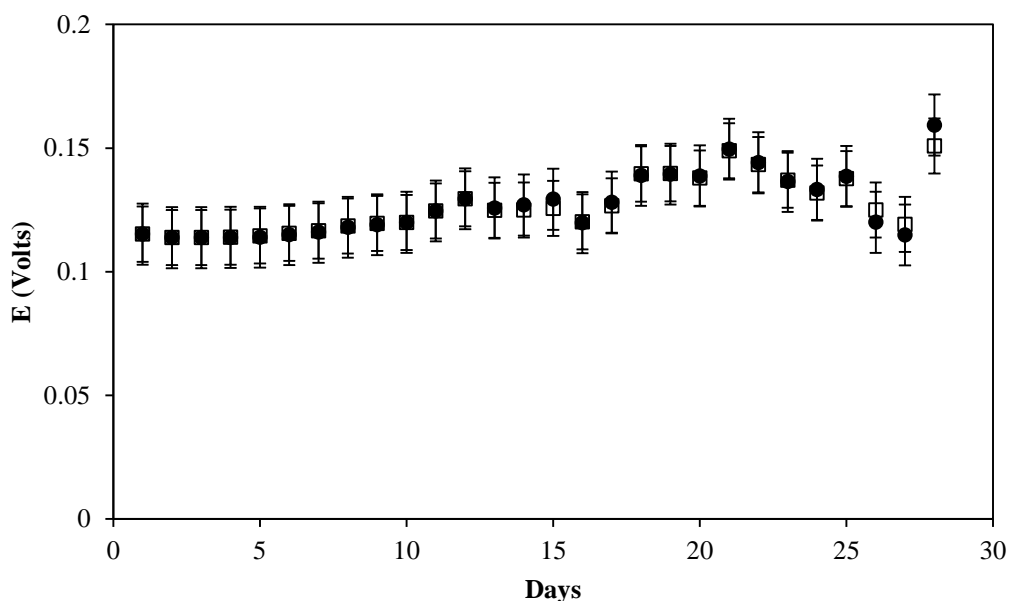


Figure 3.31: Open-circuit potential-time plots for Chit/PpyCl in 1.5 $\mu\text{g mL}^{-1}$ lysozyme (●) and 0.1 mol dm^{-3} NaCl (□). The films were prepared by potentiostatic electropolymerisation at 0.80 V vs SCE to a charge density of 2.20 C cm^{-2} from a solution of 0.1 mol dm^{-3} Py and 0.1 mol dm^{-3} NaCl on to a chitosan coated Pt electrode. $n=3$

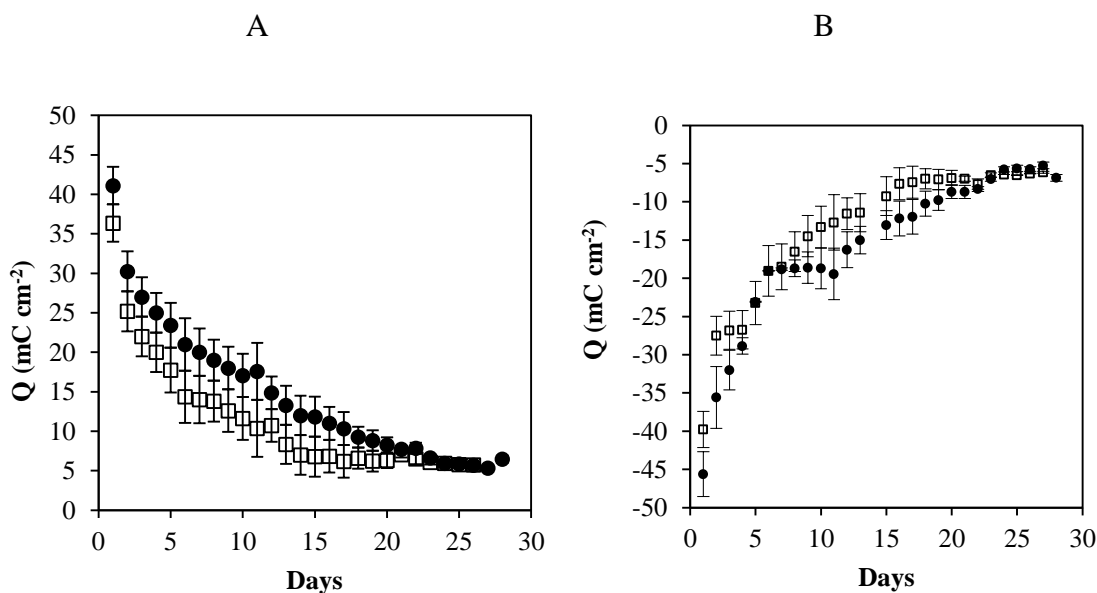


Figure 3.32: Total charge consumed during, 10th cycle. (A) oxidation (B) reduction, the Chit/PpyCl in 1.5 μg mL⁻¹ lysozyme and NaCl is represented by (●) and (□), respectively. The films were prepared by potentiostatic electropolymerisation at 0.80 V vs SCE to a charge density of 2.20 C cm⁻² from a solution of 0.1 mol dm⁻³ Py and 0.1 mol dm⁻³ NaCl on to a chitosan coated Pt electrode. n=3

3.5 Adhesion test

The adhesion of polypyrrole to a metal substrate is pivotal to its applications, especially where good electrical contact is necessary. Generally in the case of inert metals (Pt and Au) there are no issues with the deposition and adhesion of polypyrrole, but the adhesion of polypyrrole films on some medical materials, for example titanium, is quite weak and the metal has to be pre-treated with an etchant to improve the deposition and adhesion. For some applications where a reduction potential is applied there can be a loss of adhesion even on inert metals. The loss of adhesion is associated with decreased capacitance¹²³. A decrease in capacitance is observed when the dopant is released from the polymer film during reduction.^{124, 125}

The adhesion properties were determined by performing the peel-test described in Section 2.4.10. The performance was classified using the methodology summarised in Table 3.7. In this case five classifications were employed, ranging from excellent adhesion where the films were only removed with mechanical grinding, to very poor adhesion properties,

where the adhesion properties of the films were lost during electropolymerisation. A summary of the adhesion test results is provided in Table 3.8. In this table, the films indicated with E (+V) refer to the films grown at a fixed potential of 0.80 V vs SCE, while the films indicated with E (−V) refer to the reduced films. The reduced films were held at −0.90 V vs SCE for 10 min in 0.1 mol dm^{−3} NaCl after polymerisation. The films were then dried in a stream of air. It is clearly evident from Table 3.8 that the Chit/PpyCl composite has superior adhesion properties compared to the PpyCl film, with excellent adhesion properties when the composite is prepared or reduced. The adhesion properties of the chitosan film are equally good, while the reduced PpyCl films have poor adhesion properties.

Table 3.7: A summary of how adhesion was qualitatively classified and the numbers used.

Classification	Description	Result
0	In addition to showing no detachment with the peel-test, mechanical grinding with grit paper is required to remove the film (1 out of 3 times).	Excellent
1	No detachment, manual polishing is required to remove film.	Good
2	Some detachment (1 out of 3 times).	Poor
3	Detachment partially or wholly (2 out of 3 times).	Very Poor
4	Complete fail of adhesion, detachment during potentiostatic experiments.	Fail

Table 3.8: Summary of results from adhesion tests.

Sample	Classification	Result
PpyCl E (+ V)	1	Good
Ppy/Chit E (+ V)	1	Good
Chit/Ppy E (+ V)	0	Excellent
PpyCl E (− V)	2	Poor
Ppy/Chit E (− V)	1	Good
Chit/Ppy E (− V)	0	Excellent
Chitosan	1	Excellent

3.6 Wettability of the composite

According to Hallab *et al.*¹²⁶ the cell adhesion properties of a material are superior when the material is hydrophilic. The wettability (hydrophilicity) of a surface can be easily determined with the use of contact angle measurements with deionised water, where the lower the contact angle, the more wettable (hydrophilic) the surface. Contact angle measurements were made using the sessile drop technique and analysed with the goniometer method. The contact angle was immediately measured after placing a drop of deionised water on each sample. An example of the image of the droplet during the contact angle measurement is shown in Figure 3.3. The contrast between the light and dark regions is used to calculate the contact angle of the droplet.

The contact angles were measured for PpyCl, PpyCl/Chit, Chit/PpyCl and Chit and the data are summarised in Table 3.9. In some cases the contact angles were measured over a 60 s period to monitor any potential time variations. It is clear that the PpyCl films

grown to a charge density of 2.2 C cm^{-2} are the most hydrophilic with a contact angle of 52° and showed no significant change within the first 10 s.

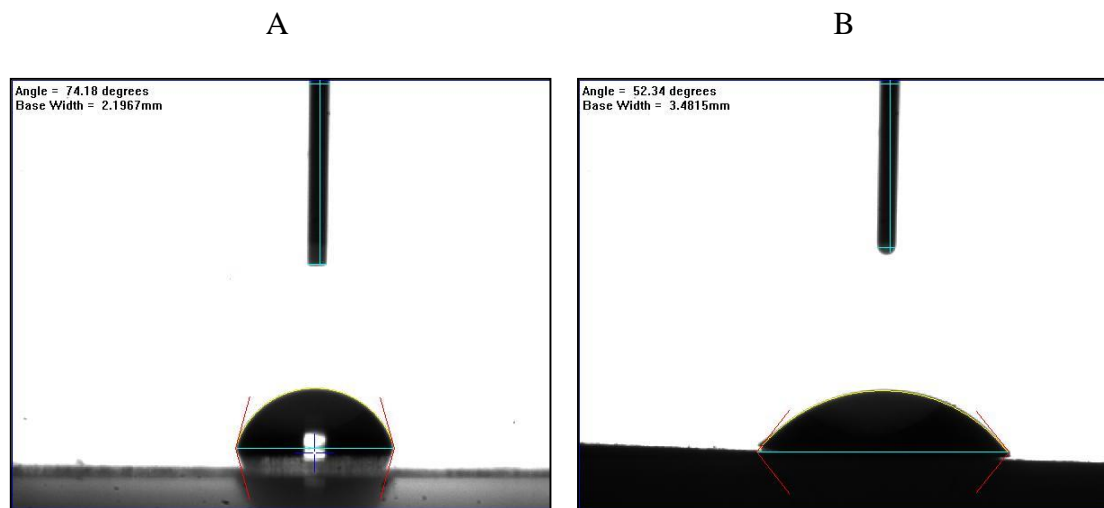


Figure 3.33: Images of the silhouettes of the droplets from the contact angel measurement for chitosan (A) and PpyCl (B). The PpyCl was prepared by potentiostatic electropolymerisation at 0.80 V vs SCE to a charge density of 2.20 C cm^{-2} from a solution of 0.1 mol dm^{-3} Py and 0.1 mol dm^{-3} NaCl.

The chitosan films gave a high contact angle measurement of 95° in the first 10 s, which is characteristic of hydrophobicity. Indeed, Silva *et al.*⁷³ reported similar results. At 60 s an average value of 75° was obtained for the chitosan film which is in good agreement with the literature values^{127,128}. For example, Hoven *et al.*¹²⁸ reported similar values, however, they took their measurements within 5 s to eliminate errors caused by adsorption process. In the case of chitosan the contact angle of the water droplet decreased with time. Chitosan is a well-known hydrophilic polymer.¹²⁹ These results can be explained by the fact that when the chitosan solution is drop cast and forced dried under an IR lamp prior to contact angle measurements it contains a negligible amount of water. Hydration then occurs, but this occurs slowly and is consistent with the decrease in the contact angles with increasing time. PpyCl has an average contact angle measurement of 52° which is in good agreement with the values reported by Thompson *et al.*¹³⁰ for Ppy doped with various dopants. The Chit/PpyCl has hydrophilic values similar to the PpyCl, indicating

that the PpyCl dominates the hydrophilic nature of the composite. In contrast, the PpyCl/Chit has a contact angle value of 70° after 1 s and this did not change significantly after 60 s even though it was dried prior to contact angle measurements. This may be connected to the fact that the PpyCl layer trapped some moisture which allowed some rehydration of the chitosan layer after curing under an IR lamp.

Table 3.9: Average contact angles using deionised water obtained on polypyrrole chloride (PpyCl), chitosan (Chit), and the composites (PpyCl/Chit and Chit/PpyCl). n=2, with the exception of chitosan; n=3.

Sample	Contact angle θ	Result
PpyCl	52°	hydrophilic
Chit (t = 1 s)	95°	hydrophobic
Chit (t = 60 s)	75°	hydrophilic
PpyCl/Chit	70°	hydrophilic
Chit/PpyCl	58°	hydrophilic

Hydrophobic and superhydrophobic chitosan films have been reported in the literature¹³¹. The superhydrophobic films are prepared in the presence of anionic surfactants and have been proposed for applications in antimicrobial surfaces.

An interesting paper by Teh *et al.*¹³² shows a correlation between contact angle measurements of PpyDBS at stepped potentials, illustrating the switching between hydrophilic properties at negative potentials and increased hydrophobicity at increasing positive potentials.

3.7 Summary of results

Conducting Chit/PpyCl composites, that retain the unique electrochemical behaviour of the inherently conducting polypyrrole component, have been electrochemically synthesised. The optimum formulation for Chit/PpyCl was found to comprise of 10 μL of 0.5 % chitosan and 0.1 mol dm^{-3} pyrrole made up in a 0.1 mol dm^{-3} NaCl supporting electrolyte. A constant potential of 0.80 V vs SCE was applied for 5 min to yield a charge density of 2.2 C cm^{-2} . The total preparation time was approximately 45 min in contrast to the hours and overnight steps required for chemical preparation documented in the literature¹³³⁻¹³⁵. The growth parameters and growth rate strongly suggest that at optimum conditions the chitosan swollen film (hydrogel) does not impede the growth of PpyCl on the electrode surface and through the hydrated film network.

The FT-IR results distinguishes the composite film as a *class I* hybrid¹³⁶ which has weak interactions, as opposed to a *class II* hybrid¹³⁶ which has strong chemical interactions such as, ionic or covalent bonding. The FT-IR spectrum in Figure 3.7 clearly shows evidence for the successful preparation of PpyCl in the presence of chitosan. The DSC plot in Figure 3.6 shows that the composite exhibits a higher thermal stability than chitosan.

The electrochemical properties were studied using cyclic voltammetry in Section 3.3.4 and electrochemical impedance spectroscopy (EIS) was investigated in Section 3.3.6. The electroactivity of chitosan and PpyCl differ significantly. The composite behaves similarly to PpyCl, indicating that the chitosan does not adversely affect the PpyCl but may influence the ion transport. The conductivity of chitosan has not been reported (in the hydrated form), and it is difficult to compute because of the magnitude of swelling. However, using impedance measurements the difference in the resistance values between chitosan and PpyCl is over 1,000 fold due to a lack of electronic conductivity in the chitosan network.

The lysozyme solution appeared to have little effect on the stability of the composite, even after an extended period of days (Section 3.4).

Improved adhesion was observed with the composite which is the most notable result on a macroscopic scale, as improved adhesion can enhance the operating lifetime and stability of polymers (Section 3.5).

The preliminary wettability test was described in Section 3.6. Chitosan, PpyCl and Chit/PpyCl appeared to be hydrophilic, which is consistent with reports in the literature.

References

1. B. Guo, L. Glavas and A.-C. Albertsson, *Progress in Polymer Science*, 2013, **38**, 1263-1286.
2. L. S. Curtin, G. C. Komplin and W. J. Pietro, *The Journal of Physical Chemistry*, 1988, **92**, 12-13.
3. Y. Li, X. Y. Cheng, M. Y. Leung, J. Tsang, X. M. Tao and M. C. W. Yuen, *Synthetic Metals*, 2005, **155**, 89-94.
4. Z. Zhang, J.-Z. Wang, S.-L. Chou, H.-K. Liu, K. Ozawa and H. Li, *Electrochimica Acta*.
5. A. Ramanavičius, A. Ramanavičienė and A. Malinauskas, *Electrochimica Acta*, 2006, **51**, 6025-6037.
6. M. S. Kim, H. K. Kim, S. W. Byun, S. H. Jeong, Y. K. Hong, J. S. Joo, K. T. Song, J. K. Kim, C. J. Lee and J. Y. Lee, *Synthetic Metals*, 2002, **126**, 233-239.
7. X. Yu and Z. Shen, *Journal of Magnetism and Magnetic Materials*, 2009, **321**, 2890-2895.
8. A. M. Fenelon and C. B. Breslin, *Electrochimica Acta*, 2002, **47**, 4467-4476.

-
9. A. M. Fenelon and C. B. Breslin, *Corrosion Science*, 2003, **45**, 2837-2850.
 10. M. I. Redondo and C. B. Breslin, *Corrosion Science*, 2007, **49**, 1765-1776.
 11. E. W. H. Jager, E. Smela, O. Inganäs and I. Lundström, *Synthetic Metals*, 1999, **102**, 1309-1310.
 12. K. Kontturi, P. Pentti and G. Sundholm, *Journal of Electroanalytical Chemistry*, 1998, **453**, 231-238.
 13. X. Bi and Q. Pei, *Synthetic Metals*, 1987, **22**, 145-156.
 14. G. Çakmak, Z. Küçükyavuz, S. Küçükyavuz and H. Çakmak, *Composites Part A: Applied Science and Manufacturing*, 2004, **35**, 417-421.
 15. S. Brahim, D. Narinesingh and A. Guiseppi-Elie, *Analytica Chimica Acta*, 2001, **448**, 27-36.
 16. S. Brahim, D. Narinesingh and A. Guiseppi-Elie, *Biosensors and Bioelectronics*, 2002, **17**, 53-59.
 17. P. Chansai, A. Sirivat, S. Niamlang, D. Chotpattananont and K. Viravaidya-Pasuwat, *International Journal of Pharmaceutics*, 2009, **381**, 25-33.
 18. C. J. Small, C. O. Too and G. G. Wallace, *Polymer Gels and Networks*, 1997, **5**, 251-265.
 19. M. N. V. R. Kumar, R. A. A. Muzzarelli, C. Muzzarelli, H. Sashiwa and A. J. Domb, *Chemical Reviews*, 2004, **104**, 6017-6084.
 20. I.-Y. Kim, S.-J. Seo, H.-S. Moon, M.-K. Yoo, I.-Y. Park, B.-C. Kim and C.-S. Cho, *Biotechnology Advances*, 2008, **26**, 1-21.
 21. J. Mo, J.-E. Hwang, J. Jegal and J. Kim, *Dyes and Pigments*, 2007, **72**, 240-245.
 22. T. Uragami and K. Takigawa, *Polymer*, 1990, **31**, 668-672.

-
23. S. B. Schreiber, J. J. Bozell, D. G. Hayes and S. Zivanovic, *Food Hydrocolloids*, 2013, **33**, 207-214.
 24. H. Ueno, T. Mori and T. Fujinaga, *Advanced Drug Delivery Reviews*, 2001, **52**, 105-115.
 25. L. G. Cima, J. P. Vacanti, C. Vacanti, D. Ingber, D. Mooney and R. Langer, *Journal of Biomechanical Engineering*, 1991, **113**, 143-151.
 26. M. Zhang, X. H. Li, Y. D. Gong, N. M. Zhao and X. F. Zhang, *Biomaterials*, 2002, **23**, 2641-2648.
 27. C. T. Tsao, C. H. Chang, Y. Y. Lin, M. F. Wu, J.-L. Wang, J. L. Han and K. H. Hsieh, *Carbohydrate Research*, 2010, **345**, 1774-1780.
 28. L. Baosong and W. Yen, *Acta Polymerica Sinica*, 2010, **010**, 1399.
 29. B. N. Grgur, N. V. Krstajić, M. V. Vojnović, Č. Lačnjevac and L. Gajić-Krstajić, *Progress in Organic Coatings*, 1998, **33**, 1-6.
 30. *Japan Pat.*, 1992.
 31. X. Feng, H. Huang, L. Xu, J.-J. Zhu and W. Hou, *Journal of Nanoscience and Nanotechnology*, 2008, **8**, 443-447.
 32. Y. Wan, Y. Fang, Z. Hu and Q. Wu, *Macromolecular Rapid Communications*, 2006, **27**, 948-954.
 33. X. Yang, T. Dai and Y. Lu, *Polymer*, 2006, **47**, 441-447.
 34. S. Yalçinkaya, C. Demetgül, M. Timur and N. Çolak, *Carbohydrate Polymers*, 2010, **79**, 908-913.
 35. N. Gomez and C. E. Schmidt, *Journal of Biomedical Materials Research Part A*, 2007, **81A**, 135-149.
 36. J. Y. Lee and C. E. Schmidt, *Acta Biomaterialia*, 2010, **6**, 4396-4404.

-
37. A. Gambhir, M. Gerard, A. K. Mulchandani and B. D. Malhotra, *Applied Biochemistry and Biotechnology*, 2001, **96**, 249-257.
 38. K. J. Gilmore, M. Kita, Y. Han, A. Gelmi, M. J. Higgins, S. E. Moulton, G. M. Clark, R. Kapsa and G. G. Wallace, *Biomaterials*, 2009, **30**, 5292-5304.
 39. J. Huang, X. Hu, L. Lu, Z. Ye, Q. Zhang and Z. Luo, *Journal of Biomedical Materials Research Part A*, 2010, **93A**, 164-174.
 40. M. F. a. L. F. a. H. N. a. J. D. B. a. Y.-F. K. a. J. S.-N. a. C. E. S. John, *Biomedical Materials*, 2008, **3**, 034124.
 41. C. Colin and M. A. Petit, *Journal of The Electrochemical Society*, 2002, **149**, E394-E401.
 42. G. Shi, M. Rouabhia, Z. Wang, L. H. Dao and Z. Zhang, *Biomaterials*, 2004, **25**, 2477-2488.
 43. C. Basavaraja, W. J. Kim, D. G. Kim and D. S. Huh, *Materials Chemistry and Physics*, 2011, **129**, 787-793.
 44. J. Y. Lee, C. A. Bashur, A. S. Goldstein and C. E. Schmidt, *Biomaterials*, 2009, **30**, 4325-4335.
 45. Y. Chen, H. Feng, L. Li, S. Shang and M. Chun-Wah Yuen, *J. Macromol. Sci., Part A: Pure Appl. Chem.*, 2013, **50**, 1225-1229.
 46. W. M. Aylward and P. G. Pickup, *Electrochimica Acta*, 2007, **52**, 6275-6281.
 47. A. J. Bard and L. R. Faulkner, *Electrochemical methods. Fundamentals and applications*, Wiley, 2001.
 48. D.-H. Kim, J. A. Wiler, D. J. Anderson, D. R. Kipke and D. C. Martin, *Acta Biomaterialia*, 2010, **6**, 57-62.
 49. D. J. Fermín, H. Teruel and B. R. Scharifker, *Journal of Electroanalytical Chemistry*, 1996, **401**, 207-214.

-
50. B. Scharifker and G. Hills, *Electrochimica Acta*, 1983, **28**, 879-889.
 51. B. C. Kim, G. M. Spinks, G. G. Wallace and R. John, *Polymer*, 2000, **41**, 1783-1790.
 52. M. Palomar-Pardavé, M. Miranda-Hernández, I. González and N. Batina, *Surface Science*, 1998, **399**, 80-95.
 53. K. Qi, Y. Qiu, Z. Chen and X. Guo, *Corrosion Science*, 2013, **69**, 376-388.
 54. I. Rodríguez, B. R. Scharifker and J. Mostany, *Journal of Electroanalytical Chemistry*, 2000, **491**, 117-125.
 55. S. Ghosh, G. A. Bowmaker, R. P. Cooney and J. M. Seakins, *Synthetic Metals*, 1998, **95**, 63-67.
 56. T. W. Lewis, G. G. Wallace, C. Y. Kim and D. Y. Kim, *Synthetic Metals*, 1997, **84**, 403-404.
 57. E. Khor and J. L. H. Whey, *Carbohydrate Polymers*, 1995, **26**, 183-187.
 58. M. E. Nicho and H. Hu, *Solar Energy Materials and Solar Cells*, 2000, **63**, 423-435.
 59. G. I. Mathys and V. T. Truong, *Synthetic Metals*, 1997, **89**, 103-109.
 60. M. Omastová, M. Trchová, J. Pionteck, J. Prokeš and J. Stejskal, *Synthetic Metals*, 2004, **143**, 153-161.
 61. M. Omastová, J. Pionteck and M. Trchová, *Synthetic Metals*, 2003, **135–136**, 437-438.
 62. M. Omastová, M. Trchová, J. Kovářová and J. Stejskal, *Synthetic Metals*, 2003, **138**, 447-455.
 63. G. D. Christian, *Analytical chemistry*, Wiley, 2004.
 64. R. G. Davidson and T. G. Turner, *Synthetic Metals*, 1995, **72**, 121-128.

-
65. M. I. Redondo, M. V. García, E. Sánchez de la Blanca, M. Pablos, I. Carrillo, M. J. González-Tejera and E. Enciso, *Polymer*, 2010, **51**, 1728-1736.
66. J. Ratto, T. Hatakeyama and R. B. Blumstein, *Polymer*, 1995, **36**, 2915-2919.
67. F. S. Kittur, K. V. Harish Prashanth, K. Udaya Sankar and R. N. Tharanathan, *Carbohydrate Polymers*, 2002, **49**, 185-193.
68. A. P. Martínez-Camacho, M. O. Cortez-Rocha, J. M. Ezquerro-Brauer, A. Z. Graciano-Verdugo, F. Rodríguez-Félix, M. M. Castillo-Ortega, M. S. Yépez-Gómez and M. Plascencia-Jatomea, *Carbohydrate Polymers*, 2010, **82**, 305-315.
69. R. A. Jeong, G. J. Lee, H. S. Kim, K. Ahn, K. Lee and K. H. Kim, *Synthetic Metals*, 1998, **98**, 9-15.
70. M. Bazzaoui, L. Martins, E. A. Bazzaoui and J. I. Martins, *Electrochimica Acta*, 2002, **47**, 2953-2962.
71. A. Madhan Kumar and N. Rajendran, *Ceramics International*, 2013, **39**, 5639-5650.
72. I. Arzate-Vázquez, J. J. Chanona-Pérez, G. Calderón-Domínguez, E. Terres-Rojas, V. Garibay-Febles, A. Martínez-Rivas and G. F. Gutiérrez-López, *Carbohydrate Polymers*, 2012, **87**, 289-299.
73. S. S. Silva, B. J. Goodfellow, J. Benesch, J. Rocha, J. F. Mano and R. L. Reis, *Carbohydrate Polymers*, 2007, **70**, 25-31.
74. P. Dyreklev, M. Granström, O. Inganäs, L. M. W. K. Gunaratne, G. K. R. Senadeera, S. Skaarup and K. West, *Polymer*, 1996, **37**, 2609-2613.
75. D. A. Buttry and M. D. Ward, *Chemical Reviews*, 1992, **92**, 1355-1379.
76. G. Sauerbrey, *Zeitschrift für Physik*, 1959, **155**, 206-222.
77. G. Inzelt, Conducting polymers a new era in electrochemistry, <http://dx.doi.org/10.1007/978-3-642-27621-7>.

-
78. A. R. Hillman, *Journal of Solid State Electrochemistry*, 2011, **15**, 1647-1660.
79. E. Andreoli, V. Annibaldi, D. A. Rooney and C. B. Breslin, *J. Phys. Chem. C*, 2011, **115**, 20076-20083.
80. P. Holzhauser and K. Bouzek, *Journal of Applied Electrochemistry*, 2006, **36**, 703-710.
81. D. Buttry, 1989.
82. A. L. Briseno, A. Baca, Q. Zhou, R. Lai and F. Zhou, *Analytica Chimica Acta*, 2001, **441**, 123-134.
83. G. A. Snook and G. Z. Chen, *Journal of Electroanalytical Chemistry*, 2008, **612**, 140-146.
84. R. Stanković, O. Pavlović, M. Vojnović and S. Jovanović, *European Polymer Journal*, 1994, **30**, 385-393.
85. F. Scholz and A. M. Bond, *Electroanalytical methods guide to experiments and applications*, Springer, 2010.
86. X. Ren and P. G. Pickup, *Journal of Electroanalytical Chemistry*, 1997, **420**, 251-257.
87. I. L. Lehr, O. V. Quinzani and S. B. Saidman, *Materials Chemistry and Physics*, 2009, **117**, 250-256.
88. G. A. Snook, G. Z. Chen, D. J. Fray, M. Hughes and M. Shaffer, *Journal of Electroanalytical Chemistry*, 2004, **568**, 135-142.
89. X. Ren and P. G. Pickup, *Canadian Journal of Chemistry*, 1997, **75**, 1518-1522.
90. J. M. Fonner, L. Forciniti, N. Hieu, J. D. Byrne, Y.-F. Kou, J. Syeda-Nawaz and C. E. Schmidt, *Biomedical Materials*, 2008, **3**, 12.
91. M. N. Akieh, Á. Varga, R.-M. Latonen, S. F. Ralph, J. Bobacka and A. Ivaska, *Electrochimica Acta*, 2011, **56**, 3507-3515.

-
92. H. Zhao, W. E. Price, P. R. Teasdale and G. G. Wallace, *Reactive Polymers*, 1994, **23**, 213-220.
 93. V. M. Schmidt and J. Heitbaum, *Electrochimica Acta*, 1993, **38**, 349-356.
 94. A. C. Partridge, C. B. Milestone, C. O. Too and G. G. Wallace, *Journal of Membrane Science*, 1999, **152**, 61-70.
 95. X. Ren and P. G. Pickup, *Journal of Physical chemistry*, 1993, **97**, 5356-5362.
 96. X. Ren and P. G. Pickup, *Electrochimica Acta*, 1996, **41**, 1877-1882.
 97. H. Grande and T. F. Otero, *The Journal of Physical Chemistry B*, 1998, **102**, 7535-7540.
 98. M. D. Levi, C. Lopez, E. Vieil and M. A. Vorotyntsev, *Electrochimica Acta*, 1997, **42**, 757-769.
 99. W. J. Albery and A. R. Mount, *Journal of Electroanalytical Chemistry and Interfacial Electrochemistry*, 1991, **305**, 3-18.
 100. G. Garcia-Belmonte, Z. Pomerantz, J. Bisquert, J.-P. Lellouche and A. Zaban, *Electrochimica Acta*, 2004, **49**, 3413-3417.
 101. G. Garcia-Belmonte, *Electrochemistry Communications*, 2003, **5**, 236-240.
 102. Y. Wan, K. A. M. Creber, B. Peppley and V. T. Bui, *Polymer*, 2003, **44**, 1057-1065.
 103. D. D. Macdonald, *Electrochimica Acta*, 2006, **51**, 1376-1388.
 104. K. Qi, Y. Qiu, Z. Chen and X. Guo, *Corrosion Science*, 2012, **60**, 50-58.
 105. H. Ge, G. Qi, E.-T. Kang and K. G. Neoh, *Polymer*, 1994, **35**, 504-508.
 106. P. A. Kilmartin and G. A. Wright, *Electrochimica Acta*, 2001, **46**, 2787-2794.

-
107. S. Leinad Gnana Lissy, S. Pitchumani and K. Jayakumar, *Materials Chemistry and Physics*, 2002, **76**, 143-150.
 108. R. A. Green, N. H. Lovell, G. G. Wallace and L. A. Poole-Warren, *Biomaterials*, 2008, **29**, 3393-3399.
 109. Y. Li and R. Qian, *Synthetic Metals*, 1994, **64**, 241-245.
 110. D. D. Ateh, H. A. Navsaria and P. Vadgama, *Journal of The Royal Society Interface*, 2006, **3**, 741-752.
 111. M. Dash, F. Chiellini, R. M. Ottenbrite and E. Chiellini, *Progress in Polymer Science*, 2011, **36**, 981-1014.
 112. W. Adachi, Y. Sakihama, S. Shimizu, T. Sunami, T. Fukazawa, M. Suzuki, R. Yatsunami, S. Nakamura and A. Takénaka, *Journal of Molecular Biology*, 2004, **343**, 785-795.
 113. S.-B. Lin, Y.-C. Lin and H.-H. Chen, *Food Chemistry*, 2009, **116**, 47-53.
 114. S. Hirano, H. Tsuchida and N. Nagao, *Biomaterials*, 1989, **10**, 574-576.
 115. E. T. Baran, K. Tuzlakoğlu, J. F. Mano and R. L. Reis, *Materials Science and Engineering: C*, 2012, **32**, 1314-1322.
 116. R. J. Nordtveit, K. M. Vaarum and O. Smidsroed, *Carbohydr. Polym.*, 1996, **29**, 163-167.
 117. K. Tomihata and Y. Ikada, *Biomaterials*, 1997, **18**, 567-575.
 118. D. Ren, H. Yi, W. Wang and X. Ma, *Carbohydrate Research*, 2005, **340**, 2403-2410.
 119. T. Freier, H. S. Koh, K. Kazazian and M. S. Shoichet, *Biomaterials*, 2005, **26**, 5872-5878.
 120. J. Bünsow and D. Johannsmann, *Journal of Colloid and Interface Science*, 2008, **326**, 61-65.

-
121. A. Richter, A. Bund, M. Keller and K.-F. Arndt, *Sensors and Actuators B: Chemical*, 2004, **99**, 579-585.
 122. E. J. Calvo and R. A. Etchenique, in *Comprehensive Chemical Kinetics*, eds. R. G. Compton and G. Hancock, Elsevier, 1999, vol. 37, ch. 12, pp. 461-487.
 123. G. Paliwoda-Porebska, M. Rohwerder, M. Stratmann, U. Rammelt, L. Duc and W. Plieth, *Journal of Solid State Electrochemistry*, 2006, **10**, 730-736.
 124. U. Rammelt, L. M. Duc and W. Plieth, *Journal of Applied Electrochemistry*, 2005, **35**, 1225-1230.
 125. W. Plieth, A. Bund, U. Rammelt, S. Neudeck and L. Duc, *Electrochimica Acta*, 2006, **51**, 2366-2372.
 126. N. J. Hallab, K. J. Bundy, K. O'Connor, R. L. Moses and J. J. Jacobs, *Tissue Eng*, 2001, **7**, 55-71.
 127. W. Graisuwan, O. Wiarachai, C. Ananthanawat, S. Puthong, S. Soogarun, S. Kiatkamjornwong and V. P. Hoven, *Journal of Colloid and Interface Science*, 2012, **376**, 177-188.
 128. V. P. Hoven, V. Tangpasuthadol, Y. Angkitpaiboon, N. Vallapa and S. Kiatkamjornwong, *Carbohydrate Polymers*, 2007, **68**, 44-53.
 129. B. Nyström, A.-L. Kjøniksen and C. Iversen, *Advances in Colloid and Interface Science*, 1999, **79**, 81-103.
 130. B. C. Thompson, S. E. Moulton, R. T. Richardson and G. G. Wallace, *Biomaterials*, 2011, **32**, 3822-3831.
 131. N. A. Ivanova and A. B. Philipchenko, *Applied Surface Science*, 2012, **263**, 783-787.
 132. K. S. Teh, Y. Takahashi, Z. Yao and Y.-W. Lu, *Sensors and Actuators A: Physical*, 2009, **155**, 113-119.

133. H. Huang, J. Wu, X. Lin, L. Li, S. Shang, M. C.-w. Yuen and G. Yan, *Carbohydrate Polymers*, 2013, **95**, 72-76.
134. R.-J. Lee, R. Temmer, T. Tamm, A. Aabloo and R. Kiefer, *Reactive and Functional Polymers*, 2013, **73**, 1072-1077.
135. R.-J. Lee, T. Tamm, R. Temmer, A. Aabloo and R. Kiefer, *Synthetic Metals*, 2013, **164**, 6-11.
136. G. Kickelbick, *Hybrid materials: synthesis, characterization and applications*, Wiley-VCH, 2007.

Chapter 4

Electrochemical synthesis and characterisation of polypyrrole methyl orange (PpyMO)/chitosan composite films

4. Electrochemical synthesis and characterisation of polypyrrole methyl orange (PpyMO)/chitosan composite films

4.1 Introduction

Films consisting of a blend of chitosan and polypyrrole doped with methyl orange were prepared and characterised for their electrical and physical properties. Methyl orange, Figure 4.1, is an intensely coloured azo compound commonly used as a dye. Its distinctive colour change from orange to red is easily observed between the narrow pH ranges of 4.4 to 3.1¹. The absorption band of methyl orange is in the visible spectrum making it a suitable indicator for the titration of strong acids and weak bases, while its characteristic bright colour makes it an important dye for many industries such as, paint², textile^{3, 4}, leather⁵, printing, cosmetics⁶ and general chemical processing⁷. The azo linkage is the most labile portion of the dye molecule and is responsible for its toxicity^{8, 9}; as a consequence it is a major industrial pollutant. Methyl orange has a hydrophilic group making it soluble in water¹⁰.

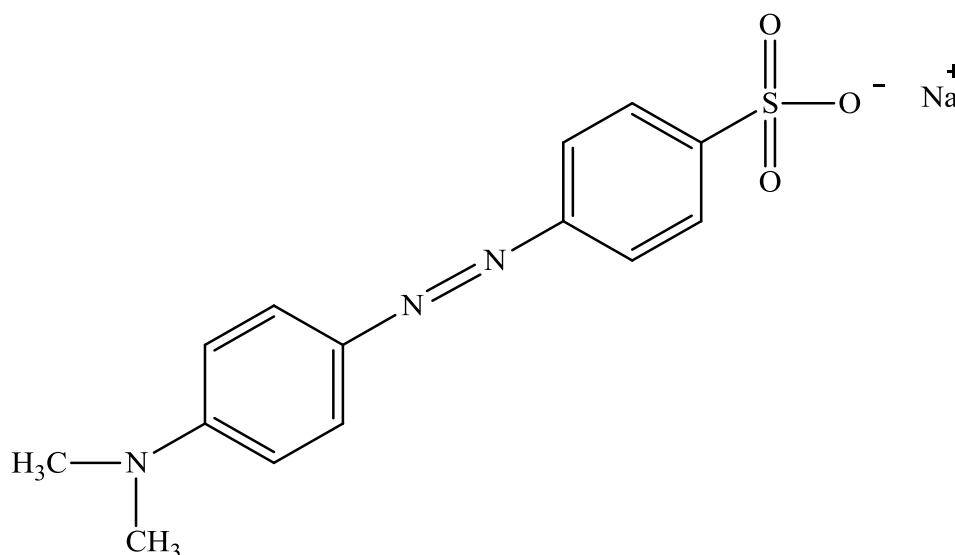


Figure 4.1: Structure of methyl orange.

Kaynak and co-workers¹¹ doped Ppy with sulfonic acid dyes varying in size. They found that Nuclear fast red has the highest conductivity of $4.7 \text{ m}\Omega^{-1} \text{ cm}^{-1}$ and Naphthol Green B has the lowest conductivity of $8.73 \text{ }\mu\Omega^{-1} \text{ cm}^{-1}$, and they suggest possible geometry effects of the dopant on the final product. In recent publications methyl orange was evaluated as a suitable candidate for semiconductor devices with a wide range of thermal stability¹²⁻¹⁴. Dyeing materials are widely used in semiconductor devices due to their stability, having a conjugate structure and being rich in π -electrons¹⁵.

Dyes like methyl orange can be found in some pharmacology studies, as an example Zbaida *et al.*¹⁶ compared the reduction of azo dyes, that are structurally related to 4-(dimethylamino)-azobenzene (DAB), by rat liver microsomal cytochrome P-450. Mazur *et al.*¹⁷ reported the preparation of polypyrrole microvessels that are capable of encapsulating Nile Red, a solvatochromic dye that served as a model lipophilic drug in their study. Lee and Chiang¹⁸ studied the drug release behaviour of poly(acrylic acid/N-vinyl pyrrolidone)/chitosan hydrogels using phenol red and neutral red dyes. Lira *et al.*¹⁹ reported the synthesis of a polyaniline-polyacrylamide hydrogel hybrid material for the controlled release of safranin, a cationic dye.

In summary, methyl orange has a range of attractive properties, including its molecular size, its ability to absorb light (as it contains chromophores), it is inexpensive and possesses some interesting electrochemistry due to its conjugated structure¹⁵.

In this study methyl orange was chosen as a model anionic dopant for the fabrication of a polypyrrole/anion composite. The use of polypyrrole (Ppy) as a suitable substrate for the controlled release of methyl orange was then investigated. Polypyrrole methyl orange (PpyMO) was successfully synthesised from a solution consisting of 0.05 mol dm^{-3} pyrrole, 5.0 mmol dm^{-3} methyl orange and $0.025 \text{ mol dm}^{-3}$ NaCl. However, aggregates of methyl orange were observed in the electrolyte solution on application of the potential to the electrode. When the concentration of NaCl was reduced to 0.01 mol dm^{-3} the concentration of aggregates was lowered. The NaCl was then removed from the electrosynthesis solution and as a consequence the polypyrrole methyl orange growth was compromised as the concentrations of methyl orange and pyrrole were relatively low. The electrosynthesis solution was then modified to consist of 0.1 mol dm^{-3} pyrrole and 0.01

mol dm⁻³ methyl orange dissolved in distilled water. No additional electrolyte was used and as a result no aggregates were formed in solution and competition between anionic species was eliminated. In this system the anionic methyl orange, MO⁻, was directly incorporated into the polypyrrole matrix as a dopant during electrosynthesis. The release of the MO⁻ was investigated both with and without electrical stimulation. Attempts to make Chit/PpyMO were unsuccessful. The chitosan appeared to interact with the MO⁻ from the electrolyte solution. The pyrrole monomer could not interpenetrate the chitosan efficiently. Alternatively, chitosan was added post-electropolymerisation. The scheme for this process is depicted in Chapter 3, Figure 3.1. There are relatively few publications reported on the formation of Ppy/Chit with methyl orange. Chen *et al.*²⁰ prepared a Ppy/Chit through static polymerisation using methyl orange as the dopant and Fe₂(SO₄)₃ as the oxidant. Other citations reveal that methyl orange is useful for soft templates when growing Ppy nanocomposites^{10, 21-25}.

4.2 Experimental

Polypyrrole methyl orange films, PpyMO, were grown potentiostatically on to a platinum working electrode (surface area 0.13 cm²). The monomer solution consisted of 0.1 mol dm⁻³ pyrrole (Sigma-Aldrich, distilled under vacuum) and 0.01 mol dm⁻³ methyl orange (Sigma-Aldrich) in distilled water. The film was synthesised by applying a constant potential of 0.80 V vs SCE for approximately 3 min yielding a charge density of 0.25 C cm⁻². The PpyMO films were rinsed with acetone, ethanol and distilled water to remove any unreacted monomer and undoped methyl orange. The chitosan film was prepared by drop casting 10 μL of 0.5% (w/v) chitosan solution directly on to the washed PpyMO film and then force dried under an infrared lamp for 10 min.

4.3 Results and discussion

4.3.1 Redox properties of Methyl Orange

Cyclic voltammetry was used to gain information on the stability of a methyl orange solution towards oxidation and reduction. The experiments were carried out on a bare Pt electrode by cycling between -1.20 V vs SCE and 1.00 V vs SCE, at a scan rate of 50 mV s^{-1} , in 0.01 mol dm^{-3} methyl orange or 0.1 mol dm^{-3} NaCl. Typical cyclic voltammograms are shown in Figure 4.2. The voltammograms recorded in NaCl display redox properties which are dominated by H^+ adsorption and $\text{H}_{2(\text{g})}$ evolution between approximately -0.90 V and -1.20 V vs SCE. This indicates that the electrochemistry of the bare Pt is dominant²⁶. The voltammogram recorded in the presence of methyl orange has a similar profile but the current is considerably lower as a result of the lower conductivity. The methyl orange solution has a conductivity value of 0.7 $\text{m}\Omega^{-1} \text{cm}^{-1}$ compared to a conductivity of 1.6 $\text{m}\Omega^{-1} \text{cm}^{-1}$ for the NaCl solution. No reduction or oxidation peaks were observed indicating that the MO solution is stable in this electrochemical window. Levine *et al.*¹⁶ reported the formal redox potential of methyl orange to be -1.48 V, with the oxidation and the reduction potentials at 1.02 V and -1.55 V, respectively, with respect to SHE. It is evident from Figure 4.2 that there is a slight increase in the current at potentials higher than 0.85 V vs SCE, which may indicate some oxidation of methyl orange. However, there is no evidence of any redox reactions between -1.20 V and 0.85 V vs SCE and the PpyMO film can be formed at potentials below 0.85 V vs SCE and the methyl orange released at potentials in the vicinity of -1.20 V vs SCE.

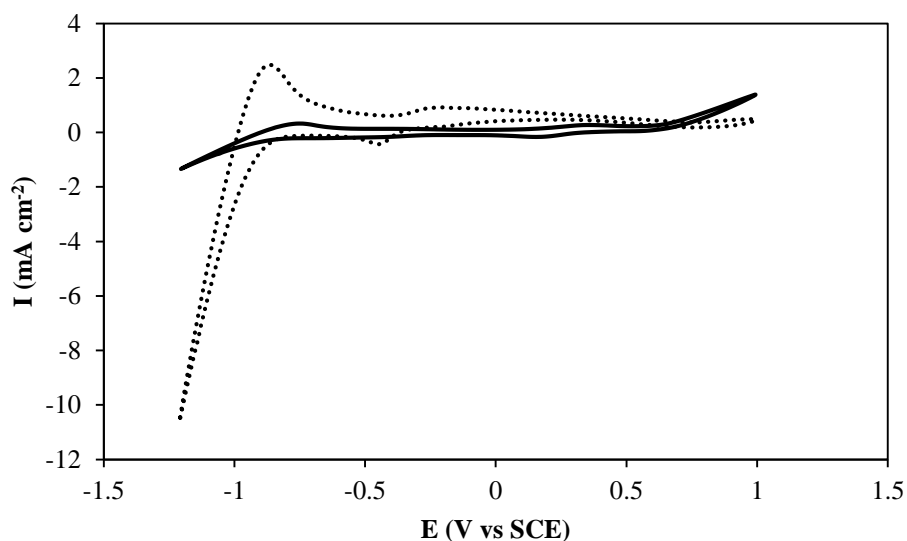


Figure 4.2: Cyclic voltammogram of a 0.13 cm² bare platinum electrode (20th cycle) at 50 mV s⁻¹ in 0.01 mol dm⁻³ methyl orange (—) and 0.1 mol dm⁻³ NaCl (····).

4.3.2 Electrochemical synthesis of the polypyrrole methyl orange film and composite

In the literature, PpyMO was synthesised from a solution containing nitrates (NO_3^-) as a supporting electrolyte during galvanostatic synthesis²⁷. Here, potentiostatic synthesis, similar to that shown in the previous chapter, was employed. It has been reported that changes of electrode potential in the early stages of film formation can disturb steady polymer growth, leading to poorer adhesion of the polymer film while films grown at a constant potential can achieve higher qualities, in terms of smoothness and adherence, than those grown at constant current²⁸. In this study, no supporting electrolyte was used for the electrosynthesis of PpyMO to ensure that Ppy was only doped by the MO^- . Initial attempts to synthesis Chit/PpyMO were unsuccessful so a decision was made to add the chitosan post-electropolymerisation. Figure 3.1 in Chapter 3 illustrates the sequential steps used to prepare a PpyA/Chit composite film. A range of monomer and dopant concentrations were tested until a formulation yielded a film grown to a charge of 0.25 C cm⁻² in less than 5 min at 0.80 V vs SCE to prevent irreversible over-oxidation²⁹. Typical current-time and charge-time plots recorded during the formation of PpyMO at 0.80 vs SCE are shown in Figure 4.3, while a schematic outlining the formation of PpyMO is

presented in Figure 4.4. For comparison, the profiles recorded during the formation of PpyCl, recorded under similar conditions with 0.1 mol dm^{-3} pyrrole and 0.1 mol dm^{-3} NaCl at 0.80 V vs SCE , are shown. There is a considerable difference between the rates of electropolymerisation in the methyl orange and chloride-containing solutions. The PpyCl is deposited to a charge of 0.25 C cm^{-2} in 40 s , while 250 s are required to deposit the PpyMO. The charge increases in a linear manner during the formation of PpyCl. The average rate of growth for PpyCl grown to a charge density of 0.25 C cm^{-2} on a conventional Au disc electrode and Pt disc electrode was computed as 8.02 mC s^{-1} and 7.53 mC s^{-1} , respectively, indicating efficient growth of the polymer film³⁰. The charge-time plot is very different during the formation of PpyMO, Figure 4.3. The charge increases in a linear manner, but at a lower rate during the early stages of electropolymerisation, from 0 to 40 s . Then there is an increase in the rate of polymer deposition. The average rate of growth for PpyMO deposited to a charge density of 0.25 C cm^{-2} on a conventional Au disc electrode and Pt disc electrode was computed to be 0.67 mC s^{-1} and 0.64 mC s^{-1} , respectively, which is considerably slower than the rate of formation of PpyCl. The slower growth rate may be explained by the slow diffusion of the relatively large MO^- anion to the electrode surface³¹.

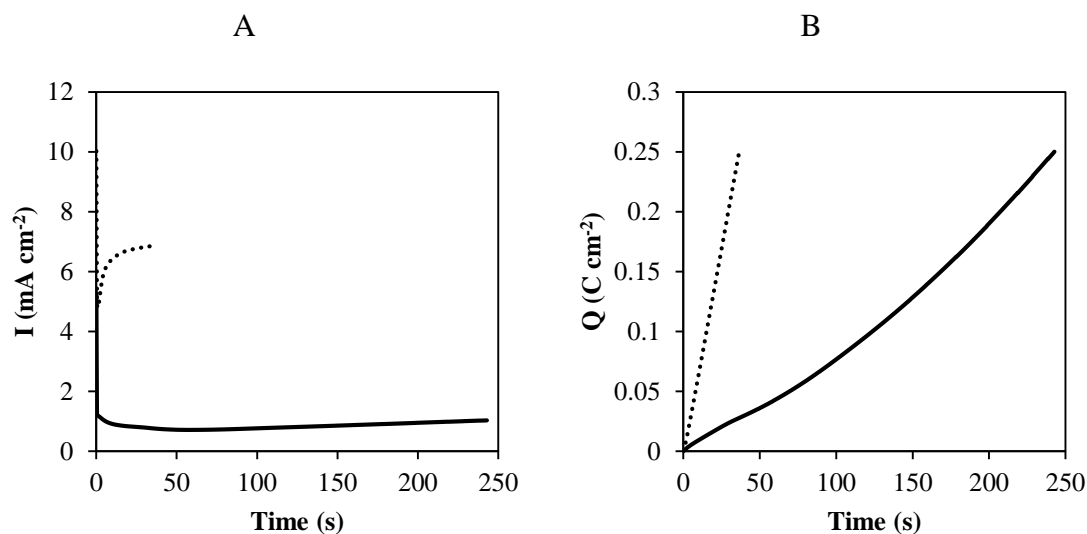


Figure 4.3: Current-time plots (A) and charge-time plots (B) for the growth of (— PpyMO) and (···· PpyCl). The PpyCl was prepared from a solution of 0.1 mol dm^{-3} Py and 0.1 mol dm^{-3} NaCl and the PpyMO was prepared from a solution of 0.1 mol dm^{-3} Py and 0.01 mol dm^{-3} MO. The films were electropolymerisation at 0.80 V vs SCE yielding a charge density of 0.25 C cm^{-2} .

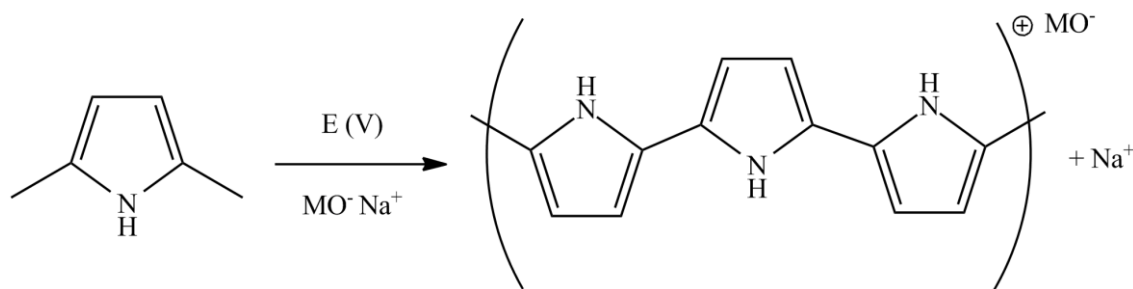


Figure 4.4: Synthesis of polypyrrole with the incorporation of the methyl orange anion (MO^-).

To explore further the nature of the anion in the formation of the polypyrrole films, dexamethasone 21-phosphate disodium salt (Dex) was chosen as the anion. It has a $\text{p}K_a$ of 6.4^{32} and its chemical structure is shown in Figure 4.5. The presence of the phosphate group on the dexamethasone steroid ring structure imparts a negative charge to the drug (Dex^{2-}) making it suitable for incorporation as a dopant in polypyrrole³³.

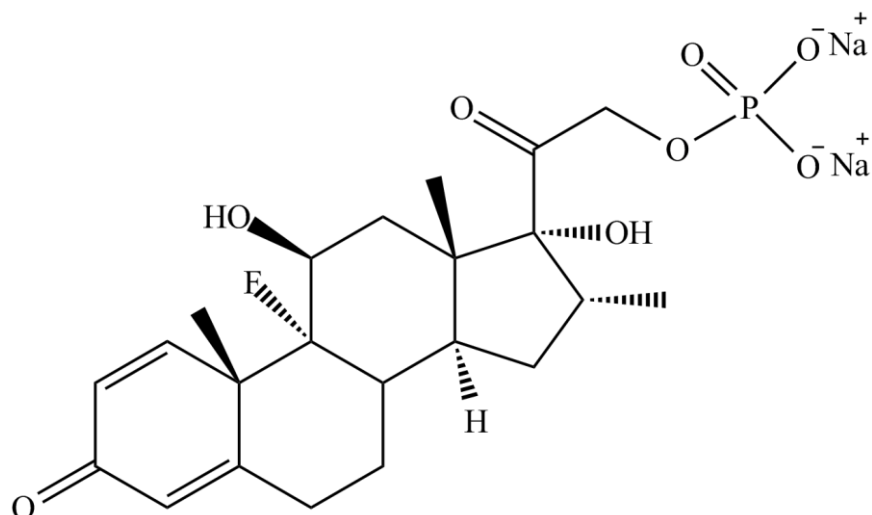


Figure 4.5: Structure of Dexamethasone 21-phosphate disodium salt (Dex²⁻).

Dexamethasone is classified as a synthetic glucocorticosteroid and is used in several treatments, including the reduction of inflammation in the central nervous system and in the treatment of cancer³⁴. It is thought to act through the glucocorticosteroid receptors found in most neurons and glial cells throughout the brain³⁵. These pathways are involved in the inhibition of astrocyte proliferation³⁶ and microglial activity³⁷. Brand names of dexamethasone include Decadron®, Dexasone®, Diodes®, Hexadrol® and Maxidex®. It can also be given in tablet form or intravenously. It is also an ophthalmic drug³⁸⁻⁴⁰ and it is used to treat a variety of ocular diseases. Topical preparations are available as cream, gel and aerosol solution to treat skin disorders. There are several pro-drug forms of dexamethasone⁴¹⁻⁴³ used for the treatments mentioned above. There has been increasing reports in the literature of the use of dexamethasone in controlled release studies⁴⁴⁻⁴⁹. Wadha *et al*⁴⁴. studied the controlled release of Dex²⁻ from Ppy. The drug was incorporated into the polymer using a galvanostatic mode, while its release was carried out using cyclic voltammetry over a wide potential window, which is likely to compromise the integrity of the Ppy film. Wallace and co-workers^{45, 46} reported the electrochemical release of therapeutic levels of Dex²⁻ from polyterthiophene. An oxidation potential was applied to inhibit the release of Dex²⁻. They found that by applying a reduction potential the rate of drug release was not significantly increased when compared to an unstimulated film. It is clear from these studies that dexamethasone is an interesting drug and an ideal drug to compare with methyl orange.

The current-time and charge-time plots recorded during the formation of PpyDex are presented in Figure 4.6, while a schematic representing the formation of the film is presented in Figure 4.7. Again the rate of electropolymerisation was compared with the formation of PpyCl. It was found that by increasing the pyrrole concentration and reducing the concentration of dexamethasone a dilute formulation was sufficient to grow PpyDex on a Pt disc electrode at 0.80 V vs SCE to a charge of 0.25 C cm^{-2} in 3 min. The data presented in Figure 4.6 were recorded in 0.01 mol dm^{-3} dexamethasone with 0.1 mol dm^{-3} pyrrole. Again, the rate of electropolymerisation is lower than that recorded during the formation of PpyCl. The average rate of growth for PpyCl grown to a charge density of 0.25 C cm^{-2} on a Pt disc electrode was computed as 7.53 mC s^{-1} . The average rate of growth for PpyDex was computed as 1.80 mC s^{-1} , which is considerably slower than PpyCl but not as slow as PpyMO. The average rate of growth for PpyDex deposited at 0.90 V vs SCE was computed to be 3.80 mC s^{-1} , clearly showing that the rate of electropolymerisation is increased on the application of higher potentials.

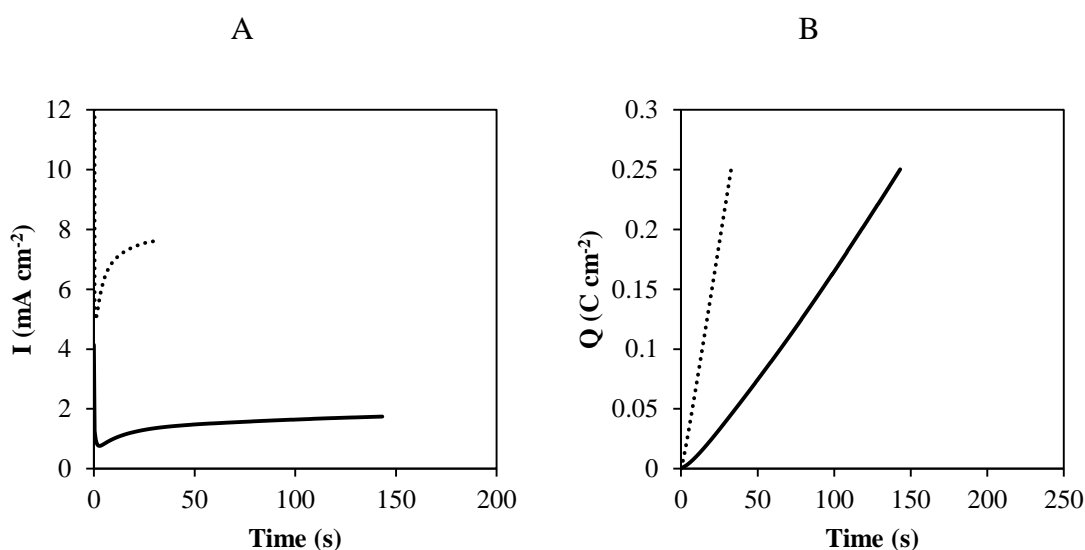


Figure 4.6: Current-time plots (A) and charge-time plots (B) for the growth of (— PpyDex) and (···· PpyCl) at 0.80 V vs SCE yielding a charge density of 0.25 C cm^{-2} . The PpyCl was prepared from a solution of 0.1 mol dm^{-3} Py and 0.1 mol dm^{-3} NaCl and the PpyDex was prepared from a solution of 0.1 mol dm^{-3} Py and 0.01 mol dm^{-3} Dex.

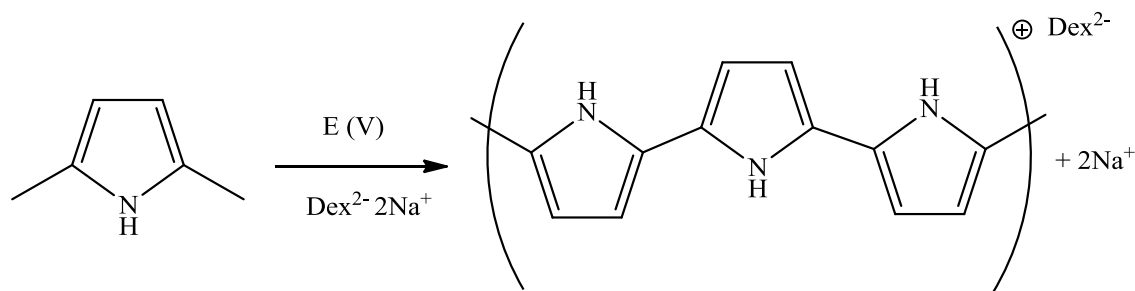


Figure 4.7: Synthesis of polypyrrole with the incorporation of the dexamethasone.

It is evident from these data that the rate of electropolymerisation is higher with the PpyDex compared to the PpyMO system, however on comparing the costs of the dopants, summarised in Table 4.1, it is clear that the dexamethasone is considerably more expensive making methyl orange the preferred dopant.

Table 4.1: Comparison of the cost of dopants used, price taken from Sigma-Aldrich (October 2013).

Dopant	Concentration (mol dm ⁻³)	Cost ex. VAT (per gram)
chloride (Cl)	0.10	€ 0.03
methyl orange (MO)	0.01	€ 0.35
dexamethasone (Dex)	0.01	€ 331.50

Although the PpyDex film was successfully formed at 0.80 V vs SCE and 0.90 V vs SCE, the dopant is expensive, as shown in Table 4.1, and all further studies were focussed on PpyMO.

4.3.2.1 Morphology (SEM)

The surface topography and morphology of the polymers was studied using SEM. The polymer was grown on a customised Pt electrode (Section 2.4.6) with a surface area of 0.13 cm². The polymer films were washed thoroughly with acetone, ethanol, and distilled water until washing ran clear to ensure the removal of excess electrolyte (MO⁻) on the

surface. They were air dried for several hours before imaging. These samples were sputter coated with 1.4 nm of gold prior to imaging.

In Figures 4.8, 4.9 and 4.10, SEM micrographs of PpyCl and PpyMO grown to a charge density of 0.25 C cm^{-2} are shown. The polymer films appear as globule structures or “cauliflower” structures^{50, 51}. As mentioned in Section 3.3.3.3 this morphology is typical of bulk polypyrrole. The globules are composed of micro-spherical grains, it has been reported that this particular morphology is caused by the dopant intercalation difficulty in the disordered polymeric chain^{4, 52}. The presence of these cauliflower structures in the PpyMO film is more clearly evident in Figure 4.10. It is also evident from Figure 4.9, that rods or tubular-like structures, consisting of methyl orange, are distributed across the surface of the film. It is clear from these micrographs that the morphology of the polypyrrole film changes in the presence of methyl orange. Although the typical cauliflower-like structures seen for polypyrrole films are present, tubular-like structures which decorate the surface are also evident with the PpyMO film²⁷. These tubes have lengths up to $10 \mu\text{m}$ and in some cases appear as branched structures. These significant changes in the morphology of the polymers formed in the presence of methyl orange, clearly confirm that the methyl orange is effectively incorporated into the polypyrrole film. During the electropolymerisation of PpyMO, MO is also present as a precipitate on the surface of the polymer and as there is no other dopant available in the electrolyte to dope the polymer this film will be just referred to as PpyMO.

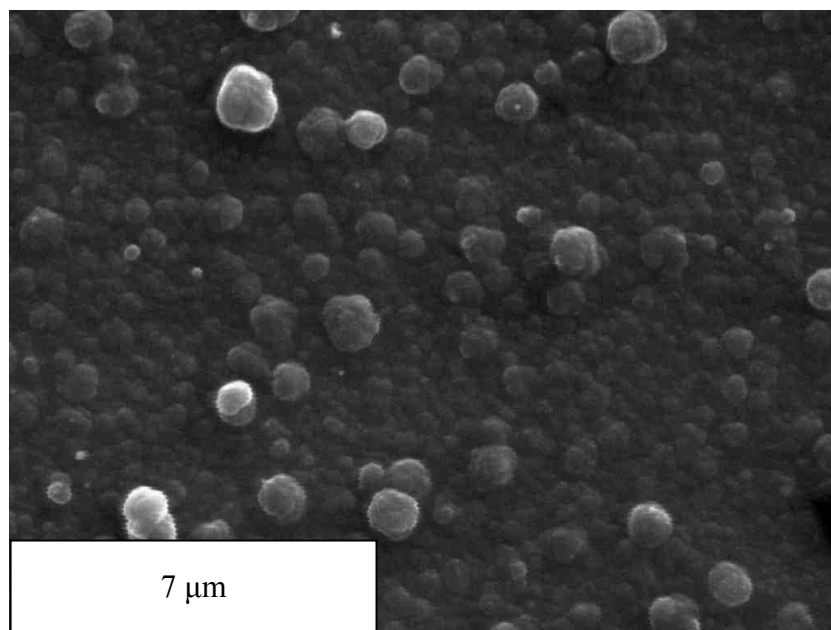


Figure 4.8: SEM micrograph of polypyrrole-chloride, PpyCl, grown on a 0.13 cm^2 customised Pt electrode showing “cauliflower” morphology. The film was prepared by potentiostatic electropolymerisation at 0.80 V vs SCE in 0.1 mol dm^{-3} Py 0.1 mol dm^{-3} NaCl grown to a charge density of 0.25 C cm^{-2} .

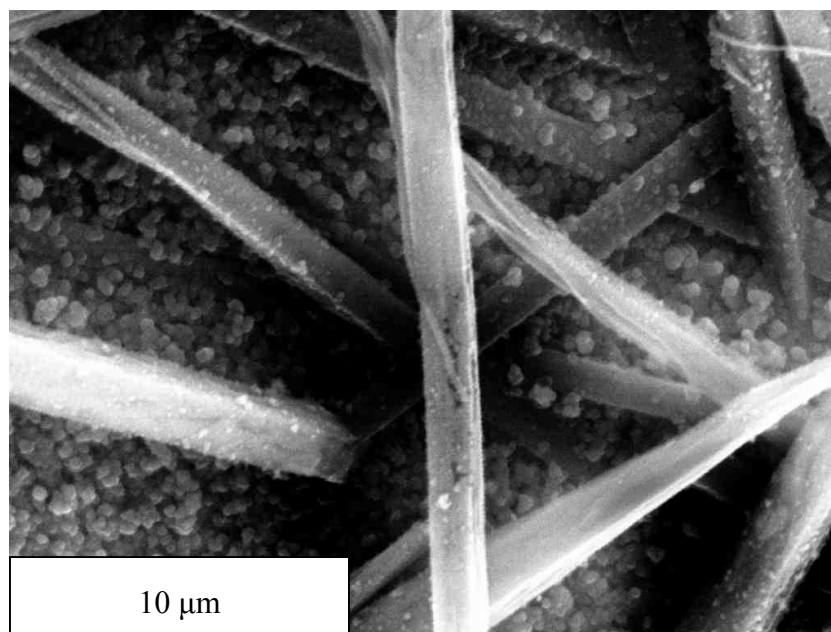


Figure 4.9: SEM micrograph of polypyrrole methyl orange, PpyMO, grown on a 0.13 cm^2 customised Pt electrode showing “cauliflower” morphology with rod-like crystals of methyl orange adhered to the surface of the polymer. The film was prepared by potentiostatic electropolymerisation at 0.80 V vs SCE in 0.1 mol dm^{-3} Py 0.01 mol dm^{-3} MO grown to a charge density of 0.25 C cm^{-2} .

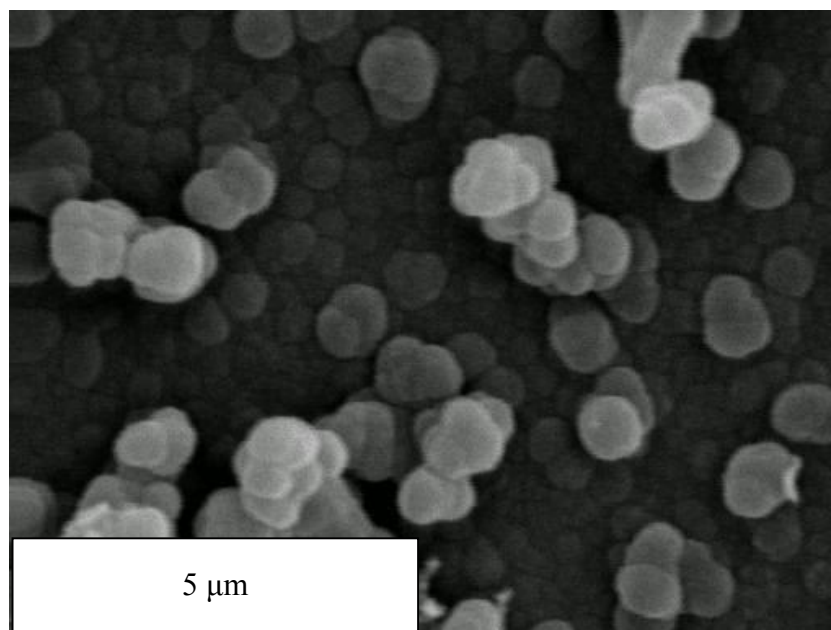


Figure 4.10: SEM micrograph of polypyrrole methyl orange, PpyMO, at a higher magnification. The film was prepared by potentiostatic electropolymerisation at 0.80 V vs SCE in 0.1 mol dm⁻³ Py 0.01 mol dm⁻³ MO grown to a charge density of 0.25 C cm⁻².

Real film thickness (δ_{film}) of PpyMO grown to different charge densities ranging from 0.1 C cm⁻² to 0.5 C cm⁻² were measured from scanning electron microscopy (SEM) micrographs. The relationship between charge consumed during polymerisation and thickness is shown in Equation 3.3, Chapter 3. In Figure 4.11 B the thickness of the films is shown plotted as a function of the charge density and the linear regression provides the volume-to-charge ratio (K)⁵³. The K value was found to be 2.25×10^4 cm³ C⁻¹ for the polypyrrole methyl orange films.

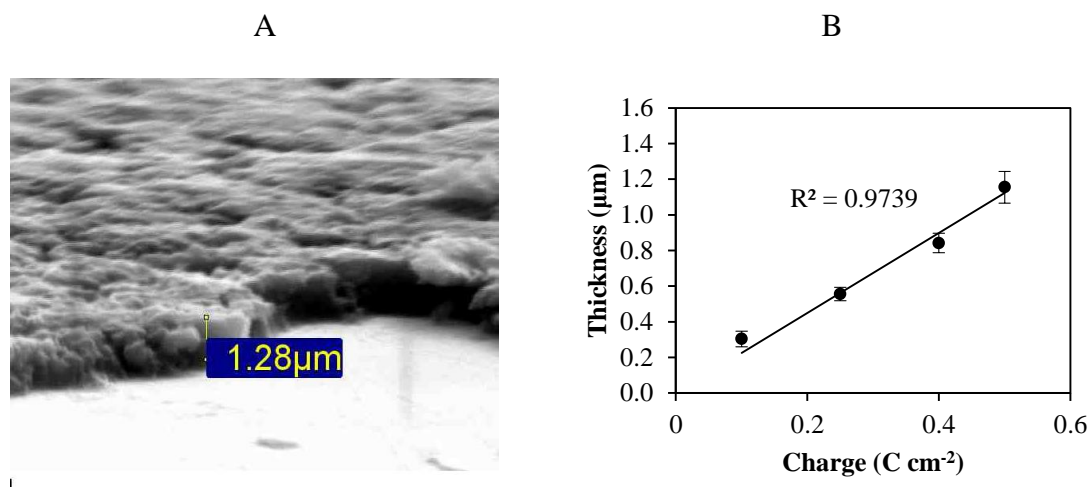


Figure 4.11: Representative micrograph of PpyMO thickness (0.5 C cm^{-2}), showing callipers (A) and a plot showing the dependence of charge consumed during synthesis with thickness, $n = 4$.

4.3.2.2 EDX analysis

EDX analysis was carried out to verify the presence of the methyl orange. The EDX spectrum in Figure 4.12 confirms the presence of carbon at 0.3 keV, sulphur at 2.45 keV and oxygen at 0.52 keV. Carbon is an elemental component of both polypyrrole and methyl orange, however, the sulphur and oxygen are elemental components of the anionic methyl orange (MO^-). The incorporation of MO as a dopant and precipitate on the surface of the polymer was shown previously (Section 4.3.2.1). Interestingly chloride also appears at 2.62 keV in the EDX spectra. EDX analyses of methyl orange on its own showed traces of chloride and this could explain the presence of chloride in the EDX spectrum. Other routes of contamination of Cl^- anions could be from the reference electrode leaking into the electrolyte during synthesis as a consequence of the low conductivity of the electrosynthesis solution ($0.7 \text{ m}\Omega^{-1} \text{ cm}^{-1}$).

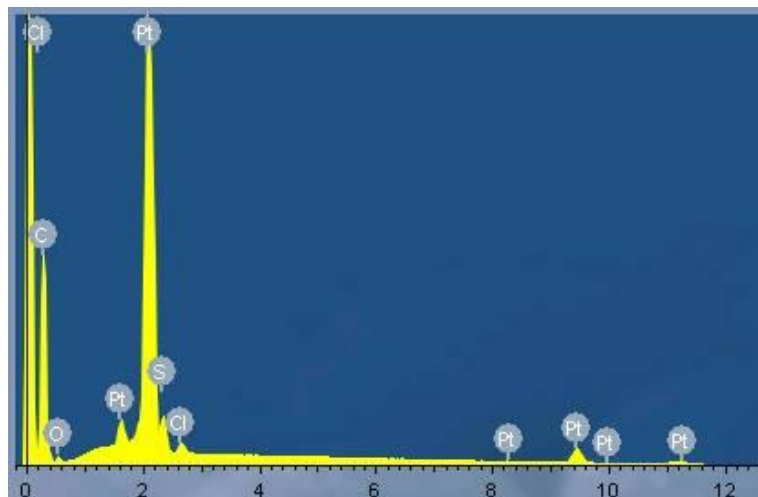


Figure 4.12: Representative EDX spectrum of PpyMO, showing x-axis from 0 to 12.5 keV.

4.3.3 Cyclic Voltammetry (CV)

The electrochemical properties of PpyCl and PpyMO were characterised using cyclic voltammetry. The polymers were grown to a charge density of 0.25 C cm^{-2} . They were cycled in $0.1 \text{ mol dm}^{-3} \text{ NaCl}$ and the potential was swept from -0.95 V to 0.35 V vs SCE to avoid over-oxidising the polymer⁵⁴. Different scan rates, ranging from 5, 10, 25, 50, 100 to 150 mV s^{-1} , were used. The voltammograms of PpyCl and PpyMO were compared to that recorded for Pt in the NaCl solution.

4.3.3.1 Redox properties of PpyCl and PpyMO grown to a charge of 0.25 C cm^{-2}

Representative voltammograms are shown in Figure 4.13 for the PpyCl and PpyMO films deposited to a charge of 0.25 C cm^{-2} and cycled in $0.1 \text{ mol dm}^{-3} \text{ NaCl}$. The data presented in the plots labelled A and C show the voltammograms recorded at different scan rates and the plots labelled B and D show a magnification of the voltammograms recorded at 10 mV s^{-1} and compared to the electrochemical response of the bare Pt electrode. It is clear from the data presented in Figure 4.13 B and D that the voltammograms recorded for bare Pt are very different to the response obtained with the PpyCl and PpyMO modified Pt electrodes. There is no evidence for the adsorption of hydrogen ions or the

evolution of hydrogen gas when the Pt electrodes are modified with the polymer films. Reproducible voltammetric behaviour was attained with the polymer films after the first few cycles, usually 3 to 4 cycles and the data shown in Figure 4.13 were recorded following 9 cycles. It is clear that the voltammograms recorded for PpyMO (Figure 4.13 C) and PpyCl (Figure 4.13 A) are different. Lower currents, particularly at the higher scan rates, are observed with the PpyMO films and the peak potentials vary considerably for the two polymer films. For the PpyCl film, the main redox peak for anion transport is centred at -0.10 V vs SCE, and the main anodic peak potential (E_{pa}) and the cathodic peak potential (E_{pc}) shift as the scan rate increases. A second cathodic peak appears at approximately -0.55 V vs SCE at a scan rate of 10 mV s^{-1} , it also shifts in the cathodic direction by 160 mV and becomes more pronounced as the scan rate is increased to 150 mV s^{-1} . For PpyCl the dominating redox process is for anion transport, indeed similar voltammograms for PpyCl have been published and discussed⁵⁵⁻⁵⁸ and ion transport has been extensively studied⁵⁹⁻⁶⁴. Small ions like Cl^- exhibit predominantly anion transport because of their mobility⁶⁵.

In contrast, Figure 4.13 C clearly shows that the main redox peak for PpyMO is at lower potentials than PpyCl. There is little voltammetric data published or discussed with regard to PpyMO, however the redox wave is in the region associated with cation transport⁶⁶. The anodic peak potential (E_{pa}) shifts by 142 mV in the anodic direction as scan rate increases from 5 to 150 mV s^{-1} . The cathodic peak potential (E_{pc}) is centred at -0.50 V vs SCE. No other significant peaks are observed although a mix of anion and cation transport has been reported for other small to medium sized sulphate based dopants^{67, 68} and this may be the case for the PpyMO system. The PpyCl and PpyMO films demonstrate redox asymmetry typical of conducting polymers⁶⁹.

In Figure 4.14, plots are shown for the peak potential (E_p) and peak current (I_p) as a function of the scan rate for the cyclic voltammograms of PpyCl and PpyMO (shown in Figure 4.13). These data are also presented in Table 4.2. In PpyCl, the voltammetric peak associated with Cl^- insertion is more susceptible to the change in scan rate than the voltammetric peak associated with Cl^- expulsion. The peak associated with the transient Cl^- insertion shifts to lower potentials with increased scan rate while the corresponding

cathodic peak remains at $-0.13 \text{ V} \pm 23 \text{ mV}$ as the scan rate increases with the exception of the data recorded at 5 mV s^{-1} .

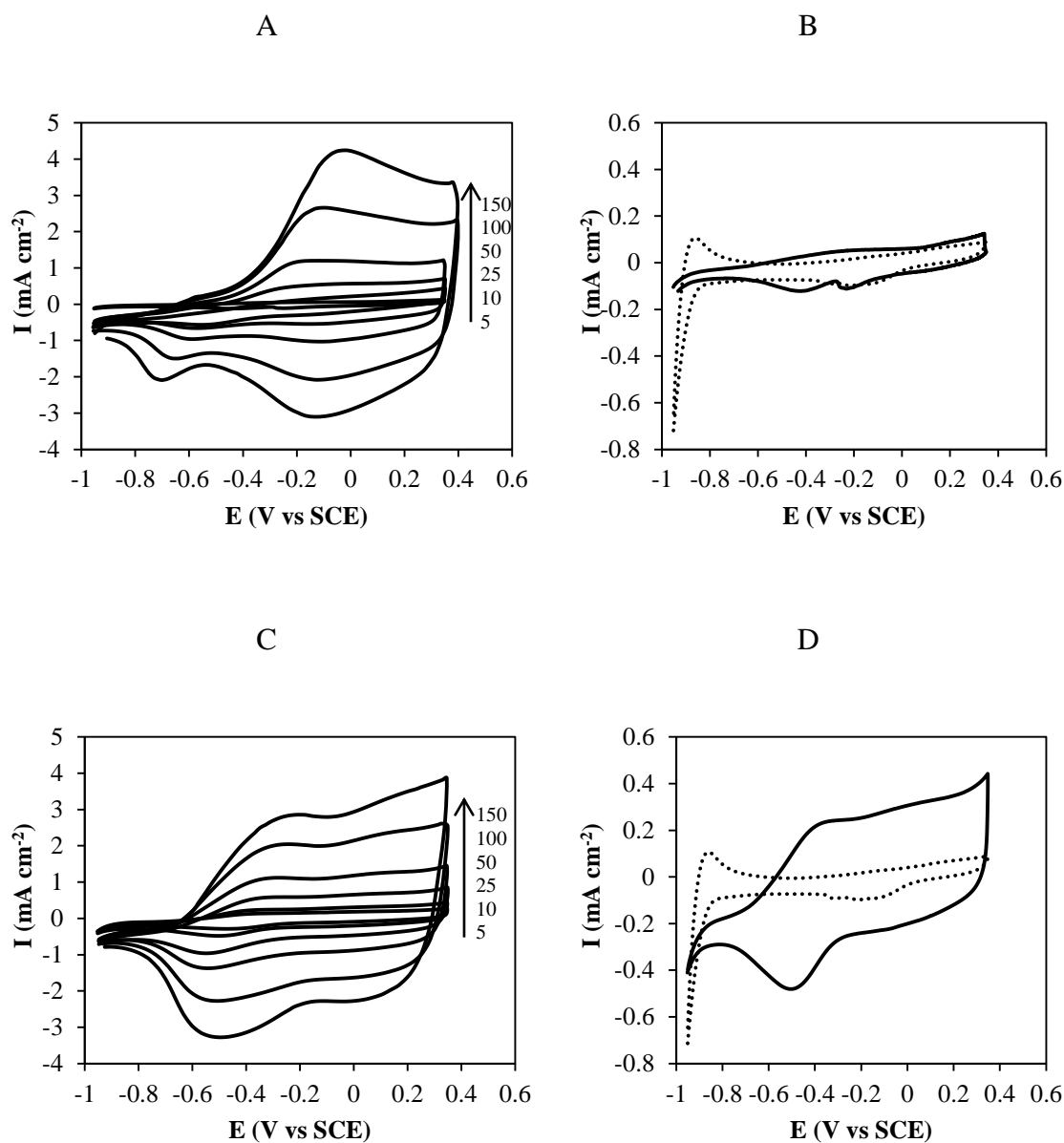


Figure 4.13: Cyclic voltammograms (10th cycle) of PpyCl (A and B) and PpyMO (C and D) coated Pt electrode in $0.1 \text{ mol dm}^{-3} \text{ NaCl}$. The dashed traces in (B) and (D) correspond to the voltammograms of bare Pt electrode. The scan rates in mV s^{-1} are indicated on the plot. The films were prepared by potentiostatic electropolymerisation at 0.80 V vs SCE to a charge density of 0.25 C cm^{-2} . The PpyCl was prepared from a solution of $0.1 \text{ mol dm}^{-3} \text{ Py}$ and $0.1 \text{ mol dm}^{-3} \text{ NaCl}$ and the PpyMO was prepared from a solution of $0.1 \text{ mol dm}^{-3} \text{ Py}$ and $0.01 \text{ mol dm}^{-3} \text{ MO}$.

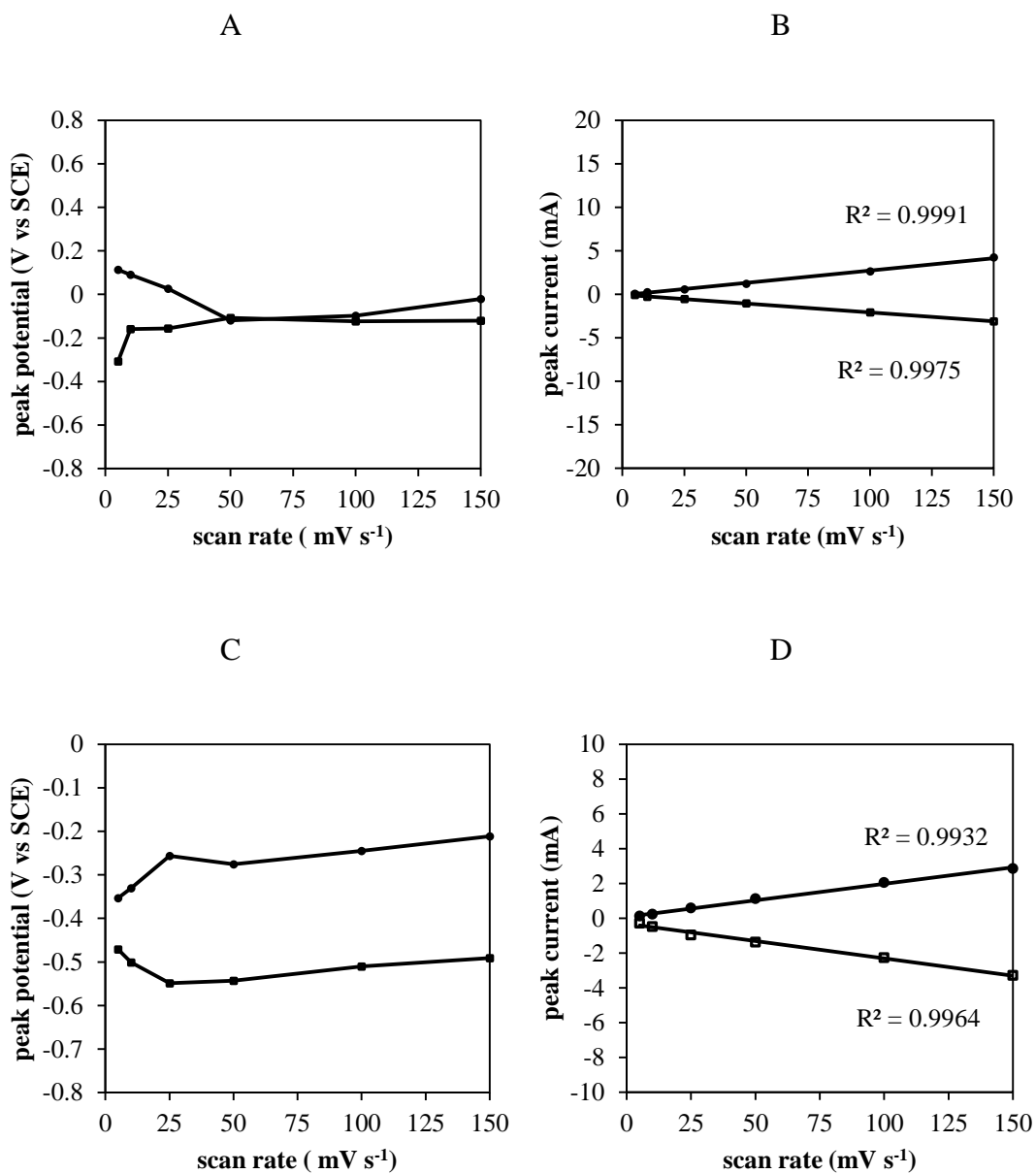


Figure 4.14: Peak potential plotted as a function of scan rate for PpyCl (A) and PpyMO (C) and peak current plotted as a function of scan rate PpyCl (B) and PpyMO (D) taken from the cyclic voltammograms (10th cycle) shown in Figure 4.13 A and C. The main anodic peak (●) and the main cathodic peak (□). The R^2 values for the linear trendline are indicated. The films were prepared by potentiostatic electropolymerisation at 0.80 V vs SCE to a charge density of 0.25 C cm^{-2} . The PpyCl was prepared from a solution of 0.1 mol dm^{-3} Py and 0.1 mol dm^{-3} NaCl and the PpyMO was prepared from a solution of 0.1 mol dm^{-3} Py and 0.01 mol dm^{-3} MO.

Table 4.2: Cyclic voltammetric data for the redox properties of PpyCl and PpyMO in 0.1 mol dm⁻³ NaCl.

PpyCl				
Scan rate (mV s ⁻¹)	E_{mid} (V vs SCE) ^a	ΔE_p (mV) ^b	I_{pa} (mA cm ⁻²)	I_{pc} (mA cm ⁻²)
5	-0.10	420	0.07	-0.08
10	-0.03	250	0.25	-0.29
25	-0.07	182	0.57	-0.55
50	-0.11	-12	1.20	-1.03
100	-0.11	25	2.66	-2.09
150	-0.07	101	4.24	-3.10
PpyMO				
Scan rate (mV s ⁻¹)	E_{mid} (V vs SCE) ^a	ΔE_p (mV) ^b	I_{pa} (mA cm ⁻²)	I_{pc} (mA cm ⁻²)
5	-0.41	118	0.14	-0.29
10	-0.42	170	0.24	-0.48
25	-0.40	293	0.59	-0.96
50	-0.41	267	1.12	-1.37
100	-0.38	266	2.05	-2.27
150	-0.35	280	2.86	-3.27

^a Calculated from $1/2 (E_{p,c} + E_{p,a})$.

^b $\Delta E_p = E_{pa} - E_{pc}$.

It is clear from a comparison of the data presented in Figure 4.14 A and Figure 4.14 C that the peak separation is more significant in the PpyMO than in the PpyCl film. For PpyMO the voltammetric peak associated with Na⁺ expulsion shifts to more positive potentials by 142 mV as the scan rate increases from 5 to 150 mV s⁻¹. The peak associated with the transient Na⁺ insertion is centred at $-0.50 \text{ V} \pm 30 \text{ mV}$. When anionic transport is dominant the insertion of the anion species from the solution into the Ppy film is associated with a larger ohmic potential drop than its expulsion⁶³. When cation transport is dominant the insertion of the cation species into the film is associated with a larger ohmic potential drop than its expulsion. In both cases, the peak current increases in a linear manner with the scan rate, Figure 4.14 B and Figure 4.14 D, and higher currents are obtained with the PpyCl films.

Table 4.2 shows the cyclic voltammetric data for the main redox process of PpyCl and PpyMO. The ratios of the peak currents (I_{pa}/I_{pc}) were determined for the main redox peaks, and average values of 0.8 and 0.7 were calculated for PpyCl and PpyMO, respectively. The peak current ratios increased as the scan rate increased. This deviates from a reversible voltammetric response with a peak ratio of 1.0⁷⁰. The average peak-to-peak separation, ΔE_p , for PpyCl and PpyMO in 0.1 mol dm⁻³ NaCl was calculated to be 121 mV and 232 mV, respectively. The other parameter determined from the cyclic voltammetric data is the midpoint potential, E_{mid} , which is very different for the PpyCl and PpyMO films. The E_{mid} values were computed as -0.08 V vs SCE for PpyCl and -0.39 V vs SCE for PpyMO, at 298 K. For reversible systems, the E_{mid} values coincide with the thermodynamically defined formal potential⁷⁰.

4.3.3.2 Redox properties of PpyCl/Chit and PpyMO/Chit grown to a charge density of 0.25 C cm^{-2}

As detailed earlier, the chitosan layer was formed post-electropolymerisation to give the PpyCl/Chit and PpyMO/Chit composite. Figure 4.15 shows the cyclic voltammograms of the PpyCl/Chit and PpyMO/Chit deposited on a Pt electrode and cycled in 0.1 mol dm^{-3} NaCl at $23 \text{ }^\circ\text{C}$. Again, the data presented in Figure 4.15 A show the voltammograms recorded for PpyCl/Chit at various scan rates, while the data shown in Figure 4.15 C represents the PpyMO/Chit film. The chitosan component does not significantly alter the overall redox properties of the chloride based composite. Figure 4.15 A shows a broad redox waves centred at 0.0 V vs SCE which is consistent with anion transport. The main anodic peak potential (E_{pa}) and cathodic peak potential (E_{pc}) shift as the scan rate is increased. A second cathodic peak appears at -0.50 V vs SCE at a scan rate of 5 mV s^{-1} and remains centred at this potential, however it becomes less pronounced as the scan rate is increased to 50 mV s^{-1} . Clearly the dominating redox process is for anion transport, which is similar to that obtained with the PpyCl film in Figure 4.13. The corresponding current-potential curves for PpyMO/Chit are shown in Figure 4.15 C. The anodic peak potential (E_{pa}) shifts in the anodic direction from about 0.0 V to 0.30 V vs SCE as the scan rate is increased from 5 to 150 mV s^{-1} . The cathodic peak potential (E_{pc}) shifts in the cathodic direction from approximately -0.10 V to -0.40 V vs SCE as the scan rate is increased. At the low scan rates ($< 25 \text{ mV s}^{-1}$) a second cathodic peak is observed at -0.50 V vs SCE. Again, these voltammograms are consistent with cation transport, which is similar to that observed with the PpyMO film, Figure 4.12. However, there is also evidence of anion transport, with the incorporation and expulsion of chloride anions.

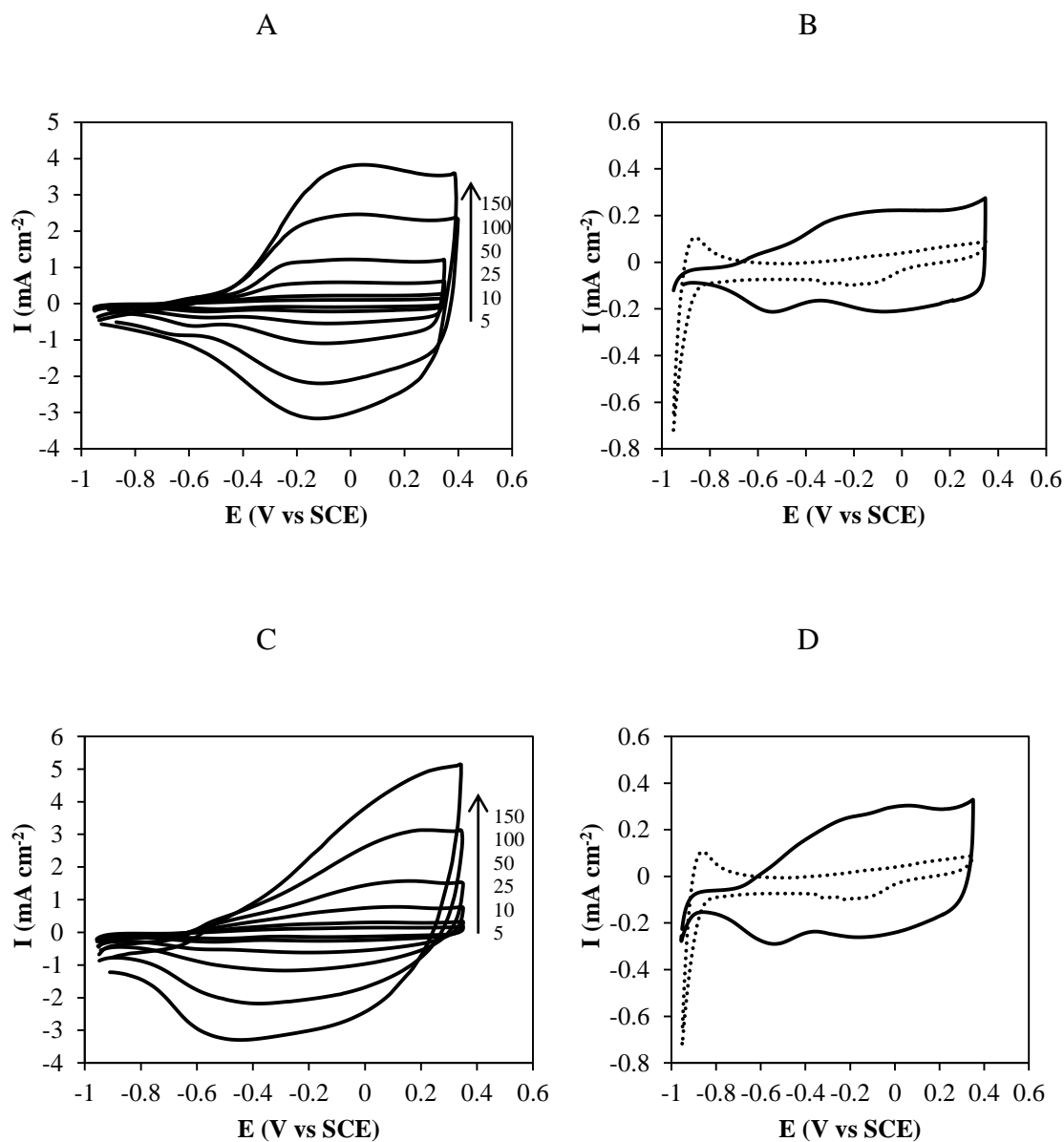


Figure 4.15: Cyclic voltammograms (10th cycle) of PpyCl/Chit (A and B) and PpyMO/Chit (C and D) coated Pt electrode in 0.1 mol dm⁻³ NaCl. The dashed traces in (B) and (D) correspond to the voltammograms of bare Pt electrode. The scan rates in mV s⁻¹ are indicated on the plot. The films were prepared by potentiostatic electropolymerisation at 0.80 V vs SCE to a charge density of 0.25 C cm⁻². The PpyCl was prepared from a solution of 0.1 mol dm⁻³ Py and 0.1 mol dm⁻³ NaCl and the PpyMO was prepared from a solution of 0.1 mol dm⁻³ Py and 0.01 mol dm⁻³ MO. Chitosan was added post-polymerisation.

In Figure 4.16, plots are shown for the peak potential (E_p) and peak current (I_p) as a function of the scan rate for the cyclic voltammograms of PpyCl/Chit and PpyMO/Chit presented in Figure 4.15. In PpyCl/Chit (Figure 4.16 A) there is a difference of 100 mV between the maximum and minimum values of (E_{pa}) which occur at 5 and 25 mV s^{-1} , respectively. This voltammetric peak associated with Cl^- insertion is more susceptible to the change in scan rate than the voltammetric peak associated with Cl^- expulsion.

The peak associated with the transient Cl^- insertion shifts slightly to lower potentials with increased scan rate, possibly due to uncompensated resistance as the scan rate increases.

The peak separation is more significant in the PpyMO/Chit than in the PpyCl/Chit, as evident from a comparison of Figure 4.16 A and Figure 4.16 C. For PpyMO/Chit the voltammetric peak associated with Na^+ insertion is difficult to discern at the higher scan rates, as shown in Figure 4.15. However the peak potentials recorded at the lower scan rates are clear and these are plotted in Figure 4.16 C. The corresponding cathodic peak varies significantly with the scan rate, giving a peak separation of 0.78 V at 150 mV s^{-1} .

In contrast to PpyMO, Figure 4.14, which has a peak associated with Na^+ insertion at -0.50 V vs SCE, the PpyMO/Chit appears to be dominated also by anionic transport. The insertion of the ionic species from the solution into the Ppy film is associated with a larger ohmic potential drop than its expulsion⁶³. Clearly the ionic species interact with the chitosan-modified surface of the electrode. The peak currents for PpyCl/Chit and PpyMO/Chit increase linearly with increasing scan rate, indicating the absence of a kinetic or charge-transport limitation⁶³. The linear current increase with scan rate may suggest good rate ability⁷¹ attributed to the effective accessibility of electrolyte through the PpyCl/Chit and PpyMO/Chit composites.

Table 4.4 shows the cyclic voltammetric data for the main redox process of PpyCl/Chit and PpyMO/Chit. The peak current ratios (I_{pa}/I_{pc}) were determined and average values of 1.1 and 1.3 were calculated for PpyCl/Chit and PpyMO/Chit, respectively. The peak current ratios increased as the scan rate increased. This deviates from a reversible voltammetric response with a peak ratio of 1.0⁷⁰. The average peak-to-peak separation, ΔE_p , for PpyCl/Chit and PpyMO/Chit in 0.1 mol dm^{-3} NaCl was calculated to be 115 mV

and 425 mV, respectively. The peak-to-peak separation values are similar for PpyCl and PpyCl/Chit, however, there is almost a two-fold higher value obtained for PpyMO/Chit compared to PpyMO. The E_{mid} values were computed to be -0.03 V vs SCE for PpyCl/Chit and -0.06 V vs SCE for PpyMO/Chit, at 298 K.

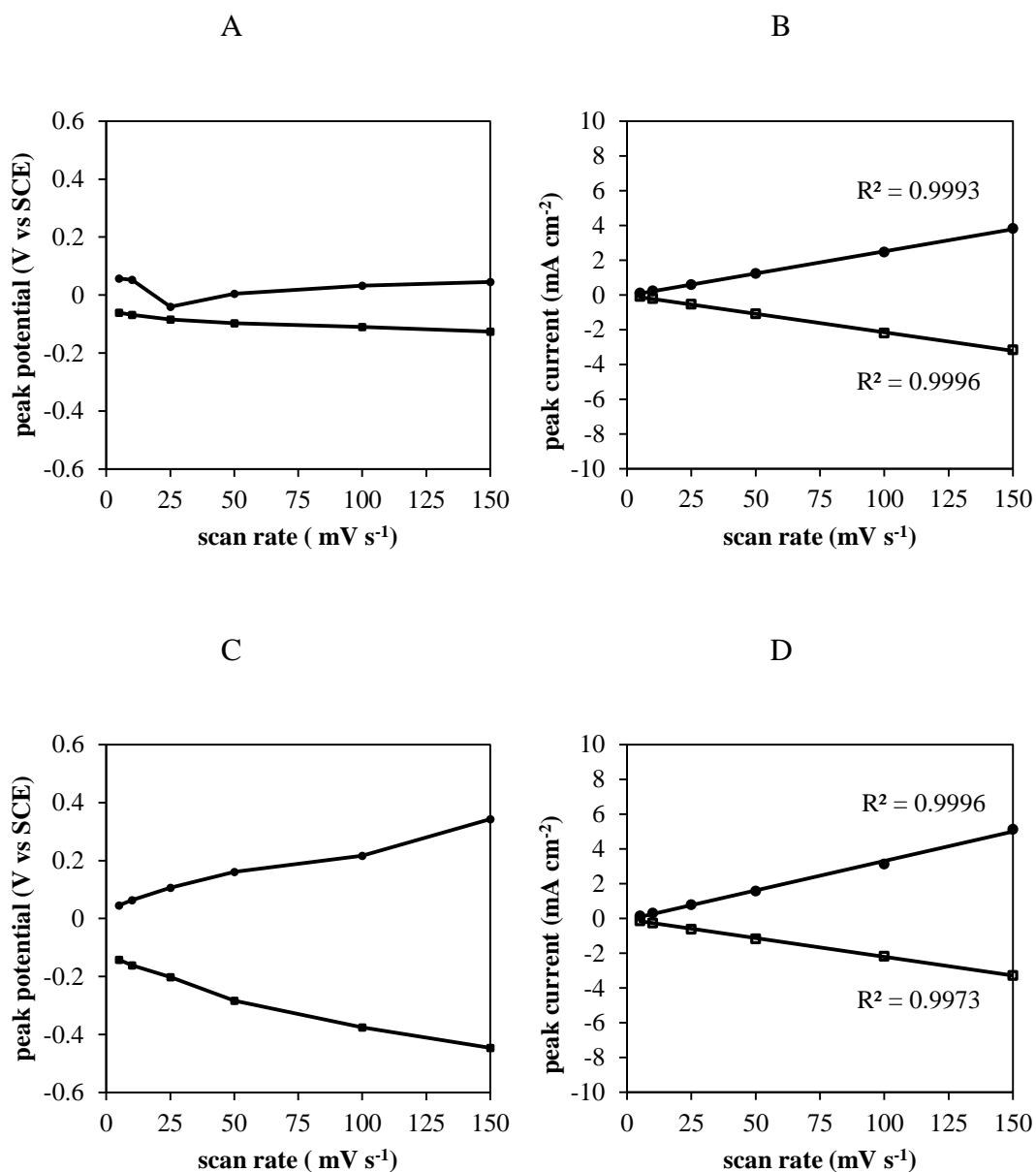


Figure 4.16: Peak potential plotted as a function of scan rate for PpyCl/Chit (A) and PpyMO/Chit (C) and peak current plotted as a function of scan rate PpyCl/Chit (B) and PpyMO/Chit (D) taken from the cyclic voltammograms (10th cycle) shown in Figure 4.13 A and C. The main anodic peak (●) and the main cathodic peak (□). The R^2 values for the linear trendline are indicated. The films were prepared by potentiostatic electropolymerisation at 0.80 V vs SCE to a charge density of 0.25 C cm^{-2} . The PpyCl was prepared from a solution of 0.1 mol dm^{-3} Py and 0.1 mol dm^{-3} NaCl and the PpyMO was prepared from a solution of 0.1 mol dm^{-3} Py and 0.01 mol dm^{-3} MO. Chitosan was added post-polymerisation.

Table 4.3: Cyclic voltammetric data for the redox properties of PpyCl/Chit and PpyMO/Chit in 0.1 mol dm⁻³ NaCl.

PpyCl/Chit				
Scan rate (mV s ⁻¹)	E_{mid} (V vs SCE) ^a	ΔE_p (mV) ^b	I_{pa} (mA cm ⁻²)	I_{pc} (mA cm ⁻²)
5	0.00	120	0.10	-0.10
10	-0.01	120	0.22	-0.21
25	-0.06	100	0.59	-0.54
50	-0.05	40	1.22	-1.10
100	-0.04	140	2.46	-2.19
150	-0.04	170	3.82	-3.16

PpyMO/Chit				
Scan rate (mV s ⁻¹)	E_{mid} (V vs SCE) ^a	ΔE_p (mV) ^b	I_{pa} (mA cm ⁻²)	I_{pc} (mA cm ⁻²)
5	-0.05	187	0.15	-0.14
10	-0.05	225	0.30	-0.26
25	-0.05	308	0.78	-0.62
50	-0.06	445	1.57	-1.17
100	-0.08	592	3.13	-2.18
150	-0.05	789	5.12	-3.29

^a Calculated from $1/2 (E_{p,c} + E_{p,a})$.

^b $\Delta E_p = E_{pa} - E_{pc}$.

A direct comparison of the cyclic voltammograms recorded for PpyMO and PpyCl is shown in Figure 4.17 A, while corresponding data are presented in Figure 4.17 B for the PpyMO/Chit and PpyCl/Chit films. These voltammograms were recorded at 50 mV s^{-1} . The significant role of the chitosan layer can be clearly seen. It is also evident that the chitosan layer exerts more influence on the PpyMO system; with evidence for both cation and anion transport with the chitosan layer, but predominately cation transport with the PpyMO films.

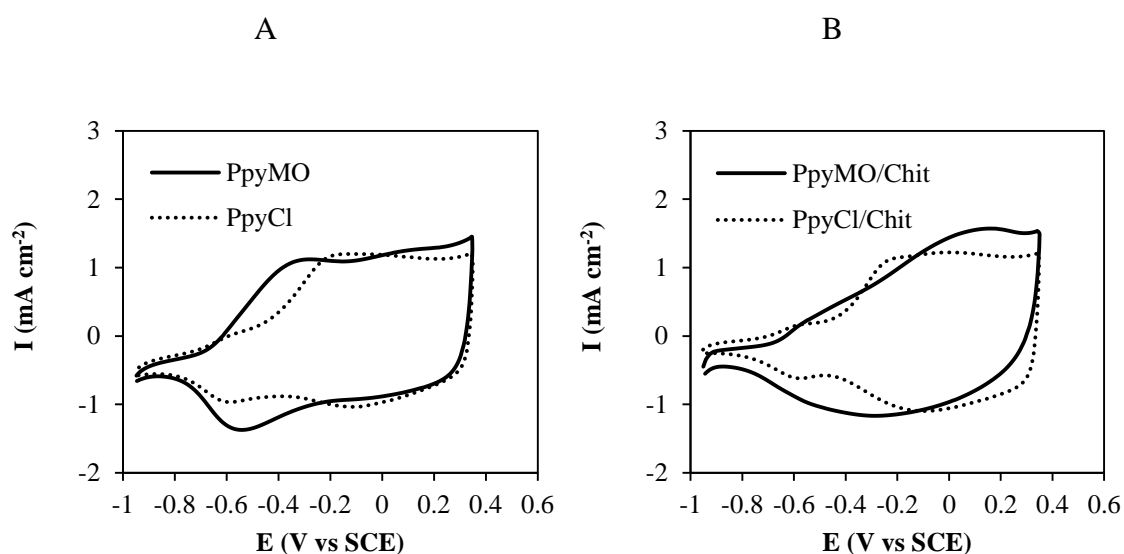


Figure 4.17: Cyclic voltammograms for the redox properties of PpyA (A) and PpyA/Chit (B) in $0.1 \text{ mol dm}^{-3} \text{ NaCl}$ on a 0.13 cm^2 Pt electrode at 50 mV s^{-1} . The films were prepared by potentiostatic electropolymerisation at 0.80 V vs SCE to a charge density of 0.25 C cm^{-2} . The PpyCl was prepared from a solution of $0.1 \text{ mol dm}^{-3} \text{ Py}$ and $0.1 \text{ mol dm}^{-3} \text{ NaCl}$ and the PpyMO was prepared from a solution of $0.1 \text{ mol dm}^{-3} \text{ Py}$ and $0.01 \text{ mol dm}^{-3} \text{ MO}$. For PpyA/Chit (B), chitosan was added post-polymerisation.

A more detailed analysis of the mass transfer process can be obtained as described by Levi *et al.*⁷² using a generalised capacitance curve (current divided by the potential scan rate). Figure 4.18 shows a typical plot for the PpyCl (A) and PpyMO (B) cycled at a scan rate of 5 mV s^{-1} . The oxidation and reduction peaks can be seen more clearly at the slow

scan rates in both the PpyCl and PpyMO films using this approach. Four peaks are visible and these are labelled as I, II, III and IV. Figure 4.18 A presents PpyCl. The secondary redox cation exchange process, Peak I and IV, is centred at -0.50 V vs SCE. During oxidation there are two competing processes: the expulsion of the cation and the inclusion of the anion. Conversely, during reduction the expulsion of the anion and inclusion of the cation are the two competing processes⁷³. Figure 4.18 B presents PpyMO. The secondary redox cation exchange process, Peak I and IV, is centred at -0.50 V vs SCE. The PpyCl/Chit film reaches a maximum capacitance of approximately 25 mF cm^{-2} , whereas the PpyMO film reaches a maximum capacitance of approximately 50 mF cm^{-2} . This suggests PpyMO has better charge storage ability⁷⁴ than PpyCl and bare Pt which has a capacitance of 6.62 mF cm^{-2} (data not shown).

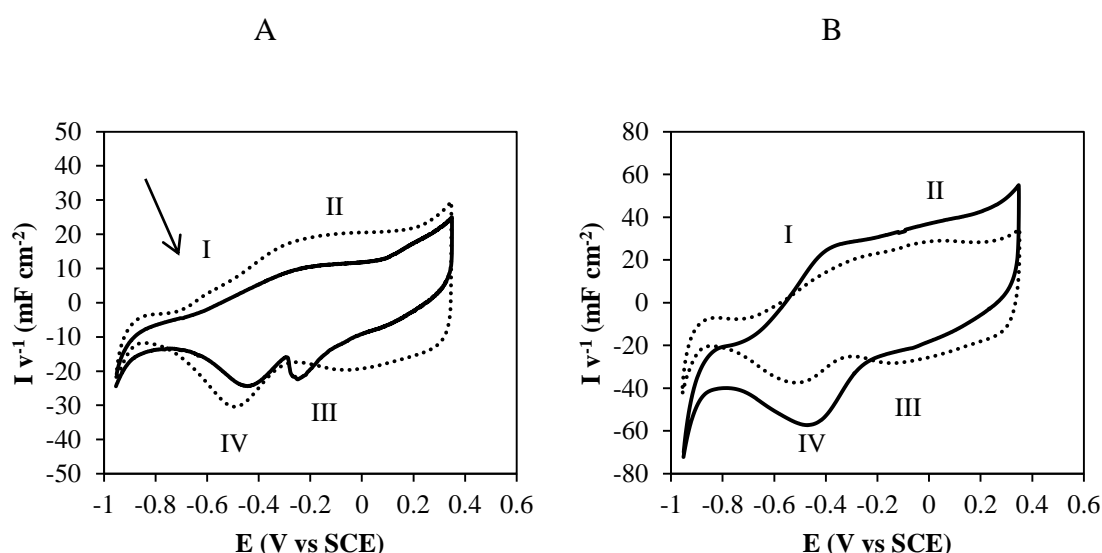
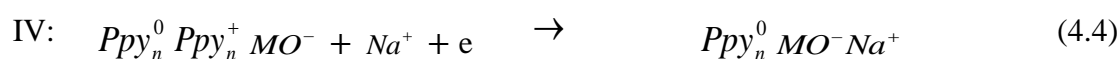
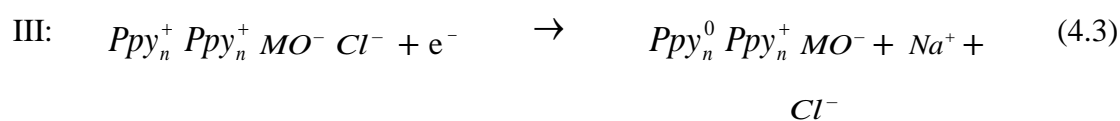
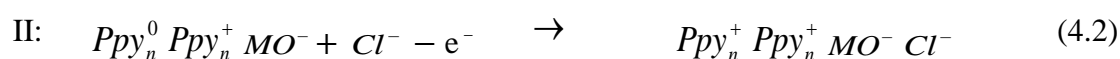
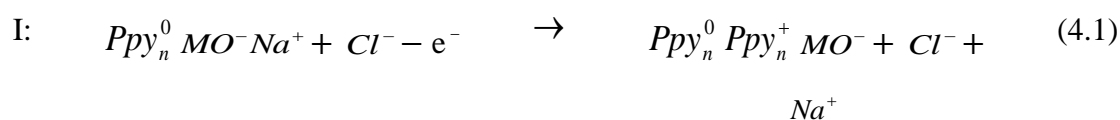


Figure 4.18: Generalised capacitance curve (where the current is divided by the scan rate v) for PpyCl (A) and PpyMO (B) cycled in 0.1 mol dm^{-3} NaCl at 5 mV s^{-1} . The dashed traces indicate the chitosan-coated composite. The films were prepared by potentiostatic electropolymerisation at 0.80 V vs SCE to a charge density of 0.25 C cm^{-2} . The PpyCl was prepared from a solution of 0.1 mol dm^{-3} Py and 0.1 mol dm^{-3} NaCl and the PpyMO was prepared from a solution of 0.1 mol dm^{-3} Py and 0.01 mol dm^{-3} MO. For PpyA/Chit (B), chitosan was added post-polymerisation.

The possible processes occurring at the peaks labelled I, II, III, and IV are described in Equations 4.1, 4.2, 4.3 and 4.4. On re-oxidation of the PpyMO (Figure 4.18 B, peaks I and II) the polymer backbone becomes positively charged. The charge neutrality is achieved by the expulsion of the sodium ion (Equation 4.1) and the incorporation of the chloride ion (Equation 4.2) from the electrolyte. When the PpyMO is reduced during subsequent cycles (Figure 4.18 B, peaks III and IV), the chloride anion is expelled into the electrolyte (Equation 4.3) and in order to maintain overall charge neutrality a sodium ion from the electrolyte is incorporated into the polymer (Equation 4.4).



4.3.4 Electrochemical impedance spectroscopy (EIS)

Complex plane-impedance plots (Nyquist plots) and Bode plots were recorded for PpyMO, PpyMO/Chit, PpyCl and PpyCl/Chit. The PpyMO and PpyCl films were grown to a charge density of 0.25 C cm^{-2} at a Pt electrode. The impedance measurements were recorded at fixed potentials of -0.90 , -0.60 , -0.30 , -0.10 , 0.0 , 0.10 and 0.30 V vs SCE in $0.1 \text{ mol dm}^{-3} \text{ NaCl}$. Four measurements were recorded at each potential with a 60 min period between each measurement, to reduce the effect of hysteresis⁶³. The polymer film

is in a totally reduced state at -0.90 V vs SCE⁵⁴, and as the potential is increased the films are oxidised, and the different applied potentials represent varying degrees of oxidation.

These data sets were fitted to the equivalent circuits illustrated in Figure 4.19 using a non-linear least squares fitting minimisation method in the ZView fitting programme described in Section 2.4.4. The real axis intercept at high frequency coincides with the uncompensated solution resistance (R_s) and is independent of the applied potential⁶³. A Randles circuit (Figure 4.19) was used to model the impedance response at each applied potential, and then additional circuit elements were considered. A more complex circuit was used to model the impedance of PpyMO at -0.90 V vs SCE, with a second RC time constant incorporated into the model, which describes two RC processes occurring at different rates⁷⁵, Figure 4.19 B. All data were normalised to the surface area of the Pt electrode, 0.13 cm².

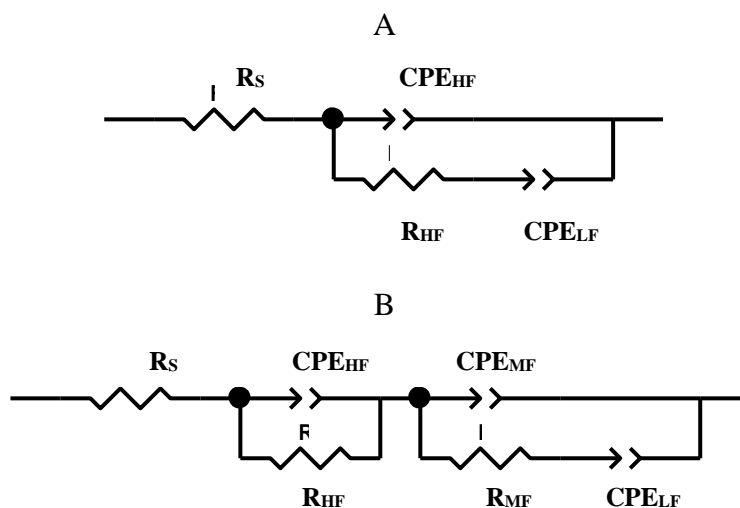


Figure 4.19: Equivalent circuits used for modelling the impedance data.

4.3.4.1 EIS of PpyMO films

The complex-plane impedance (Nyquist) plots and Bode plots for PpyMO are shown in Figure 4.20 A and B, respectively. The parameters extracted from the equivalent circuit model were used to determine the double layer capacitance (C_{dl}) which was corrected to units of capacitance. Some of the parameters from the equivalent circuit for PpyMO films at different redox states are shown in Table 4.5 and this includes the solution resistance, R_s , the constant phase element (CPE_{HF}), which has an exponent between 0.5 and 1.0, and the charge-transfer resistance, R_{HF} is also included. The capacitance term, C_{LF} , was estimated directly from the Bode plot ($C_{LF} = 1/\text{slope}$)^{76, 77} as described in Section 2.4.4 equation 2.8.

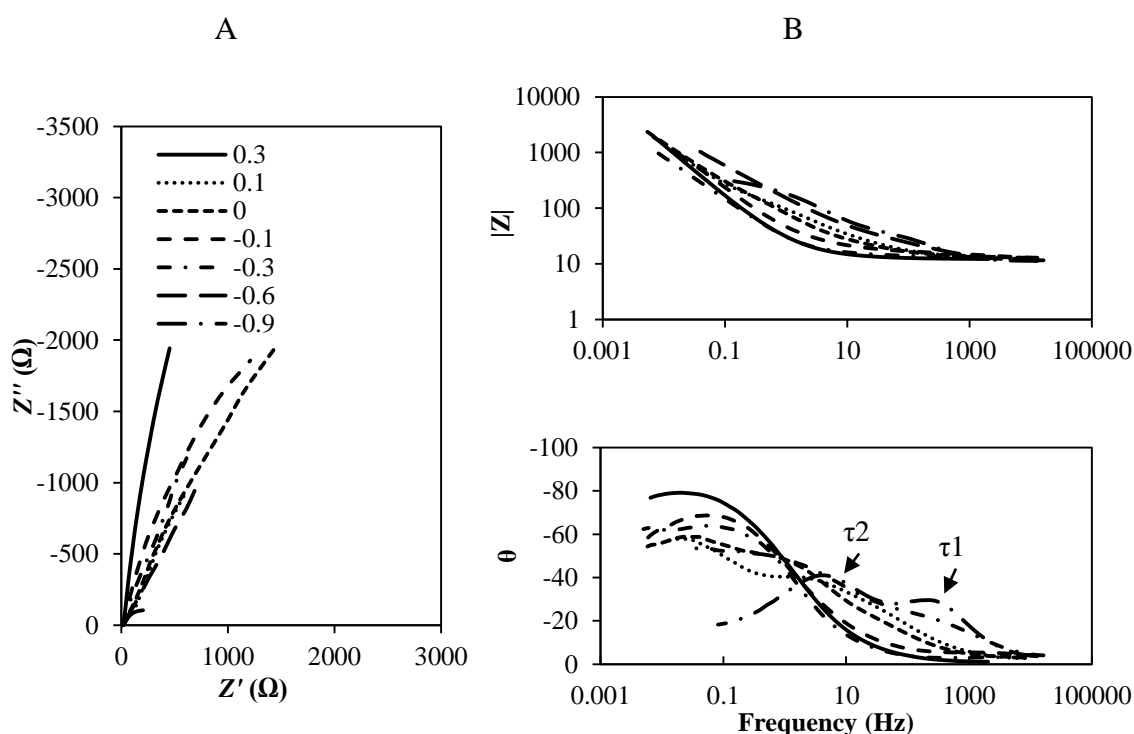


Figure 4.20: Complex-plane impedance plot (A) for PpyMO coated 0.13 cm^2 Pt electrodes at various potentials in 0.1 mol dm^{-3} NaCl. The Bode plot (B) shows the logarithm of the impedance and the phase angle against the logarithm of frequency. Potentials are indicated in V vs SCE. Frequency range shown from 65 kHz to 0.005 Hz. The films were prepared by potentiostatic electropolymerisation at 0.80 V vs SCE to a charge density of 0.25 C cm^{-2} . The PpyCl was prepared from a solution of 0.1 mol dm^{-3} Py and 0.1 mol dm^{-3} NaCl and the PpyMO was prepared from a solution of 0.1 mol dm^{-3} Py and 0.01 mol dm^{-3} MO.

At higher potentials a 45° “Warburg-type” linear region is observed in the high-medium frequency range as the redox reaction induced by the ac potential wave penetrates the PpyMO film. This is more clearly shown in Figure 4.21 A. At lower potentials a compressed semicircular arc is observed in the high frequency range, due to parallel resistance-capacitance elements which is typical of polymer coated electrodes exhibiting ion transport⁷⁸. This is clearly evident in Figure 4.21 B. The impedance response in these regions is particularly important for determining mass transfer parameters. As the frequency is decreased the transmission line becomes nearly vertical where the polymer|metal electrode behaves like a capacitor. The deviation from an ideal impedance spectrum is thought to be due to irregular thickness and morphology of the polymer surface⁷⁹. Tables 4.4 and 4.5 summarise the parameters for the circuit elements evaluated by fitting the impedance data of PpyCl and PpyMO, respectively.

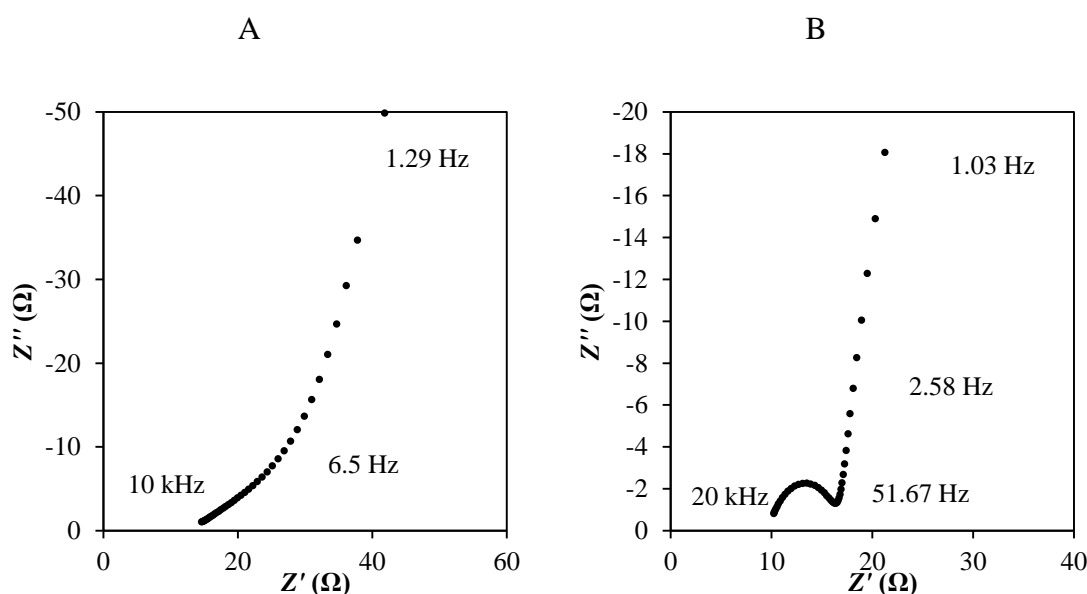
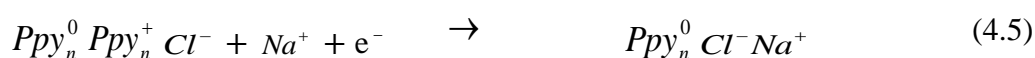


Figure 4.21: Complex plane-impedance plot of a PpyMO coated 0.13 cm² Pt electrode measured at 0.30 V vs SCE (A) and -0.30 V vs SCE (B) in 0.1 mol dm⁻³ NaCl. The frequency is indicated on the plot. The films were prepared by potentiostatic electropolymerisation at 0.80 V vs SCE to a charge density of 0.25 C cm⁻². The PpyCl was prepared from a solution of 0.1 mol dm⁻³ Py and 0.1 mol dm⁻³ NaCl and the PpyMO was prepared from a solution of 0.1 mol dm⁻³ Py and 0.01 mol dm⁻³ MO.

The R_{HF} resistance term presented in Tables 4.4 and 4.5 can be considered as the charge-transfer resistance. The R_{HF} increases sharply by three orders of magnitude with a minimum at 0.30 V vs SCE and a maximum at -0.60 V vs SCE ($1.35 \text{ k}\Omega \text{ cm}^2$) for the PpyCl film, Table 4.4. As the potential is varied from 0.30 V vs SCE to -0.60 V vs SCE the PpyCl is reduced from an oxidised state to a neutral state and the resistance increases. However, a decrease in the resistance is observed at -0.90 V vs SCE. This may be attributed to a decrease in the ionic resistance due to the insertion of Na^+ , as shown in Equation 4.5.



The ingress of cations in a Ppy film was studied by Plieth *et al.*⁸⁰ and they found a strong increase in mass at potentials below -0.70 V during EQCM measurements as the pores in the film became saturated with hydrated cations.

The R_{HF} values obtained for PpyMO, Table 4.5, appear independent of potential for redox potentials higher than -0.30 V vs SCE. At potentials lower than -0.30 V vs SCE, it can be clearly seen that the R_{HF} becomes potential dependent and the resistance increases sharply by approximately $230 \Omega \text{ cm}^2$, with a maximum at -0.90 V vs SCE.

The total resistance, R_T , was computed using the expression in Equation 4.6 for resistors in series. This resistance was then used to calculate the conductivity, σ_T , as shown in Equation 4.6, where d is the nominal thickness of the dry film, 5.0×10^{-5} and 5.6×10^{-5} cm for PpyCl and PpyMO respectively, and A is the geometric surface area of the electrode (0.13 cm^2).

$$R_T = R_{HF} + R_{MF} \quad (4.6)$$

$$\sigma_T = \frac{1}{R_T} \times \frac{d}{A} \quad (4.7)$$

The total resistance, R_T , and the conductivity, σ_T , of the PpyCl and PpyMO films were plotted as a function of applied potential and representative plots are presented in Figure

4.22. The conductivity of the PpyCl decreases sharply by $100.6 \mu\text{S cm}^{-1}$ with a maximum at 0.30 V vs SCE and a minimum at -0.60 V vs SCE as the Ppy is reduced and the charge carrier (Cl^-) concentration in the film decreases. A slight increase of $0.3 \mu\text{S cm}^{-1}$ is observed at -0.90 V vs SCE , which is consistent with the ingress of Na^+ , Equation 4.5. The resistance decreases as the applied potential is varied from 0.30 V vs SCE to -0.60 V vs SCE and again there is a slight decrease in the resistance at -0.90 V vs SCE .

Table 4.4: Parameters for the circuit elements evaluated by fitting the impedance data of PpyCl to the equivalent circuit shown in Figure 4.19, n=3.

E (V vs SCE)	0.3	0.1	0.0	-0.1	-0.3	-0.6	-0.9
R_s (Ω cm²)	12.21 ± 0.05	14.34 ± 0.18	13.83 ± 0.22	13.65 ± 0.17	15.02 ± 0.05	30.14 ± 0.63	36.44 ± 3.44
CPE-T_{HF} (mF cm⁻²)	3.98 ± 0.23	3.72 ± 0.23	1.23 ± 0.14	0.56 ± 0.02	0.76 ± 0.01	0.33 ± 0.01	0.42 ± 0.05
CPE-P_{HF}	0.79 ± 0.01	0.66 ± 0.01	0.62 ± 0.02	0.63 ± 0.01	0.65 ± 0.00	0.54 ± 0.01	0.34 ± 0.01
R_{HF} (Ω cm²)	3.95 ± 0.23	14.96 ± 0.80	71.70 ± 5.31	487 ± 15.8	592 ± 5.70	1346 ± 46.7	757 ± 105
CPE-T_{LF} (mF cm⁻²)	7.99 ± 0.24	6.17 ± 0.25	4.03 ± 0.16	3.78 ± 0.10	6.57 ± 0.09	3.01 ± 0.13	0.52 ± 0.07
CPE-P_{LF}	1 ± 0	0.99 ± 0.02	0.79 ± 0.02	0.68 ± 0.01	0.69 ± 0.00	0.74 ± 0.02	0.58 ± 0.03
χ^2	0.007	0.008	0.004	0.002	0.0003	0.003	0.0007
SS	0.815	0.833	0.489	0.292	0.031	0.334	0.068

The CPE was replaced with a capacitor (C) in the lower branch of the circuit for parameters with a P value of 1 ± 0

Table 4.5: Parameters for the circuit elements evaluated by fitting the impedance data of PpyMO to the equivalent circuit shown in Figure 4.19, $n=3$.

E (V vs SCE)	0.3	0.1	0.0	-0.1	-0.3	-0.6	-0.9^a
R_s ($\Omega \text{ cm}^2$)	15.69 \pm 0.20	11.85 \pm 0.06	12.55 \pm 0.24	12.84 \pm 0.19	10.93 \pm 0.11	11.78 \pm 0.06	12.49 \pm 0.06
CPE-T_{HF} (mF cm^{-2})	2.02 \pm 0.06	1.79 \pm 0.03	0.80 \pm 0.25	0.05 \pm 0.01	0.03 \pm 0.00	0.07 \pm 0.00	0.05 \pm 0.00
CPE-P_{HF}	0.70 \pm 0.01	0.59 \pm 0.00	0.64 \pm 0.04	1 \pm 0	1	0.88 \pm 0.01	1 \pm 0
R_{HF} ($\Omega \text{ cm}^2$)	39.82 \pm 1.73	75.42 \pm 2.38	14.73 \pm 1.27	4.90 \pm 0.26	6.16 \pm 0.15	150 \pm 4.84	16.3 \pm 0.41
CPE-T_{LF} (mF cm^{-2})	2.97 \pm 0.09	1.17 \pm 0.03	4.11 \pm 0.26	5.79 \pm 0.06	11.84 \pm 0.09	0.76 \pm 0.00	0.69 \pm 0.02
CPE-P_{LF}	1 \pm 0	0.88 \pm 0.01	0.81 \pm 0.02	0.76 \pm 0.00	0.78 \pm 0.00	0.58 \pm 0.00	0.83 \pm 0.01
χ^2	0.014	0.0008	0.0065	0.011	0.0055	0.0014	0.0019
SS	1.66	0.101	1.345	0.713	0.1923	0.2602	

The CPE was replaced with a capacitor (C) in the circuit parameters with a P value of 1.

^a The circuit in 4.18 B consists of additional elements: $R_{\text{MF}} 257 \pm 7.79$, $\text{CPE}_{\text{LF-T}} 18.7 \text{ mF cm}^{-2} \pm 1.79$, $\text{CPE}_{\text{LF-P}} 0.43 \pm 0.02$

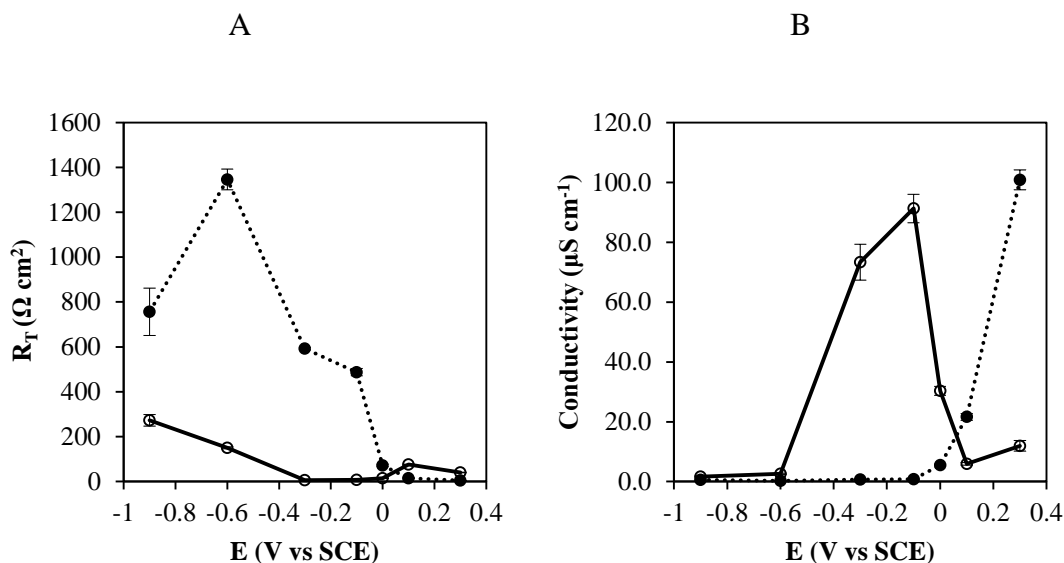


Figure 4.22: Plots of resistance, R_T , (A), and conductivity, σ_T , (B), as a function of applied potential for PpyCl (●) and PpyMO (○) in 0.1 mol dm^{-3} NaCl. The films were prepared by potentiostatic electropolymerisation at 0.80 V vs SCE to a charge density of 0.25 C cm^{-2} . The PpyCl was prepared from a solution of 0.1 mol dm^{-3} Py and 0.1 mol dm^{-3} NaCl and the PpyMO was prepared from a solution of 0.1 mol dm^{-3} Py and 0.01 mol dm^{-3} MO.

The conductivity of the PpyMO film is comparably lower than the PpyCl when polarised in the oxidised state, Figure 4.22 B. Similarly, the resistance is somewhat higher, Figure 4.22 A. The conductivity increases as the PpyMO is reduced, Equation 4.8, and the concentration of the charge carriers (Na^+) is increased.



The high frequency capacitance, C_{HF} , shown in Tables 4.4 and 4.5, was calculated using the expression provided in Equation 4.9 and the low frequency capacitance, C_{LF} , was estimated directly from the Bode plot ($C_{\text{LF}} = 1/\text{slope}$).

$$\text{corrected } C_{HF} = T_{HF}^{(1/P)} \left(\frac{R_S R_{HF}}{R_S + R_{HF}} \right)^{1-P/P} \quad (4.9)$$

In Figure 4.23, the high frequency capacitance, C_{HF} , and the low frequency capacitance, C_{LF} are plotted as a function of the applied potential for the PpyMO and PpyCl films. It is evident from these plots that there is some variation between the capacitance of the PpyCl and PpyMO films. The PpyCl film shows a decrease in C_{HF} as the Ppy film releases chloride anions to the surrounding electrolyte, with a maximum at 0.30 V vs SCE and a minimum at -0.60 V vs SCE. The C_{HF} of PpyMO is comparably lower than PpyCl when polarised in the oxidised state and decreases tenfold between 0.20 and 0.0 V vs SCE. At potentials lower than 0.0 V vs SCE, the C_{HF} appears to be independent of potential. The C_{LF} decreases steadily for PpyCl as the charge storage capacity of the film matrix decreases. Interestingly, the C_{LF} increases for PpyMO as the applied potential is reduced from 0.10 V to -0.30 V vs SCE followed by a minimum value at -0.60 V vs SCE. This high capacity is attributed to cation transport and corresponds to the cyclic voltammogram in Figure 4.13 B.

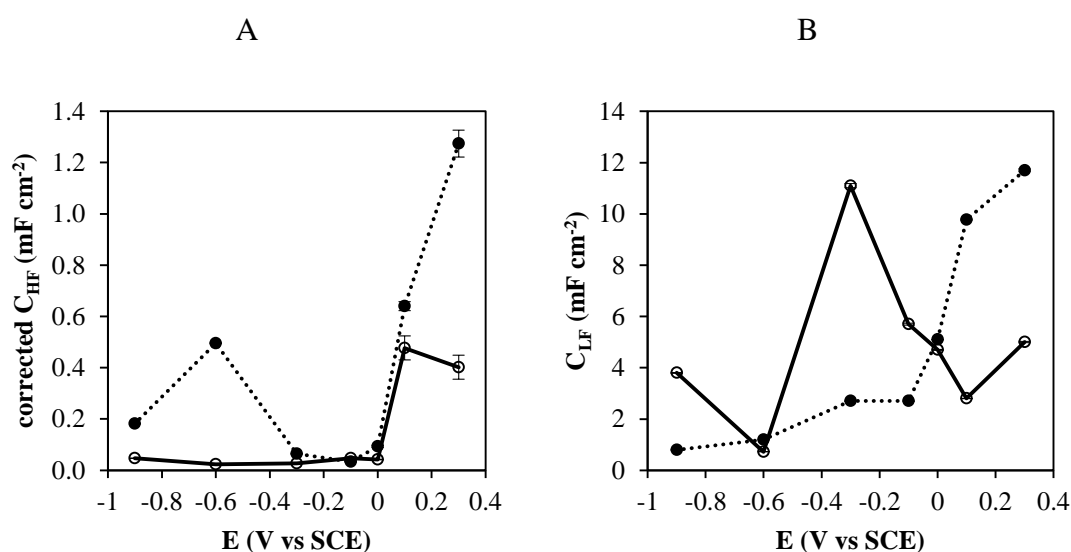


Figure 4.23: Plots of corrected double layer capacitance, C_{HF} , (A), and low frequency capacitance, C_{LF} , (B), as a function of applied potential for PpyCl (●) and PpyMO (○) in 0.1 mol dm^{-3} NaCl. The films were prepared by potentiostatic electropolymerisation at 0.80 V vs SCE to a charge density of 0.25 C cm^{-2} . The PpyCl was prepared from a solution of 0.1 mol dm^{-3} Py and 0.1 mol dm^{-3} NaCl and the PpyMO was prepared from a solution of 0.1 mol dm^{-3} Py and 0.01 mol dm^{-3} MO.

4.3.4.2 EIS analysis of PpyMO/Chit

The impedance of PpyCl/Chit and PpyMO/Chit was measured as a function of the applied potential, using an approach similar to that used to record the impedance in Section 4.3.4.1. Typical complex-plane impedance plots and Bode plots recorded for PpyMO/Chit at potentials varying from 0.30 V to -0.90 V vs SCE are shown in Figure 4.24. Again, it is evident from these data that the impedance response changes as the applied potential is varied. The impedance is lower at 0.30 V vs SCE and increases as the potential is varied from 0.30 V to -0.60 V vs SCE. The resistance of the PpyMO/Chit film is somewhat higher than that obtained for PpyMO. This is consistent with a higher resistance to ion transport due to the presence of the chitosan.

These data were fitted to the equivalent circuit in Figure 4.19 and the data obtained are summarised in Tables 4.6 and 4.7. The R_{HF} increases sharply by three orders of magnitude with a minimum at 0.10 V vs SCE and a maximum at -0.90 V vs SCE ($0.84 \text{ k}\Omega \text{ cm}^2$) for the PpyCl/Chit film, Table 4.6. As the potential is varied from 0.30 V vs SCE to -0.90 V vs SCE the PpyCl/Chit is reduced from an oxidised state to a neutral state and the resistance increases. However, the PpyCl/Chit is oxidised to a lesser extent than the PpyCl in Section 4.3.4.1. This may be due to the mobility of Cl^- . The R_{HF} values obtained for PpyMO/Chit, Table 4.7, appear independent of potential for redox potentials higher than -0.30 V vs SCE. At potentials lower than -0.30 V vs SCE, it can be clearly seen that the R_{HF} becomes potential dependent and the resistance increases sharply by approximately $0.73 \text{ k}\Omega \text{ cm}^2$, with a maximum at -0.60 V vs SCE and a decrease in the resistance is observed at -0.90 V vs SCE. Again, this may be attributed to a decrease in the ionic resistance due to the insertion of cations.

Again, the total resistance, R_T , was computed using the expression in Equation 4.6 for resistors in series. The presence of chitosan makes it difficult to determine the polymer films thickness and thus the conductivity, σ_T , was not determined. Figure 4.25 shows a direct comparison between the resistance of PpyCl/Chit and PpyMO/Chit where the total resistance is plotted as a function of applied potential. Again, it is clear from this plot that

the resistance of the polymer films, PpyCl/Chit and PpyMO/Chit, increases as the potential is varied from 0.10 V vs SCE to -0.90 V vs SCE.

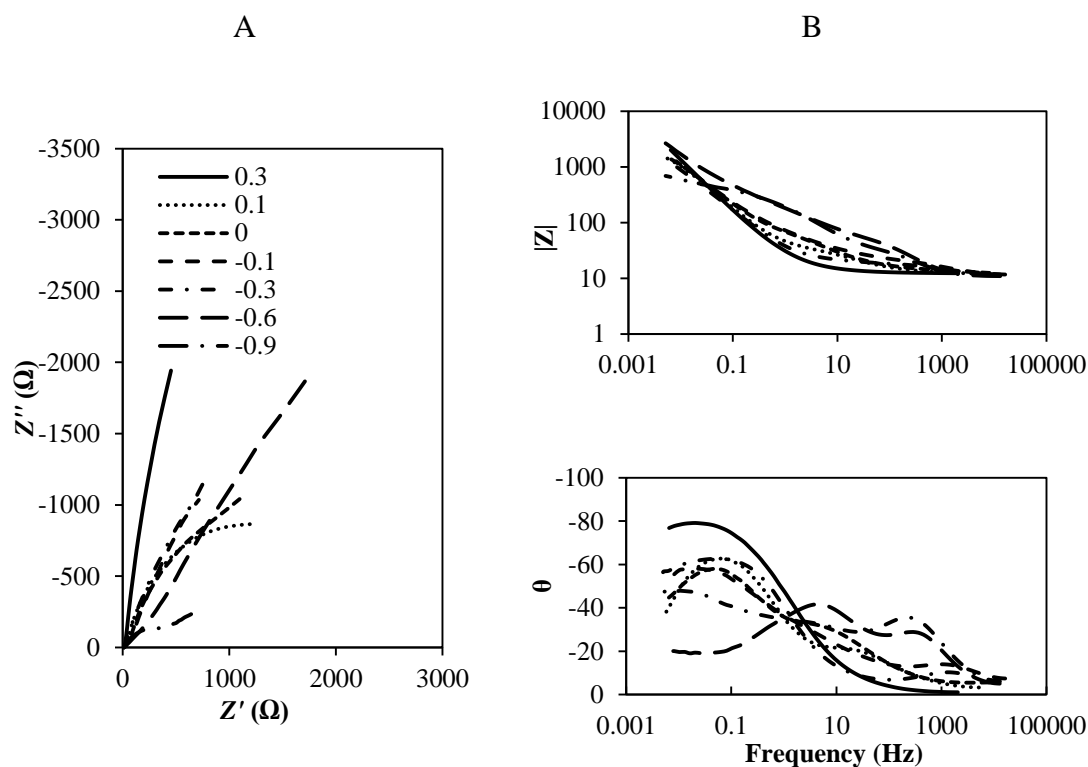


Figure 4.24: Complex-plane impedance plot (A) for PpyMO/Chit coated 0.13 cm² Pt electrodes at various potentials in 0.1 mol dm⁻³ NaCl. The Bode plot (B) shows the logarithm of the impedance and the phase angle against the logarithm of frequency. Potentials are indicated in V vs SCE. Frequency range shown from 65 kHz to 0.005 Hz. The films were prepared by potentiostatic electropolymerisation at 0.80 V vs SCE to a charge density of 0.25 C cm⁻². The PpyMO was prepared from a solution of 0.1 mol dm⁻³ Py and 0.01 mol dm⁻³ MO. Chitosan was added post-polymerisation.

Table 4.6: Parameters for the circuit elements evaluated by fitting the impedance data of PpyCl/Chit to the equivalent circuit shown in Figure 4.19, $n = 3$.

E (V vs SCE)	0.3	0.1	0.0	-0.1	-0.3	-0.6	-0.9
R_s (Ω cm²)	13.16 \pm 0.05	11.46 \pm 0.06	12.74 \pm 0.12	14.25 \pm 0.24	14.59 \pm 0.11	25.33 \pm 0.52	20.92 \pm 0.45
CPE-T_{HF} (mF cm⁻²)	6.37 \pm 0.09	3.31 \pm 0.10	1.69 \pm 0.09	0.79 \pm 0.08	0.45 \pm 0.01	0.16 \pm 0.01	0.13 \pm 0.01
CPE-P_{HF}	0.82 \pm 0.00	0.67 \pm 0.01	0.62 \pm 0.01	0.62 \pm 0.01	0.67 \pm 4.45	0.59 \pm 0.01	0.61 \pm 0.01
R_{HF} (Ω cm²)	40.95 \pm 2.58	2.54 \pm 0.08	22.39 \pm 0.51	128.8 \pm 5.98	392.4 \pm 9.96	689.4 \pm 13.4	838.4 \pm 69.4
CPE-T_{LF} (mF cm⁻²)	2.82 \pm 0.10	9.29 \pm 0.11	8.47 \pm 0.11	4.64 \pm 0.10	3.73 \pm 0.08	5.35 \pm 0.23	1.05 \pm 0.07
CPE-P_{LF}	1 \pm 0	1 \pm 0	0.89 \pm 0.01	0.76 \pm 0.01	0.54 \pm 0.01	0.71 \pm 0.01	0.38 \pm 13.7
χ^2	0.0024	0.0016	0.0022	0.0041	0.0011	0.0039	0.0032
SS	0.2406	0.1817	0.2665	0.4997	0.1416	0.4625	0.3843

The CPE was replaced with a capacitor (C) in the circuit for parameters with a P value of 1

Table 4.7: Parameters for the circuit elements evaluated by fitting the impedance data of PpyMO/Chit to the equivalent circuit shown in Figure 4.19, n=3.

E (V vs SCE)	0.3	0.1	0.0	-0.1	-0.3	-0.6	-0.9
R_S (Ω cm²)	13.10 ± 0.07	11.67 ± 0.10	11.44 ± 0.12	13.13 ± 0.12	12.71 ± 0.06	13.64 ± 0.17	13.63 ± 0.07
CPE-T_{HF} (mF cm⁻²)	6.19 ± 0.13	3.11 ± 0.05	3.43 ± 0.06	3.64 ± 0.06	5.16 ± 0.08	0.13 ± 0.01	0.05 ± 0.00
CPE-P_{HF}	0.82 ± 0.00	0.65 ± 0.00	0.65 ± 0.00	0.64 ± 0.00	0.77 ± 0.00	1 ± 0	1 ± 0
R_{HF} (Ω cm²)	37.57 ± 3.24	56.46 ± 1.64	63.76 ± 2.78	83.42 ± 4.77	29.96 ± 1.87	9.42 ± 0.82	7.96 ± 0.32
CPE-T_{LF} (mF cm⁻²)	2.89 ± 0.14	4.15 ± 0.09	2.97 ± 0.09	1.87 ± 0.08	2.12 ± 0.09	1.48 ± 0.02	0.54 ± 0.02
CPE-P_{LF}	1 ± 0	1 ± 0	1 ± 0	1 ± 0	1 ± 0	0.59 ± 0.01	0.83 ± 0.01
χ²	0.0075	0.0054	0.0069	0.0076	0.0030	0.0037	0.0012
SS	0.9423	0.6633	0.8432	0.9676	0.3444	0.4064	0.1514

The CPE was replaced with a capacitor (C) in the circuit for parameters with a P value of 1 ± 0

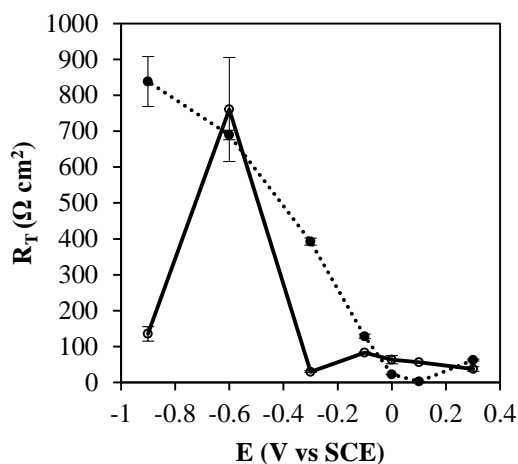


Figure 4.25: Plots of resistance, R_T , as a function of applied potential for PpyCl/Chit (●) and PpyMO/Chit (○) in 0.1 mol dm^{-3} NaCl. The films were prepared by potentiostatic electropolymerisation at 0.80 V vs SCE to a charge density of 0.25 C cm^{-2} . The PpyCl was prepared from a solution of 0.1 mol dm^{-3} Py and 0.1 mol dm^{-3} NaCl and the PpyMO was prepared from a solution of 0.1 mol dm^{-3} Py and 0.01 mol dm^{-3} MO. Chitosan was added post-polymerisation.

In Figure 4.26, the high frequency capacitance, C_{HF} , and the low frequency capacitance, C_{LF} are plotted as a function of the applied potential for the PpyMO/Chit and PpyCl/Chit films. It is evident from these plots that in the presence of chitosan the C_{HF} values are much lower for PpyCl/Chit and PpyMO/Chit films than the PpyCl and PpyMO films, Figure 4.23 A. The PpyCl/Chit film shows a decrease in C_{HF} as the Ppy film releases chloride anions to the surrounding electrolyte, with a maximum at 0.30 V vs SCE and a minimum at -0.90 V vs SCE . The C_{HF} of PpyMO in Figure 4.23 A was comparably lower than PpyCl when polarised in the oxidised state, here in Figure 4.26 A the difference is negligible. At potentials lower than 0.0 V vs SCE , the C_{HF} appears to be independent of potential. Overall the C_{LF} decreases steadily for PpyCl/Chit as the charge storage capacity of the film matrix decreases⁸⁰, with the exception of 0.00 V vs SCE . Interestingly again, the C_{LF} increases for PpyMO/Chit as the applied potential is reduced from 0.10 V to -0.30 V vs SCE , followed by a minimum value at -0.60 V vs SCE but to a lesser extent than that observed in Figure 4.23 B. This high capacity is attributed to cation transport and corresponds to the cyclic voltammograms in Figure 4.15 B.

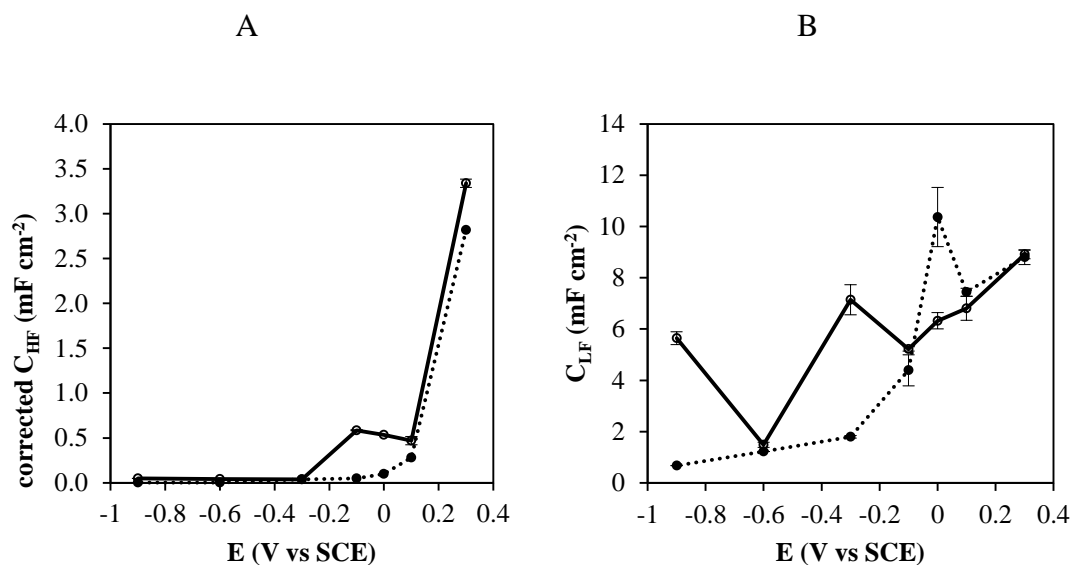


Figure 4.26: Plots of corrected double layer capacitance, C_{HF} , (A), and low frequency capacitance, C_{LF} , (B), as a function of applied potential for PpyCl/Chit (●) and PpyMO/Chit (○) in $0.1\ mol\ dm^{-3}$ NaCl. The films were prepared by potentiostatic electropolymerisation at $0.80\ V$ vs SCE to a charge density of $0.25\ C\ cm^{-2}$. The PpyCl was prepared from a solution of $0.1\ mol\ dm^{-3}$ Py and $0.1\ mol\ dm^{-3}$ NaCl and the PpyMO was prepared from a solution of $0.1\ mol\ dm^{-3}$ Py and $0.01\ mol\ dm^{-3}$ MO. Chitosan was added post-polymerisation.

4.3.4.3 A comparison between the PpyCl and PpyMO films with respect to its resistance and capacitance.

A direct comparison of the impedance responses for PpyMO, PpyMO/Chit, PpyCl and PpyCl/Chit are shown in Figure 4.27, while corresponding data are presented in Table 4.8. These spectra were recorded at $0.10\ V$ vs SCE. The significant role of the different anionic dopants can be clearly seen. The PpyCl films have lower resistance (R_T) and lower capacitance than the PpyMO films and the low frequency capacitance (C_{LF}) is higher for the PpyCl films than the PpyMO films. It is also evident that the chitosan layer exerts little effect on the PpyA systems at this applied potential. However, PpyA/Chit shows a slight decrease in the resistance. Although the conductivity of the PpyA/Chit could not

be determined, the presence of chitosan appears to hinder the mobility of the anions and results in a loss of the conductivity which is associated with reduced concentration of dopant species⁸¹.

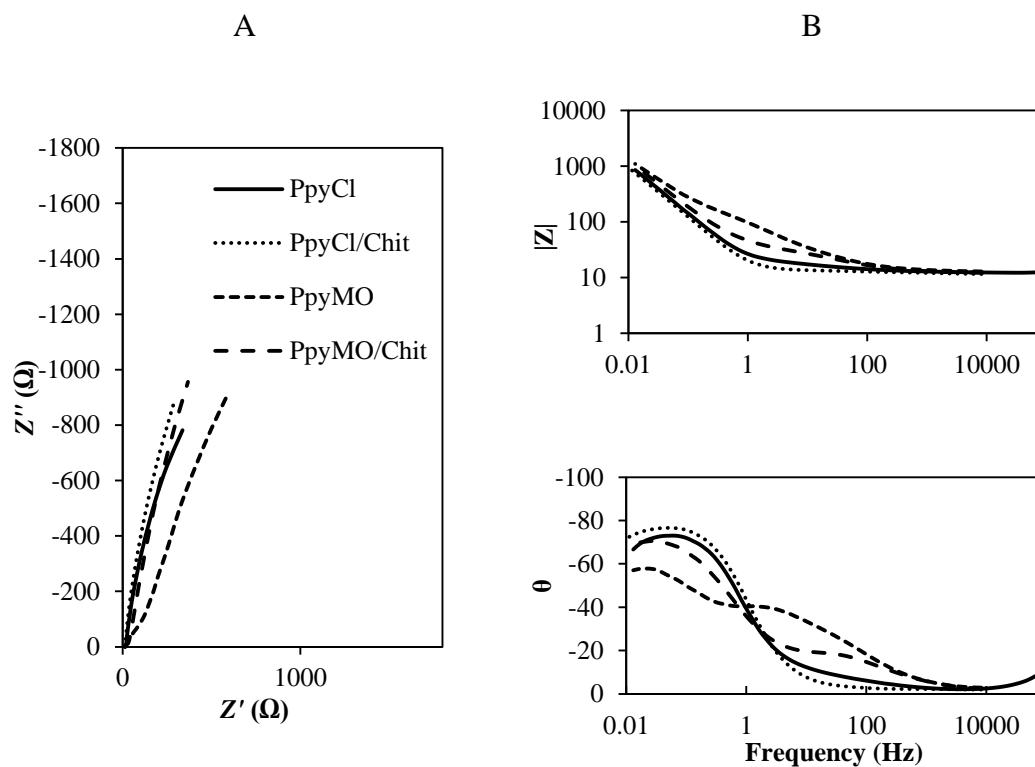


Figure 4.27: Complex-plane impedance plot (A) and Bode plot (B), for PpyA and PpyA/Chit coated 0.13 cm^2 Pt electrodes at 0.1 V vs SCE in 0.1 mol dm^{-3} NaCl. The films were prepared by potentiostatic electropolymerisation at 0.80 V vs SCE to a charge density of 0.25 C cm^{-2} . The PpyCl was prepared from a solution of 0.1 mol dm^{-3} Py and 0.1 mol dm^{-3} NaCl and the PpyMO was prepared from a solution of 0.1 mol dm^{-3} Py and 0.01 mol dm^{-3} MO. Chitosan was added post-polymerisation.

Table 4.8: Summary of the parameters extracted from fitting the impedance data recorded at 0.10 V vs SCE for the PpyA and PpyA/Chit composites in 0.1 mol dm⁻³ NaCl. PpyA films were grown to a charge density of 0.25 C cm⁻².

Sample (0.10 V)	corrected C_{HF} (mF cm⁻²)	R_T (Ω cm²)	C_{LF} (mF cm⁻²)	σ_T (μS cm⁻¹)
PpyMO	0.40 ± 0.05	75.42 ± 2.38	5.01 ± 0.00	5.91 ± 0.41
PpyCl	0.64 ± 0.03	14.96 ± 0.80	9.78 ± 1.37	21.61 ± 1.09
PpyMO/Chit	0.47 ± 0.06	56.46 ± 1.64	6.81 ± 0.47	-
PpyCl/Chit	0.28 ± 0.06	2.54 ± 0.08	7.44 ± 0.20	-

4.3.5 Adhesion test

The adhesion test were performed by applying cellotape™ onto the sample as described in Section 2.4.10. The adhesion properties were classified using the methodology summarised in Table 3.8, Chapter 3. A summary of the adhesion test results is provided in Table 4.9. In this table, the films indicated with E (+V) refer to the films grown at a fixed potential of 0.80 V vs SCE, while the films indicated with E (-V) refer to the reduced films. The reduced films were held at -0.90 V vs SCE for 10 min in 0.1 mol dm⁻³ NaCl after polymerisation. The films were then dried in a stream of air. It is clearly evident from Table 4.9 that the PpyCl/Chit composite has superior adhesion properties compared to the PpyCl and PpyMO films, with excellent adhesion properties when the composite is prepared or reduced. The adhesion properties of the chitosan film are equally good, while the reduced PpyCl and PpyMO films have poor adhesion properties.

Table 4.9: Summary of results from adhesion tests.

Sample	Classification	Result
PpyCl E (+ V)	1	Good
PpyCl/Chit E (+ V)	0	Excellent
PpyMO E (+ V)	1	Good
PpyMO/Chit E (+ V)	0	Excellent
PpyCl E (– V)	2	Poor
PpyCl/Chit E (– V)	1	Good
PpyMO E (– V)	3	Very Poor
PpyMO/Chit E (– V)	2	Poor

4.3.6 Methyl orange release studies

The methyl orange release studies were carried out by applying a constant potential as a function of time. All release experiments were carried out in a three electrode system with a SCE reference electrode, a platinum counter electrode and the working electrode was a PpyMO coated platinum electrode. The electrolyte used in the release studies was 0.1 mol dm⁻³ NaCl (4 cm³). All experiments were carried out in triplicate and with stirring to assist the diffusion of the released compound at the electrode surface through the bulk solution.

Methyl orange was detected using UV-visible spectroscopy. Spectra were recorded on a Cary 50 conc spectrophotometer controlled by Cary Win UV software and 5 cm³ plastic cuvettes (1 cm path length) were used. Typical spectra recorded at different concentrations of methyl orange are shown in Figure 4.28. It is clear that the methyl orange absorbs strongly in the region of 350 to 550 nm with a peak absorbance, or λ_{max} , at 465 nm. A calibration curve of methyl orange at the λ_{max} (465 nm) was produced to calculate the concentration of methyl orange released from the polymer films. The spectrum was recorded between 300 and 600 nm in order to confirm the absence of

interferences. The calibration curve is presented in Figure 4.29 and a straight line relationship, with a R^2 value of 0.998, was obtained, which indicates that the data agree well with the Beer-Lambert Law⁸², Equation 4.10. It is clear that the absorbance is directly proportional to the concentration of the methyl orange dissolved in solution.

$$A = \epsilon cd \quad (4.10)$$

The slope of the linear plot was $27.7 \times 10^3 \text{ mol}^{-1} \text{ dm}^3$ giving the extinction coefficient, ϵ , a value of $27.7 \times 10^3 \text{ mol}^{-1} \text{ dm}^3 \text{ cm}^{-1}$ for methyl orange at 465 nm in $0.1 \text{ mol}^{-1} \text{ dm}^3$ NaCl. Chen *et al.* reported the molar extinction coefficient of $21.6 \times 10^3 \text{ mol}^{-1} \text{ dm}^3$ for methyl orange at 464 nm in water⁸³.

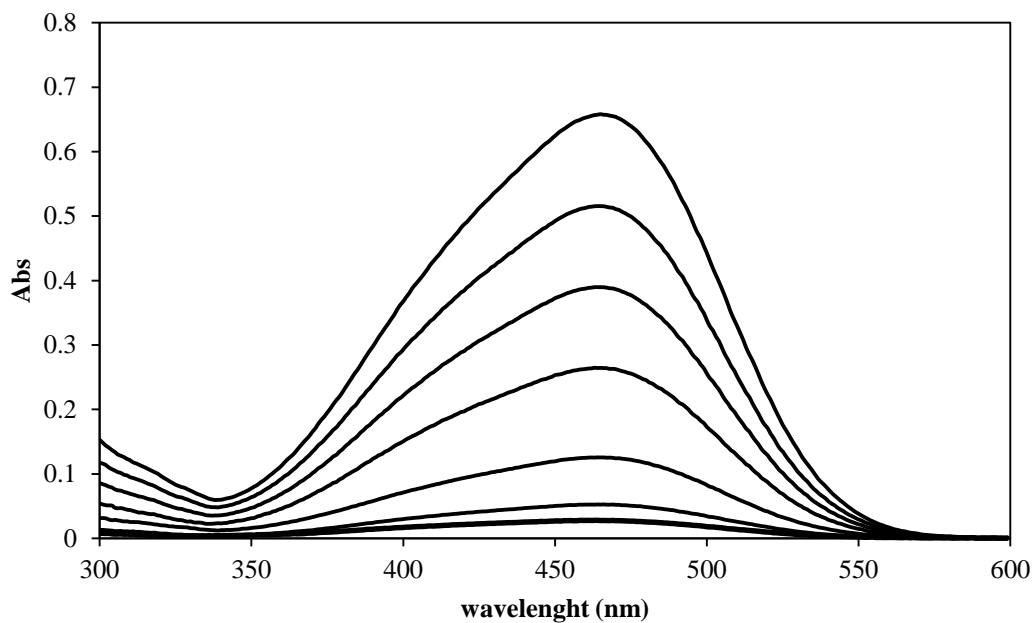


Figure 4.28: UV-visible spectra of methyl orange at different concentrations, ranging from $25 \mu\text{mol dm}^{-3}$ to $1 \mu\text{mol dm}^{-3}$ in 0.1 mol dm^{-3} NaCl.

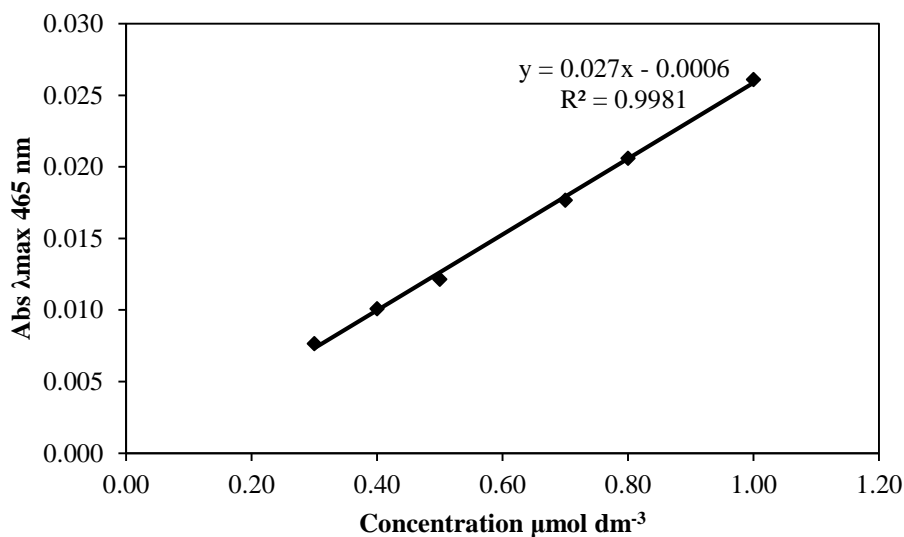


Figure 4.29: Calibration curve of methyl orange used to determine the concentration of methyl orange released from the PpyMO and PpyMO/Chit films in 0.1 mol dm^{-3} NaCl.

Figure 4.30 A and B show the release of MO^- from PpyMO and PpyMO/Chit films over a 30-min period as a function of the applied potential. For the PpyMO an excess of $0.4 \mu\text{mol dm}^{-3}$ was released after 10 min. The concentration of MO^- released from the PpyMO film increased as the applied potential decreased. The maximum concentration of MO^- ($1.0 \mu\text{mol dm}^{-3}$) released occurs at -0.60 V vs SCE after 30 min, while the minimum concentration of MO released occurred at 0.30 V vs SCE . At this potential the PpyMO film is in an oxidised state but the methyl orange is released as the methyl orange is solvated when in contact with the aqueous electrolyte¹⁴. At a release potential of -0.90 V vs SCE , the PpyMO film became delaminated, which can occur at negative potentials⁸⁴, this can be used to explain the lower released concentrations at this potential, Figure 4.30 A.

As shown in Figure 4.30 B, for the PpyMO/Chit composite, the release of MO^- is slower during the first 20 min probably because of the hydration of the dehydrated chitosan layer in the electrolyte solution. An excess of $1.2 \mu\text{mol dm}^{-3} \text{MO}^-$ was released after 30 min at all the release potentials. The minimum release of MO^- occurs at 0.30 V vs SCE , in contrast to PpyMO, the release of MO is impeded by the presence of the chitosan layer. At -0.90 V vs SCE the PpyMO/Chit remains adhered to the surface of the Pt electrode and thus relatively high concentrations of MO^- are released, particularly after 20 or 30 min. It is clear from Figure 4.30, that the concentration of MO^- increases with the release period and there is a more significant increase in the concentration of MO^- as the release period is increased from 10 to 30 min for the PpyMO/Chit composite, Figure 4.30 B. Again, this may be related to the hydration of the chitosan layer. The concentration of MO^- decreases slightly at -0.90 V , this may be due to an increase in the availability of protons in the vicinity of the electrode surface which may protonate the amine groups of the chitosan, thereby increasing the electrostatic attraction of negatively charged methyl orange species to the positively charged chitosan⁸⁵⁻⁸⁷.

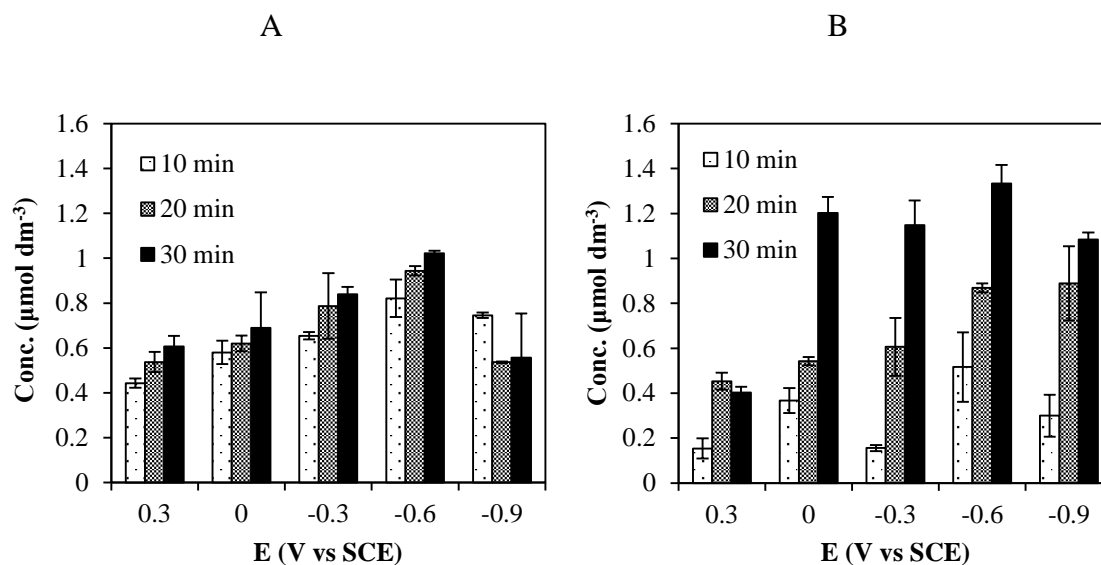


Figure 4.30: Concentration of MO^- released from PpyMO (A) and PpyMO/Chit (B) as a function of the applied potential and release period. The data were averaged over 4 determinations, $n = 4$. The films were prepared by potentiostatic electropolymerisation at 0.80 V vs SCE to a charge density of 0.25 C cm^{-2} . The PpyMO was prepared from a solution of 0.1 mol dm^{-3} Py and 0.01 mol dm^{-3} MO. Chitosan was added post-polymerisation.

The release of MO^- was also monitored at the open-circuit potential (OCP). These release studies were carried out over a longer period of time, and the average concentration of MO^- released from PpyMO at 60 min and 1440 min (24 hr) was found to be $27 \mu\text{mol dm}^{-3}$ and $60 \mu\text{mol dm}^{-3}$, respectively. The average concentration of MO^- released from PpyMO/Chit at 60 min and 1440 min (24 hr) was found to be $18 \mu\text{mol dm}^{-3}$ and $42 \mu\text{mol dm}^{-3}$, respectively. The lower concentration of MO released from PpyMO/Chit is possibly attributed to the adsorption of methyl orange onto the chitosan moiety. The cationic properties of the chitosan⁸⁸ may impart an overall positive charge at the electrode|solution interface which may slow down the ion transport⁷⁴. Huang *et al.*⁸⁹ showed the dependence of pH on adsorption kinetics due to the electrostatic attraction between protonated chitosan (RNH_3^+) and the methyl orange anion (RSO_3^-), Equation 4.11.



As the pH increases there are less protonated groups and more hydroxyl groups⁹⁰.

4.4 Summary

In this chapter, polypyrrole was successfully doped with methyl orange in the absence of an additional supporting electrolyte. The PpyMO films were characterised and discussed prior to carrying out the release of methyl orange from the film. The morphology of the PpyMO was similar to that of PpyCl; both exhibit globular “cauliflower” morphology^{50, 51}. However, tubular-like structures²⁷, consistent with methyl orange, were evident on the surface of the PpyMO films. The films appeared to be free from surface defects and the adhesion properties of PpyCl and PpyMO were overall satisfactory.

For comparison purposes, dexamethasone was incorporated into polypyrrole. The growth rates, determined from the quantitative analysis of the $Q-t$ curve, are summarised for the PpyCl, PpyMO and PpyDex films in Table 4.10. Although the growth rate of PpyDex is higher than PpyMO, the dexamethasone is very expensive and all further studies were focussed on the PpyMO system.

Table 4.10: Summary of growth rates for the formation of PpyCl, PpyMO and PpyDex.

Films (0.25 C cm ⁻²)	Growth rate (mC s ⁻¹)
PpyCl	7.8
PpyMO	0.7
PpyDex (0.8 V)	1.8
PpyDex (0.9 V)	3.8

The redox properties of PpyCl, PpyMO, PpyCl/Chit and PpyMO/Chit were analysed by CV. The films exhibit classical features of apparent non-kinetic hysteresis^{69, 91}. The peak currents were proportional to the scan rate. The peak shape and peak position varied depending on the dominant ion exchange and inclusion or expulsion process. In the case for PpyCl, the Cl⁻ is more mobile than Na⁺ and the PpyCl and PpyCl/Chit exhibit a

dominant anion exchange process, while PpyMO clearly shows a dominant cation exchange. The voltammograms of the PpyMO/Chit system are consistent with both cation and anion exchange, indicating the significant role of the chitosan layer. Electrochemical impedance data were recorded for the polymer films and the composites and a range of electrochemical behaviour was observed at different applied potentials. The charge-transfer resistance increased as the PpyCl film was reduced from an oxidised state to a neutral state. The charge-transfer resistance of PpyMO was lower and this is consistent with the ingress of Na^+ ions as the PpyMO film is reduced⁸⁰.

The concentration of methyl orange released from PpyMO and PpyMO/Chit by electrical stimulation into the cell was detected using visible spectroscopy. In both cases, for PpyMO and PpyMO/Chit, as the potential was decreased from 0.30 V to -0.60 V vs SCE, the concentration of methyl orange increased. The concentration also increased as a function of time. However, the release of MO^- from PpyMO at -0.90 V vs SCE was influenced by the adhesion properties of the PpyMO film. This was not observed with the PpyMO/Chit composite which further supports the improved adhesion properties when chitosan is present.

References

1. J. Del Nero, R. E. de Araujo, A. S. L. Gomes and C. P. de Melo, *Journal of Chemical Physics*, 2005, **122**, 104506.
2. N. F. Jaafar, A. Abdul Jalil, S. Triwahyono, M. N. Muhd Muhid, N. Sapawe, M. A. H. Satar and H. Asaari, *Chemical Engineering Journal*, 2012, **191**, 112-122.
3. L. Obeid, A. Bée, D. Talbot, S. B. Jaafar, V. Dupuis, S. Abramson, V. Cabuil and M. Welschbillig, *Journal of Colloid and Interface Science*, 2013, **410**, 52-58.

4. A. Madhan Kumar and N. Rajendran, *Ceramics International*, 2013, **39**, 5639-5650.
5. N. Pugazhenthiran, S. Ramkumar, P. Sathish Kumar and S. Anandan, *Microporous and Mesoporous Materials*, 2010, **131**, 170-176.
6. R. D. Combes and R. B. Haveland-Smith, *Mutation Research/Reviews in Genetic Toxicology*, 1982, **98**, 101-243.
7. S. Morales-Torres, L. M. Pastrana-Martínez, J. L. Figueiredo, J. L. Faria and A. M. T. Silva, *Applied Surface Science*, 2013, **275**, 361-368.
8. T. Wang, J. Su, X. Jin, Z. Chen, M. Megharaj and R. Naidu, *Journal of Hazardous Materials*, 2013, **262**, 819-825.
9. K. Tanaka, K. Padermpole and T. Hisanaga, *Water Research*, 2000, **34**, 327-333.
10. Z. Xiaomiao Feng and Zhengzong Sun and Wenhua Hou and Jun-Jie, *Nanotechnology*, 2007, **18**, 195603.
11. E. Håkansson, T. Lin, H. Wang and A. Kaynak, *Synthetic Metals*, 2006, **156**, 1194-1202.
12. C. Yelleswarapu and D. Rao, *Optics & Spectroscopy*, 2011, **111**, 208-214.
13. I. S. Yahia, M. S. Abd El-sadek and F. Yakuphanoglu, *Dyes and Pigments*, 2012, **93**, 1434-1440.
14. H. Sato, R. Okuda, A. Sugiyama, M. Hamatsu and J.-i. Anzai, *Materials Science and Engineering: C*, 2009, **29**, 1057-1060.
15. H. P. de Oliveira, E. G. L. Oliveira and C. P. de Melo, *Journal of Colloid and Interface Science*, 2006, **303**, 444-449.
16. S. Zbaida and W. G. Levine, *Chem. Res. Toxicol.*, 1991, **4**, 82-88.
17. D. Kępińska, A. Budniak, K. Kijewska, G. J. Blanchard and M. Mazur, *Polymer*, 2013, **54**, 4538-4544.

18. W.-F. Lee and W.-H. Chiang, *Journal of Applied Polymer Science*, 2004, **91**, 2135-2142.
19. L. M. Lira and S. I. Córdoba de Torresi, *Electrochemistry Communications*, 2005, **7**, 717-723.
20. Y. Chen, H. Feng, L. Li, S. Shang and Y. M. Chun-Wah, *J. Macromol. Sci., Part A: Pure Appl. Chem.*, 2013, **50**, 1225-1229.
21. I. Rawal and A. Kaur, *Sensors and Actuators A: Physical*, 2013, **203**, 92-102.
22. T. Dai, X. Yang and Y. Lu, *Nanotechnology*, 2006, **17**, 3028-3034.
23. X. Yang, Z. Zhu, T. Dai and Y. Lu, *Macromol. Rapid Commun.*, 2005, **26**, 1736-1740.
24. X. Yang, L. Li and Y. Zhao, *Synthetic Metals*, 2010, **160**, 1822-1825.
25. M. Li, W. Li, J. Liu and J. Yao, *Journal of Materials Science: Materials in Electronics*, 2013, **24**, 906-910.
26. A. J. Bard and L. R. Faulkner, *Electrochemical methods. Fundamentals and applications*, Wiley, 2001.
27. X. Yang, T. Dai, Z. Zhu and Y. Lu, *Polymer*, 2007, **48**, 4021-4027.
28. J. Tietje-Girault, C. Ponce de León and F. C. Walsh, *Surface and Coatings Technology*, 2007, **201**, 6025-6034.
29. I. Rodríguez, B. R. Scharifker and J. Mostany, *Journal of Electroanalytical Chemistry*, 2000, **491**, 117-125.
30. B. C. Kim, G. M. Spinks, C. O. Too, G. G. Wallace, Y. H. Bae and N. Ogata, *Reactive and Functional Polymers*, 2000, **44**, 245-258.
31. J. M. Davey, S. F. Ralph, C. O. Too and G. G. Wallace, *Synthetic Metals*, 1999, **99**, 191-199.

-
32. J. Cázares-Delgadillo, C. Balaguer-Fernández, A. Calatayud-Pascual, A. Ganem-Rondero, D. Quintanar-Guerrero, A. C. López-Castellano, V. Merino and Y. N. Kalia, *European Journal of Pharmaceutics and Biopharmaceutics*, 2010, **75**, 173-178.
 33. K. Kontturi, P. Pentti and G. Sundholm, *Journal of Electroanalytical Chemistry*, 1998, **453**, 231-238.
 34. Y.-X. Chen, Y. Wang, C.-C. Fu, F. Diao, L.-N. Song, Z.-B. Li, R. Yang and J. Lu, *Endocrine-Related Cancer*, 2010, **17**, 39-50.
 35. M. Nishi, N. Takenaka, N. Morita, T. Ito, H. Ozawa and M. Kawata, *European Journal of Neuroscience*, 1999, **11**, 1927-1936.
 36. K. L. Crossin, M. H. Tai, L. A. Krushel, V. P. Mauro and G. M. Edelman, *Proc Natl Acad Sci U S A*, 1997, **94**, 2687-2692.
 37. L. Minghetti, A. Nicolini, E. Polazzi, A. Greco, M. Perretti, L. Parente and G. Levi, *British Journal of Pharmacology*, 1999, **126**, 1307-1314.
 38. A. F. Clark and T. Yorio, *Nat Rev Drug Discov*, 2003, **2**, 448-459.
 39. L. C. Bengani and A. Chauhan, *Biomaterials*, 2013, **34**, 2814-2821.
 40. J. Kim and A. Chauhan, *International Journal of Pharmaceutics*, 2008, **353**, 205-222.
 41. R. N. Fedorak, B. Haeberlin, L. R. Empey, N. Cui, H. Nolen Iii, L. D. Jewell and D. R. Friend, *Gastroenterology*, 1995, **108**, 1688-1699.
 42. G. Hochhaus, J. Barth, S. Al-Fayoumi, S. Suarez, H. Derendorf, R. Hochhaus and H. Möllmann, *The Journal of Clinical Pharmacology*, 2001, **41**, 425-434.
 43. T. Loftsson, H. Sigurdsson, D. Hreinsdóttir, F. Konrádsdóttir and E. Stefánsson, *Journal of Inclusion Phenomena and Macrocyclic Chemistry*, 2007, **57**, 585-589.

-
44. R. Wadhwa, C. F. Lagenaur and X. T. Cui, *Journal of Controlled Release*, 2006, **110**, 531-541.
 45. G. Stevenson, S. E. Moulton, P. C. Innis and G. G. Wallace, *Synthetic Metals*, 2010, **160**, 1107-1114.
 46. S. Naficy, J. M. Razal, G. M. Spinks and G. G. Wallace, *Sensors and Actuators A: Physical*, 2009, **155**, 120-124.
 47. L. Leprince, A. Dogimont and D. Magnin, *Journal of Materials Science: Materials in Medicine*, 2010, **21**, 925-930.
 48. J. W. Sirinrath Sirivisoot and Rajesh Pareta and Thomas, *Nanotechnology*, 2011, **22**, 085101.
 49. S. Sirivisoot, R. A. Pareta and T. J. Webster, *J. Biomed. Mater. Res., Part A*, 2011, **99A**, 586-597.
 50. B. Scharifker and G. Hills, *Electrochimica Acta*, 1983, **28**, 879-889.
 51. P. Dyreklev, M. Granström, O. Inganäs, L. M. W. K. Gunaratne, G. K. R. Senadeera, S. Skaarup and K. West, *Polymer*, 1996, **37**, 2609-2613.
 52. M. Bazzaoui, L. Martins, E. A. Bazzaoui and J. I. Martins, *Electrochimica Acta*, 2002, **47**, 2953-2962.
 53. P. Holzhauser and K. Bouzek, *Journal of Applied Electrochemistry*, 2006, **36**, 703-710.
 54. K. Qi, Y. Qiu, Z. Chen and X. Guo, *Corrosion Science*, 2013, **69**, 376-388.
 55. J. M. Fonner, L. Forciniti, N. Hieu, J. D. Byrne, Y.-F. Kou, J. Syeda-Nawaz and C. E. Schmidt, *Biomedical Materials*, 2008, **3**, 1-12.
 56. I. L. Lehr, O. V. Quinzani and S. B. Saidman, *Materials Chemistry and Physics*, 2009, **117**, 250-256.

-
57. G. A. Snook, G. Z. Chen, D. J. Fray, M. Hughes and M. Shaffer, *Journal of Electroanalytical Chemistry*, 2004, **568**, 135-142.
 58. X. Ren and P. G. Pickup, *Canadian Journal of Chemistry*, 1997, **75**, 1518-1522.
 59. M. N. Akieh, Á. Varga, R.-M. Latonen, S. F. Ralph, J. Bobacka and A. Ivaska, *Electrochimica Acta*, 2011, **56**, 3507-3515.
 60. H. Zhao, W. E. Price, P. R. Teasdale and G. G. Wallace, *Reactive Polymers*, 1994, **23**, 213-220.
 61. V. M. Schmidt and J. Heitbaum, *Electrochimica Acta*, 1993, **38**, 349-356.
 62. A. C. Partridge, C. B. Milestone, C. O. Too and G. G. Wallace, *Journal of Membrane Science*, 1999, **152**, 61-70.
 63. X. Ren and P. G. Pickup, *Journal of Physical chemistry*, 1993, **97**, 5356-5362.
 64. X. Ren and P. G. Pickup, *Electrochimica Acta*, 1996, **41**, 1877-1882.
 65. C. Weidlich, K. M. Mangold and K. Jüttner, *Electrochimica Acta*, 2005, **50**, 1547-1552.
 66. X. Ren and P. G. Pickup, *Journal of Electroanalytical Chemistry*, 1997, **420**, 251-257.
 67. H. Zhao, W. E. Price, C. O. Too, G. G. Wallace and D. Zhou, *Journal of Membrane Science*, 1996, **119**, 199-212.
 68. T. Raudsepp, M. Marandi, T. Tamm, V. Sammelselg and J. Tamm, *Electrochimica Acta*.
 69. H. Grande and T. F. Otero, *The Journal of Physical Chemistry B*, 1998, **102**, 7535-7540.
 70. F. Scholz and A. M. Bond, *Electroanalytical methods guide to experiments and applications*, Springer, 2010.

-
71. H. Mi, X. Zhang, Y. Xu and F. Xiao, *Applied Surface Science*, 2010, **256**, 2284-2288.
 72. M. D. Levi, C. Lopez, E. Vieil and M. A. Vorotyntsev, *Electrochimica Acta*, 1997, **42**, 757-769.
 73. M. N. Akieh, W. E. Price, J. Bobacka, A. Ivaska and S. F. Ralph, *Synthetic Metals*, 2009, **159**, 2590-2598.
 74. S. Brahim and A. Guiseppi-Elie, *Electroanalysis*, 2005, **17**, 556-570.
 75. B. R. Hinderliter, S. G. Croll, D. E. Tallman, Q. Su and G. P. Bierwagen, *Electrochimica Acta*, 2006, **51**, 4505-4515.
 76. G. Garcia-Belmonte, Z. Pomerantz, J. Bisquert, J.-P. Lellouche and A. Zaban, *Electrochimica Acta*, 2004, **49**, 3413-3417.
 77. G. Garcia-Belmonte, *Electrochemistry Communications*, 2003, **5**, 236-240.
 78. T. Komura, S. Goisihara, T. Yamaguti and K. Takahasi, *Journal of Electroanalytical Chemistry*, 1998, **456**, 121-129.
 79. B. Hirschorn, M. E. Orazem, B. Tribollet, V. Vivier, I. Frateur and M. Musiani, *Electrochimica Acta*, 2010, **55**, 6218-6227.
 80. W. Plieth, A. Bund, U. Rammelt, S. Neudeck and L. Duc, *Electrochimica Acta*, 2006, **51**, 2366-2372.
 81. R. A. Green, N. H. Lovell, G. G. Wallace and L. A. Poole-Warren, *Biomaterials*, 2008, **29**, 3393-3399.
 82. D. F. Swinehart, *Journal of Chemical Education*, 1962, **39**, 333-335.
 83. H. Liu, Y. Chen, D. Zhu, Z. Shen and S.-E. Stiriba, *Reactive and Functional Polymers*, 2007, **67**, 383-395.
 84. G. Paliwoda-Porebska, M. Rohwerder, M. Stratmann, U. Rammelt, L. Duc and W. Plieth, *Journal of Solid State Electrochemistry*, 2006, **10**, 730-736.

85. W. A. Morais, A. L. P. de Almeida, M. R. Pereira and J. L. C. Fonseca, *Carbohydrate Research*, 2008, **343**, 2489-2493.
86. M.-S. Chiou and H.-Y. Li, *Journal of Hazardous Materials*, 2002, **93**, 233-248.
87. G. Annadurai, L. Y. Ling and J.-F. Lee, *Journal of Hazardous Materials*, 2008, **152**, 337-346.
88. M. N. V. R. Kumar, R. A. A. Muzzarelli, C. Muzzarelli, H. Sashiwa and A. J. Domb, *Chemical Reviews*, 2004, **104**, 6017-6084.
89. R. Huang, Q. Liu, J. Huo and B. Yang, *Arabian Journal of Chemistry*, 2013, <http://dx.doi.org/10.1016/j.arabjc.2013.1005.1017>.
90. J. Nunthanid, S. Puttipipatkachorn, K. Yamamoto and G. E. Peck, *Drug Dev. Ind. Pharm.*, 2001, **27**, 143-157.
91. S. W. Feldberg and I. Rubinstein, *Molecular Crystals and Liquid Crystals Incorporating Nonlinear Optics*, 1988, **160**, 101-101.

Chapter 5

Electrochemical synthesis and characterisation of polypyrrole oxacillin (PpyOx)/chitosan composite films

5. Electrochemical synthesis and characterisation of polypyrrole oxacillin (PpyOx)/chitosan composite films

5.1 Introduction

Oxacillin sodium (5 methyl-3 phenyl-4-isoxazolyl penicillin sodium) is classified as a beta-lactam antibiotic in the penicillin class¹. Oxacillin (Ox) is derived from 6-aminopenicillanic acid, and it is a semisynthetic penicillinase-resistant penicillin. It was developed by Beechams by adding an acyl side chain to a penicillin molecule. The acyl side chain sterically inhibits the action of penicillinase by preventing disruption (opening) of the β -lactam ring. Thus oxacillin, along with methicillin and nafcillin, is a member of a group of β -lactams referred to as penicillinase resistant penicillins. It is used in its sodium salt, Figure 5.1, for parenteral administration. It is not destroyed by the penicillinase and it has low toxicity for the host but it is effective against most gram-positive bacteria in humans and animals² including pathogens (streptococci, staphylococci, pneumococci), clostridia, some gram-negative gonococci, some spirochetes (*Treponema pallidum* and *T. pertenuis*) and some fungi³. Certain strains of some target species, e.g., staphylococci, secrete the enzyme penicillinase, which inactivates penicillin and confers resistance to the antibiotic. Oxacillin is used in the treatment of osteomyelitis, septicaemia and endocarditis¹.

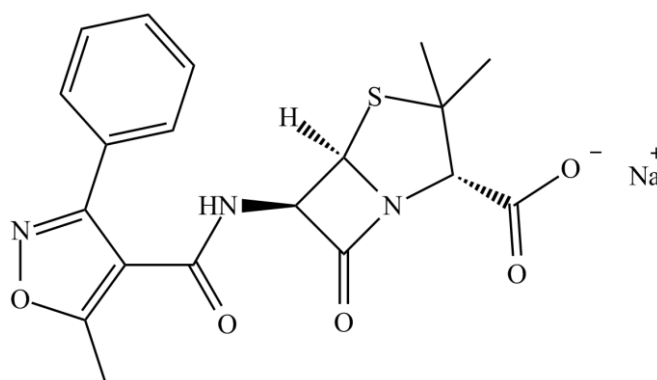


Figure 5.1: Structure of oxacillin sodium salt.

With regard to the pharmacology of oxacillin, it acts by binding to serum proteins, mainly albumin. The mechanism of action of oxacillin is by attachment to penicillin-binding proteins (PBPs), which results in the inhibition of cell wall peptidoglycan synthesis and inactivation of inhibitors to autolytic enzymes. The degree of protein binding reported for oxacillin is $94.2\% \pm 2.1\%$. Brand names of oxacillin include Bactocill®, Bristopen®, Cryptocillin® and Oxacillin for injection, USP *ADD-Vantage*®. Administration of 500 mg gives a peak serum level of 43 $\mu\text{g/mL}$ after 5 min with a half-life of 20-30 min. It has a pKa of 2.7³. Antibiotics investigated for implantable devices include amoxicillin, carbenicillin, cefanamol^{4, 5}, gentiamicin⁶ ofloxacin⁷ trobramycin⁸ rifampicin⁹ and vanomycin¹⁰. A six hour post implantation “decisive period” has been identified during which prevention of bacterial adhesion is critical to the long-term success of an implant¹¹. Various synthetic polymers and natural polymers have been evaluated as suitable antibiotic carriers. Chitosan has emerged as an attractive material as it exhibits superior biocompatibility and promotion of healthy cell growth^{12, 13}.

There are no publications of polypyrrole doped with oxacillin, but there are a few citations containing conducting polymers doped with other antibiotics^{14, 15}. Clinical studies have shown synergistic effects with chitosan and β -lactams against MRSA¹⁶. Oxacillin dissociates as a salt and it has good solubility in water making it a suitable anionic dopant for polypyrrole. The cost of oxacillin is compared with methyl orange, dexamethasone and chloride in Table 5.1. Oxacillin is considerably more expensive than methyl orange, but it is favourable when compared with the cost of dexamethasone.

Table 5.1: Comparison of the cost of dopants used, price taken from Sigma-Aldrich (October 2013).

dopant	Concentration (mol dm^{-3})	Cost ex. VAT (per gram)
chloride (Cl)	0.10	€ 0.03
methyl orange (MO)	0.01	€ 0.35
dexamethasone (Dex)	0.01	€ 331.50
oxacillin (Ox)	0.02	€30.50

5.2 Experimental

Polypyrrole oxacillin films were grown potentiostatically on to a platinum working electrode (surface area 0.13 cm^2). The monomer solution consisted of 0.2 mol dm^{-3} pyrrole (Sigma-Aldrich, distilled under vacuum) and 0.02 mol dm^{-3} oxacillin (Sigma-Aldrich) in distilled water. The electropolymerisation solution has a pH of 6.3. The film was synthesised by applying a constant potential of 0.80 V vs SCE for 5 min yielding a charge density of 0.25 C cm^{-2} . The polypyrrole oxacillin films were rinsed with ethanol and distilled water to remove any unreacted monomer and oxacillin. The chitosan film was prepared by drop casting $10 \mu\text{L}$ of 0.5% (w/v) chitosan solution directly on to the washed polypyrrole oxacillin film. The chitosan-loaded film was force dried under an infrared lamp for 10 min. The electroanalytical experiments, such as cyclic voltammetry (CV) and electrochemical impedance spectroscopy (EIS), were carried out in a solution of phosphate buffer saline (PBS) solution. The PBS solution contained $0.15 \text{ NaCl mol dm}^{-3}$, $0.04 \text{ NaH}_2\text{PO}_4 \text{ mol dm}^{-3}$ and $0.04 \text{ NaOH mol dm}^{-3}$ made up in deionized water to give pH 7.4¹⁷.

5.3 Results and discussion

5.3.1 Redox properties of Oxacillin

Cyclic voltammetry was used to determine the electrochemical stability of an oxacillin solution during oxidation and reduction. The experiments were carried out on a bare Pt electrode by cycling between -1.20 V vs SCE and 1.00 V vs SCE at a scan rate of 50 mV s^{-1} in 0.02 mol dm^{-3} Ox and 0.1 mol dm^{-3} PBS. Typical voltammograms, recorded in the presence and absence of oxacillin, are shown in Figure 5.2. The redox properties of Pt in the PBS solution are dominated by H^+ adsorption and $\text{H}_2(\text{g})$ evolution¹⁸ between approximately -0.90 V and -1.20 V vs SCE . The voltammogram recorded in the oxacillin

solution has a similar profile to the methyl orange shown in Chapter 4 (Section 4.3.1). The conductivity of the oxacillin solution was $1.2 \text{ m}\Omega^{-1} \text{ cm}^{-1}$ compared to $19.7 \text{ m}\Omega^{-1} \text{ cm}^{-1}$ for the PBS solution. This variation in the conductivity of the two solutions can be used to explain the lower currents recorded in the oxacillin solution. Importantly, no reduction or oxidation peaks were observed indicating that the Ox solution is stable. It is worth mentioning that no formal redox potential, oxidation or reduction potentials have been reported for oxacillin.

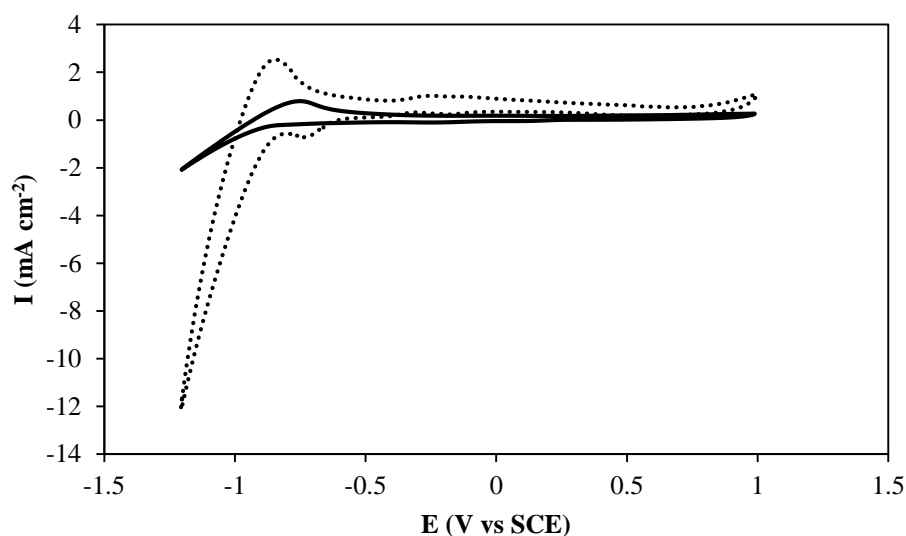
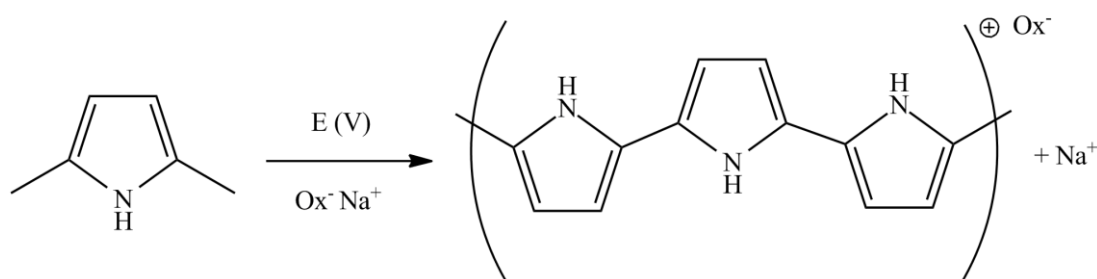


Figure 5.2: Cyclic voltammograms of a bare platinum electrode (20th cycle) at 50 mV s^{-1} in 0.02 mol dm^{-3} Ox (—) PBS solution (····).

5.3.2 Electrochemical synthesis of the polypyrrole oxacillin (PpyOx) films

There are very few publications on conducting polymers doped with antibiotics. Sirivisoot *et al.* have studied polypyrrole doped with penicillin/streptomycin^{15, 19, 20}. However, no publications were found to contain polypyrrole doped with oxacillin. The polypyrrole oxacillin films were deposited from an electropolymerisation solution containing 0.2 mol dm^{-3} pyrrole, which is higher than the concentration used in previous chapters. However this higher concentration was required for optimum growth. No additional anions were added to the electrosynthesis solution to ensure that polypyrrole

(Ppy) was only doped by the oxacillin (Ox). The concentration of the oxacillin solution was 0.02 mol dm^{-3} . Potentiostatic growth was the preferred method of electrosynthesis. A constant potential of 0.80 V vs SCE was used to achieve electropolymerisation until a charge density of 0.25 C cm^{-2} was obtained. A typical current-time ($I-t$) curve is shown in Figure 5.3 A, where the time required for achieving a charge density of 0.25 C cm^{-2} is approximately 8 min. On application of the potential, there is an initial rapid decrease in the current, which arises from the charging of the double layer²¹. This charging current decays rapidly and is then followed by a slower rise, at about 5 to 10 s, as the polypyrrole film begins to nucleate and deposit at the surface of the electrode²². At longer times, greater than 50 s, the current reaches a steady state. A homogenous black, glossy film was obtained on the surface of the electrode. Figure 5.3 B shows the comparative $I-t$ curves and charge-time ($Q-t$) plots for the nucleation process^{23, 24} of PpyCl and PpyOx. There is a steep linear charge-time plot for the formation of the PpyCl film and the charge-time plot is linear at longer electropolymerisation times, from 50 to 500 s, for the PpyOx film. It can be clearly seen that the currents and the rate of electropolymerisation are higher for the PpyCl system and that it takes a much shorter period, 30 s for the PpyCl to deposit. The difference in growth rate is likely to be due to the size of the anions, Cl^- (58.44 g mol^{-1}) and Ox^- ($423.42 \text{ g mol}^{-1}$), there may be a slow diffusion of the relatively large Ox^- anion to the electrode²⁵, another possibility is that the higher charge density on the oxygen atoms of the oxacillin causes a much stronger interaction with the pyrrole oligomer, altering the configuration of the oligomer²⁶. In Scheme 5.1 the proposed synthesis of PpyOx during electropolymerisation is illustrated. The anionic oxacillin, Ox^- , becomes incorporated in to the polypyrrole to satisfy electroneutrality.



Scheme 5.1: Synthesis of polypyrrole oxacillin with the incorporation of oxacillin.

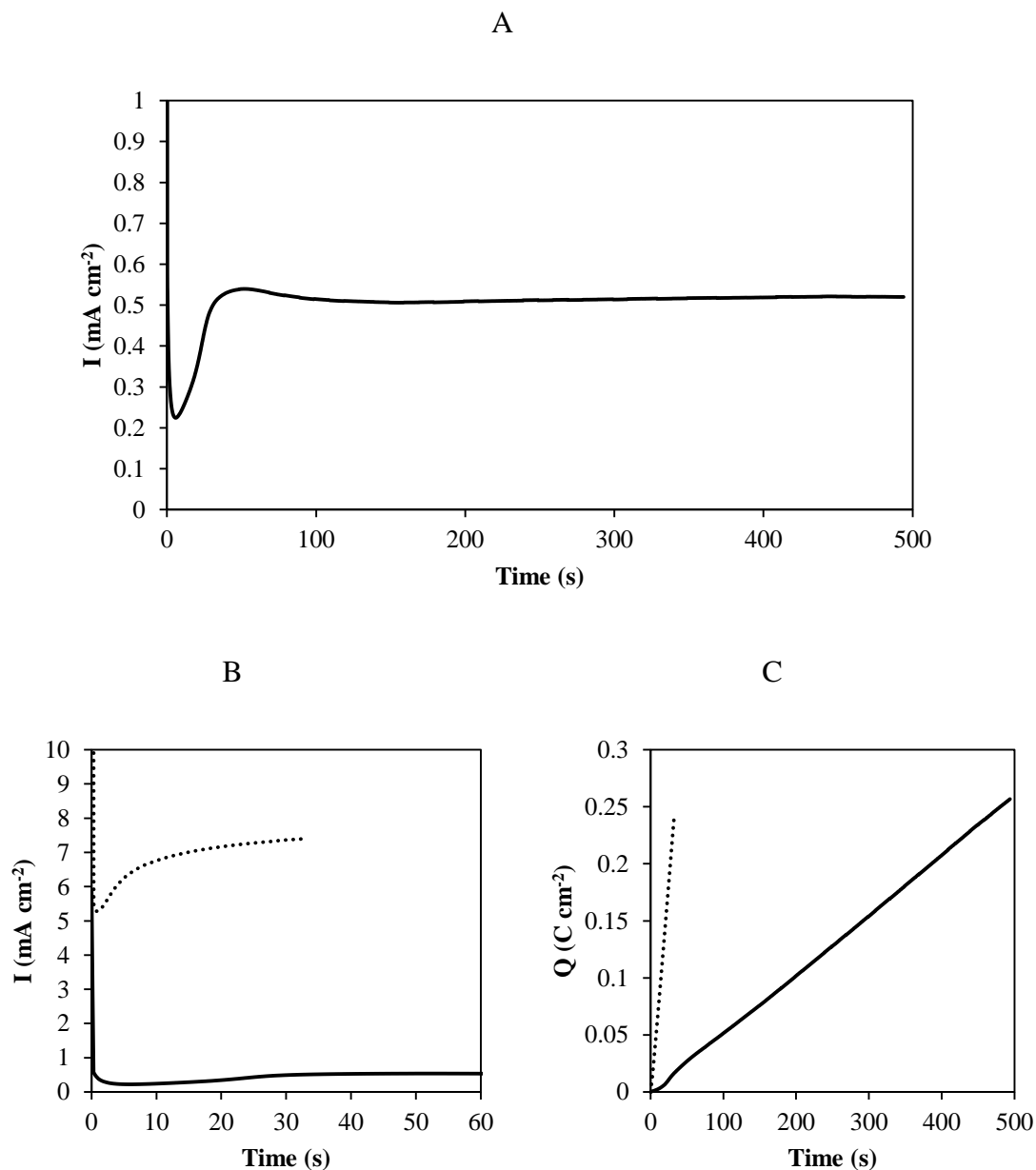


Figure 5.3: Current-time plots (A) for the growth of (— PpyOx) and current-time plots (B) for the formation of (⋯⋯ PpyCl) and (— PpyOx) at 0.80 V vs SCE yielding a charge density of 0.25 C cm⁻². Charge-time plots (C) for the growth of (— PpyOx) and (⋯⋯ PpyCl). The PpyCl was prepared from a solution of 0.1 mol dm⁻³ Py and 0.1 mol dm⁻³ NaCl and the PpyOx was prepared from a solution of 0.2 mol dm⁻³ Py and 0.02 mol dm⁻³ Ox. The films were electropolymerisation at 0.80 V vs SCE yielding a charge density of 0.25 C cm⁻².

5.3.2.1 Rates of growth on different metallic substrates

The deposition of PpyOx on different substrates was studied at 0.80 V vs SCE from a solution containing 0.2 mol dm^{-3} pyrrole and 0.02 mol dm^{-3} oxacillin. Figure 5.4 shows the current-time and charge-time curves for PpyOx on different metallic substrates. In all cases very good reproducibility was obtained. It is evident that the PpyOx grows at different rates. During the early stages of deposition, the rate of electropolymerisation is higher at the Pt electrode, however at longer electropolymerisation periods more efficient deposition is achieved with the Ti-EQCM (quartz crystal microbalance) electrode. This is evident in the charge-time plots, Figure 5.4 B. The average rate of growth of PpyOx was computed to be 0.39 mC s^{-1} for a Pt disc electrode, 0.30 mC s^{-1} for an Au disc electrode and 0.55 mC s^{-1} on a Ti-EQCM electrode. These rates for the formation of PpyOx are considerably slower than those obtained for PpyCl. The average rate of growth for PpyCl to a charge density of 0.25 C cm^{-2} on a conventional Au disc electrode and Pt disc electrode was calculated as 8.03 mC s^{-1} and 7.81 mC s^{-1} , respectively. Interestingly, PpyOx was successfully deposited at the Ti-EQCM electrodes, however, the PpyCl and PpyMO films did not form on the Ti-EQCM electrode.

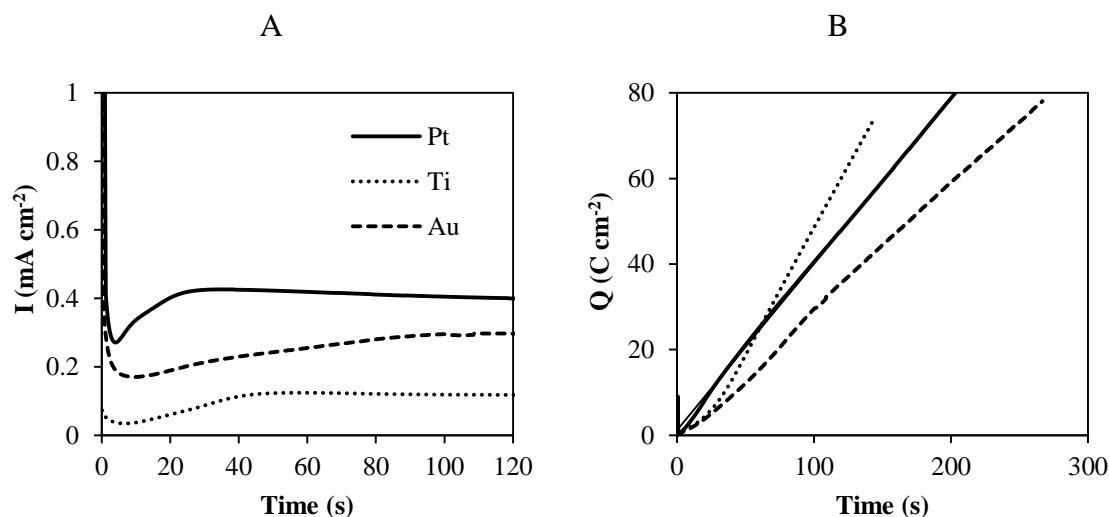


Figure 5.4: Current-time and charge-time plots for the formation of PpyOx on Pt, Au and Ti-EQCM electrodes. PpyOx was prepared from a solution of 0.2 mol dm^{-3} Py and 0.02 mol dm^{-3} Ox. The films were electropolymerisation at 0.80 V vs SCE.

5.3.2.2 Estimation of mass and doping levels using EQCM method

Quartz crystal microbalance measurements (EQCM) were performed and analysed to obtain information on the mass and the doping level of the deposited PpyOx film. In these studies, the PpyOx was grown on a Ti-EQCM electrode to a charge of 15 mC (75 mC cm⁻²) by applying a constant potential of 0.85 V vs Ag|AgCl. The frequency-charge plot and mass-charge plots for PpyOx are shown in Figure 5.5 A and B, respectively. A decrease in frequency is related to an increase in mass²⁷ according to the Sauerbrey relationship²⁸, the terms are defined in Section 2.4.5. The Sauerbrey equation can be re-arranged to solve for the mass change, as shown in Equation 5.1. The mass values plotted in Figure 5.5 B were obtained using this relationship. The sensitivity factor (C_f) was found experimentally to be 7.9897×10^8 Hz cm² g⁻¹.

$$\Delta m = - \frac{A \sqrt{(\rho_q \mu_q)}}{2f_o^2} = \frac{1}{C_f} \Delta f \quad (5.1)$$

There is a linear increase in mass with charge when the charge exceeds 5 mC cm⁻² (approximately 17 s), as shown in Figure 5.5. The R² value of 0.9996 indicates good linearity. The doping level, p , of the polymer was estimated using Equation 5.2 and the average slope of these mass-charge curves was computed as $R = 0.4436$ mg C⁻¹.

$$R = \frac{m}{Q} = \frac{M_m + p M_A}{(n + p)F} \quad (5.2)$$

Here M_m and M_A are the formula weights of the monomer and anion. In the case of polypyrrole oxacillin, the molecular weight of pyrrole is 65.07 g mol⁻¹ and oxacillin is 423.42 g mol⁻¹, and the number of electrons, $n = 2$. The value of p was calculated as 0.04 which is very low but reasonable when the size of the Ox⁻ is considered. The value of p for Ppy has been reported to range from 0.2 to 0.5 dopant species per pyrrole unit²⁹⁻³¹. For simple dopant anions such as Cl⁻, the value of p is approximately 0.33, i.e., a 1:3 doping level. This value of 0.04 is much less than the calculated value for Cl⁻ and corresponds to a 1:13 doping level. However, this value is in good agreement with the analysis reported by Song *et al.*³² where dopant levels ranging from 2.5 to 15 were

obtained for polypyrrole doped with dodecylbenzenesulfonic acid. The equation used to calculate the theoretical mass does not take into account solvent participation and it also assumes the current efficiency for the electropolymerisation of the monomer is 100 %³³.

The calculated mass and doping levels of the PpyOx and PpyCl films are summarised in Table 5.1. There is a considerable variation in the doping levels and it is also clear that the mass of the final film, deposited to a charge density of 0.25 C cm^{-2} , is higher for the PpyOx film. Again, this is connected with the larger mass of the oxacillin²⁵.

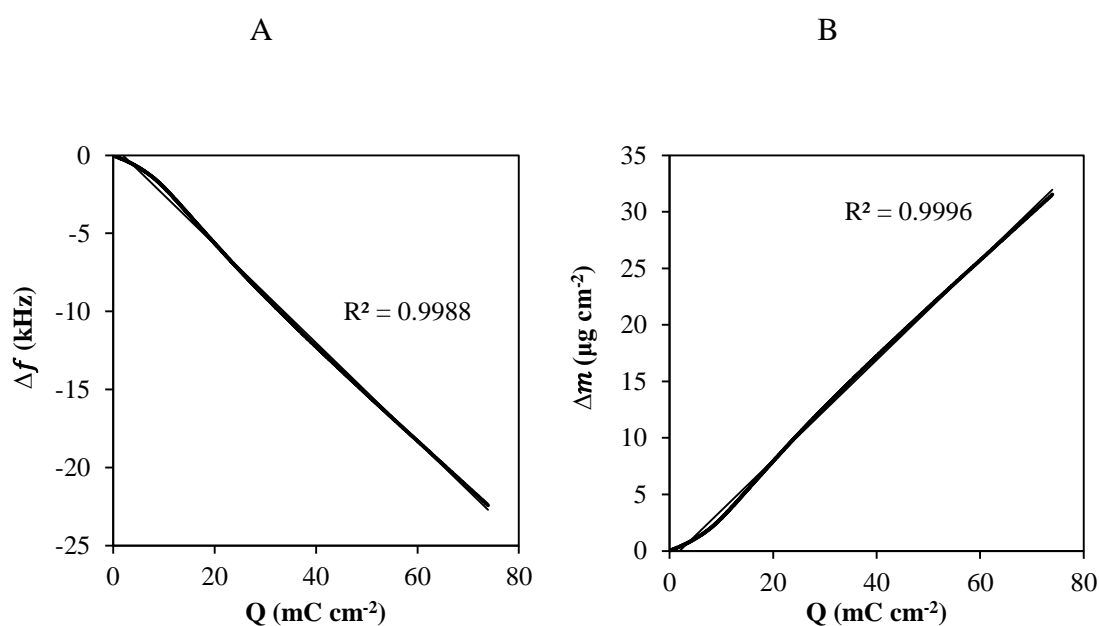


Figure 5.5: Frequency-charge plot (A) and mass-charge plot (B) for the electropolymerisation of pyrrole to generate PpyOx recorded by EQCM measurements. PpyOx was prepared from a solution of 0.2 mol dm^{-3} Py and 0.02 mol dm^{-3} Ox. The films were electropolymerised at 0.80 V vs SCE to a charge density of 75 mC cm^{-2} on a Ti-EQCM crystal (0.20 cm^2).

Table 5.2: Summary of EQCM results, calculated mass, doping levels and doping ratio of PpyOx.

PpyOx ($Q = 75 \text{ mC cm}^{-2}$)	
Mass ($\mu\text{g cm}^{-2}$)	31
Doping level, p	0.04
Doping ratio	1:13

5.3.3 SEM-EDX

The surface topography and morphology of the polymers was studied using SEM. The polymer films were grown on a customised Pt electrode (Section 2.4.6) with a surface area of 0.126 cm^2 . The polymer films were washed thoroughly with ethanol and distilled water to ensure the removal of excess electrolyte (Ox^-) on the surface. They were air dried for several hours before imaging. These samples were sputter coated with 1.5 nm of gold prior to imaging.

A typical micrograph of PpyOx is shown in Figure 5.6, while the micrograph obtained for PpyCl is shown in the inset of Figure 5.6. The PpyOx and PpyCl films (inset) were deposited to a charge density of 0.25 C cm^{-2} . The PpyCl shows the typical “cauliflower” structure of bulk polypyrrole^{21, 34}. The surface of the PpyOx film was very smooth, as evident from Figure 5.6, and had no visible contrast which made imaging difficult. In the previous chapter, methyl orange was also present as a precipitate on the surface of the polymer. It is clear from these micrographs that the morphology of the polypyrrole film changes in the presence of oxacillin. Here the evidence of a precipitate may be subtle and cannot be disregarded, however, the film will be just referred to as PpyOx as there are no other dopants available to dope it.

The cross sections of PpyOx deposited to a charge density of 0.25 C cm^{-2} and 0.40 C cm^{-2} are shown in Figure 5.7. Using these cross sections, the film thickness of PpyOx deposited to a charge density of 0.25 C cm^{-2} was estimated at $1.50 \pm 0.15 \text{ }\mu\text{m}$. The film thickness of PpyCl grown to the same charge density was calculated as $0.5 \text{ }\mu\text{m}$. The higher film thickness obtained with the PpyOx film is consistent with the higher mass values, shown in Table 5.2. Although the PpyOx films appear compact it is clear that the cross sections possess some structure, this is clearly evident in Figure 5.7 B, where a greater film thickness is achieved. Stankovic *et al.*³⁷ reported that films doped with ClO_4^- yielded films thicker than the theoretical prediction. Other studies have experienced variability in correlating film thickness with charge passed; they suggest that the current density during synthesis affects the chain length and disorder³⁸⁻⁴⁰.

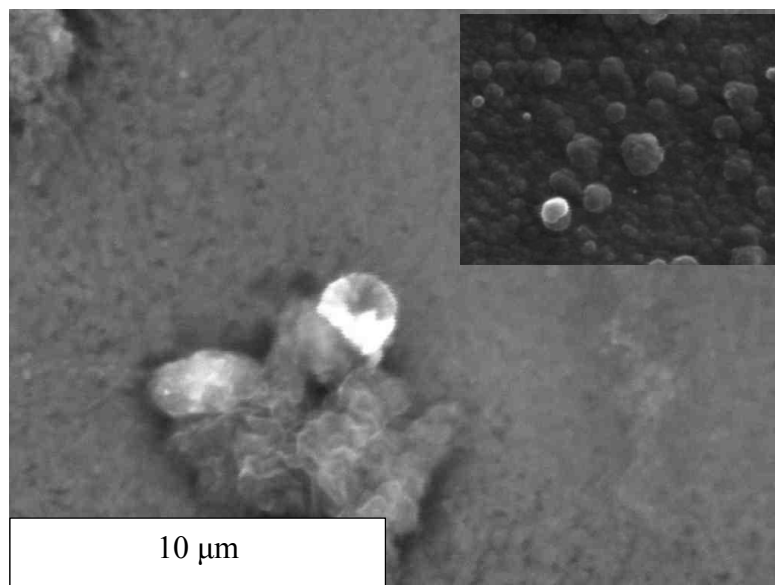


Figure 5.6: SEM micrograph of PpyOx and PpyCl is shown in the inset. The films were grown on a 0.13 cm^2 customised Pt electrode by potentiostatic electropolymerisation at 0.80 V vs SCE to yield a charge density of 0.25 C cm^{-2} . The PpyOx was prepared from a solution of 0.2 mol dm^{-3} Py 0.02 mol dm^{-3} Ox and the PpyCl was prepared from a solution of 0.1 mol dm^{-3} Py 0.1 mol dm^{-3} NaCl.

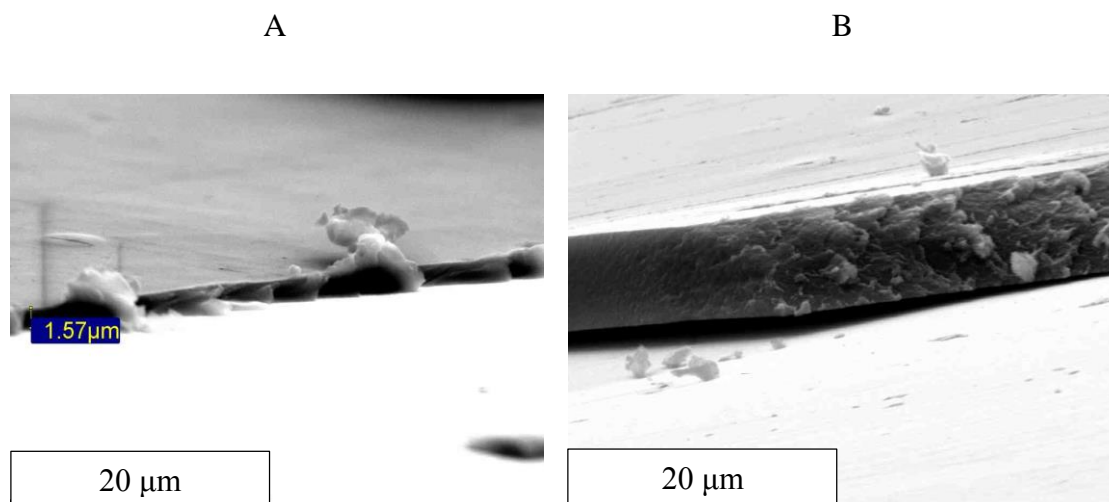


Figure 5.7: Cross section areas of PpyOx grown to a charge density of 0.25 C cm^{-2} (A) and 0.40 C cm^{-2} (B) on a 0.13 cm^2 customised Pt electrode. The films were prepared by potentiostatic electropolymerisation at 0.80 V vs SCE in 0.2 mol dm^{-3} Py 0.02 mol dm^{-3} Ox.

5.3.3.1 EDX analysis

EDX analysis was carried out to verify the presence of oxacillin. The EDX spectrum presented in Figure 5.8 confirms the presence of carbon at 0.3 keV, sulphur at 2.45 keV and oxygen at 0.52 keV. Carbon is an elemental component of both polypyrrole and oxacillin, however, the sulphur and oxygen are elemental components of anionic dopant (Ox^-), clearly indicating the incorporation of Ox^- during the formation of the polypyrrole film.

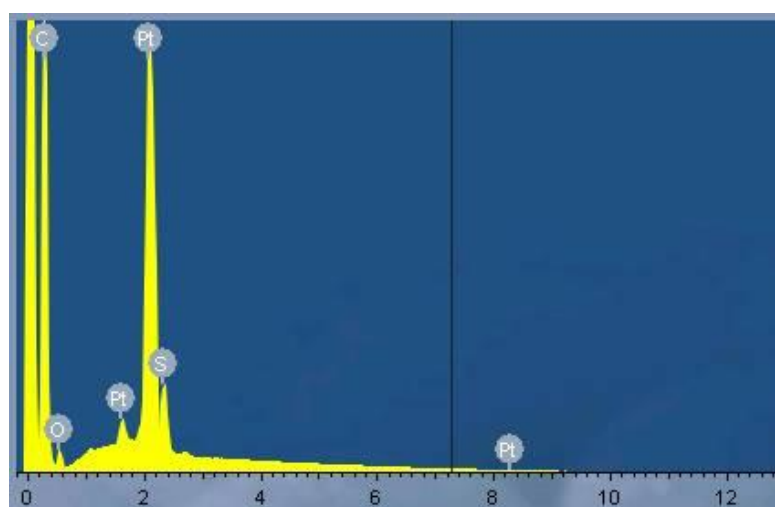


Figure 5.8: Representative EDX spectrum of PpyOx, showing x-axis from 0.0 to 12.5 keV.

5.3.4 Cyclic Voltammetry

The electrochemical properties of PpyCl and PpyOx in the presence and absence of chitosan were characterised using cyclic voltammetry. The polymers were grown to a charge density of 0.25 C cm^{-2} . They were cycled in a 0.1 mol dm^{-3} PBS solution (pH 7.4 and a conductivity of 17 mS cm^{-1}) and the potential was swept from -0.95 V to 0.35 V vs SCE to avoid over-oxidising the polymer⁴¹. Different scan rates, ranging from 5, 10, 25, 50, 100 to 150 mV s^{-1} , were used. Representative data are shown in Figure 5.9 for the

PpyCl and PpyOx films and the voltammograms shown in Figure 5.10 were recorded for the PpyCl/Chit and PpyOx composites. The voltammograms presented in the plots labelled A and C show the current-potential response at different scan rates and the plots labelled B and D show a magnification of the voltammograms recorded at 10 mV s^{-1} compared to the electrochemical response of the bare Pt electrode using the same parameters. Reproducible voltammetric behaviour was attained after the first few cycles, usually 3 to 4 cycles and the data shown in Figure 5.9 and Figure 5.10 are of the 10th cycles.

5.3.4.1 Redox properties of PpyCl and PpyOx

The voltammograms recorded for PpyCl in PBS are presented in Figure 5.9 A and Figure 5.9 B. These voltammograms are similar to the voltammograms for PpyCl in NaCl solution (Figure 4.14 A) but there is some difference in the shape of the peaks. This may be attributed to the difference in the nature of the anions incorporated into the film during cycling⁴². In the NaCl solution, small and mobile Cl^- anions are available, while the phosphate anions, HPO_4^{2-} and H_2PO_4^- , are larger. At slow scan rates ($< 25 \text{ mV s}^{-1}$) the most prominent peak is centred at -0.50 V vs SCE and is associated with cation (Na^+) insertion⁴³ from the electrolyte (PBS solution). At increasing scan rates ($> 25 \text{ mV s}^{-1}$) the redox peaks associated with the insertion of the Na^+ species and the anionic species are all clearly visible and increase in intensity. The redox peaks for anion transport appear centred at approximately -0.10 V vs SCE and shift to lower potentials as the scan rate is increased to 150 mV s^{-1} . The anodic peak which extends from -0.40 V vs SCE to 0.20 V vs SCE is broad and the anodic peak potential (E_{pa}) increases with scan rate. The dominating redox process is for anion transport. Indeed, similar voltammograms for PpyCl have been published and discussed⁴³⁻⁴⁶ and ion transport has been extensively studied⁴⁷⁻⁵². Figure 5.9 C shows that the main redox peaks for PpyOx are at lower potentials than PpyCl. This is more clearly evident on comparing the voltammograms presented in Figure 5.9 B and D. These potentials are in the region associated with cation transport^{53, 54}. The anodic peak potential (E_{pa}) remains centred at -0.37 V vs SCE. The

cathodic peak potential (E_{pc}) shifts from -0.48 V to -0.65 V vs SCE as the scan rate increases. The PpyOx films do not show any other significant peaks during cycling in PBS solution; this indicates that cation transport is dominant^{51, 54, 55}.

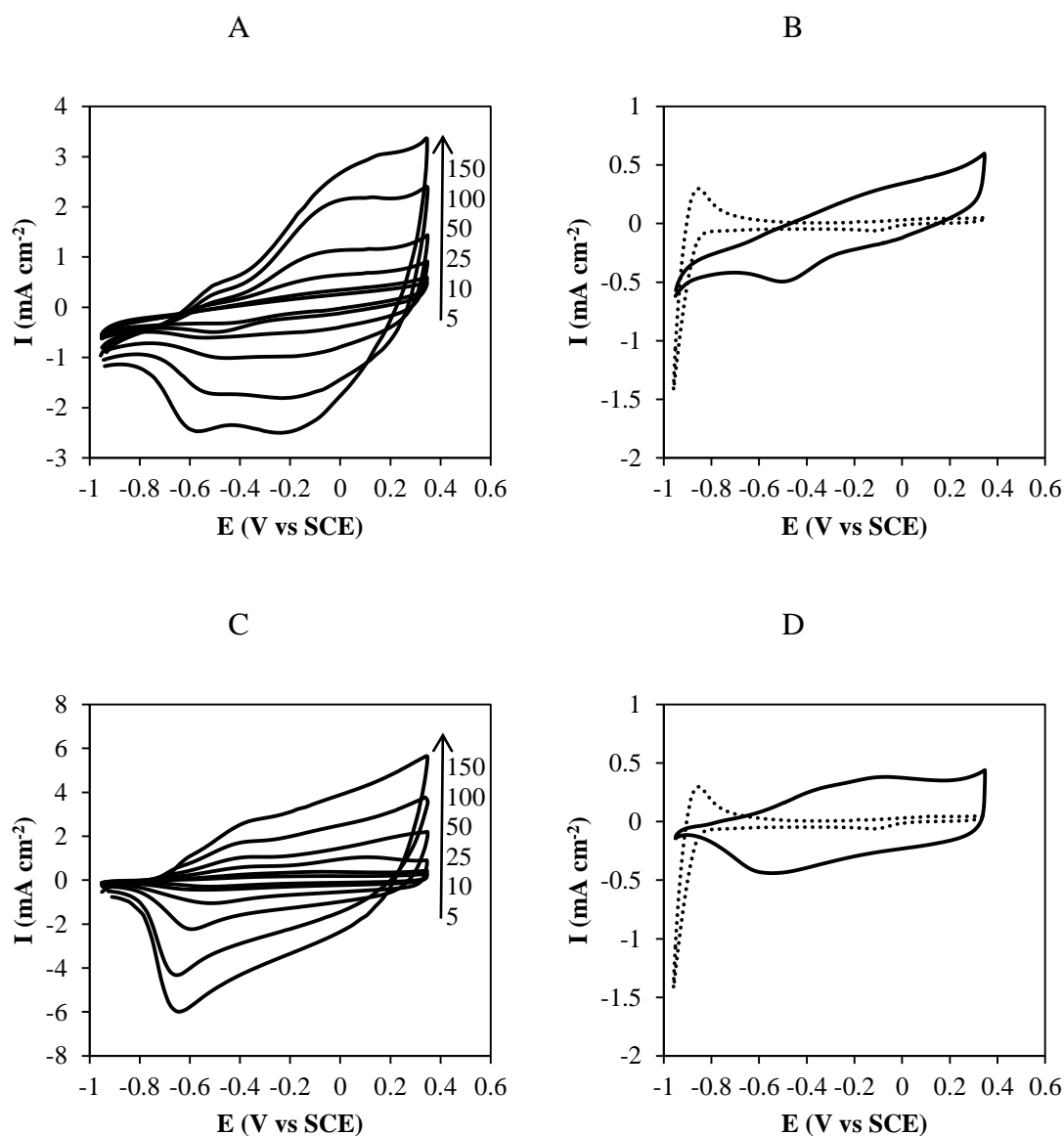


Figure 5.9: Cyclic voltammograms (10th cycle) of PpyCl (A and B) and PpyMO (C and D) coated Pt electrode in PBS solution. The dashed traces in (B) and (D) correspond to the voltammograms of bare Pt electrode. The scan rates in mV s^{-1} are indicated on the plot. The films were prepared by potentiostatic electropolymerisation at 0.80 V vs SCE to a charge density of 0.25 C cm^{-2} . The PpyCl was prepared from a solution of 0.1 mol dm^{-3} Py and 0.1 mol dm^{-3} NaCl and the PpyOx was prepared from a solution of 0.2 mol dm^{-3} Py and 0.02 mol dm^{-3} Ox.

The peak potentials and peak currents were recorded as a function of the scan rate from the cyclic voltammograms of the PpyCl and PpyOx films cycled in PBS solution. These data are plotted in Figure 5.10 where the peak potential (E_p) and peak current (I_p) are shown as a function of scan rate. For PpyCl (Figure 5.10 A) the voltammetric peaks associated with cation (Na^+) exchange are not significantly susceptible to changes in the scan rate, the anodic peak occurs at -0.49 ± 0.05 V vs SCE for Na^+ expulsion and the corresponding cathodic peak for Na^+ insertion occurs at -0.51 ± 0.04 V vs SCE. For PpyOx (Figure 5.10 C) the cathodic peak potential associated with cation (Na^+) insertion varies with scan rate while the anodic peak potential associated with cation (Na^+) expulsion varies only slightly with increasing scan rate. The anodic peak potential remains centred at approximately -0.37 ± 0.04 V vs SCE, while the cathodic peak potential shifts by 167 mV as the scan rate increases. This may suggest that when cation transport is dominant the insertion of the cation species into the film is associated with a larger ohmic potential drop than its expulsion. When anionic transport is dominant the insertion of the ionic species from the solution into the Ppy film is associated with a larger ohmic potential drop than its expulsion⁵¹. It is clear that the peak separation is more significant for PpyOx than PpyCl. As shown in Figure 5.10 B and Figure 5.10 D the peak current increases in a linear manner with the scan rate. It is also evident that the peak currents are higher for the PpyOx film.

Table 5.3 shows data for the cation redox process of PpyCl and PpyOx. The peak current ratios (I_{pa}/I_{pc}) were determined for the main redox peaks, and averages values of 0.08 and 0.14 were calculated for PpyCl and PpyOx, respectively. This deviates from a reversible voltammetric response with a peak ratio of 1.0. The average peak-to-peak separation, ΔE_p , for PpyCl and PpyOx in 0.1 mol dm^{-3} PBS solution was calculated to be 11 mV and 190 mV, respectively. The midpoint potential, E_{mid} , was computed to be -0.50 V vs SCE for PpyCl and -0.10 V vs SCE for PpyOx, at 298 K.

Table 5.3: Cyclic voltammetric data for the redox properties of PpyCl and PpyOx in PBS solution.

PpyCl				
Scan rate (mV s ⁻¹)	<i>E</i> _{mid} (V vs SCE) ^a	ΔE_p (mV) ^b	<i>I</i> _{pa} (mA cm ⁻²)	<i>I</i> _{pc} (mA cm ⁻²)
5	-0.47	78	0.02	-0.32
10	-0.48	56	0.02	-0.50
25	-0.54	-7	0.03	-0.61
50	-0.49	-81	0.06	-1.01
100	-0.48	-35	0.26	-1.73
150	-0.54	56	0.43	-2.47
PpyOx				
Scan rate (mV s ⁻¹)	<i>E</i> _{mid} (V vs SCE) ^a	ΔE_p (mV) ^b	<i>I</i> _{pa} (mA cm ⁻²)	<i>I</i> _{pc} (mA cm ⁻²)
5	-0.04	78	0.11	-0.29
10	-0.06	118	0.29	0.20
25	-0.09	173	0.62	-1.05
50	-0.13	250	1.06	-2.23
100	-0.13	253	1.71	-4.33
150	-0.13	267	2.65	-5.98

^a Calculated from $1/2 (E_{p,c} + E_{p,a})$.

^b $\Delta E_p = E_{pa} - E_{pc}$.

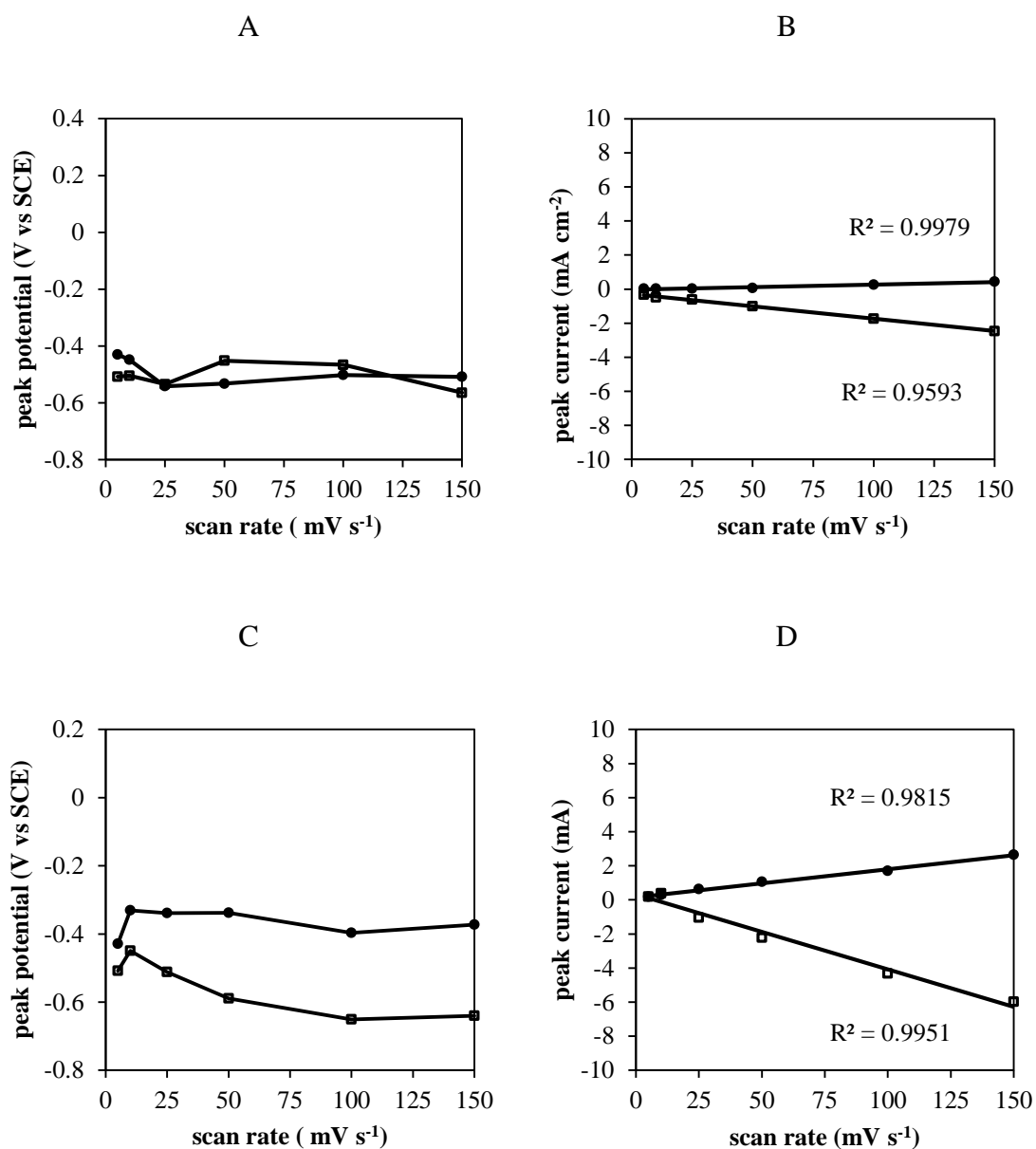


Figure 5.10: Peak potential plotted as a function of scan rate for PpyCl (A) and PpyOx (C) and peak current plotted as a function of scan rate PpyCl (C) and PpyOx (D) taken from the cyclic voltammograms (10th cycle) in PBS solution shown in Figure 5.9 A and C. The main anodic peak (●) and the main cathodic peak (□). The R^2 values for the linear trendline are indicated. The films were prepared by potentiostatic electropolymerisation at 0.80 V vs SCE to a charge density of 0.25 C cm^{-2} . The PpyCl was prepared from a solution of 0.1 mol dm^{-3} Py and 0.1 mol dm^{-3} NaCl and the PpyOx was prepared from a solution of 0.2 mol dm^{-3} Py and 0.02 mol dm^{-3} Ox.

5.3.4.2 Redox properties of PpyCl/Chit and PpyOx/Chit grown to a charge density of 0.25 C cm^{-2}

As detailed earlier, the chitosan layer was formed post-electropolymerisation to give the PpyCl/Chit and PpyOx/Chit composite. Figure 5.11 shows the cyclic voltammograms of the PpyCl/Chit and PpyMO/Chit deposited on a Pt electrode and cycled in 0.1 mol dm^{-3} PBS at $23 \text{ }^\circ\text{C}$. Again, the data presented in Figure 5.11 A show the voltammograms recorded for PpyCl/Chit at various scan rates, while the data shown in Figure 5.11 C represents the PpyOx/Chit film. In Figure 5.11 B and Figure 5.11 D the voltammograms recorded for bare Pt are compared with the PpyCl/Chit and PpyOx/Chit composites. It is clear that the chitosan component does alter the overall shape of the voltammograms when cycled in PBS solution. Figure 5.11 A shows the I - E curve for the PpyCl/Chit coated electrode. In the presence of chitosan the main redox peaks are centred at -0.54 V vs SCE similar to PpyCl in Figure 5.9. The cathodic peak potential (E_{pc}) and the anodic peak potential (E_{pa}) shifts slightly by approximately 50 mV with increasing scan rate. The anodic peak current associated with cation expulsion is slightly higher for the PpyCl/Chit composite than the PpyCl film. Clearly the dominating redox process is for cation transport in the PpyCl/Chit composite. This may be as a result of the chitosan layer hindering the egress of anions, if an anion is unable to leave the film during the reduction process than cation (Na^+) insertion is expected⁵⁶.

The corresponding I - E curve for PpyOx/Chit is shown in Figure 5.11 C. The anodic peak potential (E_{pa}) remains centred at -0.23 V vs SCE. The cathodic peak potential (E_{pc}) shifts to more negative potentials from approximately -0.40 V vs SCE to -0.70 V vs SCE as the scan rate is increased from 25 to 150 mV s^{-1} . Furthermore, the peaks become sharper and increase in intensity as the scan rate is increased.

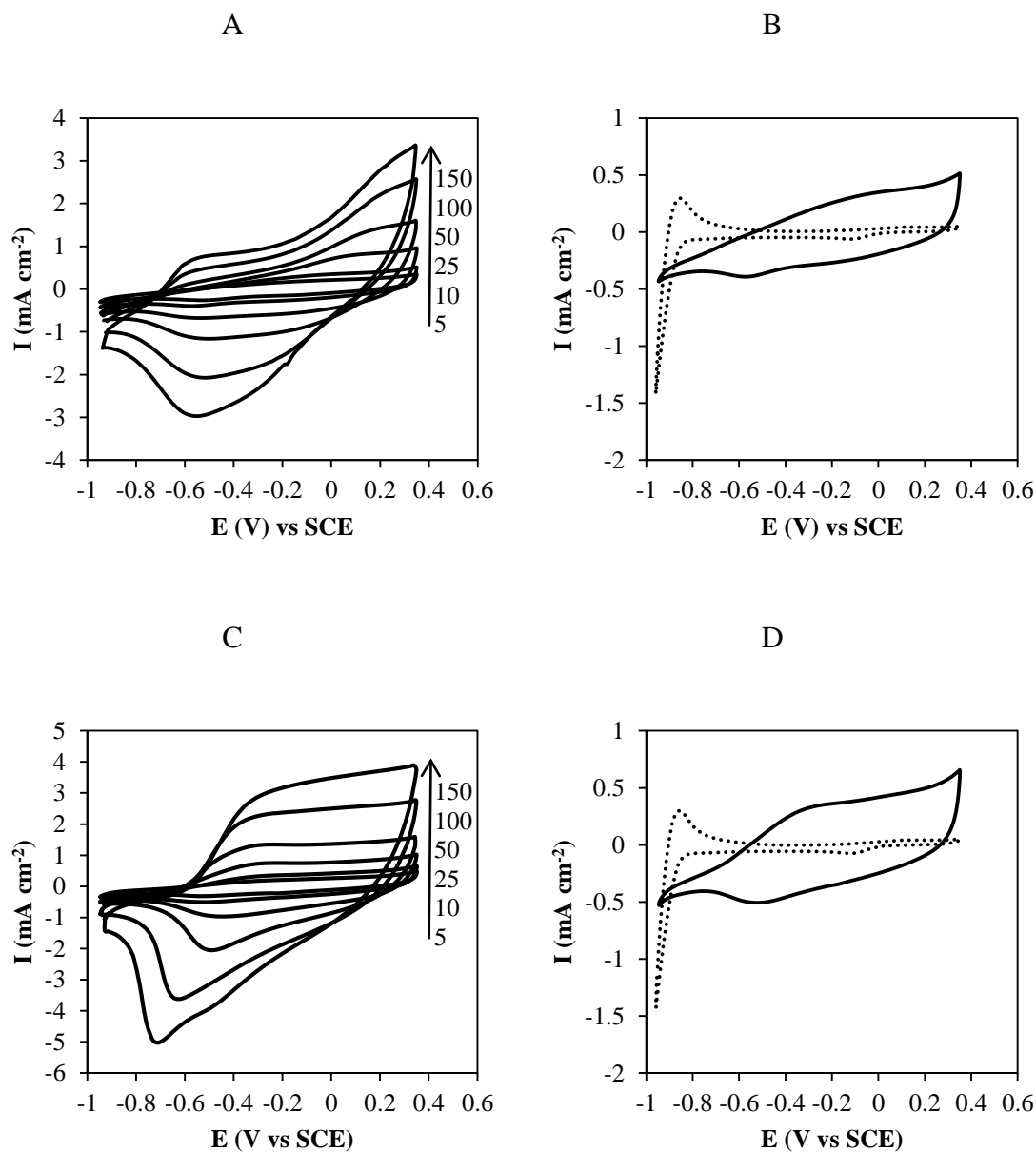


Figure 5.11: Cyclic voltammograms (10th cycle) of PpyCl/Chit (A and B) and PpyOx/Chit (C and D) coated Pt electrode in PBS solution. The dashed traces in (B) and (D) correspond to the voltammograms of bare Pt electrode. The scan rates in mV s^{-1} are indicated on the plot. The films were prepared by potentiostatic electropolymerisation at 0.80 V vs SCE to a charge density of 0.25 C cm^{-2} . The PpyCl was prepared from a solution of 0.1 mol dm^{-3} Py and 0.1 mol dm^{-3} NaCl and the PpyOx was prepared from a solution of 0.2 mol dm^{-3} Py and 0.02 mol dm^{-3} Ox. Chitosan was added post-polymerisation.

In Figure 5.12, plots are shown for the peak potential (E_p) and peak current (I_p) as a function of the scan rate for the cyclic voltammograms of PpyCl/Chit and PpyOx/Chit shown in Figure 5.11. There is a linear relationship between the peak current and the scan rate, which is similar to the response obtained with the PpyCl and PpyOx films, Figure 5.10. In PpyCl/Chit (Figure 5.12 A) there is a difference of 100 mV between the maximum and minimum values of (E_{pa}) which occur at 5 and 25 mV s^{-1} , respectively. The voltammetric peak associated with Na^+ insertion is more susceptible to the change in scan rate than the voltammetric peak associated with Na^+ expulsion.

The peak separation is more significant in the PpyOx/Chit than in the PpyCl/Chit. The peak current ratios (I_{pa}/I_{pc}) were determined for the main redox peaks, and average values of 0.08 and 0.67 were calculated for PpyCl/Chit and PpyOx/Chit, respectively. This deviates from a reversible response with a peak ratio of 1.0¹⁸. The peak-to-peak separation, ΔE_p , at 50 mV s^{-1} for PpyCl/Chit and PpyOx/Chit in 0.1 mol dm^{-3} PBS solution was calculated to be 68 mV and 257 mV, respectively. The other parameter determined from the cyclic voltammetric data is the midpoint potential, E_{mid} which was computed to be -0.54 V vs SCE for PpyCl/Chit and -0.39 V vs SCE for PpyOx/Chit, at 298 K. These data are summarised in Table 5.4.

Table 5.4: Cyclic voltammetric data for the redox properties of PpyCl/Chit and PpyOx/Chit recorded in PBS solution.

PpyCl/Chit				
Scan rate (mV s ⁻¹)	E_{mid} (V vs SCE) ^a	ΔE_p (mV) ^b	I_{pa} (mA cm ⁻²)	I_{pc} (mA cm ⁻²)
5	-0.58	104	0.04	-0.26
10	-0.60	55	0.08	-0.39
25	-0.51	42	0.09	-0.67
50	-0.47	68	0.28	-1.16
100	-0.52	6	0.48	-2.07
150	-0.55	16	0.74	-2.97

PpyOx/Chit				
Scan rate (mV s ⁻¹)	E_{mid} (V vs SCE) ^a	ΔE_p (mV) ^b	I_{pa} (mA cm ⁻²)	I_{pc} (mA cm ⁻²)
5	-0.39	281	0.20	-0.32
10	-0.39	263	0.34	-0.51
25	-0.34	217	0.75	-0.97
50	-0.36	257	1.35	-2.06
100	-0.40	385	2.37	-3.54
150	-0.46	493	3.15	-5.01

^a Calculated from $1/2 (E_{pc} + E_{pa})$.

^b $\Delta E_p = E_{pa} - E_{pc}$.

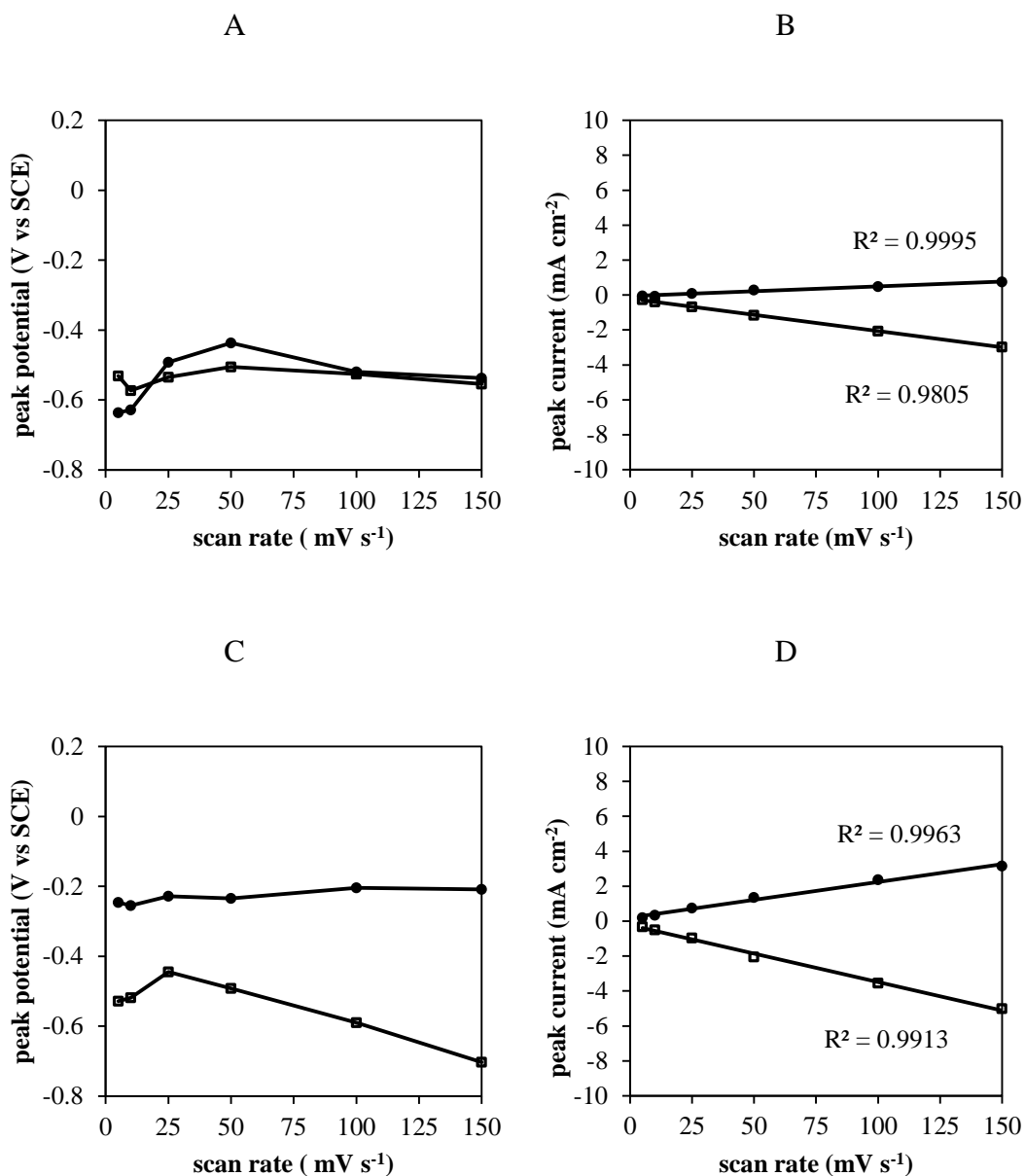


Figure 5.12: Peak potential plotted as a function of scan rate for PpyCl/Chit (A) and PpyOx/Chit (C) and peak current plotted as a function of scan rate PpyCl/Chit (B) and PpyOx/Chit (D) taken from the cyclic voltammograms (10th cycle) in PBS shown in Figure 5.11 A and C. The main anodic peak (●) and the main cathodic peak (□). The R^2 values for the linear trendline are indicated. The films were prepared by potentiostatic electropolymerisation at 0.80 V vs SCE to a charge density of 0.25 C cm^{-2} . The PpyCl was prepared from a solution of 0.1 mol dm^{-3} Py and 0.1 mol dm^{-3} NaCl and the PpyOx was prepared from a solution of 0.2 mol dm^{-3} Py and 0.02 mol dm^{-3} Ox. Chitosan was added post-polymerisation.

A direct comparison of the cyclic voltammograms recorded for PpyCl and PpyOx in PBS is shown in Figure 5.13 A, while corresponding data are presented in Figure 5.13 B for the PpyCl/Chit and PpyOx/Chit. These voltammograms were recorded at 50 mV s^{-1} . In Figure 5.13 A, there is evidence of mixed ion transport for the PpyCl films, with peaks I, II, III and IV clearly visible, but for the PpyOx film, the transport appears to be predominately cationic. This has been reported for other large sulfonate doped polypyrrole films^{41, 55, 57-59}. Again, the significant role of the chitosan layer can be clearly seen on comparing the voltammograms in Figure 5.13 A and Figure 5.13 B.

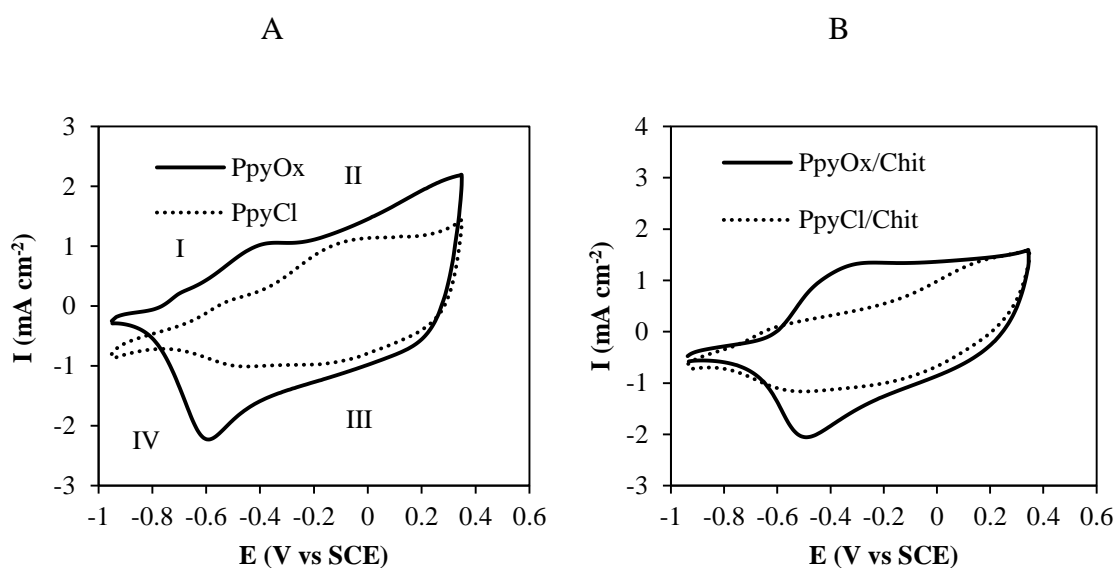
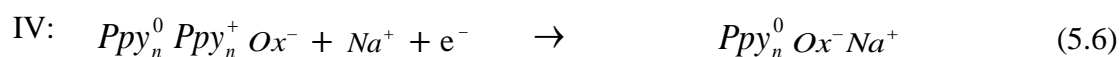
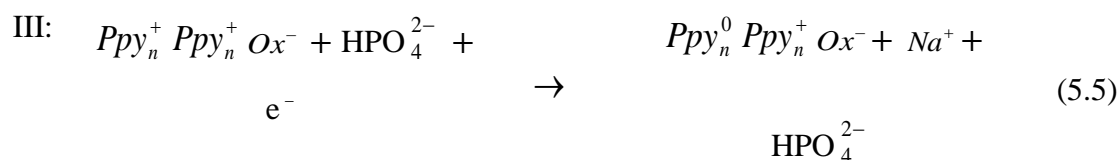
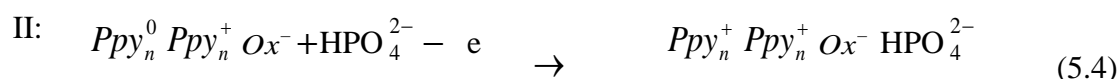
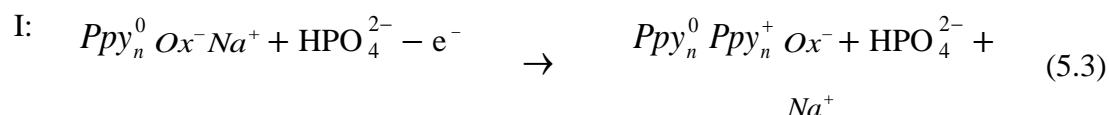


Figure 5.13: Generalised capacitance curve (where the current is divided by the scan rate v) for PpyCl (A) and PpyOx (B) cycled in PBS solution at 5 mV s^{-1} . The dashed traces indicate the chitosan-coated composite. The films were prepared by potentiostatic electropolymerisation at 0.80 V vs SCE to a charge density of 0.25 C cm^{-2} . The PpyCl was prepared from a solution of 0.1 mol dm^{-3} Py and 0.1 mol dm^{-3} NaCl and the PpyOx was prepared from a solution of 0.2 mol dm^{-3} Py and 0.02 mol dm^{-3} Ox. For PpyA/Chit (B), chitosan was added post-polymerisation.

The possible processes occurring at the peaks labelled I, II, III, and IV are described in Equations 5.3, 5.4, 5.5 and 5.6. On re-oxidation of the PpyOx (Figure 5.13 A, peaks I and II) the polymer backbone becomes positively charged. The charge neutrality is achieved by the expulsion of the sodium ion (Equation 5.3) and the incorporation of the phosphate

ions (HPO_4^{2-} or H_2PO_4^-) from the electrolyte as shown in Equation 5.4. When the PpyOx is reduced during subsequent cycles (Figure 5.13 B, peaks III and IV), the phosphate anion is expelled into the electrolyte (Equation 5.5) and in order to maintain overall charge neutrality a sodium ion from the electrolyte is incorporated into the polymer film (Equation 5.6).



5.3.5 Electrochemical Impedance spectroscopy

Complex plane-impedance plots (Nyquist plots) and Bode plots were recorded for PpyOx and PpyOx/Chit. The impedance data were recorded for a Pt electrode coated with PpyOx and PpyOx/Chit films, and the PpyOx moiety was grown to a charge density of 0.25 C cm^{-2} . The imaginary and real components of the impedance are plotted to give the complex plane or Nyquist plots, while the modulus of the impedance and the phase angle are presented as a function of frequency to give the Bode plot. Reproducible results were obtained by polarising the electrodes at the required potential for 60 min. This period was sufficiently long to achieve steady-state conditions to reduce the effect of hysteresis⁶⁰. The frequency range was varied from 65 kHz to 0.005 Hz.

The impedance measurements were recorded at fixed potentials of -0.90 , -0.60 , -0.30 , -0.10 , 0.0 , 0.10 and 0.30 V vs SCE in PBS solution. The polymer film is in a totally reduced state at -0.90 V vs SCE, and as the potential is increased the films are oxidised, and the different applied potentials represent varying degrees of oxidation.

The real axis intercept at high frequency (> 12.5 kHz) coincides with the uncompensated solution resistance (R_s) and is independent of the applied potential⁵¹. A simple Randles circuit (Figure 5.14) was used as a starting point to model the impedance response at each applied potential, and then additional circuit elements were considered. A more complex circuit was used to model the impedance of PpyOx at -0.90 V vs SCE, with a second RC time constant incorporated into the model, which describes two RC processes occurring at different rates⁶¹. Figure 5.14 B. All data were normalised to the surface area of the Pt electrode, 0.13 cm².

The parameters extracted from the equivalent circuit model were used to determine the high frequency capacitance or (CPE_{HF}) which was corrected to units of capacitance.

The low frequency capacitance C_{LF} , can be estimated directly from the Bode plot ($C_{LF} = 1/\text{slope}$). The calculation for determining C_{LF} is described in Section 2.4.4 equation 2.8 and is independent of film thickness^{62, 63}.

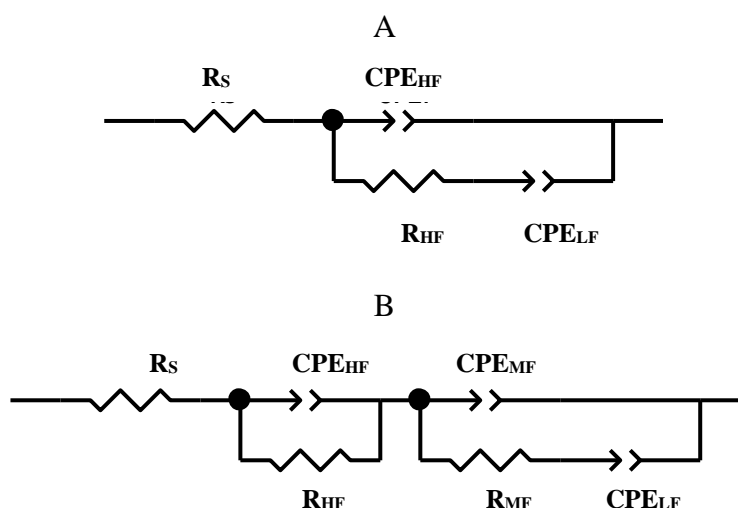


Figure 5.14: Equivalent circuits used for modelling the impedance data.

5.3.5.1 EIS of PpyOx films

The complex-plane impedance (Nyquist) plots and Bode plots for PpyOx are shown in Figure 5.15 A and B, respectively. Some of the parameters from the equivalent circuit for PpyOx films at different redox states are shown in Table 5.5.

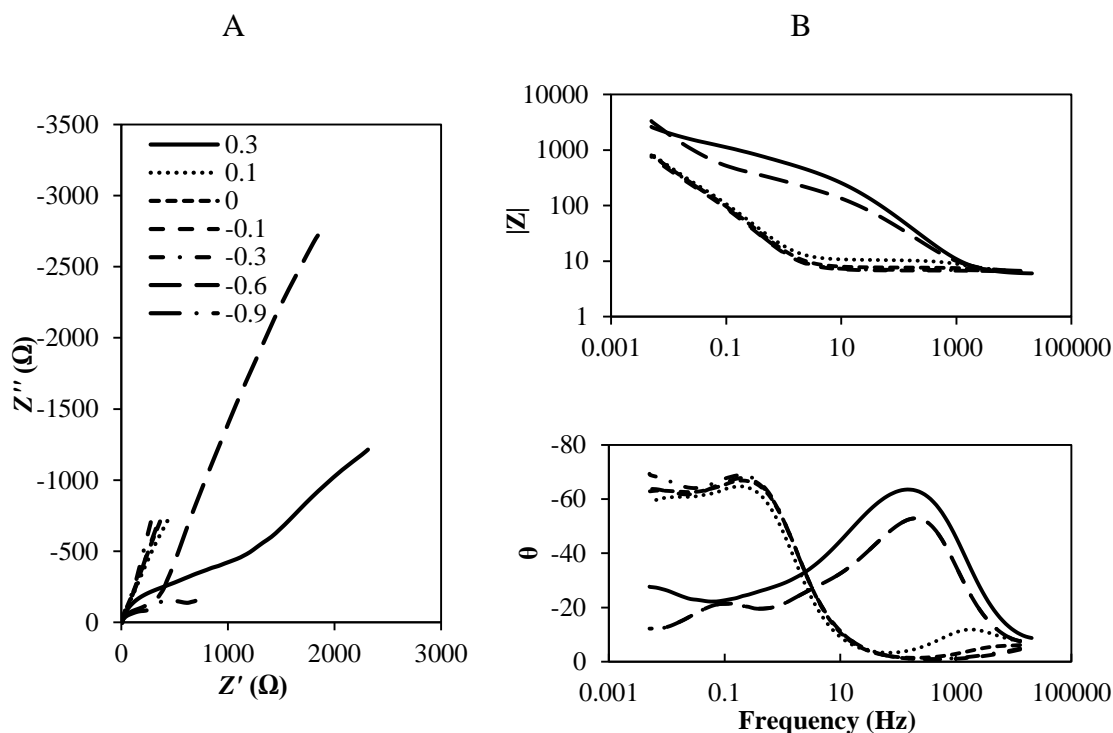


Figure 5.15: Complex-plane impedance plot (A) for PpyOx coated 0.13 cm^2 Pt electrodes at various potentials in PBS solution. The Bode plot (B) shows the logarithm of the impedance and the phase angle against the logarithm of frequency. Potentials are indicated in V vs SCE. Frequency range shown from 65 kHz to 0.005 Hz. The films were prepared by potentiostatic electropolymerisation at 0.80 V vs SCE to a charge density of 0.25 C cm^{-2} . The PpyCl was prepared from a solution of 0.1 mol dm^{-3} Py and 0.1 mol dm^{-3} NaCl and the PpyOx was prepared from a solution of 0.2 mol dm^{-3} Py and 0.02 mol dm^{-3} Ox.

At higher potentials a “Warburg-type” linear region is observed in the high-medium frequency range. At lower potentials a compressed semicircular arc is observed in the high frequency range, due to parallel resistance-capacitance elements which is typical of polymer coated electrodes exhibiting ion transport⁴³. The impedance response in these regions is particularly important for determining mass transfer parameters^{53, 64}. As the

frequency is decreased the transmission line becomes nearly vertical where the polymer|metal electrode behaves like a capacitor. The deviation from an ideal impedance spectrum is thought to be due to irregular thickness and morphology of the polymer surface^{65, 66}. In Tables 5.5 and 5.6 the parameters obtained from fitting the impedance data to the circuit elements are summarised for the PpyCl and PpyOx films, respectively.

Table 5.5: Parameters for the circuit elements evaluated by fitting the impedance data of PpyCl in 0.1 mol dm⁻³ PBS to the equivalent circuit shown in Figure 5.14, n=3.

E (V vs SCE)	0.3	0.1	0.0	-0.1	-0.3	-0.6	-0.9
R_s (Ω cm²)	5.63 ± 0.07	6.67 ± 0.16	6.69 ± 0.08	10.82 ± 0.18	7.85 ± 0.11	17.95 ± 0.54	16.15 ± 0.20
CPE-T_{HF} (mF cm⁻²)	2.34 ± 0.04	1.90 ± 0.05	2.50 ± 0.05	0.82 ± 0.05	0.41 ± 0.02	0.50 ± 0.02	0.10 ± 0.00
CPE-P_{HF}	0.56 ± 0.00	0.55 ± 0.00	0.61 ± 0.00	0.62 ± 0.01	0.71 ± 0.01	0.47 ± 0.01	0.69 ± 0.01
R_{HF} (Ω cm²)	32.15 ± 0.48	97.67 ± 2.54	49.43 ± 0.80	385.1 ± 25.6	288.8 ± 13.1	1312 ± 76.7	343.0 ± 17.4
CPE-T_{LF} (mF cm⁻²)	8.68 ± 0.11	7.70 ± 0.17	7.50 ± 0.12	4.34 ± 0.20	3.92 ± 0.14	3.49 ± 0.22	1.00 ± 0.01
CPE-P_{LF}	1 ± 0	1 ± 0	1 ± 0	0.71 ± 0.02	0.60 ± 0.01	0.82 ± 0.03	0.40 ± 0.00
χ²	0.0038	0.0073	0.0043	0.0035	0.0074	0.0065	0.0010
SS	0.4782	0.9097	0.5255	0.4165	1.054	0.9117	0.1250

The CPE was replaced with a capacitor (C) in the lower branch of the circuit

Table 5.6: Parameters for the circuit elements evaluated by fitting the impedance data of PpyOx to the equivalent circuit shown in Figure 5.14, $n=3$.

E (V vs SCE)	0.3	0.1	0.0	-0.1	-0.3	-0.6	-0.9
R_s (Ω cm^2)	5.79 \pm 0.08	6.39 \pm 0.09	7.12 \pm 0.26	6.45 \pm 0.05	6.64 \pm 0.05	5.84 \pm 0.11	5.73 \pm 0.13
CPE-T_{HF} (mF cm^{-2})	0.06 \pm 0.00	0.02 \pm 0.00	0.02 \pm 0.00	9.60 \pm 0.66	10.79 \pm 0.89	0.23 \pm 0.01	0.20 \pm 0.02
CPE-P_{HF}	0.87 \pm 0.00	1.00 \pm 0.00	1.00 \pm 0.00	0.60 \pm 0.01	0.67 \pm 0.02	0.74 \pm 0.01	0.79 \pm 0.02
R_{HF} (Ω cm^2)	184.9 \pm 17.7	8.65 \pm 0.16	1.28 \pm 0.04	0.60 \pm 0.08	0.64 \pm 0.11	267.5 \pm 7.14	140.8 \pm 12.1
CPE-T_{LF} (mF cm^{-2})	1.12 \pm 0.02	14.22 \pm 0.15	17.50 \pm 0.94	10.25 \pm 0.20	9.57 \pm 0.28	3.46 \pm 0.08	3.73 \pm 0.27
CPE-P_{LF}	0.29 \pm 0.00	0.81 \pm 0.00	1.00 \pm 0.00	1 \pm 0.00	1 \pm 0.00	0.67 \pm 0.01	0.58 \pm 0.03
χ^2	0.00094	0.0094	0.0002	0.0046	0.0073	0.0044	0.0056
SS	0.1190	0.8106	0.2861	0.5761	0.9183	0.5551	0.7025

The CPE was replaced with a capacitor (C) in the lower branch of the circuit

The R_{HF} resistance term presented in Tables 5.5 and 5.6 can be considered as the charge-transfer resistance. The values obtained for PpyCl in PBS are similar to that of PpyCl in NaCl, Section 4.3.4 (Table 4.4). The R_{HF} increases sharply by three orders of magnitude with a minimum at 0.30 V vs SCE and a maximum at -0.60 V vs SCE ($1.31 \text{ k}\Omega \text{ cm}^2$) for the PpyCl film, Table 5.5. As the potential is varied from 0.30 V vs SCE to -0.60 V vs SCE, the PpyCl is reduced from an oxidised state to a neutral state and the resistance increases⁵⁴. Again, a decrease in the resistance is observed at -0.90 V vs SCE. This may be attributed to a decrease in the ionic resistance due to the insertion of cations⁶⁷ (Na^+).

The R_{HF} values obtained for PpyOx, Table 5.6, decrease from 0.30 V vs SCE and remain low between 0.00 V vs SCE and -0.30 V vs SCE at $1.12 \pm 0.15 \text{ }\Omega \text{ cm}^2$. The resistance increases sharply by approximately $260 \text{ }\Omega \text{ cm}^2$, with a maximum at -0.60 V vs SCE.

The total resistance, R_T , was computed using the expression in Equation 5.7 for resistors in series. This resistance was then used to calculate the conductivity, σ_T , as shown in Equation 5.8, where d is the nominal thickness of the dry film, 5.0×10^{-5} cm and 1.5×10^{-4} cm for PpyCl and PpyOx respectively, and A is the geometric surface area of the electrode (0.13 cm^2).

$$R_T = R_{HF} + R_{MF} \quad (5.7)$$

$$\sigma_T = \frac{1}{R_T} \times \frac{d}{A} \quad (5.8)$$

The total resistance, R_T , and the conductivity, σ_T , of the PpyCl and PpyOx films were plotted as a function of the applied potential and representative plots are presented in Figure 5.16. The conductivity of the PpyCl film decreases sharply by $12.07 \text{ }\mu\text{S cm}^{-1}$ with a maximum at 0.30 V vs SCE and a minimum at -0.60 V vs SCE as the Ppy is reduced and the charge carrier (Cl^-) concentration in the film decreases. A slight increase of $0.88 \text{ }\mu\text{S cm}^{-1}$ is observed at -0.90 V vs SCE, which is consistent with the ingress of cations^{67, 68} (Na^+).

For PpyOx the conductivity is lower than PpyCl at 0.30 V vs SCE, however the conductivity increases and remains high, at approximately $721 \pm 95 \mu\text{S cm}^{-1}$, when the potential is varied from 0.00 V vs SCE to -0.30 V vs SCE. The conductivity decreases sharply at -0.60 V vs SCE and there is a further slight decrease in the conductivity at -0.90 V vs SCE. This high conductivity may be associated with the high concentration of ions trapped in the PpyOx film. Also, the PpyOx film has a thicker film than the PpyCl film, Figure 5.7, and it appears less porous, Figure 5.6. Zhang *et al.*⁶⁹ compared the R_{ct} (R_{HF}) values of a Cl^- doped and sulfonate doped Ppy films and found lower resistance values for the sulfonate doped Ppy, which agrees well with the values obtained for the PpyOx films.

The corrected C_{HF} and C_{LF} capacitance terms of the PpyCl and PpyOx films are plotted as a function of potential in Figure 5.17. It is evident from the plots in Figure 5.17 that there is some variation between the capacitance of the PpyCl and PpyOx films. The PpyCl film shows a decrease in C_{HF} as the Ppy film releases chloride anions to the surrounding electrolyte, with a maximum at 0.00 V vs SCE and a minimum at -0.60 V vs SCE. The C_{HF} of PpyOx is lower when polarised in the oxidised state and increases tenfold between -0.10 V and -0.30 V vs SCE. The C_{LF} decreases steadily for PpyCl as the charge storage capacity of the film matrix decreases⁶⁷. Interestingly, the C_{LF} increases for PpyOx as the applied potential is reduced from 0.30 V to -0.30 V vs SCE followed by a minimum value at -0.60 V vs SCE. This high capacitance is attributed to cation transport and corresponds to the cyclic voltammograms in Figure 5.13 A.

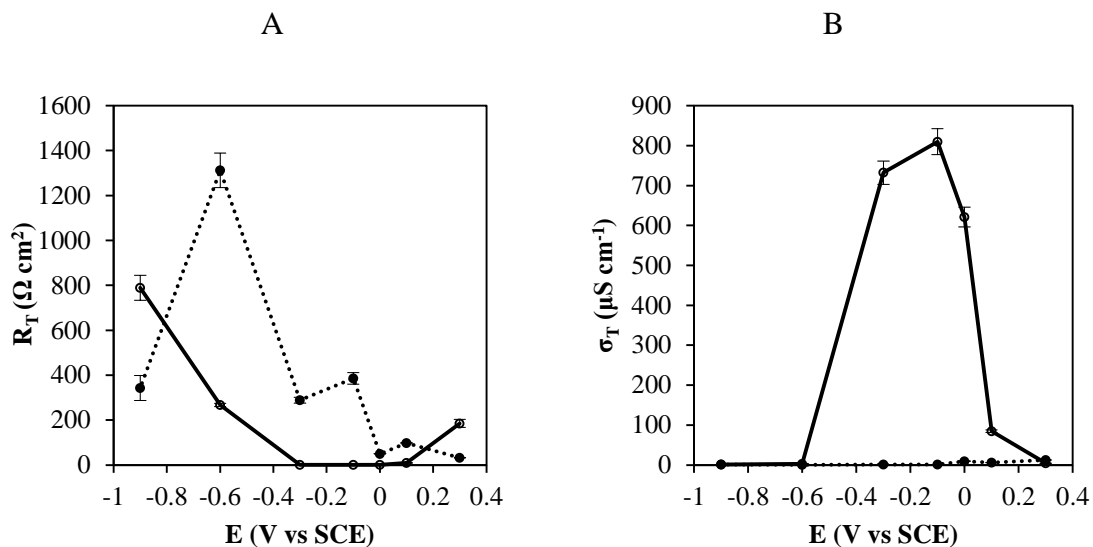


Figure 5.16: Plots of resistance, R_T , (A), and conductivity, σ_T , (B), as a function of applied potential for PpyCl (●) and PpyOx (○) in PBS solution. The films were prepared by potentiostatic electropolymerisation at 0.80 V vs SCE to a charge density of 0.25 C cm⁻². The PpyCl was prepared from a solution of 0.1 mol dm⁻³ Py and 0.1 mol dm⁻³ NaCl and the PpyOx was prepared from a solution of 0.2 mol dm⁻³ Py and 0.02 mol dm⁻³ Ox. n=3

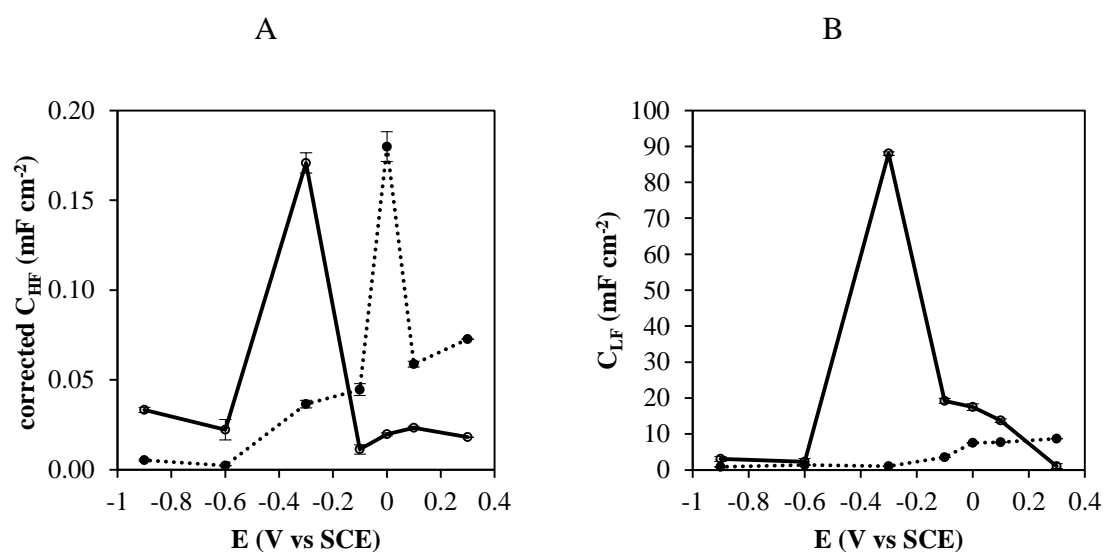


Figure 5.17: Plots of corrected double layer capacitance, C_{HF} , (A), and low frequency capacitance, C_{LF} , (B), as a function of applied potential for PpyCl (●) and PpyMO (○) in PBS solution. The films were prepared by potentiostatic electropolymerisation at 0.80 V vs SCE to a charge density of 0.25 C cm⁻². The PpyCl was prepared from a solution of 0.1 mol dm⁻³ Py and 0.1 mol dm⁻³ NaCl and the PpyOx was prepared from a solution of 0.1 mol dm⁻³ Py and 0.02 mol dm⁻³ Ox. n=3

5.3.5.2 EIS of PpyOx/Chit films

The impedance of PpyCl/Chit and PpyOx/Chit was measured as a function of the applied potential, using an approach similar to that used to record the impedance in Section 5.3.5.1. Typical complex-plane impedance plots and Bode plots recorded for PpyOx/Chit at potentials varying from 0.30 V to -0.90 V vs SCE are shown in Figure 5.18. Again, it is evident from these data that the impedance response changes as the applied potential is varied. The impedance is lower at 0.30 V vs SCE and increases as the potential is varied from 0.30 V to -0.60 V vs SCE. The resistance of the PpyOx/Chit film is somewhat higher than that obtained for PpyOx. This is consistent with a higher resistance to ion transport due to the presence of the chitosan.

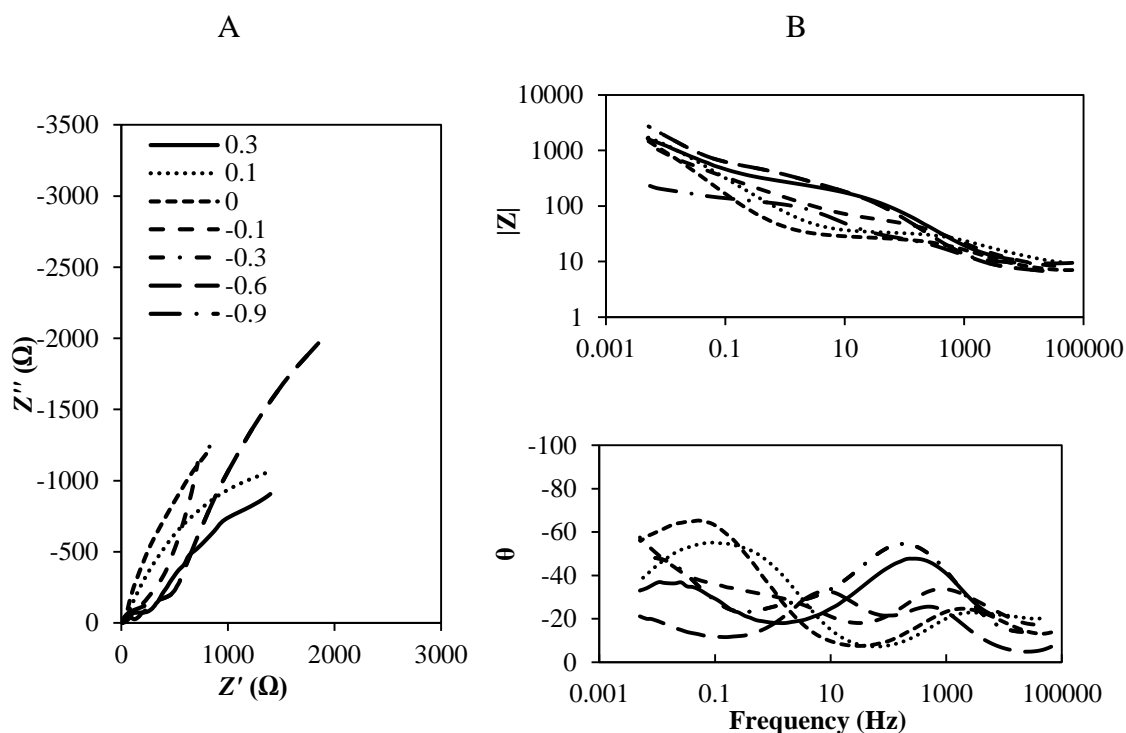


Figure 5.18: Complex-plane impedance plot (A) for PpyOx/Chit coated 0.13 cm^2 Pt electrodes at various potentials in PBS solution. The Bode plot (B) shows the logarithm of the impedance and the phase angle against the logarithm of frequency. Potentials are indicated in V vs SCE. Frequency range shown from 65 kHz to 0.005 Hz. The films were prepared by potentiostatic electropolymerisation at 0.80 V vs SCE to a charge density of 0.25 C cm^{-2} . PpyOx was prepared from a solution of 0.2 mol dm^{-3} Py and 0.02 mol dm^{-3} Ox. Chitosan was added post-polymerisation.

These data were fitted to the equivalent circuit in Figure 5.14 and the data obtained are summarised in Tables 5.7 and 5.8. The R_{HF} values for the PpyCl/Chit reach a minimum of $63 \Omega \text{ cm}^2$ at 0.30 V vs SCE and a maximum at -0.90 V vs SCE , Table 5.7. As the potential is varied from 0.30 V vs SCE to -0.90 V vs SCE the PpyCl/Chit film is converted from an oxidised state to a neutral state and the resistance increases.

The R_{HF} values obtained for PpyOx/Chit, Table 5.8, range from a minimum value of $21.5 \Omega \text{ cm}^2$ obtained at 0.0 V vs SCE to a maximum value of $314 \Omega \text{ cm}^2$ obtained at -0.60 V vs SCE and a further slight decrease in the resistance is observed at -0.90 V vs SCE . This may be attributed to a decrease in the ionic resistance due to the insertion of cations.

Again, the total resistance, R_T , was computed using the expression in Equation 4.6 for resistors in series. The presence of chitosan makes it difficult to determine the polymer film thickness and thus the conductivity, σ_T , was not determined. Figure 5.19 shows a direct comparison between the resistance of PpyCl/Chit and PpyOx/Chit where the total resistance is plotted as a function of applied potential. It is clear from this plot that the resistance of the polymer films, PpyCl/Chit and PpyOx/Chit, increases as the potential is varied from 0.10 V vs SCE to -0.60 V vs SCE . The lowest resistance (R_T) value for PpyOx/Chit was found at -0.10 V vs SCE while the lowest resistance was observed at 0.00 V vs SCE for the PpyCl/Chit.

The capacitance terms are plotted as a function of applied potential in Figure 5.20. For PpyCl/Chit, the high frequency capacitance, C_{HF} , shows a decrease as the potential is varied from 0.10 V vs SCE to -0.90 V vs SCE , Figure 5.20 A. This corresponds to the reduction of the film and the release of anions. The high frequency capacitance of PpyOx/Chit remains constant between 0.30 V and -0.30 V vs SCE . It is evident from these plots that the chitosan slows down the ion transport prolonging the charge storage capability⁷⁰.

Table 5.7: Parameters for the circuit elements evaluated by fitting the impedance data of PpyCl/Chit to the equivalent circuit shown in Figure 5.14, $n=3$.

E (V vs SCE)	0.3	0.1	0.0	-0.1	-0.3	-0.6	-0.9 ^a
R_s (Ω cm²)	7.33 ± 0.08	7.21 ± 0.09	7.05 ± 0.08	8.25 ± 0.07	7.61 ± 0.10	7.99 ± 0.17	25.78 ± 0.29
CPE-T_{HF} (mF cm⁻²)	0.38 ± 0.03	0.15 ± 0.01	0.08 ± 0.01	0.15 ± 0.01	0.07 ± 0.01	0.05 ± 0.00	0.86 ± 0.01
CPE-P_{HF} (mF cm⁻²)	0.72 ± 0.01	0.85 ± 0.01	0.84 ± 0.01	0.79 ± 0.01	0.85 ± 0.01	0.74 ± 0.01	0.45 ± 0.00
R_{HF} (Ω cm²)	62.64 ± 2.68	107.6 ± 6.73	75.78 ± 4.15	84.99 ± 2.36	124.0 ± 7.13	349.8 ± 6.94	407.3 ± 16.6
CPE-T_{LF} (mF cm⁻²)	3.21 ± 0.03	1.70 ± 0.02	1.89 ± 0.02	2.17 ± 0.02	1.86 ± 0.03	3.71 ± 0.11	0.16 ± 0.01
CPE-P_{LF} (mF cm⁻²)	0.63 ± 0.01	0.54 ± 0.00	0.49 ± 0.00	0.64 ± 0.00	0.48 ± 0.01	0.61 ± 0.01	0.92 ± 0.02
χ^2	0.0014	0.0033	0.0037	0.0027	0.0058	0.0070	0.0005
SS	0.11502	0.4120	0.5152	0.3694	0.7978	0.9587	0.0590

^aThe circuit in 5.14 B consists of additional elements: R_{MIF} 21089 ± 1418.8

Table 5.8: Parameters for the circuit elements evaluated by fitting the impedance data of PpyOx/Chit to the equivalent circuit shown in Figure 5.14, $n=3$.

E (V vs SCE)	0.3	0.1	0.0	-0.1	-0.3	-0.6	-0.9^a
R_s (Ω cm^2)	8.78 \pm 0.22	6.66 \pm 0.30	5.85 \pm 0.07	6.72 \pm 0.12	4.93 \pm 0.13	5.96 \pm 0.12	9.37 \pm 0.08
CPE-T_{HF} (mF cm^{-2})	0.13 \pm 0.01	0.10 \pm 0.02	0.19 \pm 0.01	0.08 \pm 0.01	0.03 \pm 0.00	0.19 \pm 0.01	0.03 \pm 0.00
CPE-P_{HF} (mF cm^{-2})	0.70 \pm 0.01	0.64 \pm 0.02	0.66 \pm 0.01	0.74 \pm 0.01	0.80 \pm 0.01	0.71 \pm 0.01	1.00 \pm 0.00
R_{HF} (Ω cm^2)	166.6 \pm 4.33	24.34 \pm 0.68	21.54 \pm 0.22	43.78 \pm 1.47	199.6 \pm 4.70	313.9 \pm 9.75	14.68 \pm 0.31
CPE-T_{LF} (mF cm^{-2})	4.20 \pm 0.08	4.99 \pm 0.05	9.26 \pm 0.05	4.39 \pm 0.04	5.16 \pm 0.17	3.22 \pm 0.09	0.42 \pm 0.01
CPE-P_{LF} (mF cm^{-2})	0.52 \pm 0.01	0.71 \pm 0.01	0.80 \pm 0.00	0.45 \pm 0.01	0.48 \pm 0.01	0.59 \pm 0.01	1 \pm 0.00
χ^2	0.0031	0.0045	0.0013	0.0016	0.0071	0.0050	0.0063
SS	0.3866	0.5453	0.1545	0.1715	0.9055	0.6368	0.8821

^a The circuit in 5.14 B consists of additional elements: R 45.73 \pm 3.46, CPE-T 18.12 \pm 1.17, and CPE-P 0.29 \pm 0.01

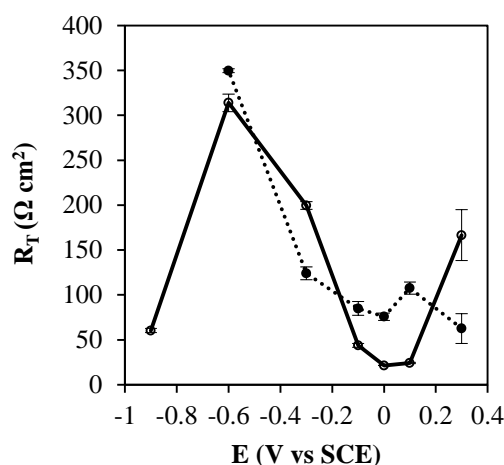


Figure 5.19: Plots of resistance, R_T , as a function of applied potential for PpyCl/Chit (●) and PpyOx/Chit (○) in PBS solution. The films were prepared by potentiostatic electropolymerisation at 0.80 V vs SCE to a charge density of 0.25 C cm^{-2} . The PpyCl was prepared from a solution of 0.1 mol dm^{-3} Py and 0.1 mol dm^{-3} NaCl and the PpyMO was prepared from a solution of 0.2 mol dm^{-3} Py and 0.02 mol dm^{-3} Ox. Chitosan was added post-polymerisation. $n=3$

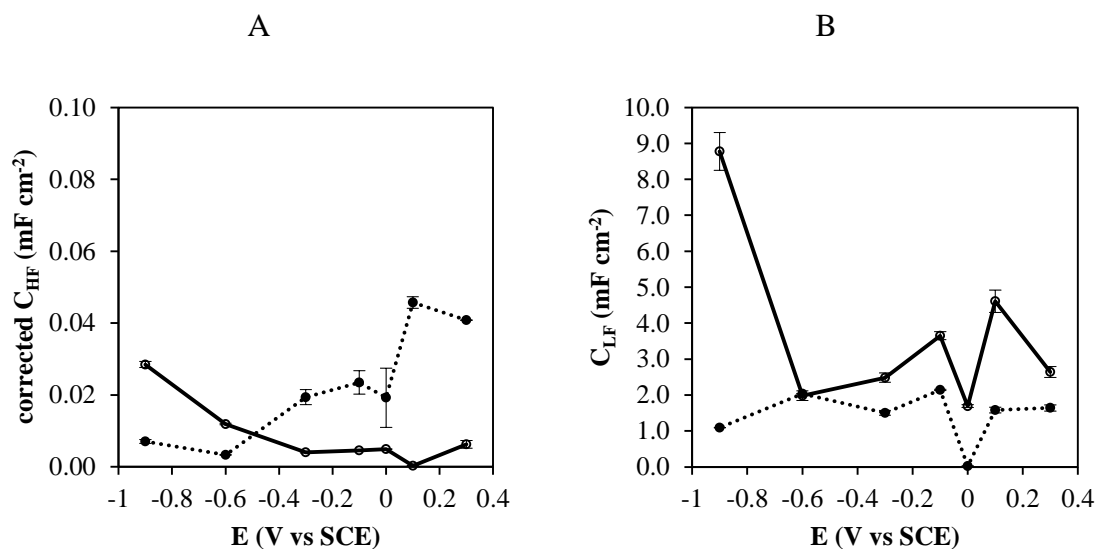


Figure 5.20: Plots of corrected double layer capacitance, C_{HF} , (A), and low frequency capacitance, C_{LF} , (B), as a function of applied potential for PpyCl/Chit (●) and PpyOx/Chit (○) in PBS solution. The films were prepared by potentiostatic electropolymerisation at 0.80 V vs SCE to a charge density of 0.25 C cm^{-2} . The PpyCl was prepared from a solution of 0.1 mol dm^{-3} Py and 0.1 mol dm^{-3} NaCl and the PpyOx was prepared from a solution of 0.2 mol dm^{-3} Py and 0.01 mol dm^{-3} Ox. Chitosan was added post-polymerisation. $n=3$

5.3.5.3 A comparison between the PpyCl and PpyOx films

A direct comparison of the impedance responses for PpyOx, PpyOx/Chit, PpyCl and PpyCl/Chit are shown in Figure 5.21, while corresponding data are presented in Table 5.9. These spectra were recorded at 0.10 V vs SCE. The significant role of the different anionics can be clearly seen. The PpyCl films have higher resistance (R_T) values and a higher capacitance than the PpyOx films and the low frequency capacitance (C_{LF}) is lower for the PpyCl films. It is also evident that the chitosan layer exerts little effect on the PpyA systems at this applied potential. Although the conductivity of the PpyA/Chit could not be determined the presence of chitosan appears to increase the resistance slightly which would reduce the conductivity. This is somewhat different to the data recorded for PpyA in NaCl, Chapter 4, indicating that the electrolyte (PBS or NaCl) has an effect on these systems⁷¹.

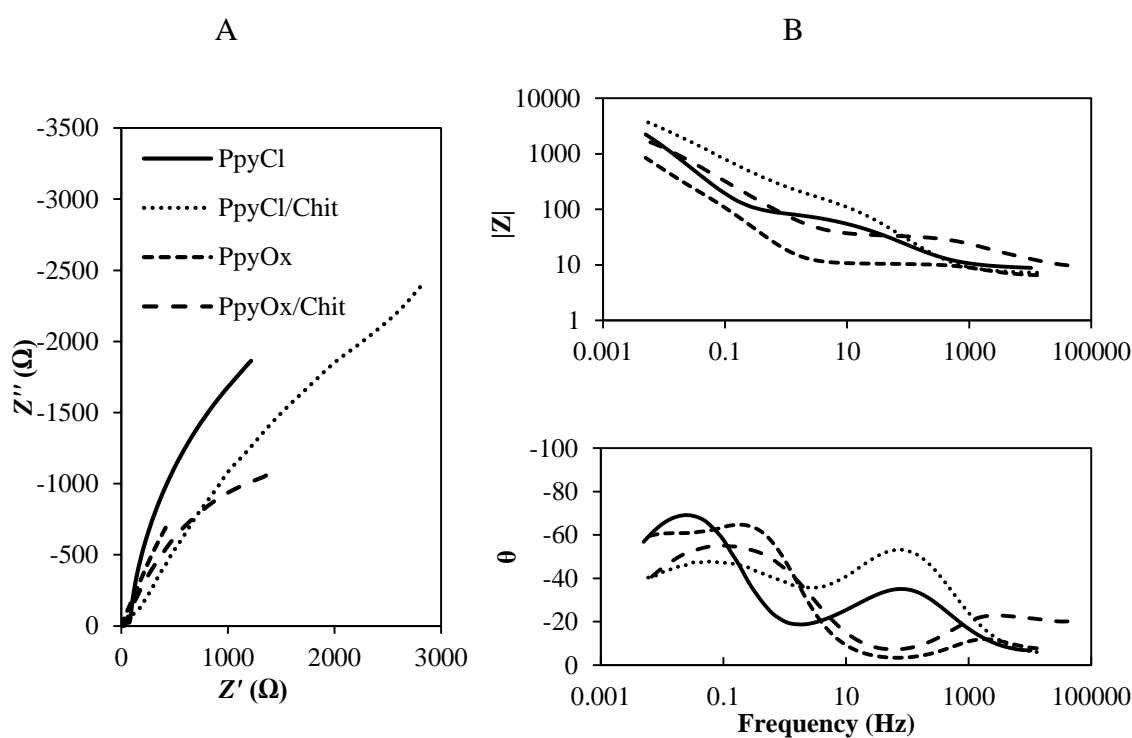


Figure 5.21: Complex-plane impedance plot (A) and Bode plot (B), for PpyA and PpyA/Chit coated 0.13 cm² Pt electrodes at 0.1 V vs SCE in PBS solution. The films were prepared by potentiostatic electropolymerisation at 0.80 V vs SCE to a charge density of 0.25 C cm⁻². The PpyCl was prepared from a solution of 0.1 mol dm⁻³ Py and 0.1 mol dm⁻³ NaCl and the PpyOx was prepared from a solution of 0.2 mol dm⁻³ Py and 0.02 mol dm⁻³ Ox. Chitosan was added post-polymerisation.

Table 5.9: Summary of the parameters extracted from fitting the impedance data recorded at 0.1 V vs SCE for the PpyA and PpyA/Chit composites in PBS solution. All PpyA films were grown to a charge density of 0.25 C cm⁻².

Sample (0.10 V)	C_{HF} (μF cm⁻²)	R_T (Ω cm²)	C_{LF} (mF cm⁻²)	σ_T (μS cm⁻¹)
PpyOx	2.33 ± 0.10	9.4 ± 1.76	13.72 ± 0.50	84.5 ± 3.38
PpyCl	5.87 ± 0.16	97.6 ± 2.54	7.70 ± 0.17	6.0 ± 0.14
PpyOx/Chit	0.03 ± 0.01	24.3 ± 0.68	4.61 ± 0.31	-
PpyCl/Chit	4.57 ± 0.15	107.6 ± 6.73	1.58 ± 0.08	-

5.3.6 Adhesion test

The adhesion tests were classified using the methodology summarised in Table 3.8, Chapter 3. A summary of the adhesion test results obtained for PpyCl, PpyCl/Chit, PpyOx and PpyOx/Chit is provided in Table 5.10. In this table, the films indicated with E (+V) refer to the films grown at a fixed potential of 0.80 V vs SCE, while the films indicated with E (-V) refer to the reduced films. The reduced films were held at -0.90 V vs SCE for 10 min in 0.1 mol dm⁻³ PBS solution after polymerisation. The films were then dried in a stream of air. The overall adhesion properties of PpyOx were satisfactory. There was somewhat of a decline in the adhesion performance of PpyCl in the presence of PBS solution when a positive potential was applied, possibly due to some nucleophilic attack of the OH⁻ ions in PBS^{41, 71}. The addition of chitosan to the PpyOx film to give the PpyOx/Chit composite improved the adhesion properties of the polymer film.

Table 5.10: Summary of results from adhesion tests.

Sample	Classification	Result
PpyCl E (+ V)	1	Good
PpyCl/Chit E (+ V)	0	Excellent
PpyOx E (+ V)	1	Good
PpyOx/Chit E (+ V)	1	Good
PpyCl E (– V)	2	Poor
PpyCl/Chit E (– V)	1	Good
PpyOx E (– V)	3	Very Poor
PpyOx/Chit E (– V)	2	Poor

5.3.7 Release of oxacillin

The release of oxacillin from the PpyOx and PpyOx/Chit films was studied and compared. Prior to the release studies, the films were washed in ethanol followed by washing in distilled water. A typical three electrode cell set-up was used, the cell was wrapped in aluminum foil and a gentle stirring motion with a magnetic stirrer and bead was used to aid the homogenising of the solution. Three protocols were chosen to study the release of oxacillin from the PpyOx and PpyOx/Chit films into 10 cm³ of 0.1 mol dm⁻³ PBS solution (pH 7.4), release at 0.30 V, –0.60 V vs SCE and at the open-circuit potential (OCP). These constant potentials were chosen based on the methyl orange release performance, Chapter 4. At 0.30 V vs SCE, the polymer film is maintained in the oxidised state, while at –0.60 V vs SCE the film is reduced. The final protocol used in this study was the release from an unstimulated film at its OCP value.

5.3.8 Detection of oxacillin

The amount of oxacillin released from the polymer film was quantitatively determined using UV spectroscopy by measuring the maximum absorbance at 205 nm. The detection of oxacillin is usually performed using gas chromatography and a UV detector at 225 nm, using the pharmacopeia method. The pharmacopeia drug, dissolved in an organic solvent, detects the oxacillin. The difference in wavelength between the pharmacopeia method and the method employed here is possibly due to the different nature of the solvent. Prior to carrying out the 24 hour release study, the UV spectrum of oxacillin in PBS solution ($8.5 \mu\text{g mL}^{-1}$) was recorded at 0, 6, 12 and 24 hours to validate the quality of detection. A broad wave between 230 and 250 nm became slightly more pronounced but the peak at 205 nm remained constant. Typical UV spectra recorded of oxacillin in PBS are shown in Figure 5.22, while the corresponding calibration curve is presented in the inset. A linear calibration curve was obtained and this was used to give the concentration of oxacillin released from the PpyOx and PpyOx/Chit films. The slope of the linear plot was $56.7 \times 10^3 \mu\text{g}^{-1} \text{dm}^3$ giving the extinction coefficient, ϵ , a value of $56.7 \times 10^3 \mu\text{g}^{-1} \text{dm}^3 \text{cm}^{-1}$.

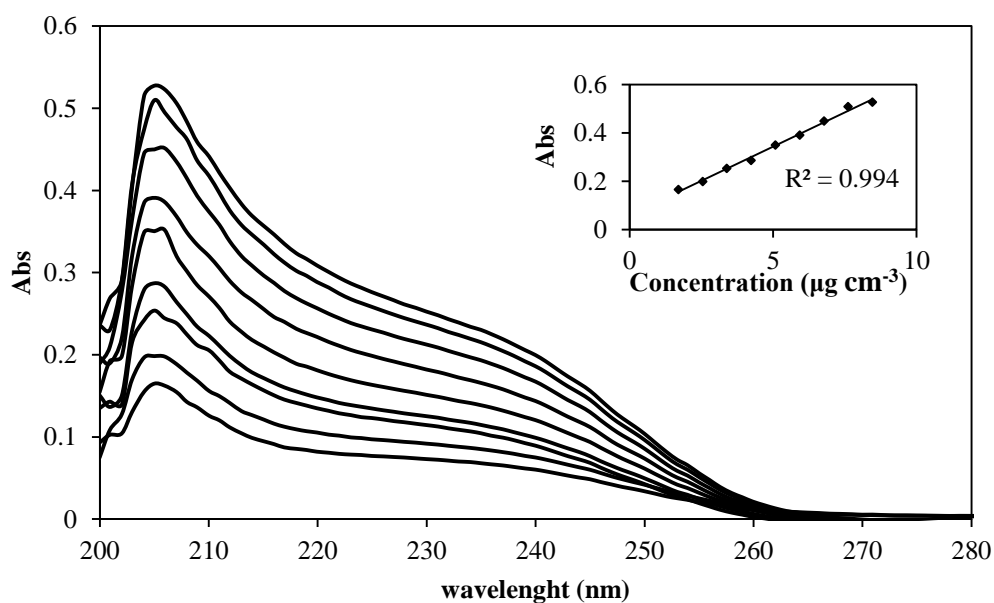


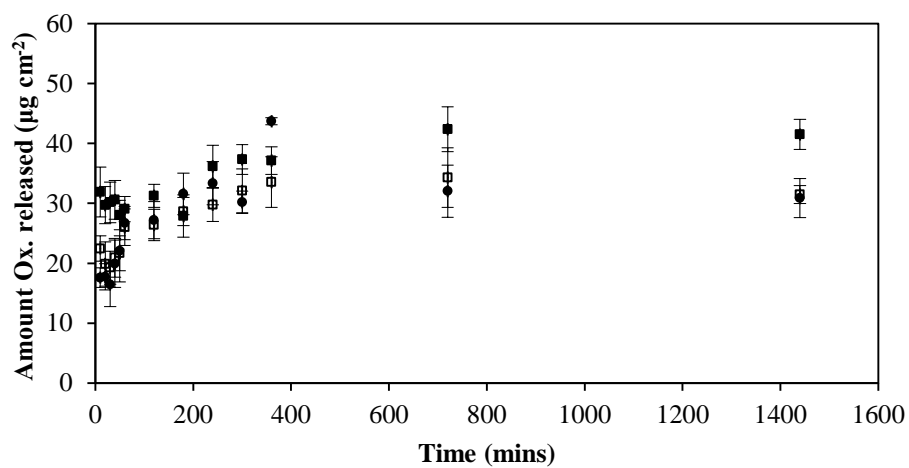
Figure 5.22: UV spectra of Ox in PBS solution. Calibration curve is shown in inset.

The amount of oxacillin released was measured as a function of time. Intervals of 10 min were used during the first hour, then one hour intervals were used until 6 hours followed by a measurement taken at 12 hours and 24 hours. To measure the amount of oxacillin released at each time interval, a 3 cm³ sample was taken from the release medium. The Ox concentration for each aliquot was compared against the calibration curve shown in Figure 5.22. Each data point represents an average of three measurements, $n = 3$.

The release of oxacillin over a 24 hour period from PpyOx film (A) and PpyOx/Chit (B) films is shown in Figure 5.23, while the oxacillin release at shorter times is shown in Figure 5.24. These data are also presented as a bar chart in Figure 5.25. At open-circuit potential conditions, or unstimulated release, the average oxacillin released in the first hour was 26.72 $\mu\text{g cm}^{-3}$ and 27.44 $\mu\text{g cm}^{-3}$ from PpyOx and PpyOx/Chit, respectively. At 12 hours, the amount of oxacillin released from PpyOx was 43.72 $\mu\text{g cm}^{-3}$ and from PpyOx/Chit was 38.03 $\mu\text{g cm}^{-3}$. This indicates that the presence of chitosan may slow the release of oxacillin. Another important finding is that no electrical stimuli were required to release the oxacillin and the release occurred probably through solvation effects. There are several applications where this would be beneficial^{11, 72}. At an applied potential of 0.30 V vs SCE, the average amount of oxacillin released in the first hour was 25.05 $\mu\text{g cm}^{-3}$ for PpyOx and 25.13 $\mu\text{g cm}^{-3}$ for PpyOx/Chit. At 12 hours, the amount of oxacillin released was 43.28 $\mu\text{g cm}^{-3}$ for PpyOx and 36.91 $\mu\text{g cm}^{-3}$ for PpyOx/Chit. At -0.60 V vs SCE, the average amount of oxacillin released in the first hour was 26.01 $\mu\text{g cm}^{-3}$ for PpyOx and 31.25 $\mu\text{g cm}^{-3}$ for PpyOx/Chit and after 12 hours the amount of oxacillin released was 34.29 $\mu\text{g cm}^{-3}$ and 31.81 $\mu\text{g cm}^{-3}$ for the PpyOx and PpyOx/Chit films, respectively. Statistically these values are similar and this is clearly evident from the data presented in Figures 5.23, 5.24 and 5.25. This may suggest that oxacillin is trapped inside the film and the applied potential has little influence on the release. When the polypyrrole is reduced it becomes neutral and in order to remain neutral either the Ox⁻ that was incorporated has to be expelled or if the Ox⁻ is immobile, a cation (Na⁺) from the surrounding electrolyte will be incorporated to satisfy charge neutrality, Equation 5.9. When the polypyrrole is reoxidised the positive charge is returned to the polypyrrole backbone. The cation (Na⁺) previously incorporated must be expelled or alternatively anions present in the electrolyte may be incorporated.



A



B

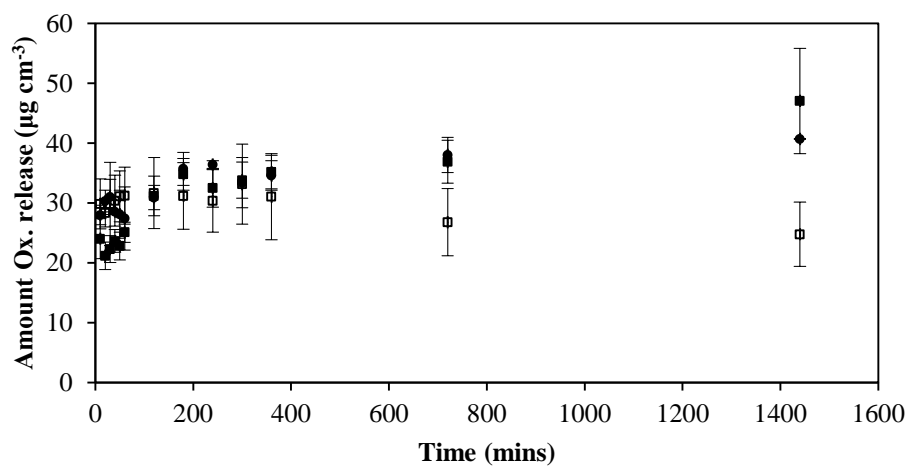


Figure 5.23: The amount of oxacillin released from PpyOx (A) and PpyOx/Chit (B) as a function of time over 1440 min, or 24 h, at 0.30 V vs SCE (■), OCP (●) and -0.60 V vs SCE (□). n =3

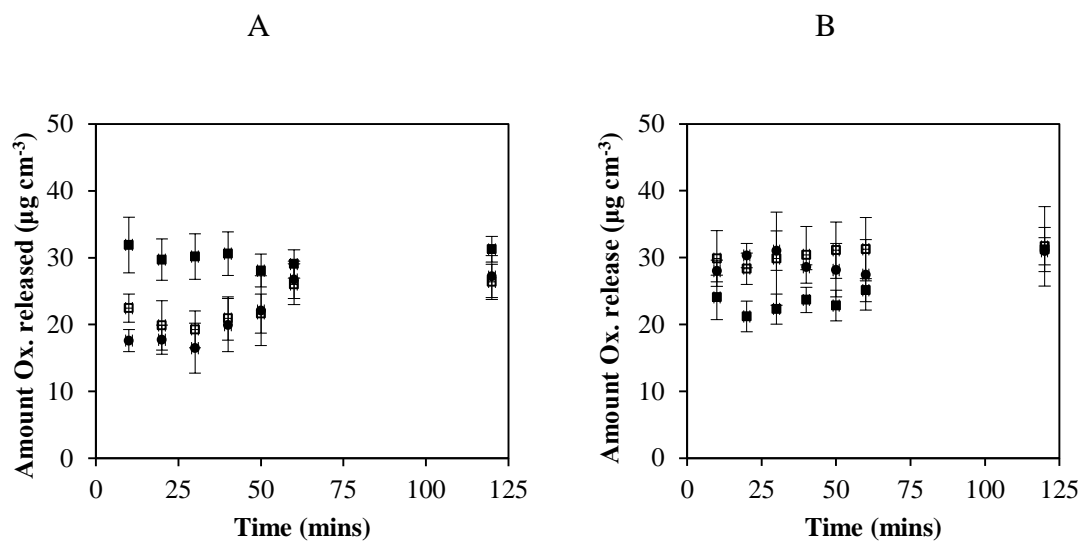


Figure 5.24: The amount of oxacillin released from PpyOx (A) and PpyOx/Chit (B) as a function of time over 120 min, or 2 h, at 0.30 V vs SCE (■), OCP (●) and -0.60 V vs SCE (□). The data were averaged over 4 determinations, $n = 4$. The films were prepared by potentiostatic electropolymerisation at 0.80 V vs SCE to a charge density of 0.25 C cm^{-2} . The PpyMO was prepared from a solution of 0.2 mol dm^{-3} Py and 0.02 mol dm^{-3} Ox. Chitosan was added post-polymerisation. $n=3$

A number of investigations into antibiotic eluting polymers have reported less than 10 % accumulated yields^{11, 73, 74}. A qualitative observation was that after the 24 h period of immersion in the dilute oxacillin-PBS solution the chitosan film became white and opaque. The colour change was not observed on completion of the 6 or 8 h studies, e.g., electrochemical impedance spectroscopy. Nunthanid *et al.*⁷⁵ observed a similar change from a colourless to white in their chitosan films following swelling release studies in PBS. They proposed cross-linking between the cationic amino group and phosphate anions. However, in this case, the white colour is possibly due to the adsorption of oxacillin this may explain the decrease in oxacillin concentration at -0.6 V vs SCE.

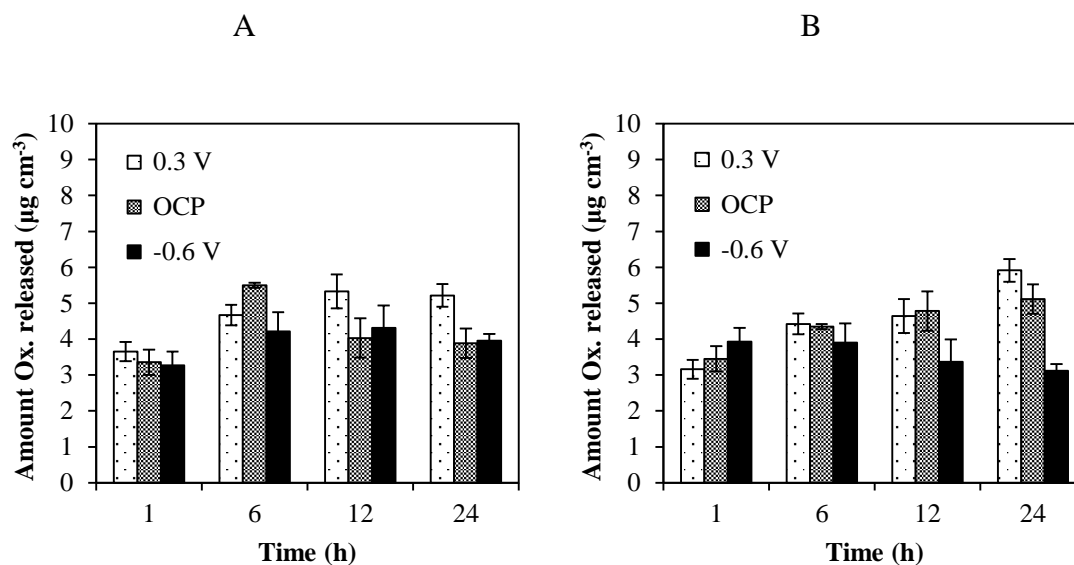


Figure 5.25: Bar chart indicating the amount of oxacillin released as a function of time for (A) PpyOx and (B) PpyOx/Chit at OCP, 0.30 V and -0.60 V, vs SCE in PBS solution. n=3

5.4 Summary

In this chapter, polypyrrole was successfully doped with oxacillin in the absence of an additional supporting electrolyte. The PpyOx films were characterised prior to carrying out the release of oxacillin from the films. The morphology of the PpyOx film was very different to that of PpyCl, which exhibits the globular “cauliflower” morphology. The PpyOx film was smooth and lacked contrasting features. The films appeared to be free from surface defects and the adhesion properties of PpyCl and PpyOx were overall satisfactory.

The redox properties of PpyCl, PpyOx, PpyCl/Chit and PpyOx/Chit were analysed using cyclic voltammetry. The peak currents were proportional to the scan rate. The peak shape and peak position varied depending on the dominant ion exchange and inclusion or expulsion process. In the case for PpyCl, the Cl⁻ is more mobile than Na⁺ and the PpyCl and PpyCl/Chit exhibit a dominant anion exchange process, while PpyOx clearly shows

a dominant cation exchange. The doping level of the PpyOx film was estimated at 1:13 using EQCM measurements.

Electrochemical impedance data were recorded for the polymer films and the composites and a range of electrochemical behaviour was observed at different applied potentials. The charge-transfer resistance increased as the PpyCl film was reduced from an oxidised state to a neutral state. The charge-transfer resistance of PpyOx was lower and this is consistent with the ingress of Na⁺ ions as the PpyOx film is reduced.

The concentration of oxacillin released from PpyOx and PpyOx/Chit by electrical stimulation into the cell was detected using UV spectroscopy. In both cases, for PpyOx and PpyOx/Chit, the concentration of oxacillin increased as a function of time but there was statistically no difference between the applied potentials, with the exception of PpyOx at -0.6 V vs SCE.

References

1. G. Carja, Y. Kameshima, G. Ciobanu, H. Chiriac and K. Okada, *Micron*, 2009, **40**, 147-150.
2. G. Yang, S. Feng, H. Liu, J. Yin, L. Zhang and L. Cai, *Journal of Chromatography B*, 2007, **854**, 85-90.
3. S. S. Castle, in *xPharm: The Comprehensive Pharmacology Reference*, eds. S. J. Enna and D. B. Bylund, Elsevier, New York, 2007, pp. 1-5.
4. N. J. Hickok and I. M. Shapiro, *Advanced Drug Delivery Reviews*, 2012, **64**, 1165-1176.

5. M. Stigter, J. Bezemer, K. de Groot and P. Layrolle, *Journal of Controlled Release*, 2004, **99**, 127-137.
6. L. Pichavant, G. Amador, C. Jacqueline, B. Brouillaud, V. Héroguez and M.-C. Durrieu, *Journal of Controlled Release*, 2012, **162**, 373-381.
7. O. Guillaume, X. Garric, J.-P. Lavigne, H. Van Den Berghe and J. Coudane, *Journal of Controlled Release*, 2012, **162**, 492-501.
8. D. Campoccia, L. Montanaro, P. Speziale and C. R. Arciola, *Biomaterials*, 2010, **31**, 6363-6377.
9. Y. Gu, X. Chen, J.-H. Lee, D. A. Monteiro, H. Wang and W. Y. Lee, *Acta Biomaterialia*, 2012, **8**, 424-431.
10. M. Fernandez-Gutierrez, E. Olivares, G. Pascual, J. M. Bellon and J. S. Román, *Acta Biomaterialia*, 2013, **9**, 6006-6018.
11. M. Zilberman and J. J. Elsner, *Journal of Controlled Release*, 2008, **130**, 202-215.
12. J. H. Sung, M.-R. Hwang, J. O. Kim, J. H. Lee, Y. I. Kim, J. H. Kim, S. W. Chang, S. G. Jin, J. A. Kim, W. S. Lyoo, S. S. Han, S. K. Ku, C. S. Yong and H.-G. Choi, *International Journal of Pharmaceutics*, 2010, **392**, 232-240.
13. H. Tan, S. Guo, S. Yang, X. Xu and T. Tang, *Acta Biomaterialia*, 2012, **8**, 2166-2174.
14. D. Esrafilzadeh, J. M. Razal, S. E. Moulton, E. M. Stewart and G. G. Wallace, *Journal of Controlled Release*, 2013, **169**, 313-320.
15. J. W. Sirinrath Sirivisoot and Rajesh Pareta and Thomas, *Nanotechnology*, 2011, **22**, 085101.
16. D.-S. Lee, Y.-M. Kim, M.-S. Lee, C.-B. Ahn, W.-K. Jung and J.-Y. Je, *Bioorganic & Medicinal Chemistry Letters*, 2010, **20**, 975-978.

17. F. B. Bolger, S. B. McHugh, R. Bennett, J. Li, K. Ishiwari, J. Francois, M. W. Conway, G. Gilmour, D. M. Bannerman, M. Fillenz, M. Tricklebank and J. P. Lowry, *Journal of Neuroscience Methods*, 2011, **195**, 135-142.
18. A. J. Bard and L. R. Faulkner, *Electrochemical methods. Fundamentals and applications*, Wiley, 2001.
19. S. Sirivisoot, R. A. Pareta and T. J. Webster, *Diffus. Defect Data, Pt. B*, 2009, **151**, 197-202.
20. S. Sirivisoot, R. A. Pareta and T. J. Webster, *J. Biomed. Mater. Res., Part A*, 2011, **99A**, 586-597.
21. B. Scharifker and G. Hills, *Electrochimica Acta*, 1983, **28**, 879-889.
22. B. C. Kim, G. M. Spinks, C. O. Too, G. G. Wallace, Y. H. Bae and N. Ogata, *Reactive and Functional Polymers*, 2000, **44**, 245-258.
23. T. F. Otero, I. Boyano, M. T. Cortés and G. Vázquez, *Electrochimica Acta*, 2004, **49**, 3719-3726.
24. C. K. Baker and J. R. Reynolds, *Journal of Electroanalytical Chemistry and Interfacial Electrochemistry*, 1988, **251**, 307-322.
25. J. M. Davey, S. F. Ralph, C. O. Too and G. G. Wallace, *Synthetic Metals*, 1999, **99**, 191-199.
26. T. Raudsepp, M. Marandi, T. Tamm, V. Sammelselg and J. Tamm, *Electrochimica Acta*.
27. D. A. Buttry and M. D. Ward, *Chemical Reviews*, 1992, **92**, 1355-1379.
28. G. Sauerbrey, *Zeitschrift für Physik*, 1959, **155**, 206-222.
29. A. L. Briseno, A. Baca, Q. Zhou, R. Lai and F. Zhou, *Analytica Chimica Acta*, 2001, **441**, 123-134.

-
30. E. M. Genies and J. M. Pernaut, *Synthetic Metals*, 1984, **10**, 117-129.
 31. M. Hepel and F. Mahdavi, *Microchemical Journal*, 1997, **56**, 54-64.
 32. M.-K. Song, Y.-T. Kim, B.-S. Kim, J. Kim, K. Char and H.-W. Rhee, *Synthetic Metals*, 2004, **141**, 315-319.
 33. F. Scholz and A. M. Bond, *Electroanalytical methods guide to experiments and applications*, Springer, 2010.
 34. P. Dyreklev, M. Granström, O. Inganäs, L. M. W. K. Gunaratne, G. K. R. Senadeera, S. Skaarup and K. West, *Polymer*, 1996, **37**, 2609-2613.
 35. J. Serra Moreno, S. Panero, M. Artico and P. Filippini, *Bioelectrochemistry*, 2008, **72**, 3-9.
 36. H. Bai, Q. Chen, C. Li, C. Lu and G. Shi, *Polymer*, 2007, **48**, 4015-4020.
 37. R. Stanković, O. Pavlović, M. Vojnović and S. Jovanović, *European Polymer Journal*, 1994, **30**, 385-393.
 38. C. C. Bof Bufon, J. Vollmer, T. Heinzel, P. Espindola, H. John and J. Heinze, *The Journal of Physical Chemistry B*, 2005, **109**, 19191-19199.
 39. D. Schmeisser, H. Naarmann and W. Göpel, *Synthetic Metals*, 1993, **59**, 211-221.
 40. J. M. Fonner, L. Forciniti, N. Hieu, J. D. Byrne, Y.-F. Kou, J. Syeda-Nawaz and C. E. Schmidt, *Biomedical Materials*, 2008, **3**, 1-12.
 41. K. Qi, Y. Qiu, Z. Chen and X. Guo, *Corrosion Science*, 2013, **69**, 376-388.
 42. C. Weidlich, K. M. Mangold and K. Jüttner, *Electrochimica Acta*, 2005, **50**, 1547-1552.
 43. X. Ren and P. G. Pickup, *Canadian Journal of Chemistry*, 1997, **75**, 1518-1522.
 44. M. F. a. L. F. a. H. N. a. J. D. B. a. Y.-F. K. a. J. S.-N. a. C. E. S. John, *Biomedical Materials*, 2008, **3**, 034124.

-
45. I. L. Lehr, O. V. Quinzani and S. B. Saidman, *Materials Chemistry and Physics*, 2009, **117**, 250-256.
 46. G. A. Snook, G. Z. Chen, D. J. Fray, M. Hughes and M. Shaffer, *Journal of Electroanalytical Chemistry*, 2004, **568**, 135-142.
 47. M. N. Akieħ, Á. Varga, R.-M. Latonen, S. F. Ralph, J. Bobacka and A. Ivaska, *Electrochimica Acta*, 2011, **56**, 3507-3515.
 48. H. Zhao, W. E. Price, P. R. Teasdale and G. G. Wallace, *Reactive Polymers*, 1994, **23**, 213-220.
 49. V. M. Schmidt and J. Heitbaum, *Electrochimica Acta*, 1993, **38**, 349-356.
 50. A. C. Partridge, C. B. Milestone, C. O. Too and G. G. Wallace, *Journal of Membrane Science*, 1999, **152**, 61-70.
 51. X. Ren and P. G. Pickup, *Journal of Physical chemistry*, 1993, **97**, 5356-5362.
 52. X. Ren and P. G. Pickup, *Electrochimica Acta*, 1996, **41**, 1877-1882.
 53. X. Ren and P. G. Pickup, *Journal of Electroanalytical Chemistry*, 1997, **420**, 251-257.
 54. V. Syrĭtski, A. Öpik and O. Forsén, *Electrochimica Acta*, 2003, **48**, 1409-1417.
 55. M. N. Akieħ, W. E. Price, J. Bobacka, A. Ivaska and S. F. Ralph, *Synthetic Metals*, 2009, **159**, 2590-2598.
 56. W. M. Aylward and P. G. Pickup, *Electrochimica Acta*, 2007, **52**, 6275-6281.
 57. K. P. Vidanapathirana, M. A. Careem, S. Skaarup and K. West, *Solid State Ionics*, 2002, **154–155**, 331-335.
 58. M. A. Careem, Y. Velmurugu, S. Skaarup and K. West, *Journal of Power Sources*, 2006, **159**, 210-214.

-
59. S. Skaarup, M. J. M. Jafeen and M. A. Careem, *Solid State Ionics*, 2010, **181**, 1245-1250.
 60. M. E. Orazem and B. Tribollet, *Electrochemical Impedance Spectroscopy*, John Wiley & Sons, Inc., Hoboken, New Jersey, 2008.
 61. B. R. Hinderliter, S. G. Croll, D. E. Tallman, Q. Su and G. P. Bierwagen, *Electrochimica Acta*, 2006, **51**, 4505-4515.
 62. G. Garcia-Belmonte, Z. Pomerantz, J. Bisquert, J.-P. Lellouche and A. Zaban, *Electrochimica Acta*, 2004, **49**, 3413-3417.
 63. G. Garcia-Belmonte, *Electrochemistry Communications*, 2003, **5**, 236-240.
 64. X. Ren and P. G. Pickup, *Journal of Electroanalytical Chemistry*, 1995, **396**, 359-364.
 65. J. Mostany and B. R. Scharifker, *Synthetic Metals*, 1997, **87**, 179-185.
 66. M. R. Warren and J. D. Madden, *Synthetic Metals*, 2006, **156**, 724-730.
 67. W. Plieth, A. Bund, U. Rammelt, S. Neudeck and L. Duc, *Electrochimica Acta*, 2006, **51**, 2366-2372.
 68. T. Komura, S. Goisihara, T. Yamaguti and K. Takahasi, *Journal of Electroanalytical Chemistry*, 1998, **456**, 121-129.
 69. X. Zhang, S. Wang, S. Lu, J. Su and T. He, *Journal of Power Sources*, 2014, **246**, 491-498.
 70. S. Brahim and A. Guiseppi-Elie, *Electroanalysis*, 2005, **17**, 556-570.
 71. K. Qi, Y. Qiu, Z. Chen and X. Guo, *Corrosion Science*, 2012, **60**, 50-58.
 72. D. Svirskis, J. Travas-Sejdic, A. Rodgers and S. Garg, *Journal of Controlled Release*, 2010, **146**, 6-15.

73. L. Bunetel, A. Segui, M. Cormier, E. Percheron and F. Langlais, *Clinical Pharmacokinetics*, 1989, **17**, 291-297.
74. F. R. Dimaio, J. J. O'Halloran and J. M. Quale, *Journal of Orthopaedic Research*, 1994, **12**, 79-82.
75. J. Nunthanid, S. Puttipipatkachorn, K. Yamamoto and G. E. Peck, *Drug Dev. Ind. Pharm.*, 2001, **27**, 143-157.

Chapter 6

Conclusion

6. Conclusions

The main objective of this research was to prepare polypyrrole in the presence of chitosan with the aim of improving the mechanical and the adhesion properties of polypyrrole, while retaining the low resistance or high conductivity, which is characteristic of polypyrrole¹.

Initially, a novel approach was taken to prepare the polypyrrole-chitosan composite films by electrochemically polymerising pyrrole in a chitosan hydrogel network directly on an electrode surface. The advantage of this procedure is that a comprehensive electrochemical characterisation can be obtained. The electrochemical properties of polypyrrole-chloride, PpyCl, and the Chit/PpyCl composites were studied using cyclic voltammetry and the dominant redox process was found to be anion transport (Cl^-), which is in good agreement with the literature²⁻⁵. Electrochemical impedance spectroscopy (EIS) was used to further characterise the electrochemical properties of the composites. The impedance response of the chitosan was significantly different from the PpyCl film. A semi-circular transmission line was obtained for the chitosan, indicating restricted diffusion conditions⁶. The Chit/PpyCl showed similar properties to PpyCl, indicating that chitosan has no adverse influence on the ion-transport properties, while the adhesion performance of Chit/PpyCl was superior to PpyCl. These results suggest that chitosan provides a suitable matrix for ion transport in polypyrrole films and offers some mechanical reinforcement⁷.

In the subsequent chapters an alternative method was used to prepare PpyA-chitosan composites as difficulties were encountered when trying to prepare Chit/PpyA directly at the surface. The sequential steps are illustrated in Figure 3.1 where chitosan was cast on to the doped polypyrrole post electropolymerisation and cured under an infrared lamp. This method was found to be more suitable for incorporating larger anionic species. The

adhesion properties performed better in the presence of chitosan but were not as superior as the initial Chit/PpyCl composite.

In Chapter 4, methyl orange is introduced as the first anion or dopant for incorporation and release from polypyrrole and the polypyrrole/chitosan composites. Methyl orange served as a suitable alternative to dexamethasone due to its size, charge, solubility, and cost. Although doping polypyrrole with methyl orange is not an entirely novel concept⁸⁻¹⁰, here it was incorporated in the absence of additional electrolytes, contrary to the literature. The methyl orange doped polymer films, PpyMO, were deposited to a charge density of 0.25 C cm^{-2} . The charge-time ($Q-t$) plots for PpyCl produced steeper slopes than PpyMO demonstrating a slower growth rate for PpyMO. This slower growth rate may be explained by the slow diffusion of the relatively large MO^- anion to the electrode surface¹¹. Although similar film thickness values were obtained for PpyCl and PpyMO when deposited to the same charge density¹², the surface morphology of the films were very different. The typical globular morphology was observed for PpyCl^{13,14} however the PpyMO gave tubular-like structures¹⁰.

Cyclic voltammetry measurements were used to identify the redox processes at the PpyCl, PpyMO, Chit/PpyCl and Chit/PpyMO composite films. The electrochemical properties of the PpyCl film were dominated by anion transport and cation transport was observed for the PpyMO film. Although the redox peaks were observed in the presence of chitosan they did appear slightly obscured. The conductivity values of PpyMO and PpyCl in 0.10 mol dm^{-3} NaCl were found to be $91.28 \text{ } \mu\text{S cm}^{-1}$ at -0.10 V vs SCE and $100.81 \text{ } \mu\text{S cm}^{-1}$ at 0.30 V vs SCE , respectively, using electrochemical impedance spectroscopy. This corresponds with the anion incorporation in PpyCl and the cation release in PpyMO. The release of MO^- from the PpyMO films was studied using UV-visible spectroscopy. The concentration of MO^- increased as the applied potential was decreased from 0.30 V to -0.60 V vs SCE , and the release time was increased. An increase in the concentration of MO^- was also observed at open-circuit potentials, indicating a mixed release mechanism. However, the release of MO^- from PpyMO at -0.90 V vs SCE was influenced by the loss of the adhesion properties of the PpyMO film. This was not observed with the Chit/PpyMO composite.

Finally, polypyrrole doped with oxacillin, PpyOx, was prepared by applying a constant potential at 0.80 V vs SCE for approximately 8 min until a charge density of 0.25 C cm^{-2} was achieved. To the authors knowledge there are no publications of polypyrrole doped with this class of β -lactam penicillin. The growth rate was slower for PpyOx than the rates observed with the PpyMO and PpyCl polymer films. The slower growth rate may be explained by the slow diffusion of the large Ox^- anion to the electrode surface¹¹. Interestingly, the same amount of charge passed per area yielded different film thickness and morphology for the PpyCl and PpyOx films. The thickness of the PpyOx film was estimated to be $1.5 \mu\text{m}$ compared $0.5 \mu\text{m}$ for the PpyCl film. In addition, the PpyCl film showed the typical globular morphology^{13, 14} while the PpyOx appeared smooth, and lacking in contrasting features. The redox properties of PpyOx were dominated by cation transport. The conductivity of PpyOx in PBS at -0.10 V vs SCE was found to be $809.7 \mu\text{S cm}^{-1}$, while the conductivity of PpyCl at 0.30 V vs SCE was considerably lower at $12.37 \mu\text{S cm}^{-1}$. This difference in the magnitude of the conductivity is possibly due to the significant variation in the film thickness.

UV-visible spectroscopy was used to determine the release of oxacillin. Three protocols were chosen to study the release of oxacillin from the PpyOx and PpyOx/Chit films into 10 cm^3 of PBS solution (pH 7.4), released at 0.30 V , -0.60 V vs SCE and at the open-circuit potential (OCP). These constant potentials were chosen based on the methyl orange release performance in Chapter 4. The release was measured over a 24 h period an even though the release of Ox did not vary significantly as a function of the applied potential it did vary over time. The chitosan layer did not significantly influence the release of oxacillin at 0.30 V vs SCE or at open-circuit potentials, but it did have a negative influence at -0.60 V vs SCE . It is possible that the adsorption properties of chitosan interact with oxacillin, this may explain the observed colour change from colourless to white, and the decrease in the oxacillin concentrations observed at -0.60 V vs SCE (Figure 5.25) as the release time was increased from 6 h to 24 h.

Overall, the main goals of this thesis were achieved. It has been shown that cyclic voltammetry and electrochemical impedance measurements are suitable techniques for the characterisation of these drug-doped conducting composites.

6.1 Future work

As future work, it would be interesting to continue the systematic approach of testing different drugs in the doping and drug release processes. New drugs arrive on the market annually and drug/device combinations do not necessarily have to be developed simultaneously. As an example, coronary stents were on the market well in advance of drug-eluting stents¹⁵. An investigation on the growth of PpyOx on titanium would be beneficial for applications for orthopaedic implants, particularly for the prevention of implant associated infection¹⁶.

To further develop these systems for suitable implantation, biocompatibility studies followed by in vivo studies would have to be performed. On reviewing the literature it is clear that there is significant interest in inherently conducting polymers, particularly polypyrrole, for biomedical applications.¹⁷⁻¹⁹ Of the drugs studied, dexamethasone is receiving increased attention as a suitable dopant²⁰⁻²³, because PpyDex is a true electrically controlled drug system²¹, and it has a broad therapeutic index²⁴. Accordingly, it would be interesting to further study the properties and release profiles of PpyDex. It would also be necessary to monitor the shelf-life of the materials over an extended period of time and to study the drug release properties and electroactivity over extended periods²⁵.

References

1. W. M. Saslow, in *Electricity, Magnetism, and Light*, ed. W. M. Saslow, Academic Press, San Diego, 2002, pp. 281-335.

2. J. M. Fonner, L. Forciniti, N. Hieu, J. D. Byrne, Y.-F. Kou, J. Syeda-Nawaz and C. E. Schmidt, *Biomedical Materials*, 2008, **3**, 1-12.
3. I. L. Lehr, O. V. Quinzani and S. B. Saidman, *Materials Chemistry and Physics*, 2009, **117**, 250-256.
4. G. A. Snook, G. Z. Chen, D. J. Fray, M. Hughes and M. Shaffer, *Journal of Electroanalytical Chemistry*, 2004, **568**, 135-142.
5. X. Ren and P. G. Pickup, *Canadian Journal of Chemistry*, 1997, **75**, 1518-1522.
6. D. D. Macdonald, *Electrochimica Acta*, 2006, **51**, 1376-1388.
7. W. M. Aylward and P. G. Pickup, *Electrochimica Acta*, 2007, **52**, 6275-6281.
8. M. Li, W. Li, J. Liu and J. Yao, *Journal of Materials Science: Materials in Electronics*, 2013, **24**, 906-910.
9. X. Yang, Z. Zhu, T. Dai and Y. Lu, *Macromolecular Rapid Communications*, 2005, **26**, 1736-1740.
10. X. Yang, T. Dai, Z. Zhu and Y. Lu, *Polymer*, 2007, **48**, 4021-4027.
11. J. M. Davey, S. F. Ralph, C. O. Too and G. G. Wallace, *Synthetic Metals*, 1999, **99**, 191-199.
12. P. Holzhauser and K. Bouzek, *Journal of Applied Electrochemistry*, 2006, **36**, 703-710.
13. B. Scharifker and G. Hills, *Electrochimica Acta*, 1983, **28**, 879-889.
14. P. Dyreklev, M. Granström, O. Inganäs, L. M. W. K. Gunaratne, G. K. R. Senadeera, S. Skaarup and K. West, *Polymer*, 1996, **37**, 2609-2613.
15. P. Wu and D. W. Grainger, *Biomaterials*, 2006, **27**, 2450-2467.
16. M. Zilberman and J. J. Elsner, *Journal of Controlled Release*, 2008, **130**, 202-215.

17. C. L. Bayer and N. A. Peppas, *Journal of Controlled Release*, 2008, **132**, 216-221.
18. J. Z. Hilt and N. A. Peppas, *International Journal of Pharmaceutics*, 2005, **306**, 15-23.
19. R. Langer and N. A. Peppas, *AIChE Journal*, 2003, **49**, 2990-3006.
20. R. Wadhwa, C. F. Lagenaur and X. T. Cui, *Journal of Controlled Release*, 2006, **110**, 531-541.
21. L. Leprince, A. Dogimont and D. Magnin, *Journal of Materials Science: Materials in Medicine*, 2010, **21**, 925-930.
22. S. Naficy, J. M. Razal, G. M. Spinks and G. G. Wallace, *Sensors and Actuators A: Physical*, 2009, **155**, 120-124.
23. G. Stevenson, S. E. Moulton, P. C. Innis and G. G. Wallace, *Synthetic Metals*, 2010, **160**, 1107-1114.
24. J. R. Backes, J. C. Bentley, J. R. Politi and B. T. Chambers, *The Journal of Arthroplasty*, 2013, **28**, 11-17.
25. R. A. Green, N. H. Lovell, G. G. Wallace and L. A. Poole-Warren, *Biomaterials*, 2008, **29**, 3393-3399.

